

Transcriptomic analysis of synergy between antifungal drugs and iron chelators for alternative antifungal therapies

Yu-Wen Lai

School of Life and Environmental Sciences (SoLES)

Faculty of Science

The University of Sydney

2017

A thesis submitted in fulfilment of the requirements of the degree of Doctor of
Philosophy.

Declaration of originality

I certify that this thesis contains no materials which have been accepted for award of any other degree or diploma at any other university. To the best of my knowledge, this thesis is original and contains no material previously published or written by any other person, except where due reference has been made in the text.

Yu-Wen Lai

August 2016

Acknowledgements

This whole thesis and the years spent into completing it would not have been possible without the help and support of a lot of people. I am thankful and grateful to my supervisor Dee Carter and also to my co-supervisor Sharon Chen for giving me the opportunity to work on this project. I am also thankful to our collaborator Marc Wilkins and his team. This project has been very challenging and your inputs and advice have really helped immensely.

A big thank you goes to past and present honours students, PhD candidates and post-docs. Your prep talks, stimulating discussions, humour, baked goods and cider making sessions were my staples for keeping me mostly sane. To Kate Weatherby and Sam Cheung, we started honours and PhDs together and even travelled together in Europe. There were major ups and downs during the course of our projects, but we're finally getting to the end! Thank you Katherine Pan and Mia Zeric for always offering chocolate and snacks, I swear I mostly go over to your side of the office just to eat your food.

A huge shout out to the people in the Carter Lab, especially to Leona Campbell for letting me cry on your shoulder, tackling any tricky questions I had and letting me know my moments of frustrations with my project were normal in a PhD candidate's life. To Majorie Linares for being my writing buddy and helping me with stuff in and outside of my PhD life. To Tien Bui for helping me locate the things I needed and with general lab housekeeping procedures. To Megan Truong for sharing your slices of fruit and helping me with the supervision of other students. To Aidan Kane for helping me with follow up experiments when I was writing. To Christine Dwyer, not just because you were an entertaining honours student when we had you, but there was this one night we were both working late in the lab and I desperately needed to talk to someone as I thought my experiment had gone wrong and I was about to cry and you just happened to be there to listen as I tried to assure myself it was going to be fine.

Thank you Igy Pang for supplying me yeast strains and putting up with me when we were analysing humongous datasets. It was a huge learning experience for both of us. Also thank you Nandan Desphande for your help in assembling fungal genome sequences.

To the teaching staff who made teaching practicals smooth and enjoyable and tea ladies who always saw me get tea just outside of tea hours. To the anchors of the store, thank you for allowing me to check out huge quantities of lab goods and not say anything when I came back the following week for the same expendables. Also a huge thanks to the workshop guys who fixed our lab equipments.

I thank my friends outside of uni who kept tabs on me to make sure I was still alive. I want to especially thank Wei for making sure I wouldn't bring my laptop to her birthday lunch otherwise she'll feed it to her dog, Malik and Anne for constantly checking I'm functioning properly and Bianca for catch up dinners over cider.

Finally I need to thank my mum and dad. You encouraged me to do a PhD and thank you for being patient with me during these years. And to my sister, I've finally finished!

Abstract

There is a growing need to improve the efficacy and range of antifungal drugs. The increase in immunocompromisation among the general population due to old age, infection with immunosuppressive diseases and immunosuppressive therapies has led to a global increase in fungal infections and invasive fungal diseases. Invasive mycoses are notoriously difficult to treat and are associated with high rates of mortality. The current suite of antifungal drugs are toxic, limited in their spectrum of activity, lacking in target selection and are becoming less effective due to antifungal resistance. For *Cryptococcus*, which causes debilitating disease and fatal meningo-encephalitis, the most effective treatment is the combined use of amphotericin B (AMB) and flucytosine (5-FC). However, the toxicity of AMB and the cost of 5-FC makes this combination difficult to implement in resource poor countries where cryptococcosis is highest due to HIV/AIDS. Even in developed countries, resolution of cryptococcosis with AMB+5-FC is difficult and mortality remains high. Alternative anti-cryptococcal therapies are therefore urgently required.

Finding and developing new drugs is an expensive and time consuming process, and synergistic therapies that augment current drugs are an alternative approach. Drug synergy enhances the activity of antifungal drugs and improves the clearance of pathogens. It requires less drug, which decreases toxicity, and also slows the development of drug resistance. Iron is important for fungal virulence and pathogenicity and iron chelating agents have been used as antifungal synergents in salvage therapy. However, the mechanistic details of how iron chelators cause synergy are unknown. Advances in genome sequencing technologies and the rise of systems biology allow the cellular responses to antifungal treatments to be studied in detail. It is hypothesised that antifungal-chelator combinations are synergistic in *Cryptococcus* and that potential antifungal targets can be found by understanding the underlying mechanisms of synergy. This thesis aims to use a transcriptomic approach to understand the mechanistic detail of synergy to find potential antifungal targets.

Chapter 3 begins with characterising the interactions of five widely used antifungal drugs (AMB, FLC, itraconazole (ITC), voriconazole (VRC) and caspofungin (CAS)) and a range of iron chelators (EDTA, lactoferrin (LF), ciclopirox olamine (CPO), deferoxamine (DFO), deferiprone (DFP) and deferasirox (DSX)). This was performed in *Cryptococcus neoformans* var. *grubii* (genotypes VNI and VNII), *Cryptococcus neoformans* var. *neoformans* (genotype VNIV) and *Cryptococcus gattii* (genotype VGII) with a focus on strains with fully sequenced genomes. The *S. cerevisiae* reference strain S288C was also included to enable a detailed downstream transcriptome analysis. Antifungal-chelator interactions were tested using the CLSI protocol for checkerboard assays. Synergy was found for AMB+LF across all of the yeast strains tested, with LF causing a four- to sixteen-fold reduction in the AMB MIC.

Supplementation with iron abolished the antifungal activity of LF but did not change the activity of AMB+LF, suggesting that the potentiation of AMB by LF was not solely due to iron chelation. Antagonism was also observed between combinations of azole antifungals and EDTA, DFP and DSX, but this was only seen in *C. neoformans* var. *grubii* strains. The results of this chapter showed that diverse responses to antifungal-chelator combinations occur in different *Cryptococcus* strains and that caution is needed when considering the use of iron chelating agents as synergists for treating cryptococcosis.

Transcriptomic analyses of AMB+LF synergy and VRC+EDTA antagonism are presented in Chapter 4. The transcriptomic response to AMB, LF and AMB+LF was first analysed in *S. cerevisiae* S288C. This provided a detailed platform of gene expression and interaction data for each treatment. Treatment with LF alone did not cause any changes in cellular functions, while AMB alone caused a shutdown of cellular growth processes, up-regulation of various stress responses and activation of the iron regulon via the iron regulating transcription factor Aft1. The addition of LF to AMB caused a down-regulation of stress responses and metal homeostasis, with stress-associated responses that are normally coordinated with zinc regulation via the transcription factor Zap1 dysregulated and the iron regulon shut down. AMB+LF also induced growth-related responses. Together, these data suggested that LF-induced drug synergy was due to disruption of the cell's ability to mount an appropriate stress response.

The mechanism of synergy differed in *C. neoformans* H99, where responses to AMB and AMB+LF were similar with an induction of stress responses and repression of cellular growth that were more pronounced in the combined treatment. This increased accumulation of stress following AMB+LF treatment, which resulted from the induction of ER stress, disruption of transmembrane transporter processes and increased metal dysregulation, likely overwhelmed the cell's capacity to cope with stress, resulting in accelerated cell death. Despite different underlying mechanisms of AMB+LF synergy in S288C and H99, the disruption of metal ion homeostasis appeared to underlie both processes. This was validated by deleting iron- (Aft1, Cir1 and HapX) and zinc- (Zap1 and Zap104) regulating transcription factors, which resulted in increased AMB susceptibility. Deletion of upstream regulators of these transcription factors and their downstream targets involved in metal homeostasis did not increase AMB susceptibility, however, which suggested that the metal-regulating transcription factors were critical for synergy. Further analysis of drug-binding domains in Zap1 (in *S. cerevisiae*) and Zap104 (in *Cryptococcus*) found these proteins to contain druggable sites, which suggested their potential as antifungal drug targets.

The mechanistic basis for antagonism was analysed by comparing the transcriptomic responses of VRC+EDTA in *C. neoformans* H99 and in *C. gattii* strain 97/170, where this combination resulted in an

antagonistic and an additive response, respectively. In both species, VRC alone induced cellular responses typical for azoles, including stress responses and mitochondrial functions related to oxidation-reduction and energy generation. The addition of EDTA disrupted mitochondrial functions and this was accompanied by different cellular responses in the two species. In *C. neoformans* H99, this involved an up-regulation of drug efflux genes, suggesting a potential mechanism of antagonism by mediating the efflux of intracellular VRC. In contrast, in *C. gattii* 97/170 the alterations to mitochondrial function were accompanied by an absence of stress responses. The different interactions between VRC+EDTA in *C. neoformans* var. *grubii* and *C. gattii* highlight species-specific responses to drug combinations that remain to be understood.

Overall, the results presented in this thesis show that metal regulation is important for resisting antifungal stress and that the dysregulation of metal ion homeostasis by some iron chelators, rather than metal chelation itself, can enhance the activity of antifungal drugs. Transcriptomic analysis of the cellular response suggests synergy may be mediated by disrupting stress responses in two ways: first, by over burdening the cell's adaptive stress response through increasing stress and cellular damage, and second, by incapacitating the stress response through the down-regulation of appropriate stress-related pathways. Disrupting metal homeostasis provides a broad spectrum of activity through different stress-disrupting mechanisms and is a potential antifungal strategy. Potential targets of this strategy were metal controlling transcription factors, especially Zap1, which contains domains that can be inhibited by small molecules.

Table of Contents

| | |
|---|-----------|
| Declaration of originality | i |
| Acknowledgements | ii |
| Abstract | iv |
| Table of Contents | vii |
| List of Figures..... | xv |
| List of Tables..... | xvii |
| List of Abbreviations..... | xix |
| | |
| CHAPTER 1: Introduction | 1 |
| 1.1. <i>Cryptococcus</i> | 2 |
| 1.1.1. <i>Cryptococcus neoformans</i> | 4 |
| 1.1.2. <i>Cryptococcus gattii</i> | 4 |
| 1.2. Cryptococcosis..... | 6 |
| 1.3. Treatment..... | 6 |
| 1.3.1. Antifungal drug classes and cryptococcosis | 6 |
| 1.3.2. Cryptococcosis management guidelines and problems with treatment | 8 |
| 1.3.3. Alternative antifungal and synergistic combination therapies for cryptococcosis | 8 |
| 1.4. Iron and its importance in biological systems..... | 11 |
| 1.4.2. Iron regulation in <i>Saccharomyces cerevisiae</i> | 11 |
| 1.4.3. Iron regulation in <i>Cryptococcus</i> | 13 |
| 1.4.4. Iron and virulence in <i>Cryptococcus</i> | 15 |
| 1.5. Systems biology..... | 15 |
| 1.5.1. Systems biology – a ‘holistic’ approach to understanding how cells respond to change | 15 |
| 1.5.2. Transcriptomics and RNA-Seq | 16 |
| 1.6. Hypotheses and aims of this thesis | 17 |
| | |
| CHAPTER 2: General materials and methods | 19 |
| 2.1. General materials | 20 |

| | |
|--|-----------|
| 2.1.1. Chemicals..... | 20 |
| 2.1.2. Buffers and solutions..... | 21 |
| 2.1.3. Media..... | 22 |
| 2.1.4. Equipment | 22 |
| 2.1.5. Kits | 23 |
| 2.1.6. Yeast strains | 23 |
| 2.2. General methods..... | 24 |
| 2.2.1. Growth..... | 24 |
| 2.2.2. Glycerol stock storage | 24 |
| 2.2.3. Preparation of drug stocks | 24 |
| CHAPTER 3: Drug combination screening – assessing interactions between antifungal drugs and iron chelating agents | 25 |
| 3.1 Introduction..... | 26 |
| 3.1.1. Combination therapy in fungal diseases | 26 |
| 3.1.2. Drug interactions and their assessment..... | 26 |
| 3.1.2.1. Loewe’s additivity..... | 27 |
| 3.1.2.2. Bliss independence..... | 28 |
| 3.1.2. Current antifungal agents and cryptococcosis..... | 29 |
| 3.1.2.1. Amphotericin B (AMB) | 29 |
| 3.1.2.2. 5-Flucytosine (5-FC)..... | 29 |
| 3.1.2.3. Triazoles..... | 30 |
| 3.1.2.4. Caspofungin (CAS) | 31 |
| 3.1.3. Iron chelating agents | 33 |
| 3.1.3.1. Ethylenediaminetetraacetic acid (EDTA)..... | 33 |
| 3.1.3.2. Lactoferrin (LF) | 34 |
| 3.1.3.3. Ciclopirox Olamine (CPO) | 34 |
| 3.1.3.4. Deferoxamine (DFO)..... | 35 |
| 3.1.3.5. Deferiprone (DFP)..... | 35 |

| | |
|--|-----------|
| 3.1.3.6. Deferasirox (DSX)..... | 36 |
| 3.1.4. Aims and hypotheses of this chapter | 37 |
| 3.2. Materials and Methods | 40 |
| 3.2.1. Strains and growth media | 40 |
| 3.2.2. Iron chelating agents and antifungal drugs..... | 40 |
| 3.2.3. Minimum inhibitory concentration (MIC) testing by microdilution assay | 40 |
| 3.2.4. Synergy testing by checkerboard assay..... | 41 |
| 3.2.5. Assessment of interactions by fractional inhibitory concentration index (FICI) and MacSynergy™ II | 41 |
| 3.2.6. Iron rescue assays..... | 42 |
| 3.3. Results | 43 |
| 3.3.1. MICs of antifungal drugs and iron chelating agents..... | 43 |
| 3.3.2. Assessment of drug-chelator interactions by FICI..... | 43 |
| 3.3.3. MacSynergy™ II drug response curves..... | 45 |
| 3.3.4. Fold-change in MIC for antifungals and iron chelators in combination..... | 45 |
| 3.3.5. Iron supplementation rescues AMB+LF synergy..... | 47 |
| 3.4. Discussion..... | 49 |
| 3.4.1. LF+AMB produces potent synergism that is independent of the chelation of iron..... | 49 |
| 3.4.2. Iron chelation does not consistently produce a synergistic response with antifungal agents in <i>Cryptococcus</i> | 50 |
| 3.4.3. Species-specific antagonism is produced by some antifungal-chelator combinations..... | 51 |
| 3.4.4. Conclusions..... | 52 |
| CHAPTER 4: Transcriptomic analyses of synergy and antagonism between antifungal drugs and iron chelating agents | 53 |
| 4.1. Introduction..... | 54 |
| 4.1.1. The search for antifungal synergents and problems harnessing information for improved therapies..... | 54 |
| 4.1.2. Systems biology tools and resources | 56 |
| 4.1.3.1. Gene ontology terms..... | 56 |

| | |
|---|----|
| 4.1.3.2. Self organising maps..... | 56 |
| 4.1.3.3. Cytoscape | 57 |
| 4.1.3.4. <i>S. cerevisiae</i> as a model organism and reference genome strain S288C | 57 |
| 4.1.3. The <i>C. neoformans</i> var. <i>grubii</i> reference strain H99 and systems biology resources | 58 |
| 4.1.4. Aims and hypothesis | 59 |
| 4.2. Methods and materials | 62 |
| 4.2.1. Preparation of chemical agents and stock concentrations | 62 |
| 4.2.1.1. Stock concentration of stressing agents | 62 |
| 4.2.1.2. Stock preparations of rescue agents | 62 |
| 4.2.1.3. Preparation of chemicals and reagents for transformation..... | 62 |
| 4.2.1.4. Genomic DNA extraction..... | 62 |
| 4.2.2. Illumina sequencing and <i>de novo</i> assembly of the <i>C. gattii</i> strain 97/170 genome | 63 |
| 4.2.3. Transcriptome analysis..... | 64 |
| 4.2.3.1. Characterising the effect of the AMB+LF combination in <i>S. cerevisiae</i> S288C and <i>C. neoformans</i> H99 for RNA isolation..... | 64 |
| 4.2.3.2. Sample preparation for RNA isolation in AMB+LF synergy experiments..... | 65 |
| 4.2.3.3. Characterising the effect of VRC+EDTA in <i>C. neoformans</i> H99 and <i>C. gattii</i> 97/170 and sample preparation for RNA isolation | 66 |
| 4.2.3.4. RNA extraction from <i>S. cerevisiae</i> S288C and <i>C. neoformans</i> H99 | 67 |
| 4.2.4. Illumina RNA-Seq and data processing | 68 |
| 4.2.4.1. RNA-Seq library preparation and sequencing..... | 68 |
| 4.2.4.2. Processing of RNA-Seq data | 70 |
| 4.2.4.3. Generating differentially expressed transcripts from the effects of synergistic and antagonistic drug treatments..... | 71 |
| 4.2.4.4. Self-organising maps (SOMs)..... | 71 |
| 4.2.4.5. Gene ontology (GO) enrichment analysis | 72 |
| 4.2.4.6. Analysis of biological networks | 74 |
| 4.2.5. Validation of transcriptomic data in <i>S. cerevisiae</i> | 74 |
| 4.2.5.1. PCR confirmation of knock-out mutants..... | 74 |

| | |
|--|-----|
| 4.2.5.2. Knock-out cassette construction..... | 75 |
| 4.2.5.3. Transformation of <i>S. cerevisiae</i> with knock-out constructs..... | 77 |
| 4.2.6. Spot plate assays | 77 |
| 4.2.7. Rescue assays | 78 |
| 4.3. Results | 79 |
| 4.3.1 Effect of AMB, LF and AMB+LF on the growth of <i>S. cerevisiae</i> S288C and <i>C. neoformans</i> H99 | 79 |
| 4.3.2. Analysis of RNA-Seq data | 81 |
| 4.3.2.1. Data quality control for RNA-Seq analysis..... | 81 |
| 4.3.2.2. Comparison of differentially expressed genes in <i>S. cerevisiae</i> S288C and <i>C. neoformans</i> H99 | 84 |
| 4.4. Results – Analysis of the transcriptome of drug synergy in <i>S. cerevisiae</i> S288C..... | 87 |
| 4.4.1. GO enrichments of differentially expressed S288C genes in T _A and T _{AL} | 87 |
| 4.4.2. SOMs analyses of T _A and T _{AL} in <i>S. cerevisiae</i> S288C..... | 91 |
| 4.4.2.1. Metal ion transport and homeostasis are enriched but oppositely regulated in T _A and T _{AL} | 93 |
| 4.4.2.2. Addition of LF causes changes to the regulation of cellular stress responses..... | 97 |
| 4.4.2.3. Protein degradation is regulated differently in T _A and T _{AL} | 100 |
| 4.4.3. Network analysis reveals metal ion regulation differs in T _A and T _{AL} | 101 |
| 4.4.4. Biological validation of transcriptome analysis..... | 105 |
| 4.4.4.1. Rescue assays | 105 |
| 4.4.4.2. Validation of selected target genes using spot plate assays of gene knock-out mutants | 109 |
| 4.4.4.3. Testing downstream binding targets of Aft1 and Zap1 as possible drug targets..... | 118 |
| 4.5. Discussion – AMB+LF synergy in <i>S. cerevisiae</i> S288C..... | 120 |
| 4.5.1. Exploring the molecular mechanisms of synergy between antifungals and iron chelators for novel antifungal therapies..... | 120 |
| 4.5.2. The addition of LF to AMB caused unexpected changes in the transcriptomic response by <i>S. cerevisiae</i> that appear contrary to enhanced growth inhibition | 120 |

| | |
|--|-----|
| 4.5.2.1. The presence of LF down-regulated stress-associated responses that were induced by AMB | 121 |
| 4.5.2.2. The addition of LF decreased the need for trace metals that was required with AMB treatment | 122 |
| 4.5.3. Appropriate regulation of stress responses is required for survival against combinatorial stresses | 125 |
| 4.5.3.1. Dysregulation of stress responses in AMB+LF synergy is associated with metal ion homeostasis..... | 126 |
| 4.5.4. LF enhances disruption in membrane-mediated trafficking that is associated with AMB treatment | 128 |
| 4.6. Results – Analysis of AMB+LF synergy in <i>C. neoformans</i> H99..... | 129 |
| 4.6.1. GO enrichments of differentially expressed H99 genes in T _A and T _{AL} | 129 |
| 4.6.2. SOMs enrichment analyses of <i>C. neoformans</i> H99 transcripts in T _A and T _{AL} | 131 |
| 4.6.2.1. Metal homeostasis is affected in AMB and AMB+LF drug treatments | 133 |
| 4.6.2.2. Co-expression of stress and ER-related enrichments suggests that ER stress is repressed in T _A and induced in T _{AL} | 139 |
| 4.6.2.3. Repression of protein sorting and lipid biosynthesis in T _A and T _{AL} suggests disruptions in ER functions such as transport protein synthesis | 140 |
| 4.6.2.4. Enrichments related to vesicle-mediated transport are induced in T _{AL} | 140 |
| 4.6.2.5. Addition of LF to AMB treatment may repress cellular processes regulated by the activity of kinases | 141 |
| 4.6.3. Comparison of the response to AMB and AMB+LF treatment by <i>S. cerevisiae</i> S288C and <i>C. neoformans</i> H99 | 145 |
| 4.6.4. Dysregulation of metal homeostasis increases susceptibility to stress and antifungal drugs in <i>C. neoformans</i> H99 | 147 |
| 4.7. Discussion –AMB+LF synergy in <i>C. neoformans</i> H99..... | 150 |
| 4.7.1. Transcriptomic analysis of synergy in <i>C. neoformans</i> H99 revealed a completely different response to AMB+LF compared to <i>S. cerevisiae</i> S288C | 150 |
| 4.7.2. Up-regulation of antioxidant genes may lower the overall stress response to AMB in <i>C. neoformans</i> H99 | 152 |
| 4.7.3. Disruption to transmembrane transport synthesis may be associated with ER stress and enhanced growth inhibition in AMB+LF synergy | 152 |

| | |
|--|------------|
| 4.7.4. Increased dysregulation of metal homeostasis in AMB+LF synergy may be mediated by destabilisation of Fe-S clusters and contribute to cell stress..... | 154 |
| 4.7.5. Avenues for future work | 155 |
| 4.8. Results – Analysis of VRC+EDTA antagonism and additivity in <i>C. neoformans</i> H99 and <i>C. gattii</i> 97/170 | 157 |
| 4.8.1. Effect of VRC and VRC+EDTA on the growth of <i>C. neoformans</i> H99 and <i>C. gattii</i> 97/170... .. | 157 |
| 4.8.2. Analysis of RNA-Seq data from VRC and VRC+EDTA treatments | 158 |
| 4.8.2.1. RNA-Seq data quality..... | 158 |
| 4.8.3. Analysis of gene expression in <i>C. neoformans</i> H99 and <i>C. gattii</i> 97/170 in response to VRC and VRC+EDTA..... | 160 |
| 4.8.3.1. Analysis of orthology between genes expressed in <i>C. neoformans</i> H99 and <i>C. gattii</i> 97/170 | 160 |
| 4.8.3.2. Analysis of differentially expressed genes in response to drug treatments | 161 |
| 4.8.4. GO term enrichments for <i>C. neoformans</i> H99 and <i>C. gattii</i> 97/170 in T _V and T _{VE} | 164 |
| 4.8.4.1. GO term analysis of total differentially expressed genes to assess the individual responses by H99 and 97/170 to treatment | 164 |
| 4.8.4.2. GO analysis of differentially expressed orthologous genes to compare the antagonistic (H99) versus additive (97/170) interaction of VRC+EDTA..... | 166 |
| 4.9. Discussion – VRC+EDTA antagonism and additivity in <i>C. neoformans</i> H99 and <i>C. gattii</i> 97/170..... | 171 |
| 4.9.1. Up-regulation of efflux pumps as a mechanism of VRC+EDTA antagonism in <i>C. neoformans</i> H99 | 172 |
| 4.9.2. EDTA may potentiate VRC activity in <i>C. gattii</i> 97/170 by alterations to the stress response | 174 |
| 4.9.3. Species-specific responses to drugs and to drug combinations..... | 176 |
| 4.9.4. Future avenues for understanding the mechanisms of azole-chelator interactions..... | 178 |
| 4.10. Additional observations in the transcriptomes of drug synergy and antagonism | 179 |
| 4.10.1. Differences in RNA-Seq data between synergy and antagonism experiments reflect the different cellular effects of polyenes and azoles | 179 |
| 4.10.2. Problems and limitations in transcriptome analyses of drug synergy and antagonism | 180 |
| CHAPTER 5: Final discussion and conclusions..... | 181 |
| 5.1. The value of holistic analysis | 182 |

| | |
|--|------------|
| 5.2. Disruption of stress-related responses as an antifungal strategy..... | 183 |
| 5.3. The potential of metal homeostasis as an antifungal target | 184 |
| 5.4. Potential of Zap1 and Zap104 transcription factors as antifungal drug targets | 185 |
| 5.5. Iron chelators as therapeutic agents for antifungal treatment | 186 |
| 5.6. Diversity of fungal responses to drug treatment and implications for studying drug responses in model organisms | 187 |
| 5.7. Implications of drug antagonism for antifungal therapy | 188 |
| 5.8. Conclusions..... | 189 |
| APPENDICES..... | 191 |
| Chapter 3 Appendix..... | 192 |
| Appendix 3.1. MIC of antifungal drugs (A) and iron chelators (IC) alone and in combination (µg/mL), with fold changes (FC) | 192 |
| Chapter 4 Appendix..... | 194 |
| Appendix 4.1. <i>S. cerevisiae</i> S288C, <i>C. neoformans</i> H99 and <i>C. gattii</i> 97/170 RNA samples..... | 194 |
| Appendix 4.2. List of primers designed in this study that were used to construct and confirm knock-out mutants in <i>S. cerevisiae</i> S288C..... | 195 |
| Appendix 4.3. BCV of LF only transcripts..... | 196 |
| Appendix 4.4. BCV of <i>C. neoformans</i> H99 transcripts in AMB+LF synergy..... | 196 |
| Appendix 4.5. Plasmid cassette construct for <i>YOR387C</i> deletion | 197 |
| Appendix 4.6. Expected amplification band sizes (base pairs) of gene knock-out confirmation primer sets in <i>S. cerevisiae</i> BY4741 | 197 |
| Appendix 4.7. PCR confirmations of gene knock-outs in <i>S. cerevisiae</i> BY4741 | 198 |
| Appendix 4.8. BCV of <i>C. neoformans</i> H99 transcripts in VRC+EDTA antagonism..... | 200 |
| REFERENCES..... | 201 |

List of Figures

| | |
|---|-----|
| Figure 1.1. The <i>Cryptococcus</i> species complex. | 3 |
| Figure 1.2. Global distributions of environmental and clinical <i>C. neoformans</i> and <i>C. gattii</i> serotypes. ... | 5 |
| Figure 1.3. Environmental sources of <i>Cryptococcus</i> and the process of infection from the lungs to the brain. | 7 |
| Figure 1.4. Targets of antifungal therapy..... | 7 |
| Figure 1.5. Regulation of the iron regulon in <i>S. cerevisiae</i> | 13 |
| Figure 1.6. Iron regulation in <i>Cryptococcus</i> | 14 |
| Figure 3.1. Representative patterns of types of drug interactions in a checkerboard assay | 27 |
| Figure 3.2. Chemical structures of AMB, FLC, CAS, ITC and VRC | 32 |
| Figure 3.3. Interactions between antifungal drugs and iron chelators | 46 |
| Figure 3.4. Iron rescue assays indicate synergy is not principally due to iron chelation in <i>S. cerevisiae</i> S288C and <i>C. neoformans</i> H99 | 48 |
| Figure 4.1. An overview of RNA-Seq library preparation and sequencing | 69 |
| Figure 4.2. Primers designed to confirm gene deletions | 76 |
| Figure 4.3. Primer design for cassette construction and gene deletion..... | 76 |
| Figure 4.4. The effect of AMB+LF, AMB, and LF on the growth of <i>S. cerevisiae</i> S288C and <i>C. neoformans</i> H99 | 80 |
| Figure 4.5. RNA-Seq analyses of <i>S. cerevisiae</i> S288C samples..... | 82 |
| Figure 4.6. RNA-Seq analysis of LF treatment only..... | 83 |
| Figure 4.7. RNA-Seq analyses of <i>C. neoformans</i> H99 samples..... | 85 |
| Figure 4.8. Independent SOMs of differentially expressed genes in <i>S. cerevisiae</i> S288C (a) T _A and (b) T _{AL} , and the heat maps of averaged gene expressions of each SOMs cluster for (c) T _A and (d) T _{AL} | 92 |
| Figure 4.9. SOMs of interest and their enriched GO terms in <i>S. cerevisiae</i> S288C T _A (a) and T _{AL} (b) | 96 |
| Figure 4.10. Mapping of sulphur metabolism pathways suggests in AMB+LF synergy there is a shutdown of homocysteine production by alterations in sulphur assimilation, threonine biosynthesis and glutathione biosynthesis pathways..... | 99 |
| Figure 4.11. Regulatory networks of the transcription factors Aft1 and its gene targets in (a) T _A and (b) T _{AL} , and Zap1 and its gene targets in (c) T _A and (d) T _{AL} | 105 |

| | |
|---|-----|
| Figure 4.12. <i>Saccharomyces</i> rescue assays in RPMI-1640 medium supplemented with (a) Iron (III) (b) Iron (II) (c) Zinc (d) Calcium and (e) BAPTA | 109 |
| Figure 4.13. Spot plate assays of knock-out mutants | 117 |
| Figure 4.14. Knock-out mutants of ‘druggable’ targets tested on various stressors..... | 119 |
| Figure 4.15. Model of the transcriptome response to AMB+LF synergy in <i>S. cerevisiae</i> S288C..... | 124 |
| Figure 4.16. Independent SOMs of <i>C. neoformans</i> H99 genes differentially expressed in (a) T _A and (b) T _{AL} , and the heat maps of average gene expressions of each SOMs cluster for (c) T _A and (d) T _{AL} | 132 |
| Figure 4.17. SOMs of interest and their enriched GO terms in <i>C. neoformans</i> H99..... | 145 |
| Figure 4.18. A model of the transcriptome response to AMB+LF synergy in <i>C. neoformans</i> H99. | 151 |
| Figure 4.19. The effect of VRC and VRC+EDTA on the growth of <i>C. gattii</i> 97/170 and <i>C. neoformans</i> H99. | 157 |
| Figure 4.20. Quality analysis of RNA-Seq data from drug antagonism experiments in <i>C. neoformans</i> H99 (a) – (d) and <i>C. gattii</i> 97/170 (e) – (h) | 160 |
| Figure 4.21. Venn diagram of differentially genes in <i>C. neoformans</i> H99 and <i>C. gattii</i> 97/170 divided according to whether or not orthologues were identified in one or both strains..... | 162 |
| Figure 4.22. Comparison of the direction of expression of orthologous genes (B in Fig. 4.21) in <i>C. neoformans</i> H99 and <i>C. gattii</i> 97/170 following (a) VRC treatment and (b) VRC+EDTA treatment..... | 163 |

List of Tables

| | |
|---|-----|
| Table 2.1. Chemicals list..... | 20 |
| Table 2.2. Buffers and solutions..... | 21 |
| Table 2.3. Media used..... | 22 |
| Table 2.4. List of equipment and software | 22 |
| Table 2.5. Kits used | 23 |
| Table 2.6. Yeast strains used..... | 23 |
| Table 3.1. Structure, function, clinical use and reported antifungal activity of the iron chelating agents used in this study..... | 38 |
| Table 3.2. MIC values for antifungal drugs and iron chelating agents..... | 44 |
| Table 4.1. Percent reduction in growth relative to untreated controls at selected timepoints for AMB and AMB+LF treatment in <i>S. cerevisiae</i> S288C and <i>C. neoformans</i> H99..... | 80 |
| Table 4.2. Comparison of gene counts when <i>S. cerevisiae</i> S288C RNA samples 1B and 8A were swapped, not swapped or deleted..... | 83 |
| Table 4.3. <i>C. neoformans</i> H99 gene count comparison with and without RNA sample 5A..... | 86 |
| Table 4.4. Comparison of differentially expressed genes in <i>S. cerevisiae</i> S288C and <i>C. neoformans</i> H99 in response to the two drug treatments | 86 |
| Table 4.5. Selected gene ontology term enrichments of differentially expressed transcripts in <i>S. cerevisiae</i> S288C for T _A and T _{AL} | 88 |
| Table 4.6. Agents used for rescue assays in <i>S. cerevisiae</i> S288C | 106 |
| Table 4.7. Candidate genes for knock-out mutant generation and their selection criteria | 114 |
| Table 4.8. Major GO enrichments in T _A and T _{AL} for <i>C. neoformans</i> H99 and <i>S. cerevisiae</i> S288C | 129 |
| Table 4.9. Iron-, copper- and zinc-related transcripts identified in SOMs analysis of <i>C. neoformans</i> H99 in T _A and T _{AL} | 135 |
| Table 4.10. Phenotypes of <i>C. neoformans</i> mutants with disrupted iron, copper and zinc transcription factors that were differentially expressed in T _A and T _{AL} | 149 |
| Table 4.11. <i>C. neoformans</i> H99 gene count comparison with and without RNA sample 7J..... | 158 |
| Table 4.12. Number of genes differentially expressed in <i>C. neoformans</i> H99 and <i>C. gattii</i> 97/170 in each drug treatment compared to untreated controls | 163 |
| Table 4.13. Orthologous genes in <i>C. neoformans</i> H99 and <i>C. gattii</i> 97/170 with opposing directions of expression | 164 |

Table 4.14. Selected GO term enrichments for all differentially expressed transcripts in *C. neoformans* H99 and *C. gattii* 97/170 in T_V and T_{VE}..... 168

Table 4.15. Selected GO term enrichments for transcripts of orthologous genes in *C. neoformans* H99 and *C. gattii* 97/170 in T_V and T_{VE}..... 169

List of Abbreviations

A list of abbreviations used in this thesis is presented below.

| Abbreviation | Chemicals |
|-------------------------------|--|
| BAPTA | 1,2-Bis(2-Aminophenoxy)ethane-N,N,N',N'-tetraacetic acid |
| β-ME | β-Mecaptoethanol |
| CW | Blankaphor (Calcafluor white) |
| DMSO | Dimethyl sulfoxide |
| dNTPs | Deoxyribonucleotide |
| SS-DNA | Deoxyribonucleic acid sodium salt from salmon testes |
| H ₂ O ₂ | Hydrogen peroxide |
| EDTA | Ethylenediaminetetraacetic acid |
| MOPS | 4-Morpholinepropanesulfonic acid |
| NaCl | Sodium chloride |
| NaNO ₂ | Sodium nitrite |
| PEG | Polyethylene glycol |
| SDS | Sodium dodecyl sulphate |

| Abbreviation | Media |
|---------------------|---|
| RPMI-1640 | Roswell Park Memorial Institute media |
| SC | Synthetic complete |
| SDA | Sabouraud dextrose agar |
| SD-ura | Synthetic defined media - uracil drop out |
| YNB | Yeast nitrogen base |

| Abbreviation | Antifungal susceptibility |
|---------------------|---|
| AMB | Amphotericin B |
| CAS | Caspofungin |
| CPO | Ciclopirox olamine |
| DSX | Deferasirox |
| DFP | Deferiprone |
| DFO | Deferoxamine |
| EDTA | Ethylenediaminetetraacetic acid |
| FLC | Fluconazole |
| 5-FC | Flucytosine |
| FIC | Fractional inhibitory concentration |
| FICI | Fractional inhibitory concentration index |
| ITC | Itraconazole |
| LF | Lactoferrin |
| MIC | Minimum inhibitory concentration |
| VRC | Voriconazole |

| Abbreviation | Unit |
|---------------------|---------------------------|
| °C | Degrees Celsius |
| <i>g</i> | G-force |
| hr | Hours |
| µg/mL | Micrograms per millilitre |
| min | Minutes |
| rpm | Revolutions per minute |
| sec | Seconds |

| Abbreviation | Other |
|---------------------|--|
| T _A | Transcripts differentially expressed in AMB treatment |
| T _{AL} | Transcripts differentially expressed in AMB+LF treatment |
| T _V | Transcripts differentially expressed in VRC treatment |
| T _{VE} | Transcripts differentially expressed in VRC+EDTA treatment |

CHAPTER 1: Introduction

There is an urgent need to increase our options for treating fungal diseases. Globally, fungal infections, including invasive fungal diseases, are on the rise and are associated with changes to the host through immunosuppressive diseases such as HIV/AIDS, the increasing use of immunosuppressive therapies, the ageing population, and changes to the environment with global climate change and the increased occurrence of natural disasters changing our exposure to infective agents [1, 2]. Fungal infections are difficult to treat, and even with best current practice the mortality rates from invasive fungal diseases can be as high as 90% [3].

Finding and developing new antifungal drugs incurs significant cost and time expenditures. An alternative approach that has gained increased interest is to enhance the activity of current antifungal drugs by combining them with agents that can synergise their activity. Synergistic drug combinations have improved survival outcomes in *in vivo* models of invasive fungal diseases [4, 5], suggesting they can be employed in human infections. However, despite their promise few studies have analysed the mechanisms underlying drug synergy [6, 7] and none have been done with the aim of harnessing this knowledge to find potential targets for antifungal drugs.

This thesis focuses on understanding the mechanisms of drug synergy between antifungal drugs and iron chelating agents. Iron chelators were chosen as iron has a known role in fungal virulence and pathogenicity [8], and chelators have demonstrated synergising activity with antifungal drugs in pathogenic yeast and fungi [9, 10]. *Cryptococcus* was chosen as the study organism, as it is a major fungal pathogen and is also the focus of our laboratory; *Saccharomyces* was included as a model yeast, as it has the most curated, annotated and functionally characterised genome, along with a suite of useful resources including detailed protein interaction data and knock-out libraries. Drug-chelator interactions were explored using RNA-Seq-based transcriptomics. The outcome is a detailed picture of the surprisingly diverse cellular and molecular responses to synergy, additivity and antagonism by fungal cells.

1.1. *Cryptococcus*

Cryptococcus is a basidiomycetous yeast genus that encompasses over 37 different species, of which two are encapsulated and pathogenic in mammals. *Cryptococcus neoformans* (which includes varieties *neoformans* and *grubii*) and *Cryptococcus gattii* (formerly known as *C. neoformans* var. *gattii*) are the etiological agents of cryptococcosis, a disease that affects the immunosuppressed and immunocompetent, and is potentially fatal if presented in the meninges [11]. A new nomenclature for *Cryptococcus* was recently described by Hagen *et al.* (2015) which divides the two pathogens into seven species based on phylogenetic analysis [12]. However, as extensive genotypic and phenotypic

comparisons between these have not yet been undertaken and they can only be reliably separated using molecular techniques, this thesis will retain the established classification system of two species with different molecular genotypes.

The two pathogenic *Cryptococcus* species are further classified into nine major molecular genotypes and five serotypes based on a variety of molecular analyses and the antigenic reactivity of their capsules, respectively. *C. neoformans* var. *grubii* includes genotypes VNI, VNII and VNB, which are all serotype A. *C. neoformans* var. *neoformans* is genotype VNIV and serotype D, and a hybrid between the two varieties of *C. neoformans* is serotype AD and genotype VNIII. *C. gattii* includes serotypes B and C and genotypes VGI to VGIV (Fig. 1.1) [13, 14]. Interspecies hybrids between *C. neoformans* and *C. gattii* have also been identified [15-17].

C. neoformans and *C. gattii* are distinctly different in their natural habitat, epidemiology, genome sequence, phenotype, clinical presentation and response to antifungal treatment [18, 19]. Additionally, differences in pathogenicity and antifungal response have been observed among the genotypes of each species [20-22].

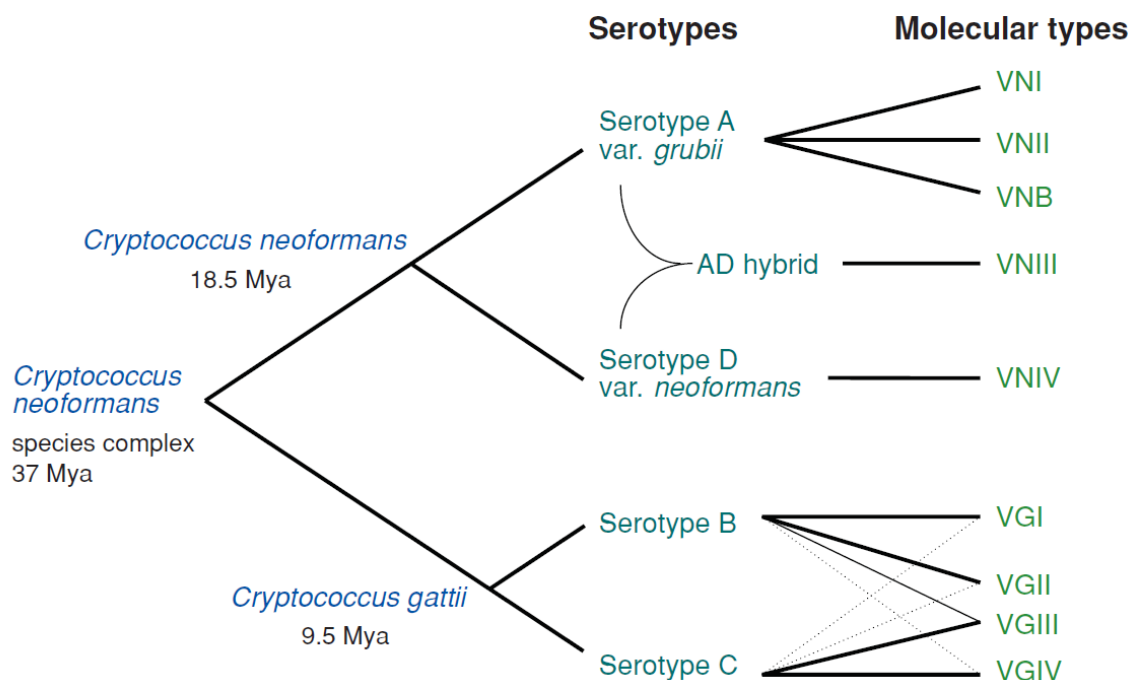


Figure 1.1. The *Cryptococcus* species complex. *C. neoformans* and *C. gattii* are shown with their respective molecular genotypes and serotypes. Bolded lines linking serotype B and C to molecular types indicate the predominant genotypes associated with each serotype. Mya is millions of years ago. From Lin and Heitman (2006) [13].

1.1.1. *Cryptococcus neoformans*

C. neoformans is a cosmopolitan and opportunistic pathogen that can be isolated from soil and trees, but more commonly obtained from pigeon guano [23]. Before the 1980s, instances of cryptococcosis were limited to patients receiving immunosuppressive therapy [24]. It was not until the HIV/AIDS epidemic, where a significant number of the infected population presented with cryptococcosis, that *C. neoformans* became an AIDS-defining illness and an important pathogen [14].

C. neoformans var. *grubii* causes the majority of cryptococcal infections in the HIV/AIDS community and is globally distributed. Within *C. neoformans* var. *grubii*, the VNI genotype is the most commonly isolated, followed by VNII. Small VNB populations, which were thought to be restricted to Southern Africa, have been found recently in different continents [22]. *C. neoformans* var. *neoformans* (VNIV) and the AD serotype hybrid (VNIII) are prevalent in Western Europe and South America [22, 25] (Fig. 1.2).

Since the introduction of highly active antiretroviral therapy (HAART) cryptococcal meningitis caused by *C. neoformans* has decreased substantially in developed countries, but it still remains a common cause of mortality in resource-limited countries like sub-Saharan African and Southeast Asia [14, 26]. In 2009 the Centers for Disease Control and Prevention (CDC) estimated there were one million cases of cryptococcal meningitis per year amongst individuals with HIV/AIDS worldwide, causing nearly 625,000 deaths [26]. This has substantially decreased with the greater use of antiretroviral therapy in Africa, however attributed mortality still remains high [27].

1.1.2. *Cryptococcus gattii*

Unlike *C. neoformans*, *C. gattii* is predominantly a primary pathogen with infection endemic in parts of Australia, Papua New Guinea and Africa [18, 28]. *C. gattii* can be biochemically distinguished from *C. neoformans* by growth on L-canavanine glycine bromothymol blue medium, which tests for the assimilation of glycine as a carbon source and in *C. gattii* strains turns the indicator in the medium blue [29]. *C. gattii* is generally less susceptible and more heteroresistant to azole antifungals than *C. neoformans* [30-32].

C. gattii was first isolated from *Eucalyptus* trees by Ellis and Pfeifer in 1990 [33], and since then it has been isolated from more than 50 species of trees including *Ficus* and *Terminalia*, suggesting trees and decaying wood are its ecological niche [34]. It was formerly thought to be restricted to tropical and sub-tropical areas, however, an outbreak of *C. gattii* cryptococcosis in the temperate region of British Columbia Vancouver Island (Canada) was recognised in 1999. This outbreak remains ongoing and has extended to the Pacific Northwest of the United States [35-37]. A growing number of isolations from

temperate regions of Asia and Europe suggests this species may have a more global distribution than was previously thought [34].

Each *C. gattii* genotype differs in distribution. VGI is the most prevalent genotype in Australia and Papua New Guinea [22], while large VGII populations are found in North and South America (Brazil, Columbia and Puerto Rico) and in some parts of Australia [22, 28]. VGIII is mainly detected in Central America and Southern California and has been isolated from HIV-infected patients [22, 28] while VGIV is most prevalent in South Africa and is identified in association with HIV/AIDS [28] (Fig. 1.2).

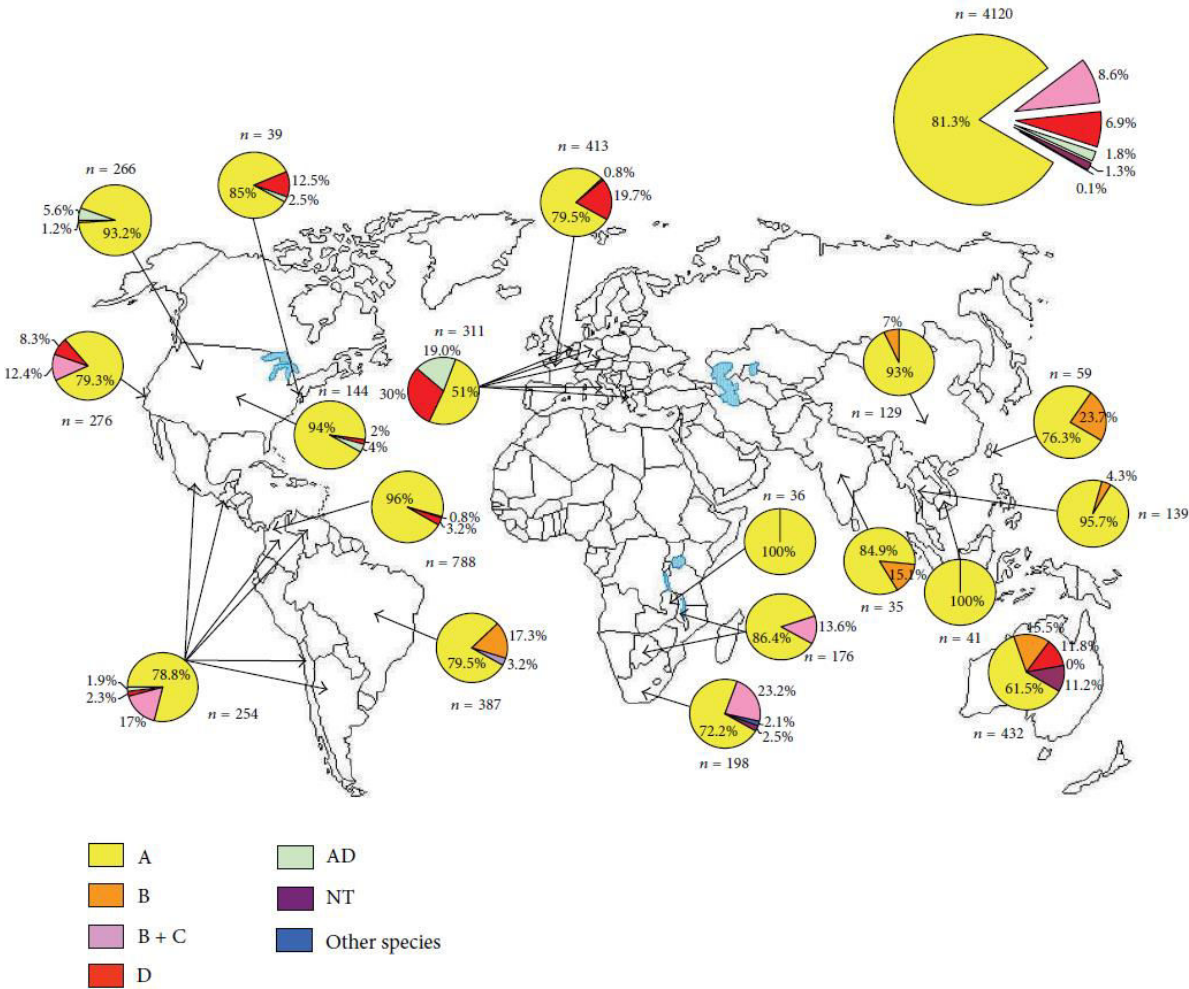


Figure 1.2. Global distributions of environmental and clinical *C. neoformans* and *C. gattii* serotypes. Percentages are compiled from individual studies, reviewed by Antonio *et al.* (2013) [25].

1.2. Cryptococcosis

Cryptococcal infection starts with the inhalation of the pathogen as desiccated yeast cells or spores from the environment. Initial infection in the lungs is typically asymptomatic and, with a normal immune response, can be either cleared or contained as a dormant latent infection. When a decline in the host's immunity occurs, the pathogen reactivates and can disseminate hematogenously with predilection for the brain, where the most common clinical manifestation of human cryptococcosis is meningoencephalitis [13] (Fig. 1.3).

During meningeal involvement, symptoms of cryptococcosis can range from headache, fever, dyspnea, neck stiffness to altered mental status and seizures. While most attention has been focused on cryptococcal meningitis because it is life threatening, cryptococcosis can also affect other organs of the body, including the eyes, skin, prostate, bones and the urinary tract [14].

The clinical presentation of cryptococcosis differs between *C. neoformans* and *C. gattii*. While *C. neoformans* infection is associated with presentation in the central nervous system as meningitis or meningoencephalitis, *C. gattii* infections are more aggressive and frequently present in the lungs and brain as cryptococcomas, which in the latter case is associated with neurological sequelae and prolonged antifungal therapy [23, 28]. AIDS patients undergoing HAART can also develop cryptococcal immune reconstitution inflammatory syndrome (IRIS), which is the over-reaction of an improved immune response to an underlying cryptococcus infection that results in clinical deterioration [38].

1.3. Treatment

1.3.1. Antifungal drug classes and cryptococcosis

Although five classes of antifungal drugs are available for the treatment of mycotic infections, only three can be used to treat cryptococcosis. The classes of drugs that are effective include the polyenes and triazoles, which target the cell membrane, and nucleic acid and/or protein synthesis inhibitors (Fig. 1.4). Examples of drugs within these classes are amphotericin B (AMB), fluconazole (FLC) and 5-fluorocytosine (5-FC). Selected antifungal drugs and their modes of action will be discussed in more detail in Chapter 3.

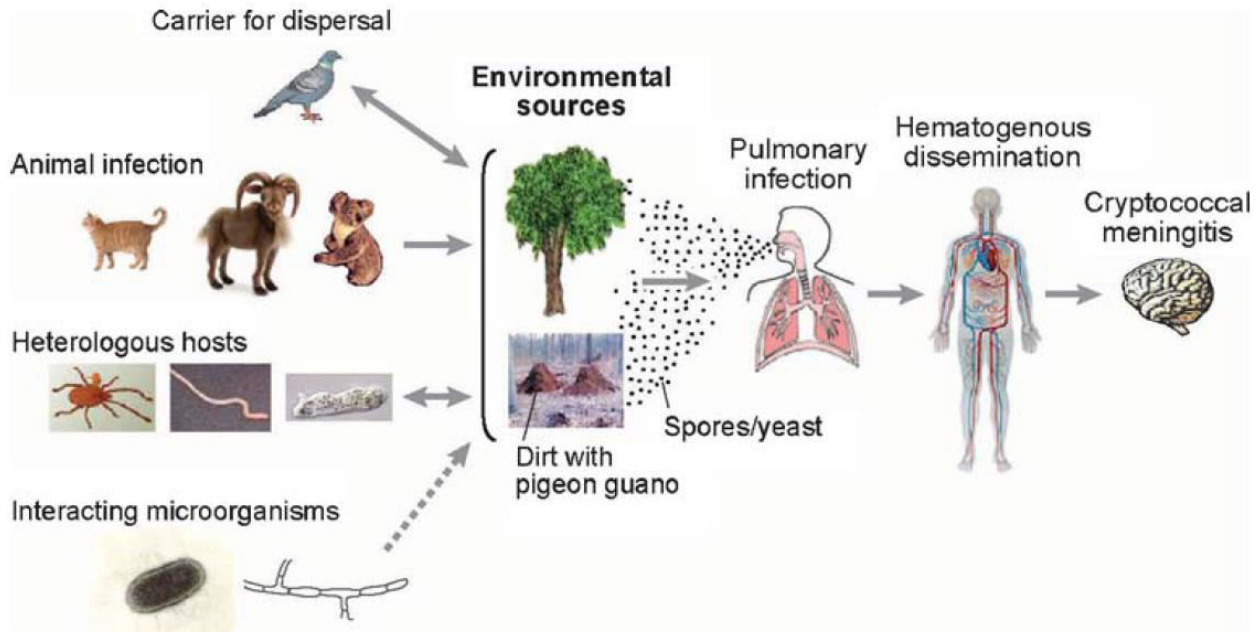


Figure 1.3. Environmental sources of *Cryptococcus* and the process of infection from the lungs to the brain. From Lin and Heitman (2006) [13].

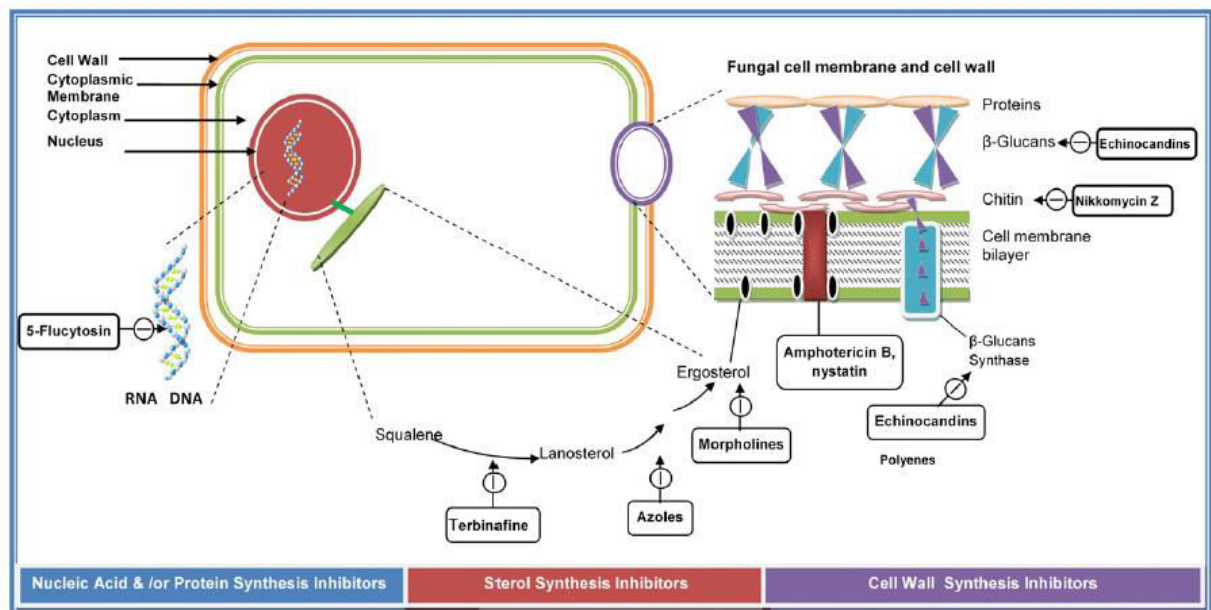


Figure 1.4. Targets of antifungal therapy. From Kathiravan *et al.* (2012) [39].

1.3.2. Cryptococcosis management guidelines and problems with treatment

In 2010, the Infectious Diseases Society of America updated the clinical practice guidelines for the management of cryptococcosis. Building from the previous edition published in 2000, this revision includes the management of cryptococcal meningoencephalitis in different populations, based on immune status, age, demographics, causative pathogen and clinical manifestation of disease. The major areas for management included the early recognition of disease, the use of lipid formulations of AMB, and therapy with the combined use of AMB with 5-FC, followed by maintenance with FLC [40].

Combination therapy with AMB+5-FC has been shown clinically to be more effective in clearing the pathogen in the cerebrospinal fluid and to improve survival outcome compared to AMB or FLC monotherapy, or AMB+FLC combination therapy [41, 42]. However, AMB or FLC monotherapies, and combined AMB+FLC therapy, are often employed in resource-poor countries in sub-Saharan Africa and South East Asia where the availability of 5-FC and AMB is often limited. These limitations are associated with the cost, distribution and lack of registration of the drugs and pose significant challenges to cryptococcosis treatment, which underlie the high rates of morbidity and mortality in those countries [43, 44].

Additionally, each drug is not without their problems. 5-FC is only used in combination with other drugs as resistance is easily acquired with monotherapy [45]. AMB, the most effective drug and considered the gold standard in mycotic therapy, is particularly toxic. Other formulations of AMB, such as liposomal AMB, are designed to exhibit less toxicity while retaining efficacy but are extremely expensive. The intravenous administration of AMB is also problematic in terms of patient care and compliance [43]. FLC has the least toxicity and the best bioavailability, however its use in monotherapy and as a prophylactic has led to concerns of developing resistance, and there are reports detailing a decrease in susceptibility to FLC in the last few years. However, whether this is emerging FLC resistance or intrinsic resistance is not known [46, 47].

1.3.3. Alternative antifungal and synergistic combination therapies for cryptococcosis

As noted above, the repertoire of anti-cryptococcal drugs is limited and current treatments, which often use old and off-patent drugs [43], remain associated with high mortalities. Unfortunately, pharmaceutical companies are less inclined to invest in the licensing and improvement of off-patent drugs as these can be made generically, making them less profitable for the company, and improving the effect of the drug may not warrant a new patent [48]. Alternative therapies with new or novel drugs are desperately required, but investments in novel drugs can be protracted; for example it took

30 years from bench to bedside for echinocandin drugs [49]. Additionally, new and better drugs are marketed at prices that are often not affordable in poorer countries.

Alternative approaches to antifungal therapies involve repurposing approved medical compounds and finding natural compounds that have antifungal activity. Repurposing approved medical compounds is advantageous in that their toxicology and pharmacology profiles are already known and can be used immediately to treat new diseases [50]. An example is 5-FC, which was originally an anti-tumour drug [45]. Compounds naturally produced by plants and microorganisms as defence mechanisms have long been investigated as a source for drug discovery [51]. Examples include AMB and caspofungin, which were originally derived from bacterial and fungal metabolites, respectively [52, 53]. Natural compounds and non-antifungal medicines have also been tested in combination with antifungal drugs as potential alternative therapies [54-56], and antifungal-iron chelating agents and antifungal-immunotherapies combinations have been used as salvage and adjuvant therapies for mucormycosis and candidiasis, respectively [57-59]. However, routine use of these salvage and adjuvant therapies has not been implemented for clinical use.

The practice of combining different antimicrobial agents is used in the treatment of many diseases. These include tuberculosis, leprosy, malaria, HIV/AIDs, and infections with antibiotic resistant bacteria, which are difficult to treat with monotherapies [60, 61]. The advantages of combination therapy coincide with many of the principles of its use, which aim to:

- Increase antimicrobial activity with two agents that may not be accomplished with one agent and hence clear the pathogen faster
- Enable the use of smaller drug dosages so that side effects and toxicity are diminished while maintaining drug efficacy
- Delay the emergence of resistant mutants that may occur from the use of a single drug
- Provide a broad spectrum of activity in seriously ill patients suspected of having either mixed infections or antimicrobial resistant infections [50, 62, 63].

Drug combinations can interact in different ways and the most desired interaction is synergy, which is where the therapeutic effect of the combined drugs or agents is significantly greater than their effects alone. Synergy satisfies the criteria for combination therapies and as it results in faster pathogen clearance and disease resolution, much attention has been given to finding synergistic drug combinations. One synergistic drug combination that is used clinically for bacterial infections is sulfamethoxazole and trimethoprim, otherwise known as co-trimoxazole, which was first

implemented in the 1960s. Co-trimoxazole greatly reduces the MICs of sulfamethoxazole and trimethoprim compared to when these agents are used alone and is broadly synergistic by disrupting folate biosynthesis [64]. It is used for treating a range of infections, however an increasing incidence of resistance to co-trimoxazole is becoming an issue, especially in developing countries where it is widely used [65]. Another synergistic antimicrobial drug combination is ceftolozane and tazobactam, which was marketed as Zerbaxa® in 2014 for the treatment of intra-abdominal and urinary tract infections (https://www.merck.com/product/usa/pi_circulars/z/zerbaxa/zerbaxa_pi.pdf). Like co-trimoxazole, ceftolozane + tazobactam has a broad spectrum of antibacterial activity, even against bacteria that commonly harbour antimicrobial resistance [66].

Repurposed medicines and bioactive compounds have been screened to find agents that potentiate antifungal activity for improved cryptococcal therapy. In pioneering studies, combinations of FLC and caspofungin (CAS) with calcineurin inhibitors and target of rapamycin (TOR) inhibitors were found to be more effective against *Cryptococcus in vitro* than FLC and CAS alone [4]. A later study found treatment combinations of calcineurin inhibitors with either AMB or FLC improved the survival of organ transplant patients with cryptococcosis [67]. Other medicines such as the antibacterial drug rifampicin and antidepressant sertraline also exhibited synergy in *Cryptococcus in vitro* with AMB and FLC, respectively, and FLC and sertraline was further demonstrated to be more effective than FLC alone in a mouse model of systemic cryptococcosis [68, 69]. Natural phenolic compounds from plants can also synergise with antifungal drugs. Examples of these include dihydroxybenzaldehydes and its structural derivatives, thymol and cinnamic acid, which enhanced *in vitro* AMB, FLC and itraconazole (ITC) activity in *Cryptococcus* [70]. While natural compounds are thought to be relatively safe for human use as most of them are extracted from medicinal and edible plants, there is surprisingly a lack of *in vivo* studies that test their interactions with antifungal drugs.

Some synergistic antifungal and non antifungal drug combinations in *Cryptococcus* are also synergistic *in vitro* in other fungal organisms, such as the calcineurin inhibitor FK-506 (Tacrolimus) with CAS in *A. fumigatus* and dihydroxybenzaldehydes with AMB in *C. albicans* [70, 71]. There are many drug combinations that are synergistic in fungal pathogens but have not yet been tested in *Cryptococcus*, for example antifungal drugs and iron chelating agents, where synergy has been reported in *Candida* and *Aspergillus* [9, 72]. Iron chelators have also been reported to potentiate antifungal activity and improve the survival of mice suffering from aspergillosis and mucormycosis [73, 74]. Based on the synergy seen *in vitro* in fungal pathogens and the improved survival from fungal infections *in vivo*, iron chelation is a possible way of enhancing antifungal drugs in *Cryptococcus*.

1.4. Iron and its importance in biological systems

Iron is an essential trace metal for living organisms. Its importance lies in the fact that it can exist in various oxidation states, of which the ferric (Fe^{3+}) and ferrous (Fe^{2+}) forms are most prevalent [75]. Due to this, iron serves as an important cofactor in enzymes that catalyse and participate in many redox reactions that are essential for maintaining metabolic functions in a cell. These functions involve (but are not limited to) DNA synthesis and repair, mitochondrial respiration and energy production, anti-oxidation and detoxification of foreign compounds, and protein and lipid biosynthesis [76, 77]. Additionally, iron is important for microbial virulence, with increased pathogenicity seen in the presence of extra iron [78].

After aluminium, iron is the second most abundant element on Earth [75]. However, it mainly exists as ferric hydroxide in aerobic and pH neutral environments, which limits bioavailability as this compound is insoluble. To combat this, hosts and microbes have evolved mechanisms to scavenge iron. Hosts impose nutritional immunity through iron-binding glycoproteins like transferrin and lactoferrin to withhold iron and prevent its use by microbes [79]. Similarly, some microorganisms like *Aspergillus* secrete low molecular weight molecules called siderophores that bind highly to iron to sequester it for their own use [8].

Within a biological system, iron is tightly controlled. Too much or too little iron can lead to detrimental consequences that in humans manifest as iron deficient and iron overload diseases, including sickle cell anaemia and Friedrich's ataxia, respectively [80].

1.4.2. Iron regulation in *Saccharomyces cerevisiae*

The regulation of iron is well characterised in the model yeast *Saccharomyces*. Here, the cellular iron response, otherwise known as the iron regulon, is controlled by the transcription factors Aft1, Aft2, and Yap5 [81]. Aft1 (Activator of Ferrous Transport) and its paralogue Aft2 are low-iron sensing transcription factors that regulate iron mainly through the activation of genes involved in iron uptake and release from cellular storage. Most of these proteins are present in the plasma membrane and the membranes of subcellular compartments. At the cell surface, these proteins include siderophore transporters (Sit1, Arn1, Taf1 and Enb1), metalloreductases to reduce ferric iron to its divalent form and cause its release from siderophores (Fre1 – 7), and ferroxidases that catalyse the oxidation of ferrous iron before cellular uptake (Fet3 and Ftr1). In addition, cell wall iron acquisition mannoproteins (Fit1 – 3) and a ferrous iron uptake protein (Fet4) have been identified. In the vacuole, which serves as an iron storage compartment, the release of iron into the cytosol is mediated by iron export (Fet5, Fth1 and Smf3) and metalloreductase (Fre6) proteins. Under iron-limited conditions, the transcription of

iron uptake and storage genes is increased [82, 83]. A representation of the *S. cerevisiae* iron regulon is shown in Figure 1.5.

Aft1 also induces regulators involved in the post-translational control of iron, mainly through Cth2 and to a lesser extent Cth1, which destabilise the AU-rich elements (ARE) within mRNAs from genes involved in iron-consuming pathways and cause their degradation. This results in the repression of non-essential but iron-dependent processes, such as Fe-S cluster and haem biosynthesis, and decreased storage of iron in the vacuole through the down-regulation of *CCC1* [84, 85] (Fig. 1.5).

The localisation of Aft1 is mediated by the iron pool within the mitochondria, which exists in the form of iron-sulphur (Fe-S) proteins and plays a role in optimal redox and respiratory functions [83, 86, 87]. Mitochondrial Fe-S clusters also regulate the activity of Yap5, a transcription factor involved in high-iron sensing [88, 89], which in turn influences the activity of Aft1. It is not known how the cell senses a disruption in the synthesis of Fe-S clusters during iron deficiency, however, the suppression of Yap5 leads to the down-regulation of *GRX4* [90]. Grx4 is a glutathione that, together with its paralogue Grx3, binds to Aft1 and prevents it from entering the nucleus and activating the iron regulon [91].

The regulation of iron through Aft1 appears to be unique to *S. cerevisiae* and a few closely related species, with orthologues only found to date in *Candida glabrata* and *Kluyveromyces lactis*. Other fungal species exert their regulation of iron through GATA-type and CCAAT-binding transcriptional repressors [92].

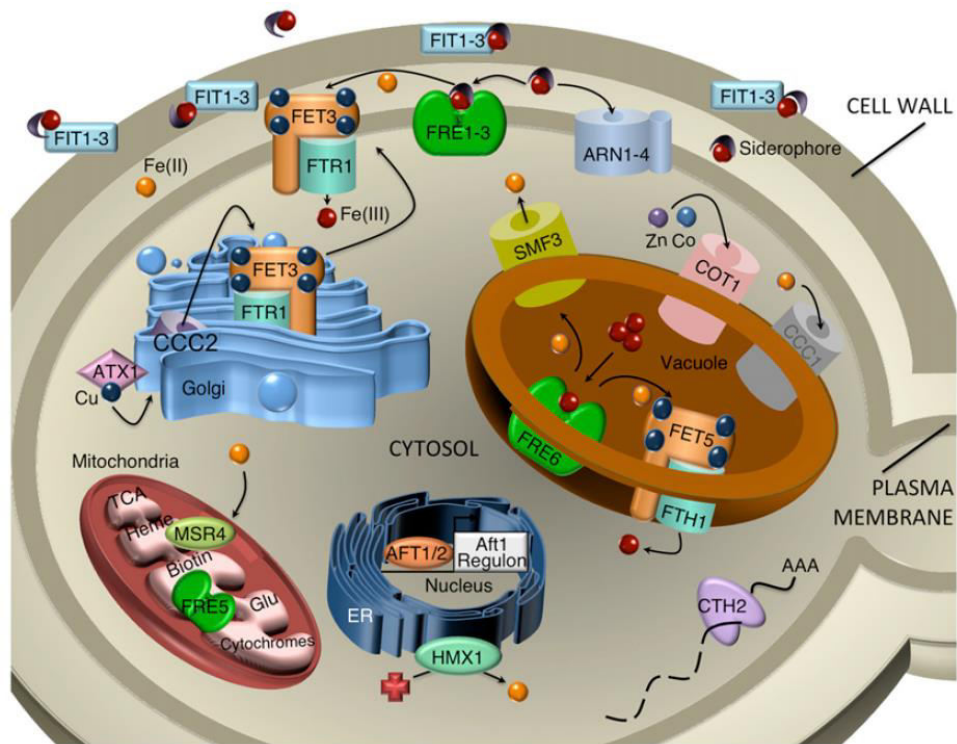


Figure 1.5. Regulation of the iron regulon in *S. cerevisiae*. Low-iron sensing transcription factors Aft1 and Aft2 regulate genes involved in iron uptake, transport and storage (genes in black). Red spheres are Fe^{3+} ; orange spheres are Fe^{2+} . Aft1 also controls the post-translational regulator Cth2, which down-regulates non essential iron-dependant processes such as haem and biotin biosynthesis, and decreases vacuole storage of iron by down-regulating CCC1 (gene in gray) From Cyert and Philpott (2003) [93].

1.4.3. Iron regulation in *Cryptococcus*

The cryptococcal iron regulon shares orthologous iron mobilisation proteins with *Saccharomyces*, with ferroxidases (Cfo1 and Cfo2) and permeases (Cft1 and Cft2) that are orthologous to Fet3 and Ftr1 [94-96]. Similarly, siderophore transporters (Sit1), a suit of ferric reductases (Fre1 – 7, Fre201) and mitochondrial iron related proteins (Frr1, Frr3 and Frr4) have also been identified [97-99]. Unlike *Saccharomyces*, however, *Cryptococcus* can use haem as an iron source through endocytosis that is mediated through the mannoprotein Cig1 and a component of the ESCRT complex Vsp23 [100, 101]. Melanin, which is synthesised by Lac1 and is present in the cryptococcal cell wall, has iron reducing properties [102]. Additionally, the homeostasis of iron in *Cryptococcus* is controlled by two regulators: the GATA-type transcription factor Cir1 (*Cryptococcus* Iron Regulator) and a bZIP transcription factor HapX [103, 104]. The regulation of iron in *Cryptococcus* is shown in Figure 1.6.

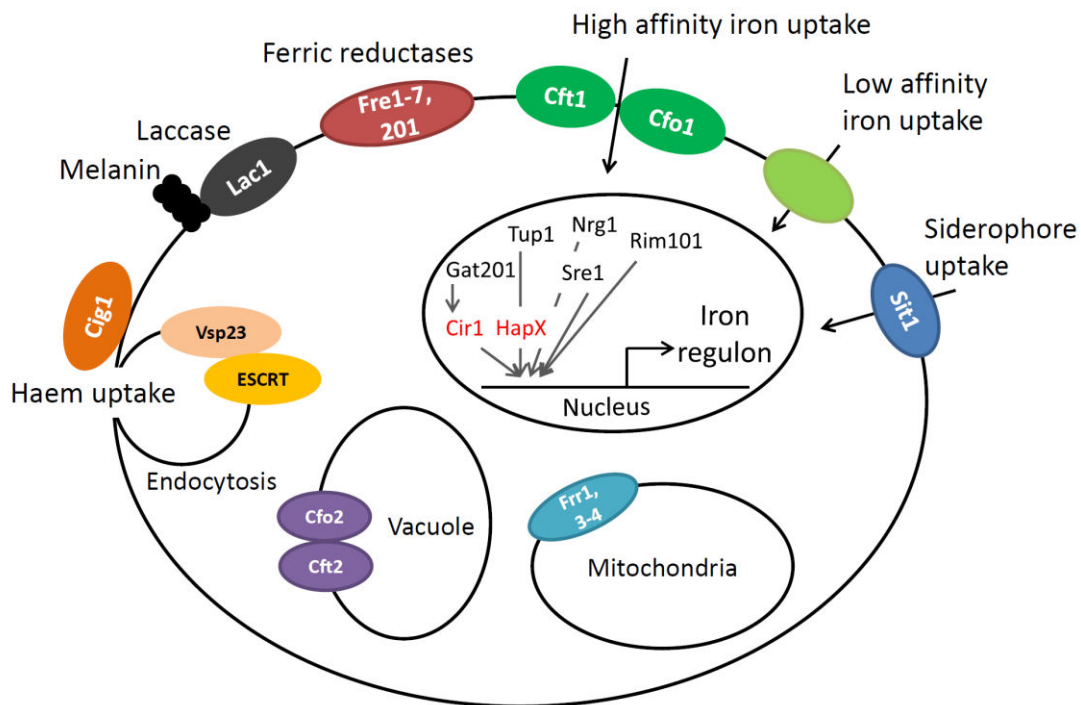


Figure 1.6. Iron regulation in *Cryptococcus*. Iron homeostasis is mainly regulated by Cir1 and HapX (in red). Other transcription factors also exert control on iron uptake genes while Gat201 regulates Cir1. Cfo2/Cft2 is thought to localise at the vacuole [105]. Low affinity uptake systems have yet to be characterised. Adapted from Ding *et al.* (2014) [106].

Cir1 is similar in sequence to other fungal GATA-type iron regulators, such as Fep1 and Sre1 in *Schizosaccharomyces* and *Aspergillus*, respectively, but lacks one of the two zinc finger binding motifs. It exerts positive and negative regulation on genes encoding iron uptake and transport proteins (such as Cft1 and Cfo1), as well as other genes involved in different functions and cellular pathways like sterol and cell wall biosynthesis [104]. HapX is part of a protein complex that binds to CCAAT motifs. During iron limitation this complex up-regulates siderophore transport genes while repressing the expression of genes involved in electron transport functions [103].

This GATA and CCAAT-type iron regulating system in *Cryptococcus* differs from other fungal species in that HapX positively regulates Cir1 in both iron replete and limited conditions, and does not act as a repressor of iron response genes [92, 103]. This may be related to the constitutive transcription of *CIR1*, which does not change regardless of iron availability, suggesting it is post-translationally regulated. Based on protein expression in different iron status and reducing conditions, Jung *et al.* (2011) proposed a model for the regulation of Cir1, where the stability of Cir1 is controlled by the iron status of the cell and it acts as a repressor of target genes [107].

In addition to Cir1 and HapX, other regulators of iron such as Tup1, Nrg1, Sre1, and Rim101 have been identified that influence iron uptake, while Gat201 interacts directly with Cir1 [108-112] (Fig. 1.6).

1.4.4. Iron and virulence in *Cryptococcus*

Like all pathogens, *Cryptococcus* requires iron for virulence and pathogenicity. Iron limitation has been reported to decrease the synthesis of melanin and cause enlargement of the polysaccharide capsule, which are both important virulence attributes [113, 114]. In addition, iron uptake genes encoding the ferric reductases Fre2 and Fre3, and the ferroxidase Cfo1, have roles during infection. Fre2 is required for the utilisation of mammalian heme and transferrin as iron sources, while *FRE3* expression was found to increase following serial passage of *Cryptococcus* through mice, which also increased their virulence [98, 115]. Finally, murine infections with *cfo1Δ* mutants were attenuated in virulence compared to a wild-type strain [104] and were more sensitive to antifungal drugs [116].

Most strikingly, capsule and melanin production are regulated by Cir1, and *cir1Δ* mutants cannot grow at body temperature, which is essential for mammalian virulence, and are defective in mating [104, 117]. The cryptococcal capsule is made primarily of the sugars glucuronoxylomannan (GXM) and galactoxylomannan (GalXM), and smaller amounts of mannoproteins. This polysaccharide matrix protects the cells from phagocytosis and can modulate the host immune response [118]. Melanin is an acid-resistant, solvent-insoluble, brown pigment that is synthesised and deposited in the cryptococcal cell wall. It has been shown to confer protection against oxygen-derived radicals, and increases tolerance to antifungal drugs such as AMB [119]. Mutants that lack capsule or melanin are avirulent in mouse infection models [120, 121]. Mutants deleted in other iron-regulating transcription factors such as HapX and Nrg1 also exhibit attenuated or avirulent phenotypes [103, 110]. Based on this, antifungal agents that disrupt iron homeostasis are being explored as alternative therapies for cryptococcosis [105].

1.5. Systems biology

1.5.1. Systems biology – a ‘holistic’ approach to understanding how cells respond to change

Systems biology can be described as the quantitative and high-throughput study of the interactions involved in biological organisation and processes as cells respond to changes in their environments [122]. It includes examining the variation of genotypes that can arise from a genome by the way genes are modified during expression, the population of RNA that may be translated to proteins, the population of proteins and the influence of post-translational modifications that contribute to phenotypic variation, and the changes in the chemical fingerprint of cells that arise from alterations in cellular processes. Systems biology integrates data from ‘omics’ studies, such as genomics, proteomics,

transcriptomics and metabolomics, with the aim of understanding and characterising a cell's biology in its whole entity as it is and as it responds to different stimuli. The approaches used in systems biology are interdisciplinary, integrating molecular biology with bioinformatics to quantify cellular constituents, model the biological system and predict an outcome from the reconstruction of an experimental situation [122-124].

1.5.2. Transcriptomics and RNA-Seq

Eukaryotic cells are complex biological systems that continually adapt and respond to external and internal stimuli by rewiring important cellular pathways, changing gene expression levels and changing gene and protein interactions. While genomics entails genetic potential from the structure and arrangement of a whole genome sequence, such as gene arrangements, chromosomal insertions and deletions, copy number variations and single nucleotide polymorphisms (SNPs), it is limited in that it does not reflect gene and protein expression or the post-transcriptional and post-translational changes that occur that alter protein functions. Proteomics enables the study of all expressed proteins, which is more beneficial than genomics in analysing biological systems as proteins are vital and have functional roles as structural elements and mediate signalling and catalysis in metabolic pathways. However, proteomics is disadvantaged by the inability to detect low-abundance proteins and membrane-bound accurately, and current protein extraction technologies have only enabled a subset of proteins within the cell to be isolated and studied [125]. Hence, proteomic data are invariably incomplete.

Transcriptomics enables the simultaneous quantification and characterisation of the entire mRNA population within a cell, which is unique to a particular time in response to a particular environment [126, 127]. Although there is a non-linear correlation between mRNA transcripts and their translation into proteins [128], the study of RNA transcripts is beneficial as the global analysis of genes and their expression profiles allows a prediction of which proteins can be translated, even if they cannot be identified through proteomics. This technique has been useful in the identification of disease biomarkers, characterisation of the cellular fingerprint of diseases like cancer [129] and the development of new therapeutic strategies and vaccines [130].

Various techniques have been developed to analyse the transcripts of a cell. These include DNA microarrays, cDNA amplified fragment length polymorphism (cDNA-AFLP), expressed sequence tag sequencing (ESTs), serial analysis of gene expression (SAGE) and massive parallel signature sequencing (MPSS) to name a few. However, each technique has issues such as background noise, sensitivity and laboriousness [127, 131, 132].

RNA-Seq, also known as whole transcriptome shotgun sequencing, is one of the latest next generation sequencing technologies. In this method, transcripts are converted into cDNA for massive parallel sequencing [127, 133]. It does not have the limitations of previous techniques, but current RNA-Seq technologies only permit transcripts to be sequenced in short cDNA fragments. Hence, reconstruction of the original transcripts either by *de novo* assembly or alignment to a reference genome requires many processing elements before analysis (to be discussed further in Chapter 4). Assembled RNA-Seq data can provide concise information on the levels of gene expressions and transcript structures, such as exon boundaries, transcriptional starting sites and the 5' and 3' ends of genes. Additionally, these data can provide information about alternative splicing and the diversity of splicing, and can reveal SNPs and novel transcribed regions [127, 131, 134].

Transcriptomics has been useful in investigating cellular responses to stimuli, such as to antifungal treatments, in order to understand their impact on the biology of fungal cells. Microarrays were used to understand the antifungal activity of the iron chelator ciclopirox olamine in *C. albicans*, at the molecular level, which had been poorly understood [135]. Transcriptomic investigations have been useful in understanding adaptive responses to drugs and drug resistance [136-138], and have been used to monitor the fungal response to chitosan in order to develop it as an antifungal drug [139]. Surprisingly, although there are many studies that have found synergistic drug combinations that enhance the antifungal activity, 'omics' type studies of synergistic combinations, such as between antifungal drugs and iron chelators, are lacking. In addition to understanding antifungal drug responses, other recent applications of transcriptomics in fungi include investigating the antagonistic interactions between fungal plant pathogens and bacteria as an alternative to chemical treatments to control fungal infections [140], and using transcriptomic comparison of a laboratory strain and its variants to investigate microevolution [141].

1.6. Hypotheses and aims of this thesis

The treatment of cryptococcosis is reliant on antifungal drugs that are associated with unacceptable rates of mortality even with current best treatment practice. New medicines are urgently needed but there are significant issues in their development. Enhancing the activities of current antifungal drugs is an attractive alternative to *de novo* drug development, and some repurposed drugs and natural products have been found to be synergistic with antifungals against *Cryptococcus*.

Iron is important for virulence and pathogenicity, and disrupting iron homeostasis has been suggested as a potential antifungal target. Iron chelating agents have been found to synergise with antifungal drugs in medically important yeast and fungi, but the mechanistic basis of how these work has not

been explored. Antifungal-iron chelator interactions have not yet been investigated in *Cryptococcus*. The overall aim of this thesis was to find alternative therapies from understanding synergy between antifungal drugs and iron chelating agents.

At the outset of this study it was hypothesised that synergistic antifungal-iron chelator interactions exist in *Cryptococcus* and that new antifungal therapies could be found through the transcriptomic analyses of these combinations. The well-characterised model *Saccharomyces* could be used to map and understand the transcriptomic profiles of synergistic combinations in detail, which would then be used to aid the analysis of synergy in *Cryptococcus* and find potential novel drug targets that could then be validated in this and other fungal pathogens.

Therefore, the aims of this project were:

1. To determine whether current antifungal drugs and various iron chelators produce synergy when used in combination against pathogenic *Cryptococcus* species and *S. cerevisiae*.
2. To understand the mechanistic basis of synergy using the extensive genetic resources available for *S. cerevisiae*, allowing the transcriptomic profile of synergistic antifungal-iron chelator combinations to be mapped, analysed and validated.
3. To use the data and resources generated in 1) and 2) to characterise the transcriptome of antifungal-iron chelator synergy in *Cryptococcus* and find potential targets for anti-*Cryptococcus* therapy.

CHAPTER 2: General materials and methods

2.1. General materials

2.1.1. Chemicals

All chemicals and their suppliers are listed in Table 2.1. All chemicals used were of analytical grade.

| Chemical | Supplier |
|---|-----------------------------|
| 1,2-Bis(2-Aminophenoxy)ethane- <i>N,N,N',N'</i> -tetraacetic acid (BAPTA) | Sigma-Aldrich |
| 3-Hydroxy-1,2-dimethyl-4(1H)-pyridone (deferiprone) | Sigma-Aldrich |
| 4-Morpholinepropanesulfonic acid (MOPS) | Sigma-Aldrich |
| Absolute ethanol | Sigma-Aldrich |
| Amphotericin B (solubilised) | Sigma-Aldrich |
| Ammonium sulphate | APS FineChem |
| Agar | Difco |
| Agarose (DNA grade) | Bioline |
| β -Mercaptoethanol | BDH Biochemicals |
| Blankaphor (Calcafluor white) | Bayer Chemicals |
| Boric acid | APS FineChem |
| Bromophenol blue | Sigma-Aldrich |
| Caffeine | Sigma-Aldrich |
| Calcium chloride | Unilab, Ajax FineChem |
| Caspofungin | Merck Research Laboratories |
| CloNAT (nourseothricin) | Werner Bioagents |
| Ciclopirox olamine | Sigma-Aldrich |
| Congo red | Sigma-Aldrich |
| Deferoxamine | Sigma-Aldrich |
| Deferasirox | Novartis |
| Deoxynucleotide triphosphates (dNTPs) | GeneWorks |
| Deoxyribonucleic acid sodium salt from salmon testes | Sigma-Aldrich |
| D-glucose (anhydrous) | Univar APS Finechem |
| Dimethyl sulfoxide (DMSO) | Sigma-Aldrich |
| EDTA | Sigma-Aldrich |
| EDTA (Na ₂) | Biochemicals |
| Ferric chloride | Sigma-Aldrich |
| Ferrous sulfate | Fisons analytical reagent |
| Fluconazole | Sigma-Aldrich |
| GelRed™ Nucleic acid gel stain | Biotum |
| Glass beads (0.5 mm) | Sapphire Bioscience |
| Glycerol | Ajax Finechem |
| Hydrogen peroxide solution (30% (w/w)) | Sigma-Aldrich |
| Hyperladder™ I | Bioline |
| Isopropanol | Sigma-Aldrich |
| Itraconazole | Sigma-Aldrich |

| | |
|---|------------------------------------|
| Kanamycin | Sigma-Aldrich |
| Lactoferrin | MP Biomedicals |
| L-glutamine | Sigma-Aldrich |
| Lithium acetate | Sigma-Aldrich |
| LongAmp® <i>Taq</i> 2 X master mix | New England BioLabs |
| Peptone | Amyl Media |
| Phenol: Chloroform (5:1, Molecular grade) | Sigma-Aldrich |
| Phytosphingosine chloride | Sigma-Aldrich |
| Polyethylene glycol (PEG) m.w. 3350 | Sigma-Aldrich |
| RPMI-1640 powder | Life technologies |
| SD-ura drop out media | Sigma-Aldrich |
| Sodium acetate anhydrous | Ajax FineChem |
| Sodium chloride | Fisons Scientific Equipment |
| Sodium dodecyl sulfate (SDS) | Sigma-Aldrich |
| Sodium hydroxide (NaOH) | Ajax FineChem Pty Ltd |
| Sodium nitrite | Sigma-Aldrich |
| <i>Taq</i> DNA Polymerase with standard <i>Taq</i> buffer | New England BioLabs |
| Tris | Ajax FineChem |
| Uracil | Sigma-Aldrich |
| Voriconazole | Sigma-Aldrich |
| Yeast nitrogen base (YNB) | Becton, Dickonson and Company (BD) |
| Zinc chloride | Sigma-Aldrich |

2.1.2. Buffers and solutions

Buffers and solutions and their components are outlined in Table 2.2.

Table 2.2. Buffers and solutions

| Buffers and solutions | Components |
|-----------------------|--|
| 20 X TBE | 800 mL RO water 215.6 g/L Tris base 110 g/L Boric acid 16.4 g/L Na ₂ EDTA Adjusted to 1 L |
| Blue juice | 1 mg/mL Bromophenol blue 20% glycerol |
| DNA extraction buffer | 50 mM Tris-HCl (pH 8) 20 mM EDTA 1% SDS |
| Tris-EDTA (TE) buffer | 1 mM Na ₂ EDTA 10 mM Tris-HCl (pH 8) |

2.1.3. Media

Media and their ingredients are shown in Table 2.3. All media were filter sterilised unless stated.

| Medium | Components |
|--|--|
| Roswell Park Memorial Institute (RPMI)-1640 (pH 7.0) | 10.4 g/L RPMI-1640 powder 34.53 g/L MOPS 18 g/L D-glucose 0.3 g/L L-glutamine |
| Sabouraud dextrose agar (SDA). Autoclaved at 151 °C for 15 min. | 10 g/L peptone 40 g/L D-glucose 15 g/L agar |
| Synthetic complete (SC) broth/agar (pH 4.5) | 1.7 g/L YNB (no amino acids and ammonium sulphate) 5 g/L ammonium sulphate 1.92 g/L synthetic drop out media without uracil 20 g/L D-glucose 76 mg/L uracil 20 g/L agar added for agar plates |
| Yeast nitrogen base (YNB) broth (pH 7.0) | 7 g/L YNB with amino acids and ammonium sulphate 34.53g/L MOPS 8 g/L glucose |

2.1.4. Equipment

A list of equipment and software used is presented in Table 2.4.

| Equipment and software | Supplier (country) |
|--|-------------------------------------|
| BenchMixer™ | Benchmark (USA) |
| Biochrom EZ Read 2000 Microplate Reader | VWR International Pty Ltd (England) |
| Centrifuge 5418 R | Eppendorf (Germany) |
| Centrifuge 5810 R | Eppendorf (Germany) |
| Dry block heater | Thermoline (Australia) |
| Experion™ automated electrophoresis system | Bio-Rad (USA) |
| Experion™ priming station | Bio-Rad (USA) |
| Experion™ vortex II station | Bio-Rad (USA) |
| Experion™ software (Version 3.2) | Bio-Rad (USA) |
| Galapagos Expert software (ver. 1.1.2.0) | VWR International Pty Ltd (England) |
| Haemocytometre | Neubauer (Germany) |
| Minilys® | Sapphire Bioscience (France) |
| NanoDrop 1000 spectrophotometer (ver. 3.6.0) | Thermo Scientific (USA) |
| Orbital mixer incubator | Ratek (Australia) |
| Qubit® 2.0 Fluorometer | Invitrogen (USA) |
| Veriti 96 well thermal cycler | Applied Biosystems (Singapore) |

2.1.5. Kits

Commercial kits that were used for general methods are listed in Table 2.5.

| Kits | Supplier |
|--|--------------------------|
| Experion™ Std Sens RNA chips | Bio-Rad |
| Experion™ RNA Std Sens reagents and supplies | Bio-Rad |
| Qiagen RNeasy mini kit | Qiagen |
| Qubit® RNA BR assay kit | Invitrogen |
| Qubit® dsDNA HS assay kit | Invitrogen |
| UltraClean® Microbial DNA Isolation kit | MoBIO Laboratories, Inc. |

2.1.6. Yeast strains

Yeast strains used in this project are listed in Table 2.6.

| Organism | Strain name | Strain origin/source | Genotype | Comments |
|----------------------|------------------------------|------------------------------|----------|---|
| <i>C. gattii</i> | R265 | Heitman Lab, Duke University | VGIIa | Genome sequenced (https://www.broadinstitute.org/annotation/genome/cryptococcus_neoformans_b/MultiHome.html) [142] |
| | R272 | Heitman Lab, Duke University | VGIIb | Genome sequenced [143] |
| | 97/170 | Heitman Lab, Duke University | VGII | Strain with high level of intrinsic FLC resistance [144] Sequenced in this study |
| <i>C. neoformans</i> | KN99α | Heitman Lab, Duke University | VNI | Genome sequenced Heitman Lab (unpublished) |
| | H99 | Heitman Lab, Duke University | VNI | <i>C. neoformans</i> reference genome (http://www.broadinstitute.org/annotation/genome/cryptococcus_neoformans/MultiHome.html) |
| | WM148 (CBS10085) | Westmead hospital | VNI | Genome sequenced (https://gold.jgi.doe.gov/project?id=38230) |
| | WM626 (MMRL 3150) (CBS10084) | Westmead hospital | VNII | Genome sequenced (https://gold.jgi.doe.gov/project?id=68032) |
| | WM629 (CBS10079) | Westmead hospital | VNIV | Genome sequenced (https://gold.jgi.doe.gov/project?id=38231) |

| | JEC21 α | Heitman Lab, Duke University | VNIV | Genome sequenced [145] |
|------------------------|----------------|--|--|--|
| <i>S. cerevisiae</i> | S288C | Wilkins Lab, University of New South Wales | <i>MATα SUC2 gal2 mal2 mel flo1 flo8-1 hap1 ho bio1 bio6</i> | Reference genome (www.yeastgenome.org/) Parent strain of BY4741 |
| | BY4741 | Wilkins Lab, University of New South Wales | <i>MATα his3Δ0 leu2Δ0 met15Δ0 ura3Δ0</i> | Daughter strain of S288C. Strain used for the Yeast deletion project |
| <i>C. parapsilosis</i> | ATCC 22019 | ATCC collection | Azole susceptible strain | MIC reference strain |
| <i>C. krusei</i> | ATCC 6258 | ATCC collection | Azole resistance strain | MIC reference strain |

2.2. General methods

2.2.1. Growth

All isolates used were streaked from glycerol stocks that were stored at -80 °C. Each isolate was grown on Sabouraud dextrose agar (SDA) and incubated at 30 °C for two days before use. Plated isolates that were more than one month old were discarded.

2.2.2. Glycerol stock storage

Glycerol stocks of yeast strains and mutants were made for long term storage. Two day old yeast cultures were grown on SDA, harvested and mixed with pre-sterilised 15 % glycerol and 0.15 % peptone. Stocks were flash frozen in liquid nitrogen and stored at -80 °C until further use.

2.2.3. Preparation of drug stocks

Antifungal drugs included amphotericin B (AMB), the azole drugs fluconazole (FLC), voriconazole (VRC) and itraconazole (ITC) and the echinocandin caspofungin (CAS). AMB and CAS were made to 1,600 μ g/mL in Milli Q water according to the drug's potency as outlined in the Clinical Laboratory Standards Institute (CLSI) guidelines [146]. FLC was dissolved in methanol (0.02%) and diluted to a stock concentration of 5,120 μ g/mL in Milli Q water, while ITC and VRC were dissolved in 100% DMSO to a final concentration of 1,600 μ g/mL.

Iron chelators tested were deferiprone (DFP), deferoxamine (DFO), deferasirox (DSX), ciclopirox olamine (CPO), EDTA and bovine lactoferrin (LF). DFP and DFO were made to stock concentrations of 5,120 μ g/mL in Milli Q water, while CPO was dissolved in water to 1,280 μ g/mL. EDTA was also made to 5,120 μ g/mL and adjusted to pH 7 by hydrochloric acid. DSX was made in 100 % dimethyl sulfoxide (DMSO) to 5,120 μ g/mL. All stock solutions were filter sterilised and stored at -20 °C in 5 mL aliquots.

CHAPTER 3: Drug combination screening – assessing interactions between antifungal drugs and iron chelating agents

This chapter begins the study of understanding synergistic drug combinations by establishing the drug interactions of commonly used antifungal drugs with a range of iron chelating agents. Two different methods of assessing drug interactions were used to find drug synergy.

Chapter 3 of this thesis has been accepted for publication in the International Journal of Antimicrobial Agents owned by Elsevier. The accepted work is under the following title:

Yu-Wen Lai, Leona T. Campbell, Marc R. Wilkins, Chi Nam Ignatius Pang, Sharon Chen, Dee A. Carter. Synergy and antagonism between iron chelators and antifungal drugs in Cryptococcus. (doi: 10.1016/j.ijantimicag.2016.06.012)

Y. W. L. contributed to the design and data acquisition of the study and the drafting of the manuscript. C. N. I. P. contributed to the data acquisition and writing of the manuscript. L. T. C., M. R. W., S. C. and D. A. C. contributed to the design and analysis of the study and the drafting of the manuscript.

3.1 Introduction

3.1.1. Combination therapy in fungal diseases

The practice of combination therapy was introduced in the 1970s to treat cryptococcal meningitis [147] and it has been an important therapeutic resource in the treatment of fungal diseases. The use of combination therapy against fungi is mostly driven by the lack of effective antifungal drugs, unlike most combination therapies in bacterial infections that are implemented to slow drug resistance. A majority of antifungal drugs have a broad spectrum of activity and most cases of antifungal resistance are intrinsic rather than developing from drug exposure [148]. Combination therapies are commonly implemented in situations where infections are hard to treat; either because patients do not respond to standard therapy or the causative pathogen is multi-resistant [149].

Combination therapy is favoured for invasive fungal diseases due to their significant morbidity and mortality levels [62, 150]. The search for synergents to increase the efficacy of antifungal drugs has seen the use of non-antifungal compounds (reviewed by Lupetti *et al.* (2003) [151]) with recent efforts focused on increasing the susceptibility of FLC with calcineurin and heat shock protein 90 inhibitors [152, 153]. Iron chelating agents have been used as salvage therapy for invasive mycoses in conjunction with polyenes, azoles and echinocandins with mixed outcomes [154], even though the treatment outcome of murine infections using similar drug combinations were favourable [74, 155, 156].

3.1.2. Drug interactions and their assessment

While the basic inhibitory actions of antifungal drugs are known, their effects on fungal cells are complex, and predicting how drug combinations interact and affect a cell can be difficult. There are various models used for determining drug interactions, of which the most commonly used are Loewe's model of additivity and the Bliss independence model [157]. Based on the outcome of these analyses, drug combinations are commonly characterised into the following four of interaction types [63, 148, 158]:

- Additivity, where the effect of the combination is equal to the sum of the effects of each drug when used alone.
- Synergism, when the combined effect of the drugs is significantly greater than their additive effect.
- Indifference, when the combined effect is no greater than that of the more effective agent when used alone.

- Antagonism, when the combined effect of drugs is less than that of the more effective agent when used alone.

3.1.2.1. Loewe's additivity

Loewe's model of additivity uses the sum of the effects of drug A and drug B when used alone to determine their interactions when used in combination. This model assumes that the drugs used target the same biological site via the same mechanisms of action [159], and is represented by the equation: $\sum \frac{a_i}{A_i} + \frac{b_i}{B_i} = 1$ where a_i and b_i refer to the inhibitory concentrations of drug a and drug b in combination and A_i and B_i are the inhibitory concentrations of the drugs by themselves. A value of 1 indicates an additive drug interaction, while < 1 and > 1 indicate synergy and antagonism, respectively [157, 159].

A widely used drug interaction method that uses this model is the fractional inhibitory concentration index (FICI), which is based on an extension of the CSLI microdilution broth susceptibility testing protocol used to measure the minimum inhibitory concentration (MIC) of drugs [160]. This assay is performed in the style of a checkerboard, in which serial dilutions of two drugs are dispensed horizontally and vertically such that different drug concentrations are combined in each well. The pattern of growth observed in checkerboard assays can determine the type of drug interaction, as Figure 3.1 illustrates.

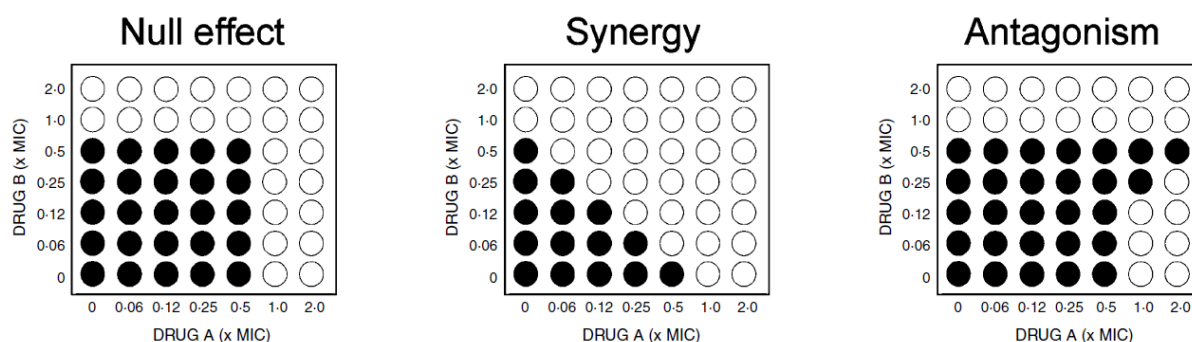


Figure 3.1. Representative patterns of types of drug interactions in a checkerboard assay. Black wells represent growth. From Kontoyiannis and Lewis (2004) [147].

Based on Loewe's equation of additivity, the FICI for the combination of drugs A and B is $FICI = FIC_A + FIC_B$, i.e.,

$$FICI = \sum \frac{MIC \text{ of drug A in combination}}{MIC \text{ of drug A alone}} + \frac{MIC \text{ of drug B in combination}}{MIC \text{ of drug B alone}}$$

The FICI value obtained for the combination determines the type drug interaction. While an FICI < 1 and > 1 might be considered synergistic and antagonistic, respectively, the interpretation of interactions have varied across different drug combination studies [161]. For clarity, this project will follow the FICI definitions of drug interactions proposed by Odds (2003) [162] as follows:

- FICI > 0.5 – 4: no interaction (either additivity or indifference).
- FICI ≤ 0.5: synergy.
- FICI > 4: antagonism.

While Loewe's additivity is a simple and popular method for testing drug interactions, it has disadvantages. The serial dilution of drugs as shown in Figure 3.1 tests exponentially increasing drug concentrations, which results in not testing many combinations of drug concentrations between the ones tested, especially at higher drug concentrations. Additionally, there is no standard for reading the MIC of drug combinations, especially when cidal and static drugs that have different endpoints are tested together. These can affect how drug interactions are interpreted and can result in variation across different studies [161].

3.1.2.2. Bliss independence

The Bliss independence model, also known as the effect multiplication or the fractional product model, is based on the statistical probability of two drugs acting independently to affect growth [163]. It assumes that the drugs used are mutually non exclusive, meaning their modes of action, and possibly their sites of action, differ [159].

This model looks at the maximal effect of drug A, drug B and the combination of drug A and B with an infinite amount of the drugs alone or in combination. The predicted drug effect is expressed as the fractional product, using the equation $f_{AB} = f_A f_B$, where f_A and f_B are the effects of drug A and drug B, respectively, and has the value $0 < f_{AB} < 1$. The drug interaction is determined by the equation $f_{AB} = f_A + f_B(1 - f_A)$, where synergy is observed when the fractional product is more than the predicted drug effect, i.e. > 1, and conversely antagonism is when this is less than the fractional product, i.e. < 0. Values between 0 and 1 are considered additive [157, 159, 164].

A method that uses this model is MacSynergy™ II [165]. MacSynergy™ II (ver 5.1) is analytical software program that describes and quantifies drug interactions as a three-dimensional dose response curve. It uses the standard deviation of the observed drug effects to determine statistical difference from the Bliss independence model [166]. The equation $f_{AB} = f_A + f_B(1 - f_A)$, is represented visually by a flat plane, and drug interactions cause synergistic peaks or antagonistic troughs on this plane. These are

significant if their interaction volumes are $> 25 \mu\text{M}^2\%$ and $< -25 \mu\text{M}^2\%$ for synergy and antagonism, respectively, at a 95% confidence interval [167].

3.1.2. Current antifungal agents and cryptococcosis

This thesis focuses on a set of antifungal drugs currently that are used to treat cryptococcosis. These are discussed below and their structures are shown in Figure 3.2.

3.1.2.1. Amphotericin B (AMB)

First discovered in 1953 [168], AMB is considered the gold standard for treatment of mycotic infections (Fig. 3.2). It is a polyene class drug produced by *Streptomyces nodosus* and binds strongly to ergosterol [52, 169]. This disrupts the integrity of the cell membrane and it was postulated that it caused cell death by creating open channels that allowed the leakage of cellular cytoplasmic contents [170]. Recent work, however, has demonstrated that just the binding of ergosterol is sufficient for the fungicidal activity of AMB, and that cellular leakage is a secondary mechanism [171].

Polyene class antifungal drugs have been used in therapy for more than 50 years [170] and the development of drug resistance is low [172]. Most incidences of polyene resistance are either intrinsic to the fungal species (eg. *Aspergillus terreus* and *Scedosporium prolificans*) or arise from cross resistance to azoles [172-176]. Although AMB is the drug of choice for mycoses, it is quite toxic and there are also issues with patient compliance as its administration requires hospitalisation and monitoring of side effects [43]. Combination therapies with AMB in general have been seen to improve therapeutic outcome, as detailed below (Sections 3.1.2.2 – 3.1.2.4, 3.1.3.1 – 3.1.3.2 and 3.1.3.6).

3.1.2.2. 5-Flucytosine (5-FC)

5-FC (Fig. 3.2) is a fluorinated pyrimidine that was originally synthesised in 1957 as a potential anticancer drug. Its antifungal action is due to intracellular conversion to 5-fluorouracil (5-FU), which is either incorporated into RNA, thus affecting protein synthesis, or is further metabolised to 5-fluorodeoxyuridylic acid, which inhibits DNA synthesis [45, 62, 177, 178]. Conversion requires cytosine deaminase, an enzyme that occurs only in fungal cells, however, high serum concentrations of 5-FC become toxic to the host [179].

5-FC is used only in combination with other antifungal drugs such as polyenes and azoles, as monotherapy readily leads to the acquisition of 5-FC resistance. Resistance can be due to decreased uptake of the drug via mutations in cellular transport and uptake systems, or through defects in the enzymes that convert 5-FC to 5-FU/5-fluorodeoxyuridylic or incorporate these into nucleic acids [45, 177].

3.1.2.3. Triazoles

Fluconazole (FLC), voriconazole (VRC) and itraconazole (ITC) are triazoles used widely in the treatment of mycotic infections (Fig. 3.2). These compounds inhibit ergosterol biosynthesis by non-competitively binding to the haem component of lanosterol 14 α -demethylase (Cyp51, encoded by *ERG11*) in the cytochrome P450 enzyme. This blocks the conversion of lanosterol to ergosterol, causing the accumulation of toxic sterol intermediates and depleting the membrane of ergosterol, which in turn leads to cell leakage and cell cycle arrest [170, 180]. Triazole drugs have different affinities for the target protein depending on how they interact with Cyp51 and are generally fungistatic, although ITC and VRC may be fungicidal in moulds like *Aspergillus*, *Rhizopus* and *Fusarium* [181-183].

As triazoles are less toxic than polyenes and are easily administered, they are favoured for prophylaxis and the treatment of fungal infections [181]. However, their increased use has seen the development of resistance in some fungal pathogens. Resistance mechanisms include overexpression of *ERG11*, mutations in *ERG11* that reduces the affinity between the drug and Cyp51, increasing efflux mechanisms, altering sterol biosynthesis and changing the structural integrity of the cell membrane [170]. All of these mechanisms can also enable cross-resistance to other triazole drugs. Heteroresistance can also occur, whereby a resistant subpopulation occurs in an otherwise susceptible strain [184]. In *Cryptococcus*, this appears to be caused by whole or segmented duplications of chromosomes, particularly chromosome 1 which contains *ERG11* [185].

FLC is a hydrophilic first generation triazole that was first approved as a treatment for vaginal candidiasis in 1994 [39]. It has the best bioavailability of the clinically approved azoles and achieves good penetration through the blood-brain barrier [186]. It also produces the least side effects in the host, and as such is widely used in treatment and as a prophylactic [39]. However, FLC has limited activity against moulds and filamentous fungi [181].

As FLC is off-patent, inexpensive and well tolerated there is increased interest in combining it with other agents to enhance efficacy against *Cryptococcus* and other fungal pathogens [54, 152, 153]. *In vitro* combinations of FLC and AMB against *Cryptococcus* strains have shown mixed drug interactions, ranging from additive to antagonistic, depending on the strain tested [187, 188]. Theoretically, antagonism might be predicted as FLC depletes ergosterol that is required for binding by AMB, however, this combination was shown to be as effective as AMB monotherapy in clearing *Cryptococcus* in a murine infection model [188]. Combining FLC with 5-FC has been reported to produce additive and synergistic interactions *in vitro* [189], to reduce meningeal cryptococcal burden in mouse infections [190] and to more effectively clear *Cryptococcus* than FLC monotherapy in clinical trials [191].

ITC, like FLC, is a first generation triazole but it is lipophilic. It is used mainly against *Aspergillus* species, and it also exhibits *in vivo* and *in vitro* antifungal activity against *Candida* and *Cryptococcus* species [181]. The bioavailability of this drug varies as its absorption is affected by food, and more than 99% of the drug is bound to plasma proteins [192]. Although it can reach infections in tissues, ITC has poor penetration through the central nervous system and is for this reason it is not used in the treatment of meningeal cryptococcosis [181, 192].

ITC has been noted to exhibit unfavourable interactions with other drugs [192], however *in vitro* combination with 5-FC has reportedly produced synergism and additivity against *C. neoformans* [188, 193]. In a murine model of cryptococcosis, ITC combined with 5-FC did not improve treatment [194]. Another study also found ITC and 5-FC did not improve survival in a guinea pig model of cryptococcosis, however, this combination was later reported to improve survival in hamsters compared to ITC and 5-FC monotherapy [195, 196].

VRC is a second-generation azole derived from FLC, and was designed to improve the limitations of FLC against mould infections and to have a better pharmacokinetic profile than ITC [180]. It was first approved by the FDA in 2002 for the treatment of invasive aspergillosis [180, 186], and has a broad spectrum of activity against a range of yeast and mould species, exhibiting fungicidal activity against *Aspergillus* and fungistatic activity against *Candida* and *Cryptococcus* species [180, 181, 197].

VRC has good penetration through the blood-brain barrier and high bioavailability [186, 197]. However, its absorption can be reduced by food co-intake and plasma binding [197]. Furthermore, bioavailability differs according to the ethnicity of patients due to genetic variability in CYP2C19, which is required to metabolise VRC [181, 186]. Careful monitoring of VRC therapy is required as the potential for unfavourable drug interactions with various co-administered drugs is high [197].

VRC combined with AMB has shown to prolong the survival of immune-deficient mice challenged with *Cryptococcus* and to reduce fungal organ burden compared to AMB and VRC monotherapy [198, 199]. In a clinical case of HIV-associated cryptococcal meningitis, therapy with VRC combined with AMB and interferon gamma was reported to clear the pathogen [200].

3.1.2.4. Caspofungin (CAS)

Caspofungin belongs to the class of echinocandins drugs, which target the fungal cell wall (Fig. 3.2). This drug is a synthetically modified lipopeptide produced by *Glarea lozoyensis*. It inhibits 1,3- and 1,6-D-glucan synthase, resulting in depletion of 1,3- β -D glucans that are responsible for most of the structural integrity and robustness of the fungal cell wall. Yeast cells that lack 1,3- β -glucan cease

growing, and eventually the cell becomes susceptible to osmotic pressure and lyses [53, 170, 180]. CAS also has secondary effects in reducing the ergosterol and lanosterol content of the cell [177].

CAS and other echinocandins are only active against species that contain 1,3- and 1,6-D-glucans, which makes these drugs safe and well tolerated in humans [39]. CAS was approved for the treatment of invasive aspergillosis and is active against *Candida* species, but not against *Cryptococcus* even though the cryptococcal 1,3- β -glucan synthase is susceptible to echinocandins [39, 180, 201]. The intrinsic resistance of *Cryptococcus* to CAS may be due to efflux from the cell, degradation, or difficulty accessing the cell wall due to the cryptococcal capsule [53, 170]. Interestingly, combination therapy with CAS+FLC, AMB or the calcineurin inhibitor FK506 have produced synergy *in vitro* and in animals for *C. neoformans* [39, 53, 170]. However, there have been no follow up reports investigating how synergy occurs in these combinations.

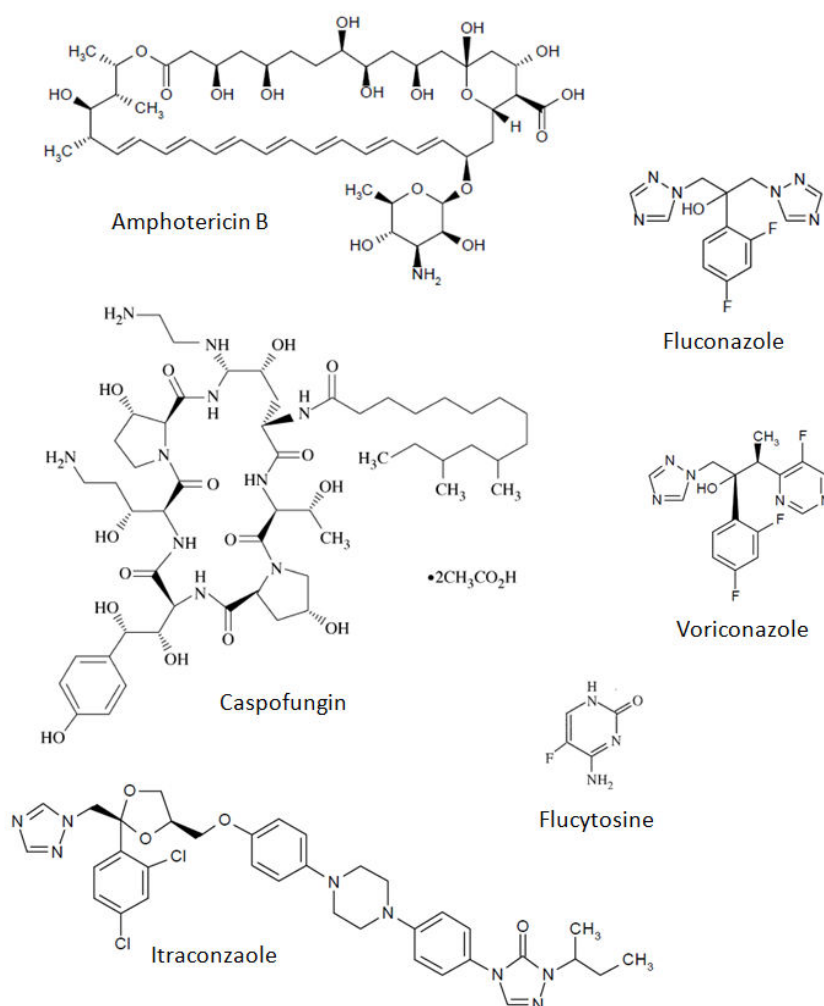


Figure 3.2. Chemical structures of AMB, FLC, CAS, ITC and VRC. From Vermes *et al.* (2000), Letscher-Bru and Herbrecht (2003), and Carillo-Munoz *et al.* (2006) [45, 53, 178].

3.1.3. Iron chelating agents

In order to investigate how iron chelation affects antifungal activity a variety of synthetic and natural chelators as well as clinically used agents were selected for use. These are described below and a summary is presented in Table 3.1.

3.1.3.1. Ethylenediaminetetraacetic acid (EDTA)

EDTA is a substituted diamine compound that chelates divalent and trivalent heavy metal ions. It is widely used in many commercial products as a preservative and stabiliser in cosmetics, pharmaceuticals and cleaning agents. Some food products contain trace amounts of EDTA as an antioxidant to prevent spoilage [202, 203]. In the clinical setting, EDTA is used for the treatment of toxic heavy metal poisoning such as Pb^{2+} and Hg^{2+} [202]. It has also found use in the treatment of cardiovascular disease by chelating Ca^{2+} that causes atherosclerotic plaques, as well as chelating Fe^{2+}/Fe^{3+} and Cu^{2+} to prevent free radical generation and lipid peroxidation [204, 205].

EDTA complexes with metal ions in a one-to-one molar ratio, where its affinity to ferric iron (Fe^{3+}) is the strongest [202, 206], followed by Pb^{2+} , Cu^{2+} , Zn^{2+} , Co^{2+} , Fe^{2+} , Ca^{2+} and Na^{2+} . It is only able to bind to free ferric iron and cannot extract the bound form from metallo-enzymes and other metal-containing proteins [206]. The side effects of EDTA are minimal and reversible, however reported ailments can include gastrointestinal upsets and musculoskeletal complaints, fever, leukopenia, thrombocytopenia, kidney damage, mineral depletion and hypocalcaemia [202, 204].

EDTA has a broad spectrum of activity against microorganisms by binding to essential trace elements required for cell growth and repair [207-210]. Studies have reported activity against a variety of gram negative bacteria, *Streptococcus* species, *Aspergillus niger*, *Candida albicans* and tobacco rattle virus [203, 210-213]. However, EDTA is more commonly used as a 'potentiator' of other antimicrobial agents as it can increase the effect of the agent by helping it gain access to the target cell [203, 207, 214, 215]. This activity has been investigated on biofilms in a variety of organisms including *Staphylococcus*, *Pseudomonas* and *Candida* [215, 216]. In *Candida*, EDTA was shown to impair the ability to form filaments, which is a prerequisite for creating biofilms [217].

Other investigations on the potentiating effect of EDTA in fungi include its use as adjunctive therapy with liposomal AMB in a rodent model of invasive pulmonary aspergillosis where it improved the survival rate of rats compared to monotherapy [208]. It has also been reported to act synergistically with chitosan in killing *Candida* species [209].

3.1.3.2. Lactoferrin (LF)

LF is a glycoprotein and a member of the transferrin family of iron-binding proteins. It is part of the mammalian innate immune response and is found mainly in mucosal secretions and in the secondary granules of neutrophils [218]. Each LF protein binds two ferric ions with high affinity. However, LF can also bind to other essential metal ions including cobalt, copper, zinc and aluminium, as well as non metal ions such as carboxylates, DNA, heparin, lipopolysaccharides and glycosaminoglycans [219]. LF is multifunctional, with immuno-modulatory, anti-inflammatory and antimicrobial properties [220].

The spectrum of activity of LF is quite broad, inhibiting bacteria, viruses, yeasts and fungi, as well as protozoa [221]. LF can inhibit growth in some organisms by chelating iron and has shown to stop hyphal formation in *Candida* and *Aspergillus* [222, 223]. Both iron free (apo-lactoferrin) and iron saturated LF (hololactoferrin) have been shown to inhibit bacterial growth, with iron free LF exhibiting greater bacterial inhibition [224]. In yeast, however, only iron free LF has antifungal activity [225, 226]. Isolated LF peptides have been found to exert antimicrobial activity on the cell surface, with membrane interactions reported in bacteria, and effects on the cell wall in yeasts [227-230].

LF has been used in conjunction with antimicrobial drugs to eradicate biofilms formed by *Pseudomonas aeruginosa* and to treat keratitis associated with fungal pathogens [231, 232]. Combination therapies with LF have also been reported, with synergy with penicillin in the treatment of drug resistant microorganisms like multi-resistant *Staphylococcus aureus* [233]. In yeasts and fungi, synergistic combinations of LF with AMB and azoles have been reported [9, 234, 235]. No toxicity or side effects have been seen in the use of LF in humans and animals [236]; indeed LF is used to prevent bacterial sepsis in pre-term neonates [237].

3.1.3.3. Ciclopirox Olamine (CPO)

Ciclopirox olamine is a hydropryridone derivative that has been used for three decades in the treatment of superficial and vaginal mycoses [238, 239]. It has a broad spectrum of activity that is not limited to the fungal kingdom, with activity against a range of gram positive and negative bacteria and *Mycoplasma*, and has been shown to be active against FLC-resistant strains of yeast [135, 240]. There have been suggestions of repurposing this drug as an antibiotic for drug resistant bacteria [241]. Pharmacological studies have shown CPO is non-toxic in animals and humans when orally administered [239].

Susceptibility to CPO comes from its high binding affinity for trivalent metal ions, where the supplementation of Fe^{3+} ions to culture media reverses the inhibitory effect in a dose-dependent manner [242-244]. Studies of gene expression in *C. albicans* exposed to CPO reported an up-regulation

of genes involved in iron sequestration, transport and uptake, which are typical cellular responses to iron-limited conditions [135, 242, 243]. CPO has been found to be more active under aerobic conditions [243, 245].

Studies investigating antifungal combination therapies with CPO have found synergy *in vitro* with ketaconazole against *Aspergillus*, and synergy with ITC and terbinafine against non-dermatophyte moulds including *Scopulariopsis*, *Aspergillus*, *Onychocola*, *Scytalidium* and *Fusarium* [9, 246].

3.1.3.4. Deferoxamine (DFO)

Deferoxamine, also known as deferrioxamine, has been used since the 1960s to relieve iron overload in haematological diseases such as beta thalassemia [247]. DFO is a bacterial siderophore produced by *Streptomyces pilosus* and it chelates iron ions in a 1:1 molar ratio [248]. DFO has a high affinity for iron but due to its molecular size and its hydrophilic properties, it is not able to readily penetrate cell membranes to chelate cytosolic iron [244, 248-250]. It is able to strip extracellular iron from ferritin and haemosiderin, but not from transferrin and lactoferrin [249-251]. Deferoxamine also binds Cu^{2+} , Al^{2+} , Mg^{2+} , Ca^{2+} and Mn^{2+} , but at a lower affinity than iron [252].

DFO is antimicrobial against a range of bacteria including *Staphylococcus*, *Neisseria* and *Proteus*, and also has been reported to increase the rate of clearance of *Plasmodium falciparum* from patients with asymptomatic malaria [253-256]. DFO has antifungal activity against *Pneumocystis* but not other fungal species [257].

The side effects from the administration of DFO involve auditory, ocular and neurological toxicity as well as musculoskeletal abnormalities [249, 258]. However, a major complication is the utilisation of DFO as a xenosiderophore, where it can provide iron to microbial pathogens and promote survival and infection in the host. Studies aimed at testing the inhibitory activity of DFO in fungi found that it could instead enhance *Aspergillus* and *Rhizopus* growth [9, 259].

3.1.3.5. Deferiprone (DFP)

Another iron chelating drug introduced in the 1990s, DFP is a synthetic oral bidentate chelator, where three molecules of DFP bind to one iron ion [260]. It is a favourable alternative to DFO in the treatment of iron overload diseases as it has better patient compliance due to less severe side effects (including zinc deficiency, joint and muscle pains and gastrointestinal upsets) that are reversible [247, 261]. However, agranulocytosis and neutropenia have been observed in some patients [247, 249, 258, 262].

DFP is more lipophilic than DFO and is able to penetrate most tissues including the skin, lungs and the brain [249, 263]. In addition to being able to chelate intracellular iron, DFP can sequester ferric iron from haemosiderin, ferritin, transferrin and lactoferrin [264]. Compared to DFO, DFP has a lower affinity for Fe^{3+} ions and is less effective at lower concentrations as it has a tendency to dissociate from iron; however it is able to shuttle iron from transferrin to DFO molecules [252, 265]. DFP can also bind to other metal ions, with affinities after iron in the order of $\text{Cu}^{2+} > \text{Al}^{2+} > \text{Zn}^{2+}$ at pH 7.4 [266]. Most importantly, DFP cannot be used as a xenosiderophore. On iron poor media, proliferation of *Yersinia enterocolitica* and staphylococcal growth occurred around a gradient disk of DFO but this was not seen around a disk of DFP [255, 267].

DFP is active against a range of gram negative and positive bacteria, such as *P. aeruginosa*, *Escherichia coli*, *Y. enterocolitica*, *Salmonella typhimurium* and *S. aureus*. It also has anti-protozoan activity against *Leishmania promastigotes* and *P. falciparum* [268]. *Aspergillus*, *Rhizopus* and *Candida* are susceptible to DFP [9, 155, 269], and combination with ketaconazole or FLC was found to be synergistic against *Aspergillus* [9].

3.1.3.6. Deferasirox (DSX)

Deferasirox is the most recently FDA-approved iron chelating agent. It is a tridentate oral iron chelator, with two molecules of DSX binding to one ferric ion [247, 260]. It belongs to the class of bishydroxyphenyltriazole chelators, and its binding affinity for iron compared with DFO and DFP is $\text{DFO} > \text{DSX} > \text{DFP}$ [262, 263]. As with DFP, DSX does not act as a xenosiderophore and does not predispose patients to mucormycosis or yersiniosis. Side effects are reversible and mostly involve stomach upsets, skin rash and headaches [247, 261-263, 270]. Bacterial species *Vibrio*, *Klebsiella* and *Aeromonas* [270, 271], and a range of fungal species including *Rhizopus*, *Mucor*, *Aspergillus*, *Cunninghamella* and *Pythium* have been reported to be susceptible to DFP [73, 74, 272, 273], however it has no effect against *Fusarium* and *Scedosporium* [274].

There have been proposals to use DSX as an adjunctive therapy for invasive fungal infections [268], however results to date have been mixed. *In vivo* studies demonstrated DSX monotherapy prolonged the survival of diabetic mice with mucormycosis, and when combined with lipid AMB produced a higher rate of survival and lower fungal burden compared to AMB monotherapy or placebo treatment [73, 74, 156]. In addition, in two separate reports treating mostly diabetic patients with mucormycosis, the use of DSX combined with antifungal drugs cured the majority from fungal disease [57, 154]. However, a randomised, double blinded placebo controlled trial found patients on DSX combined with liposomal AMB had a higher mortality rate than those on liposomal AMB alone or the placebo [275].

An additional case study involving a leukemic woman on triple antifungal therapy for zygomycosis reported the failure of DSX to resolve infection [58]. It is interesting to note that the studies detailing the successful use of DSX against mucormycosal infections involved subjects that were predisposed to some form of diabetic ailment, and Spellberg *et al.* (2012) proposed that the efficacy of DSX therapy may be related to the type of underlying disorder that made patients susceptible to mucormycosis [275].

3.1.4. Aims and hypotheses of this chapter

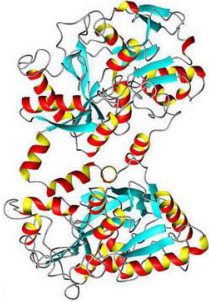
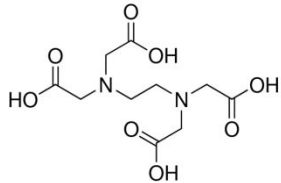
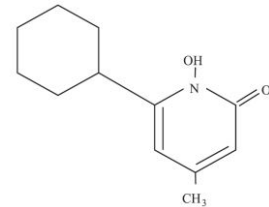
The overall aim of this thesis is to understand the mechanistic basis of synergy between antifungal drugs and iron chelating agents and to use this to discover and develop new antifungal therapies. Iron is an important trace element and many studies that disrupt iron homeostasis in *Cryptococcus* have shown its requirement for virulence and pathogenicity. Iron chelation has an antifungal effect and synergistic antifungal-chelator combinations have been observed *in vitro* in *A. fumigatus*, *C. glabrata* and *C. albicans*. Combinations of antifungal drugs and iron chelators have also been used as salvage therapy for the treatment of mucormycoses. However, MIC studies of iron chelating agents and their interaction with antifungal drugs have not been thoroughly explored in *Cryptococcus*. Given that iron is important and iron chelators have found to synergise with antifungals in other organisms, it was hypothesised that synergistic combinations of antifungal drugs and iron chelators would be found in *Cryptococcus*.

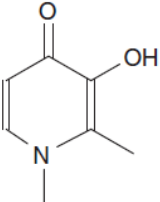
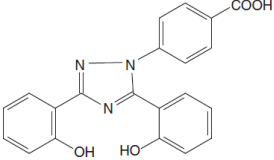
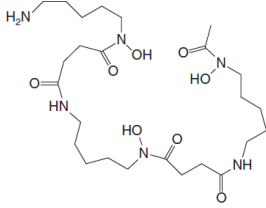
As a range of interactions between antifungal drugs and iron chelators have been reported, this chapter aims to characterise the interactions between these agents in *Cryptococcus* and *S. cerevisiae*, with the latter included to facilitate subsequent transcriptome analysis. Iron chelators were selected to encompass a range of binding types and affinities, and were tested against the antifungals most commonly employed to treat cryptococcosis. It was hypothesised that various combinations would result in synergy, and that these could be used in transcriptome studies to identify common pathways and processes that could be targeted for disruption by new antifungal therapies.

The aims specific to this chapter were therefore:

1. To determine the susceptibility of a range of *Cryptococcus* strains and *S. cerevisiae* to antifungal agents AMB, CAS, FLC, ITC and VRC and iron chelating agents CPO, DFO, DFP, DXS, LF and EDTA by CLSI microdilution assay.
2. To characterise pairwise combinations of the antifungals and iron chelators by checkerboard assay, FICI and MacSynergy™ II, and find synergistic interactions for downstream transcriptome analyses.

Table 3.1. Structure, function, clinical use and reported antifungal activity of the iron chelating agents used in this study

| Iron chelator | Structure | Compound type and chelation | Postulated mode of antifungal action | Uses | Observed Antifungal activity |
|----------------------------------|--|--|--|--|--|
| Lactoferrin (bovine) (LF) |  <p>[221]</p> | <ul style="list-style-type: none"> • Iron binding glycoprotein • 1 LF: 2 iron chelation [219] | <ul style="list-style-type: none"> • Multifunctional protein with antimicrobial activity [220, 276] • Binds to cell surface and cell membrane [228, 277-279] | <ul style="list-style-type: none"> • Given to neonates to prevent pre-term neonatal septic death [237, 280] | <ul style="list-style-type: none"> • Synergistic against <i>Aspergillus</i> and <i>Candida</i> with antifungal drugs [72, 222, 234, 235] • Biofilm disruptor [231, 232] • Antifungal activity against <i>Aspergillus</i>, <i>Trichoderma</i>, <i>Sclerotinia</i>, <i>Sclerotium</i>, <i>Rhizotonia</i> and <i>Phoma</i>, <i>Cryptococcus</i>, <i>Dekkera</i>, <i>Pichia</i>, <i>Saccharomyces</i>, <i>Zygosaccharomyces</i> species [225, 278, 281] |
| EDTA |  | <ul style="list-style-type: none"> • Substituted diamine • 1:1 chelation with iron [202] | <ul style="list-style-type: none"> • Divalent and trivalent metal ion chelator with high affinity for ferric iron [202] • Potentiator of other antimicrobial agents [203, 207, 214, 215] | <ul style="list-style-type: none"> • Cosmetic preservative [202] • Toxic heavy metal chelation therapy [282] • Cardiovascular disease therapy [205] • Adjunct therapy for murine aspergillosis [208] | <ul style="list-style-type: none"> • Disrupting agent against <i>Candida</i> and <i>Cryptococcus</i> biofilms [217, 283] • Antifungal activity against <i>Saccharomyces</i>, <i>Candida</i> and <i>Aspergillus</i> [203, 207, 210] • Synergistic with polyenes against <i>Aspergillus</i> [284], with polygodial on <i>Saccharomcyes</i>. [207] Additive with chitosan against <i>Candida</i> [209] |
| Ciclopirox olamine (CPO) |  <p>[285]</p> | <ul style="list-style-type: none"> • Hydroxyridone derivative [240] • 3 CPO : 1 iron chelation [286] | <ul style="list-style-type: none"> • Intracellular iron chelation • Binds to cell wall, membrane and organelles and inhibits function [244, 287] | <ul style="list-style-type: none"> • Topical treatment of genital and superficial mycoses [238, 240, 288, 289] • Suggestions of repurposing for antimicrobial and cancer therapy [241, 290] | <ul style="list-style-type: none"> • Antifungal activity against <i>Cryptococcus</i>, <i>Trichophyton</i>, <i>Microsporium</i>, <i>Epidermophyton</i>, <i>Candida</i>, <i>Malassezia</i> [291, 292] • Combination with ketaconazole synergistic in <i>Aspergillus</i> [9] |

| | | | | | |
|---------------------------|--|---|---|--|---|
| Deferiprone (DFP) |  <p>[263]</p> | <ul style="list-style-type: none"> • A-ketohydroxy-pyridine [266] • 3 DFP : 1 iron chelation [247] | <ul style="list-style-type: none"> • Iron chelation [155] | <ul style="list-style-type: none"> • Clinical treatment of iron overload diseases [258] | <ul style="list-style-type: none"> • Antifungal activity against <i>Aspergillus</i>, <i>Rhizopus</i> and <i>Candida</i> [9, 155, 269] • Synergistic against <i>Aspergillus</i> with FLC [9] • Synergistic against <i>Cryptococcus</i> with FLC [293] |
| Deferasirox (DSX) |  <p>[263]</p> | <ul style="list-style-type: none"> • Bishydroxy-phenyltriazole [262] • 2 DSX : 1 iron chelation [247] | <ul style="list-style-type: none"> • Iron chelation [73, 272] | <ul style="list-style-type: none"> • Clinical treatment of iron overload diseases [258] • Adjunctive/salvage therapy against mucormycosis [57, 154, 268] | <ul style="list-style-type: none"> • Antifungal activity against <i>Rhizopus</i>, <i>Mucor</i>, <i>Aspergillus</i>, <i>Cunninghamella</i> and <i>Pythium</i> [73, 74, 272, 273] • Enhanced murine clearance of aspergillosis with liposomal AMB [74] • No activity against <i>Fusarium</i> and <i>Scedosporium</i> [274] |
| Deferoxamine (DFO) |  <p>[263]</p> | <ul style="list-style-type: none"> • Siderophore from <i>Streptomyces pilosus</i> • 1:1 chelation with iron [248] | <ul style="list-style-type: none"> • Intracellular iron chelation in <i>Pneumocystis carinii</i> [257] | <ul style="list-style-type: none"> • Clinical treatment of iron overload diseases [258] | <ul style="list-style-type: none"> • Promotes growth <i>Aspergillus</i>, <i>Rhizopus</i>, <i>Cryptococcus</i> and <i>Saccharomyces</i> [9, 155, 294-296] • Clearance of <i>Pneumocystis carinii</i> infection in rats [257] |

3.2. Materials and Methods

3.2.1. Strains and growth media

Strains with fully sequenced and annotated genes were used for initial MIC and checkerboard studies as these could be used in downstream studies to characterise the cellular response to synergistic combinations. These included *C. neoformans* KN99 α (molecular genotype VNI), *C. gattii* strains R265 (VGIIa), R272 (VGIIb), and strain 97/170 (VGII) which has an intrinsically high MIC to fluconazole (MIC 64 $\mu\text{g}/\text{mL}$ [144]) and has been sequenced in our laboratory (unpublished), and *S. cerevisiae* reference strain S288C. Subsequent testing of drug-chelator pairs of interest were done on strains from major molecular genotypes in *C. neoformans* and included H99 and WM148 (*C. neoformans* var. *grubii* VNI), WM626 (*C. neoformans* var. *grubii* VNII), and WM629 and JEC21 α (*C. neoformans* var. *neoformans* VNIV). *Candida krusei* (ATCC 6248) and *C. parapsilosis* (ATCC 22019) were quality control strains for *in vitro* susceptibility assays (Table 2.6).

Cryptococcus strains were grown in yeast nitrogen broth (YNB; Becton, Dickinson and Company) buffered with 0.165 M MOPS (Sigma-Aldrich, Australia) and supplemented with 0.5% (W/V) D-glucose. RPMI-1640 media (InVitro; Australia) buffered with 0.165 M MOPS supplemented with 0.03% (W/V) L-glutamine and 2% (W/V) D-glucose was used as a growth medium for *Candida* and *Saccharomyces* as specified in the CLSI standards [146]. All media were adjusted to pH 7.0 and filter sterilised.

3.2.2. Iron chelating agents and antifungal drugs

Five different iron chelators were tested: EDTA, deferoxamine (DFO), deferiprone (DFP), ciclopirox olamine (CPO; all from Sigma-Aldrich, Australia) bovine lactoferrin (LF; MP Biomedical, Australia) and deferasirox (DSX; Novartis Pharma AG). Details of these, including their molecular structure, approval and current use are supplied in Table 3.1. Antifungal agents included amphotericin B (AMB), the azole drugs fluconazole (FLC), itraconazole (ITC), voriconazole (VRC) (Sigma-Aldrich, Australia) and caspofungin (CAS; Merck Research Laboratories).

3.2.3. Minimum inhibitory concentration (MIC) testing by microdilution assay

All MIC testing was performed according to the Clinical and Laboratory Standards Institute (CLSI) M27-A3 protocol for drug testing in yeasts [146]. All strains were subcultured onto Sabouraud dextrose agar (SDA) at 30 °C for 48 h prior to testing. Cells were standardised to a concentration of $1 - 5 \times 10^6$ cells/mL with a haemocytometer before diluting 1:1000 in the appropriate medium to yield a final concentration of $0.5 - 2.5 \times 10^3$ cells/mL.

Following preliminary analyses, iron chelators were assayed using concentrations from 0.5 – 256 µg/mL for EDTA, DFP, DFO, DSX and LF, and 0.03 – 32 µg/mL for CPO. Antifungals were assayed from 0.015 – 16 µg/mL for AMB and CAS, 0.125 – 256 µg/mL for FLC and 0.008 – 16 µg/mL for ITC and VRC. A positive (no drug) growth control and negative (sterility) control were included in each test. Plates were incubated at 37 °C for 48 h for *Saccharomyces* and *Candida* control strains and for 72 h for *Cryptococcus* strains. The MICs for the fungicidal drugs AMB and CPO were read as the lowest drug concentration that inhibited 100% of growth. MICs for the remaining fungistatic drugs were read at the lowest concentration showing 80% inhibition of growth compared to the positive growth control. Based on preliminary MIC tests with EDTA and the study done by Kobayashi *et al.* (2011) for LF [72], EDTA and LF were read at 50% inhibition.

The concentration and purity of the cell inocula were checked by back-plating onto SDA with incubation at 37°C for 48 to 72 h. All assays were tested in duplicate with each drug in a single experiment. At least two biological replicates were done on different days. All assays included the two *Candida* reference strains.

3.2.4. Synergy testing by checkerboard assay

Checkerboard assays were performed according to the CLSI checkerboard protocol [160]. Concentrations of antifungal drugs and iron chelating agents were selected to encompass the MICs determined for each strain, with the highest drug concentration beginning at 4x the MIC. Serial 2-fold dilutions of the drug and chelating agent were made horizontally and vertically, respectively, in 96 well microtitre plates. Fifty microlitres of each drug and chelator were aliquoted into the appropriate microtitre wells. Inoculations, incubation conditions, assay readings and back plating were performed as outlined above, according to the CLSI M27-A3 protocol [146]. Positive growth controls and negative sterility controls were included. At least two independent assays were performed for each yeast strain. Inhibition was read visually, and cell density was assessed by spectrometer for MacSynergy™ II analysis [167].

3.2.5. Assessment of interactions by fractional inhibitory concentration index (FICI) and MacSynergy™ II

The fractional inhibitory concentration index (FICI) was calculated as $FICI = FIC_A + FIC_B$, where $FIC = MIC$ of drug in combination/ MIC drug alone. FICI values of ≤ 0.5 are defined as synergistic, $> 0.5 - 4$ are indifferent, and > 4 is considered antagonistic [162].

MacSynergy™ II uses the Bliss independence algorithm™ to calculate synergy, which is defined by the equation $f_{AB} = f_A + f_B(1 - f_A)$ where f_{AB} is the additive effect of drugs A and B as predicted by their

individual effects (f_A and f_B) [167]. MacSynergy™II is modelled in Excel and generates a three dimensional response curve of the synergy-antagonism landscape by representing the predicted indifferent effect as a flat plane. Peaks and troughs represent synergy and antagonism, and are significant if their interaction volumes are $> 25 \mu\text{M}^2\%$ (log volume >2) or $< -25 \mu\text{M}^2\%$ (log volume <2), respectively, at a confidence interval of 95% [164, 165, 167].

3.2.6. Iron rescue assays

Iron rescue assays were performed to determine whether inhibition or synergy with AMB caused by LF was predominantly due to iron chelation. Iron (III) chloride (Sigma-Aldrich, Australia) and iron (II) sulphate (Fisson, United Kingdom) were made to stock concentrations of 5,120 $\mu\text{g}/\text{mL}$ in MilliQ water and filter sterilised. In brief, cultures of *C. neoformans* H99 and *S. cerevisiae* S288C were prepared as for MIC testing and 100 μL was dispensed into the test wells of a 96-well microtitre plate. AMB+LF was prepared at 4x the concentration found to cause maximum synergy (defined as FIC = 0.06 $\mu\text{g}/\text{mL}$ AMB + 2 $\mu\text{g}/\text{mL}$ LF for *Cryptococcus*, and 0.03 $\mu\text{g}/\text{mL}$ AMB + 2 $\mu\text{g}/\text{mL}$ LF for *Saccharomyces*) and 50 μL was dispensed across separate rows of the microtitre plate. Additional rows included AMB alone at the FIC concentration (= 0.06 $\mu\text{g}/\text{mL}$ for *Cryptococcus* and 0.03 $\mu\text{g}/\text{mL}$ for *Saccharomyces*), LF alone at its MIC (as there is no inhibition at the LF FIC; = 64 $\mu\text{g}/\text{mL}$ for *Cryptococcus* and 16 $\mu\text{g}/\text{mL}$ for *Saccharomyces*). Growth (no antifungal agents) and sterility (no yeast) controls were also included. Fifty microlitres of iron (III) chloride solutions were added to the wells to give a final concentration of 2, 4, 6, 8 or 10 $\mu\text{g}/\text{mL}$ across each row, and the process was repeated in a second plate for iron (II) sulphate. Incubation conditions and back plating were performed according to the CLSI M27-A3 protocol [146]. All tests were performed in triplicate on separate days. The effect of iron supplementation was assessed visually and by measuring the optical density at 560 nm with a spectrophotometer.

3.3. Results

3.3.1. MICs of antifungal drugs and iron chelating agents

The mode and range of MIC values for antifungal and iron chelators studied are shown in Table 3.2. All *Cryptococcus* strains were susceptible to AMB and the azole drugs according to *Cryptococcus* epidemiological cut off values (ECVs) but had CAS MICs of ≥ 2 $\mu\text{g/mL}$ (range 1–4 $\mu\text{g/mL}$) [30, 297, 298]. *S. cerevisiae* strain S288C had low MICs for all drugs except ITC where the MIC was 2 (range 2–4 $\mu\text{g/mL}$).

Among the iron chelating agents, CPO had the greatest activity against *Cryptococcus* (MIC range 0.5–2 $\mu\text{g/mL}$), followed by DSX (range 2–8 $\mu\text{g/mL}$), DFP (range 4–64 $\mu\text{g/mL}$), LF (32–64 $\mu\text{g/mL}$) and EDTA (64–128 $\mu\text{g/mL}$). For *S. cerevisiae*, CPO was most potent (1 $\mu\text{g/mL}$), followed by DSX (4 $\mu\text{g/mL}$), EDTA and LF (16 $\mu\text{g/mL}$) and DFP (64 $\mu\text{g/mL}$). DFO had no effect on any of the strains, even when the drug concentration was increased to 2,084 $\mu\text{g/mL}$ (data not shown), and was therefore excluded from further testing.

3.3.2. Assessment of drug-chelator interactions by FICI

Antifungal drugs and iron chelators that produced achievable MICs were further tested in combination by checkerboard assay with each of the five initial test strains. The resulting FICI values for each combination are shown in Figure 3.3a (top row), with the data listed in Appendix 3.1. The combination of AMB and LF was synergistic across all of the five initial strains (FICI ≤ 0.5), and this remained consistent when extended to the additional set of *Cryptococcus* strains (Fig. 3.3a bottom row). Most of the remaining drug-chelator combinations were indifferent, with FICI medians from 0.53 – 3.25 (Appendix 3.1).

Chelating agents EDTA, DFP and DSX demonstrated antagonism *in vitro* with ITC and VRC against *C. neoformans* strain KN99 α (FICI > 4; Fig. 3.3a, top row) but these combinations were indifferent for *S. cerevisiae* strain S288C and for the *C. gattii* strains. Testing of additional *C. neoformans* strains found antagonism for all *C. neoformans* var. *grubii* (VNI and VNII) strains, and this extended to FLC in some cases (Fig. 3.3a bottom row; Appendix 3.1), but this was not seen for *C. neoformans* var. *neoformans* (VNIV) strains JEC21 α and WM629, where interactions were indifferent. The MIC for VRC was consistently raised 4-fold when combined with EDTA, DFP and DSX for *C. neoformans* var. *grubii*, while for ITC and FLC interactions were strain-specific; for example in *C. neoformans* var. *grubii* VNI strain KN99 α the combination of ITC+DFP gave an FICI value of 4.25 (antagonistic), while for the *C. neoformans* var. *grubii* VNI strain WM148 this was 1.25 (indifferent).

Table 3.2. MIC values for antifungal drugs and iron chelating agents: Mode (range) in µg/mL

| Fungal species, strain and genotype | Antifungal Agent MIC (Range) | | | | | Iron Chelator MIC (Range) | | | | | |
|---|------------------------------|--------------------|-------------------------|-----------------------|----------------------|---------------------------|------------------|----------------|-------------|------|-----------------|
| | AMB | FLC | VRC | ITC | CAS | LF | EDTA | DFP | DSX | DFO | CFO |
| <i>C. neoformans</i> var. <i>grubii</i> | | | | | | | | | | | |
| H99 (VNI) | 0.25 (0.25–0.5) | 2 (1-2) | 0.007 (0.0035-0.007) | 0.03 (0.015-0.06) | 4 (2-4) | 32 (16-64) | 64 (64-128) | 8 (2-8) | 2 (1-4) | ND | 1 (1) |
| KN99α (VNI) | 0.5 (0.5-1) | 0.25 (0.25-0.5) | 0.0035 (0.0035) | 0.015 (0.015-0.03) | 2 (2-4) | 64 (64-128) | 64 (64-128) | 16 (8-16) | 4 (4-32) | >256 | 2 (1-2) |
| WM148 (VNI) | 0.5 (0.25-1) | 4 (4) | 0.03 (0.015-0.03) | 0.25 (0.06-0.25) | 2 (2-4) | 64 (16-64) | 64 (64) | 8 (2-16) | 8 (2-16) | ND | 1 (1) |
| WM626 (VNII) | 0.5 (0.25-1) | 4 (4) | 0.03 (0.015-0.06) | 0.125 (0.06-0.5) | 2 (2-4) | 64 (16-64) | 64 (32-64) | 8 (2-16) | 4 (2-16) | ND | 1 (1) |
| <i>C. neoformans</i> var. <i>neoformans</i> | | | | | | | | | | | |
| WM629 (VNIV) | 0.25 (0.125-0.5) | 1 (1) | 0.015 (0.007-0.015) | 0.03 (0.03-0.06) | 2 (2-4) | 64 (16-64) | 128 (64-128) | 4 (1-8) | 4 (1-4) | ND | 1 (1) |
| JEC21α (VNIV) | 0.25 (0.125-0.25) | 0.5 (0.5) | 0.007 (0.007) | 0.03 (0.007-0.06) | 2 (1-2) | 64 (16-64) | 64 (64-128) | 8 (1-16) | 2 (1-4) | ND | 0.5 (0.25-1) |
| <i>C. gattii</i> | | | | | | | | | | | |
| R265 (VGIIa) | 0.5 (0.25-1) | 2 (1-4) | 0.06 (0.03-0.06) | 0.125 (0.125-0.25) | 4 (4) | 64 (64-128) | 128 (128-256) | 32 (8-32) | 4 (2-32) | >256 | 2 (1-2) |
| R272 (VGIIb) | 0.5 (0.25-1) | 2 (1-4) | 0.06 (0.06-0.125) | 0.06 (0.03-0.125) | 4 (2-4) | 64 (32-128) | 128 (128-256) | 8 (4-32) | 2 (2-4) | >256 | 1 (1-2) |
| 97/170 (VGII) | 0.5 (0.25-1) | 64 (32-64) | 0.5 (0.5) | 0.5 (0.25-1) | 4 (2-4) | 64 (32-64) | 128 (128-256) | 4 (4-32) | 4 (1-8) | >256 | 1 (1-2) |
| <i>S. cerevisiae</i> | | | | | | | | | | | |
| S288C | 0.125 (0.06-0.25) | 4 (4) | 0.125 (0.125) | 2 (2-4) | 0.06 (0.06-0.125) | 16 (16-32) | 16 (8-32) | 64 (64-128) | 4 (1-8) | >256 | 1 (0.5-1) |

ND = not done

3.3.3. MacSynergy™ II drug response curves

Selected drug combinations were analysed in MacSynergy™ II to visually analyse the dose-response surface of the antifungal-chelator interactions. Figure 3.3b shows a representative three dimensional drug response plot for *C. neoformans* strain KN99 α when treated with AMB+LF. A synergistic response is seen across a range of AMB+LF combinations, with a peak at 0.25 $\mu\text{g}/\text{mL}$ AMB and 8 $\mu\text{g}/\text{mL}$ LF, and a highly significant synergy volume of 902.22 $\mu\text{M}^2\%$.

MacSynergy™ II was also used to investigate the antagonistic interaction seen when KN99 α was treated with VRC+EDTA. Figure 3.3b shows this dose response curve, where there are clear troughs below the plane of additivity at concentrations of 0.0035 VRC + 16 $\mu\text{g}/\text{mL}$ EDTA and 0.0018 VRC + 8 $\mu\text{g}/\text{mL}$ EDTA. The overall antagonism volume was -32.76 $\mu\text{M}^2\%$, which is considered “significant but minor” based on the MacSynergy™ II User Manual [167].

3.3.4. Fold-change in MIC for antifungals and iron chelators in combination

The nature of the FICI calculation means both agents must reduce their MIC by at least 4-fold to produce an FICI ≤ 0.5 . However, as our main concern is with reducing the MIC of the antifungal agent rather than the chelator, we assessed fold changes for each antifungal across all drug-chelator combinations (Fig. 3.3c; Appendix 3.1). The MICs for AMB in the presence of LF decreased at least 4-fold for all fungal strains, and the other chelators decreased the AMB MIC 2-fold for most strains. There was a substantial (8–32 fold) reduction in the MIC of LF in the presence of AMB, which was not seen when it was used in combination with other antifungal drugs. A number of combinations produced a 4-fold or greater reduction in the MIC for the antifungal agent, but as there was only small reduction in the MIC of the chelator these did not achieve an FICI of ≤ 0.5 , however, these were strain-specific and no additional combinations that consistently reduced the MIC of the antifungal partner were revealed. The majority of the antagonistic combinations increased the MIC for the antifungal agent 4-fold. Most chelators increased in efficacy in the presence of antifungal agents, however, these changes were generally quite modest; the AMB+LF combination being an exception.

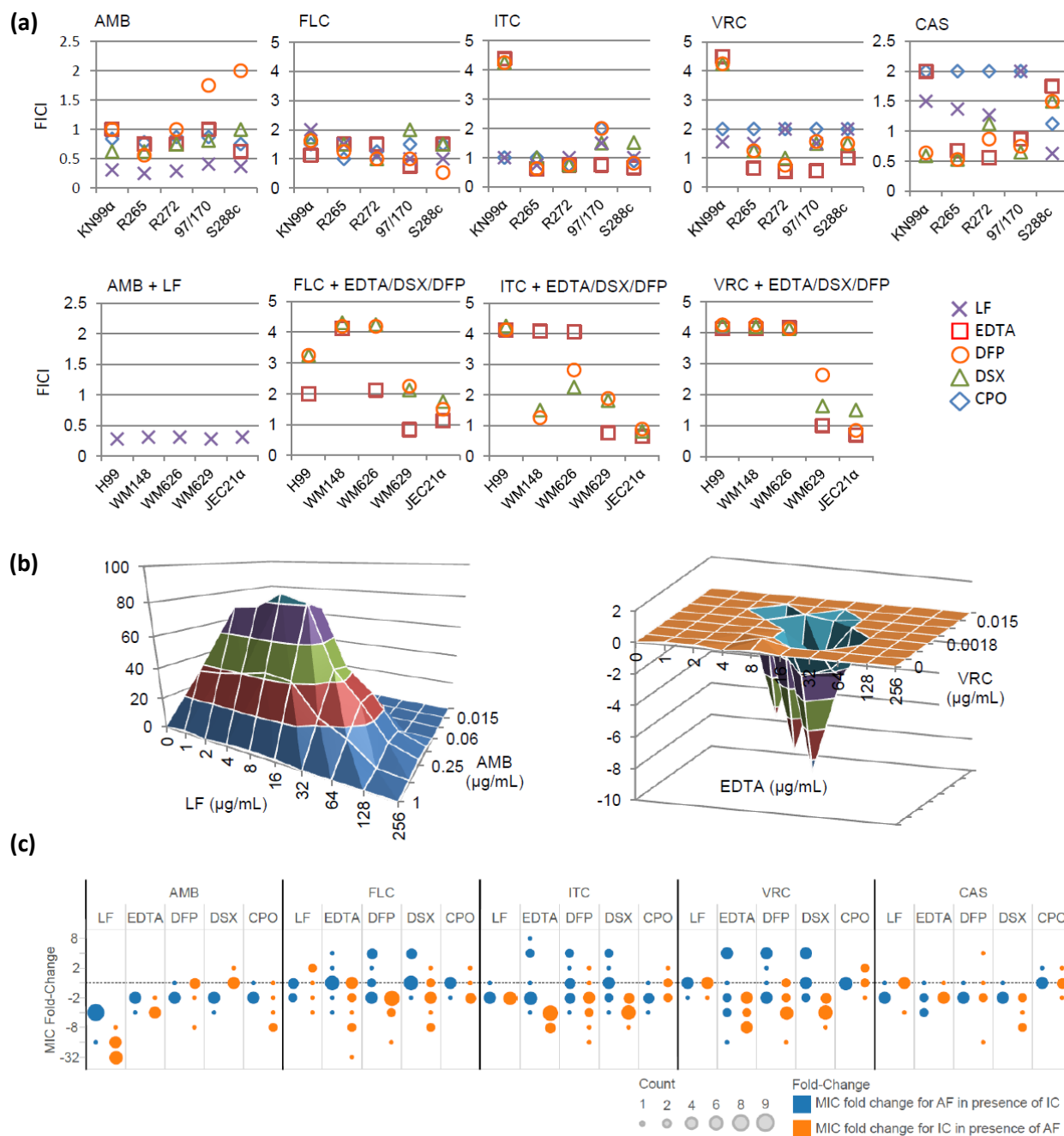


Figure 3.3. Interactions between antifungal drugs and iron chelators. **(a)** FICI values for antifungal agents combined with iron chelators. Top row: Combinations tested in an initial set of *C. neoformans*, *C. gattii* and *S. cerevisiae* isolates; Bottom row: Selected drug-chelator combinations tested in an extended set of *C. neoformans* isolates. AMB+LF is consistently synergistic (FICI ≤ 0.5) for all isolates. In contrast, some chelators are antagonist to the action of the azole drugs FLC, ITC and VRC for *C. neoformans* var. *grubii* strains (FICI > 4). **(b)** MacSynergy™ II plots showing 3-dimensional dose response curves for *C. neoformans* strain H99 treated with AMB+LF (left) and VRC+EDTA (Right). **(c)** Fold change in MIC for antifungals in the presence of iron chelators (blue dots) and for iron chelators in the presence of antifungals (orange dots).

3.3.5. Iron supplementation rescues AMB+LF synergy

To assess the contribution of iron chelation to AMB+LF synergy, inhibitory concentrations of AMB, LF and AMB+LF were tested on *Cryptococcus* and *Saccharomyces* in the presence of increasing concentrations of iron (III) (FeCl_3) and iron (II) (FeSO_4) (Fig. 3.4). Iron addition in either form fully restored growth in the LF-treated wells but did not rescue growth in cultures treated with the FIC concentration of AMB+LF to that of cultures treated with the FIC of AMB alone. This indicates that synergy is not due primarily to the ability of LF to chelate iron, and may instead be due to other antifungal properties of the LF protein, which are significantly enhanced by the presence of AMB.

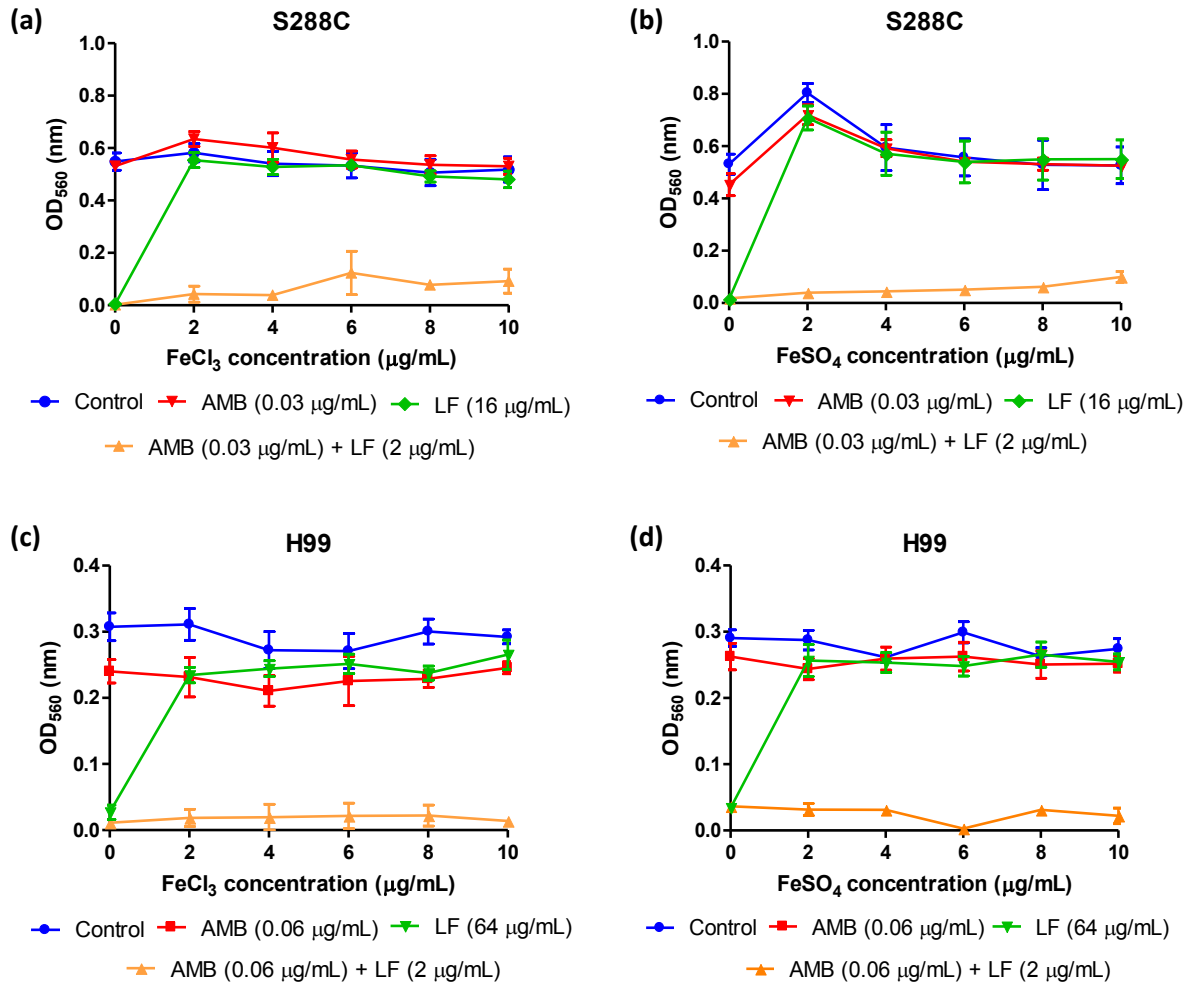


Figure 3.4. Iron rescue assays indicate synergy is not principally due to iron chelation in *S. cerevisiae* S288C and *C. neoformans* H99. The addition of exogenous ferric (Fe(III)) iron in (a) and (c) and ferrous (Fe (II)) iron in (b) and (d) completely rescued cells from MIC levels of LF but was unable to restore growth in the presence of AMB+LF to the level produced in the presence of AMB alone. LF (inverted green triangles) was tested at the MIC level; AMB alone (red squares) and AMB+LF (orange triangles) were tested at FIC levels.

3.4. Discussion

Maintaining iron homeostasis is important for all organisms, and mammalian hosts use iron sequestration to limit the growth of pathogens. *Cryptococcus* strains defective in iron homeostasis are more susceptible to antifungal drugs, including miconazole, AMB and FLC [94, 116, 293], and in the current study, it was hypothesised that iron chelation would enhance the ability of antifungal agents to inhibit *Cryptococcus*. The aim of this study was to use a diverse range of chelating agents to disrupt iron homeostasis and to test whether this would alter antifungal susceptibility, with a longer-term intention of using this to develop novel antifungal treatments. There is some controversy over drug interaction models and their application to fungi, and we applied both Loewe's additivity using FICI and Bliss independence with 3-dimensional modelling using MacSynergy™ II [299]. Good agreement was generally found with both models, which predicted synergy and antagonism resulting from some combinations.

3.4.1. LF+AMB produces potent synergism that is independent of the chelation of iron

The combination of LF+AMB was synergistic for all of the *Cryptococcus* species and strains as well as for *S. cerevisiae* strain S288C (Fig. 3.3a), with MacSynergy™ II dose response curves showing positive interactions across all AMB and LF concentrations (Fig. 3.3b). However, while supplementation with iron completely rescued cells from the MIC of LF this had very little effect on cells treated with a much lower dose of LF combined with AMB (Fig. 3.4). In fact, the lowest molar concentration of iron supplemented (12.33 μM FeCl_3 and 13.16 μM FeSO_4) was enough to saturate the two iron binding sites in LF at the FIC at 2 $\mu\text{g}/\text{mL}$ (26.32 nM) with the presence of AMB. This indicates that iron chelation is important for inhibition by LF alone but does not play the principal role in AMB+LF synergy, which appears to be mediated by other processes.

Synergism between LF and AMB has been seen previously in *C. albicans* and *A. fumigatus* (Table 3.1) [9, 235], indicating that this combination has broad antifungal activity. Although the *C. albicans* study did not perform an iron rescue assay, iron chelation was considered unlikely as the primary cause of the synergy as both apo-lactoferrin and iron-saturated LF have been reported to have similar anti-*Candida* activities [10]. LF is a multifunctional protein with antibacterial, antiviral, anti-parasitic and antifungal activities in addition to chelating properties. As a component of saliva, LF is at the frontline of innate immunity to *Candida*, and efforts to understand the mechanisms responsible for its anti-candidal activity have been the focus of recent research. Active peptides isolated from LF have been shown to interact

with the surface of *Candida* cells, causing pits on the exterior surface and a decrease in cytoplasmic membrane potential [228, 278]. LF also chelates other trace metals and binds to foreign DNA, lipopolysaccharides and carboxylates [219]. In *S. cerevisiae*, LF appears to induce cell death via the accumulation of reactive oxygen species (ROS) and mitochondrial dysfunction but it does not appear to disrupt cell membrane integrity [300]. In the current study we found LF alone had a modest effect on *Cryptococcus* cells but this was greatly augmented by the presence of AMB (≥ 16 -fold enhancement). AMB binds ergosterol in the fungal cell membrane inducing cell leakage, and recent studies have shown that AMB also induces cellular oxidative stress [301-304]. Together, these data suggest that AMB and LF likely act on the surface of fungi and their combined effect accelerates fungal inhibition, perhaps via ROS and oxidative stress, however the mechanistic details of this interaction remain unknown.

3.4.2. Iron chelation does not consistently produce a synergistic response with antifungal agents in *Cryptococcus*

With the exception of DFO, all of the iron chelators tested in this study inhibited the growth of *Cryptococcus* and *Saccharomyces*, consistent with the essential role of iron for fungal growth. However, iron chelation could not consistently synergise the various different antifungal agents *in vitro*, and some chelators were in fact antagonistic to the action of the antifungal. As noted above, even the synergy that was exhibited by AMB+LF was independent of the iron chelating properties of LF. Previous studies have found synergy between FLC+DFP and AMB+EDTA in inhibiting *Aspergillus* [9, 284] and synergy between FLC and deoxycycline against *C. albicans* has been attributed to the iron chelating properties of deoxycycline [305]. Studies of the cellular response to iron limitation indicate that even closely related species may mediate iron homeostasis by quite different mechanisms [306, 307], and it appears that fungal species must be tested empirically to determine their response to antifungal-chelator combination.

For drug synergy the dose of both agents must be reduced at least 4-fold to achieve an FICI value below the 0.5 threshold. However, in this study it was of greater interest to either reduce the need for antifungals or improve their efficacy, which might be overlooked if there were no significant reduction in the need for chelators. To explore this, we assessed each combination for changes in the requirement for the antifungal in the presence of the chelator (Fig. 3.3c; Appendix 3.1). LF consistently reduced the need for AMB at least 4-fold, and the other chelators reduced the MIC for AMB by 2-fold in most strains. As AMB is toxic, and less toxic formulations are very expensive, the general ability of chelators to enhance activity suggests therapies that target iron homeostasis might be a useful adjunct for AMB-

based therapy, even if the combination is not actually synergistic. Ideally, these would disrupt iron regulation rather than directly remove iron by chelation, as anaemia is a common side-effect of AMB treatment [308].

Some chelator-antifungal combinations reduced the antifungal MIC by 4-fold or greater, despite having an FICI greater than 0.5, however, this was sporadic and generally strain-specific. One possible exception was the combination of VRC+EDTA in *C. gattii* where the three strains tested had a 4-16 fold reduction in the VRC MIC, however, more strains should be tested to determine if this combination consistently inhibits *C. gattii*.

3.4.3. Species-specific antagonism is produced by some antifungal-chelator combinations

A surprising result of this study was that certain antifungal-chelator combinations produced an antagonistic response with an FICI greater than 4 (Fig. 3.3a and b). This was particularly the case for the azole drugs when combined with EDTA, DFP and DSX, where the antifungal MIC was raised up to 8-fold in some strains (Fig. 3.3c; Appendix 3.1). EDTA is a polyaminocarboxylic acid and is thought to inhibit *Cryptococcus* by disrupting the assembly of the polysaccharide capsule through Mg^{2+} and Ca^{2+} chelation [283], while DFP and DSX are small lipophilic molecules that can penetrate the cell membrane [263] and are antimicrobial through intracellular chelation of iron [73, 155]. The iron chelating agent DFO has been reported to enhance the growth of *Rhizopus* and *Aspergillus* due to its action as a xenosiderophore, which increases intracellular iron in the pathogens [9, 259]. EDTA, DFP and DSX are not likely to be xenosiderophores [260], however, and how they specifically interfere with azole drugs is not known. DFP has previously been reported to synergise with FLC against *A. fumigatus*, however, only a single reference strain of *A. fumigatus* was tested [9].

In the current study antagonism was highly species-specific and was confined to strains of *C. neoformans* var. *grubii*; the two strains of *C. neoformans* var. *neoformans* were not affected, and in *C. gattii* these chelators often reduced the requirement for the azole drugs. Species- and genotype-specific differences in antifungal susceptibility have been observed in *Cryptococcus* [21], and a *C. gattii* strain (97/170) that is hyper-resistant to azoles was included but no difference in its response to the addition of chelators was seen. *C. neoformans* var. *grubii* is by far the most prevalent agent of cryptococcosis globally and causes the vast majority of disease in HIV/AIDS, which is commonly treated with FLC. Although the current study was limited to analysing interactions *in vitro* that may not fully correlate to interactions *in vivo*, the results indicate a need for caution if using chelators as drug adjuvants for cryptococcosis and

recommend against the use of DFP and DSX in AIDS patients receiving azole drugs.

3.4.4. Conclusions

This study revealed considerable diversity in the interactions between antifungals and iron chelators in their ability to inhibit *Cryptococcus*. The only combination to consistently inhibit *Cryptococcus* strains was AMB+LF, however, all chelators produced a modest reduction in the need for AMB, and therapies aimed at disrupting iron homeostasis may potentiate the action of AMB and reduce the dose required for this toxic drug. There was considerable diversity in the reaction of different *Cryptococcus* strains to antifungal-chelator combinations, and the same combination could range from synergistic to antagonistic in different strains. *Cryptococcus* and *Saccharomyces* now join *Candida* and *Aspergillus*, where synergism between AMB and LF has previously been reported, and their fully sequenced strains with advanced genetic resources will provide excellent platforms where the molecular and cellular basis of synergy can be explored. This, together with *in vivo* testing, can be used to develop new, broadly active antifungal adjuvants.

CHAPTER 4: Transcriptomic analyses of synergy and antagonism between antifungal drugs and iron chelating agents

*This chapter focuses on using transcriptomics to analyse the synergistic and antagonistic responses to antifungals plus iron chelators that were found in Chapter 3. It first investigates how the addition of LF to AMB induces synergy in *S. cerevisiae* S288C by mapping a detailed transcriptome response to AMB and AMB+LF treatment. This was then used to guide the analysis of the synergistic response to AMB+LF that was also seen in *C. neoformans* H99, where detailed protein-protein interaction data and other systems biology tools are not yet available. A preliminary comparison of drug antagonism and additivity that had been observed in response to VRC+EDTA treatment by *C. neoformans* H99 and *C. gattii* 97/170 was undertaken.*

In this chapter, the results and discussions of each transcriptome analyses of AMB+LF synergy in S288C and H99 and VRC+EDTA antagonism/additivity in H99 and 97/170 are presented together.

Two publications based on this chapter are currently in preparation. One manuscript is currently under review in Scientific Reports with the working title:

Chi Nam Ignatius Pang, Yu-Wen Lai, Leona Campbell, Sharon C-A. Chen, Dee Carter, Marc R. Wilkins

*Transcriptomic and network analysis in *Saccharomyces cerevisiae* reveal that amphotericin B and lactoferrin synergy disrupt metal homeostasis and stress response.*

4.1. Introduction

4.1.1. The search for antifungal synergents and problems harnessing information for improved therapies

The search for synergents to improve current antifungal therapies and discover new drugs has seen many screens of antifungal drugs with bioactive compounds and off-patent medications, including iron chelators [54, 55, 70, 153, 309, 310]. To further aid the discovery of synergents, bioinformatic models and drug combination databases have been developed to help predict and understand synergy with antifungal drugs [310-312]. The vast majority of drug screens have been performed with FLC, which is the most widely used antifungal and is off-patent, relatively cheap and widely available. However, this has meant most research to develop and understand drug synergy has been largely limited to azole drugs [54, 313-315].

There are published approaches that attempt to predict the likelihood of synergy between combinations of compounds and antifungals that exert similar genome-wide effects [311], affect similar and topologically close genetic interactions [153, 310, 316] or have similar physiochemical properties [317]. However, these predictive models are reliant on prior knowledge of the physical and genome-wide effects that are exerted on cells by both drugs alone. Many bioactive compounds, especially natural products, have largely unknown antimicrobial mechanisms. Likewise, many repurposed medicines have unknown targets and inhibitory mechanisms in the new system in which they are employed, and even medicines that were designed to inhibit a specific target can exert additional, unknown effects [318, 319]. Finally, these bioinformatic models adopt a reductionist approach to understanding synergy by combining individual phenotypic responses of knock-out mutants to pairs of drugs and finding cellular processes and pathways that are commonly affected. However, synergy can be more complex than just two drugs specifically disrupting common cellular targets. It can also occur through promiscuous mechanisms that generally disrupt the cell, particularly when these affect the cell membrane [320]. Most importantly, these approaches do not show the dynamic and complex changes that occur in cells as they respond to synergistic drug treatments, which are where the mechanistic details of synergy can be deduced.

Despite numerous studies to find synergistic drug pairs and understand their mechanisms of synergy, there have been only three studies to date that have analysed the synergistic interaction of drugs in fungi using 'omics' and systems biology approaches. The first of these used a 2D proteomic analysis to

analyse synergy between FLC and berberine (BBR), a plant alkaloid used in many traditional Chinese medicines. FLC+BBR treatment caused an up-regulation of tricarboxylic acid cycle -related proteins and a down-regulation of proteins involved in fermentation compared to FLC and BRR treatment alone, which suggested a shift from fermentation to mitochondrial respiration. This shift was experimentally tested in all drug treatments by measuring the cellular components that correlate to increased respiratory activity: mitochondrial membrane potential and intracellular ATP level, ROS levels and ATP synthase activity. Compared to FLC and BBR alone, FLC+BBR treatment increased mitochondrial membrane potential, decreased ATP levels and inhibited ATP synthase activity. All of these processes increase endogenous ROS production, which was also detected at higher concentrations in FLC+BBR treatment compared to single treatments. Based on these changes, synergy was suggested to result from a shift in mitochondrial aerobic activity and an increase in endogenous ROS production, resulting in oxidative damage and cell death [6].

The second study of synergy also used a 2D proteomics approach, and analysed synergy between FLC and the calcium channel blocker tetrandine (TET) in *C. albicans*. In this study, only six differentially expressed proteins were identified in the combined treatment, while three and five proteins respectively were differentially expressed in response to FLC and TET alone. Adh1, an alcohol dehydrogenase involved in energy metabolism, was up-regulated when FLC and TET were used alone but was down-regulated in the combined treatment. As Adh1 has been reported to contribute to FLC resistance in *C. albicans*, its down-regulation was suggested to be responsible for the synergistic response. However, there were some issues with this study; most notably the concentration of FLC that was used to treat the cells (750 µg/mL for 6 hrs), which well exceeded the strain's FLC MIC (≤ 8 µg/mL) [7].

Most recently, Li *et al.* (2015) repeated the previous proteomic analysis of FLC+BBR synergy using B-7b, a less toxic derivative of BBR, in a different FLC-resistant strain of *C. albicans*. Instead of the changes to mitochondrial function and ROS production that were observed in their previous study, FLC+B-7b treatment was associated with increased protein processing and a down-regulation of stress response regulators. This suggested the previous responses were more likely due to a toxic response to BBR, and that a disruption to protein processing and stress responses was the more likely cause of synergy [321].

4.1.2. Systems biology tools and resources

The availability of genome sequences and the ability to analyse genome-wide gene expression using systems biology has revolutionised our knowledge of the effect of antifungal drugs. In turn, understanding these effects has aided drug discovery and development by finding newer antifungal targets and designing drugs that disrupt them.

Transcriptomics, like all system biology approaches, generate enormous datasets that are daunting and complex to analyse. A number of tools have been developed to manage and contextualise these large volumes of information in an interpretable and visual manner.

4.1.3.1. Gene ontology terms

As fully sequenced genomes became available, gene ontology (GO) terms were introduced to provide consistent descriptions of gene products so that they can be compared across databases of different organisms. Genes and proteins are characterised and annotated based on their roles in biological processes (BP), molecular function (MF) and the cellular component (CC) where they are found. Hierarchical structures were also assigned to describe the relationship of gene products to one another, such as between mother processes, which provides broader and more general descriptions, and child processes that provides more specific descriptions that are either a part of or occur as a result of the parent [322]. With the vast amount of data produced by systems biology studies, GO terms allow the data to be analysed in manageable sizes by enabling enrichment analyses on gene sets that have the same annotations. Enrichment analyses show the most over and/or under-represented GO terms in a dataset, the frequency of the number of annotated genes appearing in a GO term, and the significance of a GO term being associated with a group of genes [323]. Using GO terms, the most significant changes seen in an experimental condition are observed. The biggest limitation in using GO terms to characterise data into functional categories is its reliance on annotation, as outside model organisms many genes and products in sequenced genomes are poorly annotated.

4.1.3.2. Self organising maps

Self organising maps (SOMs) were developed by Kohonen [324] as a type of artificial neural network that identifies similar data in multidimensional datasets and clusters these together. Clustering reduces the space in the datasets into lower dimensions where the data can be visualised as a map, allowing trends in the data to be easily observed and interpreted. As this clustering is performed using an unsupervised

algorithm, it avoids the introduction of bias based on prior knowledge or assumptions [325]. One of the first uses of SOMs was the analysis of gene expression in hematopoietic differentiation. SOMs was able to find patterns in the data by clustering characterised and unknown genes involved in the different stages of cell differentiation together [326]. By revealing relationships between these, genes that were not known to have functions in cell differentiation could be found. SOMs can also identify co-expressed and co-regulated genes that may participate in a common pathway or be controlled under the same regulatory element [327].

4.1.3.3. Cytoscape

Cytoscape is an open source software platform that was designed to visualise molecular interaction networks, such as protein-protein, protein-DNA and genetic interactions. It is also an interactive platform where generated networks can be integrated with annotations, gene expression profiles and other state data (http://www.cytoscape.org/what_is_cytoscape.html). Cytoscape can create very large networks with nodes representing objects (e.g. genes or proteins) and edges showing the relationships between nodes. Experimental data, known as attributes, and annotations like GO terms can be incorporated with the nodes and edges. Visual cues, such as shapes and colours, can also be added to networks to allow for ease of viewing. Cytoscape has many features that enable networks to be managed and analysed, including different map layouts, scaling, construction, editing and the filtering of attributes and annotations to reduce network complexity. Additionally, Cytoscape incorporates statistical analysis and supports many file formats and extensions to provide different ways of analysing networks [328, 329]. These features enable the exploration of complex holistic data. The main limitation, however, is that Cytoscape requires well characterised pathways and interaction data to build and visualise networks, and is therefore most useful in model organisms.

4.1.3.4. *S. cerevisiae* as a model organism and reference genome strain S288C

S. cerevisiae has long been studied and used as a model organism in molecular and cell biology [330, 331]. Many of its genes and pathways are conserved across higher order organism [332], thus, *S. cerevisiae* has also been used to model and study a variety of processes and diseases such as cell cycle progression, aging and neurology disorders [333-335].

There are various commonly used laboratory strains of *S. cerevisiae*, all of which have different genetic backgrounds and are used for different biochemical studies [336]. One of the commonly used laboratory strains is S288C, which was genetically bred by Mortimer *et al.* (1986) for biochemical studies and was

designed to be non-flocculent under minimal nutrient conditions. The genealogy of this strain is complex, with approximately 88% of the S288C genome derived from strain EM93, which was isolated from a rotting fig. The rest of the S288C genome was derived from strains found from rotting fruits: EM126 and NRRL-210, and commercial strains of baking yeasts: FLD, LF and Yeast Foam [337].

In 1996, S288C was the first eukaryotic organism to have its genome sequenced [338], which was then updated in 2010 [339]. Shortly after the genome was published, a gene knock-out library of all known open reading frames in the S288C genome was generated to understand the biological function of each gene [340, 341]. Nearly 20 years later with 6,604 open reading frames reported in the S288C genome, 78% of the genes have been functionally characterised, while 10% remain unknown and 12% are have dubious gene assignments (<http://www.yeastgenome.org/genomesnapshot>). Technologies that investigate the interactions between proteins and genes, such as epitope tagging and synthetic gene arrays, were also developed using S288C [342]. These techniques have expanded the knowledge of individual protein functions to their functional relationships with other proteins and genes and their contributions to particular cellular processes such as filamentation, stress responses and DNA damage checkpoint signalling [343, 344]. This makes the S288C genome arguably the best annotated and functionally characterised in all eukaryotes [342]. Additionally, up-to-date genome browsers and integrative databases like the *Saccharomyces* Genome Database (SGD) and YeastMine provide information including GO annotations, mutant phenotypes and biochemical pathways that aid experimental design and analysis [332, 345]. Hence, many pioneering systems-level studies have been performed in S288C where the analysis of genome wide responses can be used to its full potential [346-348].

4.1.3. The *C. neoformans* var. *grubii* reference strain H99 and systems biology resources

Globally, more than 95% of cryptococcosis is caused by *C. neoformans* var. *grubii* [349]. In order to gain a better understanding of *Cryptococcus* as a pathogen, nearly all recent genetic, molecular, phenotypic and virulence studies have been performed in var. *grubii* strain H99. In this project, *C. neoformans* var. *grubii* strain KN99 α , which was derived from H99 by backcrossing [350] and has a congenic a mating type partner (KN99a), was initially intended for the transcriptome analysis of drug synergy. However, as there have been some issues raised with the genome of KN99 α (James Fraser, personal communication) a switch to reference strain H99 was made, which also enabled better compatibility with the majority of *Cryptococcus* studies.

H99 was isolated in 1978 from a 30 year-old male patient with Hodgkin's lymphoma at Duke University Medical Centre [351]. Its genome was sequenced by the Broad Institute and comprises 14 chromosomes with an overall size of 18.89 Mb, excluding the rDNA locus with an approximate size of 1 Mb, with 6,962 genes predicted to encode proteins (http://www.broadinstitute.org/annotation/genome/cryptococcus_neoformans/GenomeStats.html). A majority of annotations in the H99 genome have not been functionally characterised but have been predicted bioinformatically and from sequence homology to other fungi [141]. Many resources and technologies that were developed for S288C have been partially generated in H99, including a gene knock-out library of around 2,000 strains and a transcription factor knock-out library of 155 strains [310, 352, 353]. Essential *Cryptococcus* genes that lack mammalian homologues have also been identified for drug targeting [354]. A probabilistic co-functional gene network for *Cryptococcus*, CryptoNet (www.inetbio.org/cryptonet/), was developed by Kim *et al.* (2015) to predict novel genes involved in certain biological processes, such as virulence and drug response [355]. The interactions between genes and proteins, such as transcription factors and signalling proteins, are progressively being studied to understand their functions in *Cryptococcus*-specific processes like capsule production and pathogenicity [111, 355].

In *Cryptococcus*, holistic studies using transcriptomics and proteomics have focused on different approaches to finding alternative therapies, from understanding the inhibitory actions of antifungals and the development of resistance to finding pathways and proteins affected by antifungal treatment in order to target them as potential means of augmenting current antifungals [137, 356, 357]. However, no system biology studies published to date have investigated the genome-wide changes caused by drug interactions that are synergistic in *Cryptococcus*.

4.1.4. Aims and hypothesis

Drug interactions are complex and can differ with the combination of agents used and the organism in which they are tested. A number of studies have investigated the effects of single drugs on fungal cells in order to understand their mechanism of antifungal activity [135], the development of resistance [137, 358, 359] and to identify pathways that can be targeted to augment antifungal therapy [356]. However, the molecular and cellular basis of synergistic drug combinations has not been systematically studied or investigated as a source of potential new therapies.

The original aim of this chapter was to analyse gene expression in fungal cells exposed to combinations of antifungals and iron chelators that were found to act synergistically in Chapter 3, in order to find

pathways and processes that were similarly perturbed by different drug-chelator pairs that could then be tested as new therapeutic targets. Unexpectedly, however, only one antifungal-chelator combination was synergistic, and some antagonistic combinations were found. Based on this, the aims in this chapter refocused to conducting a detailed analysis of the synergy found between AMB+LF, and to investigating the species-specific antagonism seen between VRC+EDTA.

The hypothesis underlying this chapter was that changes to gene expression in a fungal cell exposed to antifungal-chelator combinations could be identified using a systems biology approach, and that these changes would help elucidate the molecular mechanisms behind synergy and antagonism.

The specific aims of this chapter were therefore:

1. To understand the effect of AMB+LF synergy on the transcriptome of *S. cerevisiae* S288C and *C. neoformans* H99.

This was achieved by:

- a. characterising the growth of S288C and H99 cells treated with AMB and AMB+LF to determine optimal time points for RNA extraction;
 - b. performing RNA-Seq, assembling the transcriptomes and analysing these by
 - i. identifying differentially expressed genes and grouping these into functional groups via GO term analysis; and
 - ii. contextualising and visualising the transcriptomic data using SOMs and Cytoscape.
2. To identify genes in altered pathways or processes that may be suitable for targeting by novel antifungal drugs.

This was achieved by

- a. comparing the transcriptomes generated above and using the S288C transcriptome as a scaffold for missing transcriptome data in H99;
- b. validating the transcriptome analysis using gene knock-outs and phenotypic testing, to find targets in S288C and H99 that may induce synergy with AMB.

3. To understand how VRC+EDTA induces antagonism in *C. neoformans* H99 and additivity in *C. gattii* 97/170.

This was achieved by

- a. characterising the effect of VRC+EDTA on the growth of H99 and 97/170 to determine the time point to extract RNA;
- b. performing RNA-Seq, assembling the transcriptomes and comparing the response of H99 and 97/170 to VRC+EDTA by
 - i. identifying reciprocally orthologous transcripts present in H99 and 97/170; and
 - ii. identifying differentially expressed genes for each treatment type and grouping these into functional groups via GO term analysis.

4.2. Methods and materials

4.2.1. Preparation of chemical agents and stock concentrations

4.2.1.1. Stock concentration of stressing agents

AMB and FLC stocks were prepared as outlined in Section 2.2.3. Stock concentrations of calcofluor white (blankaphor) and congo red were made at 10 mg/mL in Milli Q water. 10% (w/v) SDS, 5 M NaCl, 1 M sodium nitrite were made in Milli Q water. 500 mM caffeine was dissolved in Milli Q water with heat. All stressing agents were filter sterilised.

4.2.1.2. Stock preparations of rescue agents

Iron chloride stocks were prepared as outlined in Section 3.2.6. Stock concentrations of zinc chloride and calcium chloride were made in Milli Q water at 4,096 µg/mL and 32 mg/mL, respectively. BAPTA was dissolved in RPMI-1640 media at 8 mg/mL and all chemicals were filter sterilised.

4.2.1.3. Preparation of chemicals and reagents for transformation

Salmon sperm DNA (SS-DNA) was dissolved in TE buffer overnight at 4 °C to make a stock concentration of 4 mg/mL and frozen at – 20 °C until use. Stock concentrations of 1 M LiAc and 50% (w/v) PEG (molecular weight 3350) were made in Milli Q water and heat sterilised. 50 mg/mL of hygromycin B was purchased from GibcoBRL. Kanamycin and nourseothricin were made in Milli Q water at 50 mg/mL and filter sterilised. The drugs were kept frozen at – 20 °C unless otherwise specified by manufacturer's instructions.

4.2.1.4. Genomic DNA extraction

Genomic DNA was extracted from *Cryptococcus* and *Saccharomyces* cultures by mechanical breakage with glass beads. Approximately 20 µL of cells cultured on SDA were harvested and vortexed in 500 µL extraction buffer and 500 µL of 0.5 mm glass beads for 10 min. The mixture was incubated at 70 °C for 10 min and briefly vortexed. 200 µL of both 5 M potassium acetate and 5 M sodium chloride were added and mixed by inversion. After 5 min incubation in ice, the mixture was centrifuged for 10 min at 14,000 rpm.

The upper aqueous phase was transferred to a new eppendorf tube and mixed with 500 µL of 5:1 phenol/chloroform before another round of centrifugation for 5 min. The aqueous phase was

transferred into a new tube, 500 μL of chloroform was added, mixed by inversion and further centrifuged for 5 min. The aqueous layer was once again removed into a fresh tube and one volume of isopropanol was added, mixed and incubated at room temperature for 20 min. The precipitated DNA was pelleted by centrifugation at the maximum speed and washed with 75% isopropanol before the DNA was dissolved in 100 μL of TE.

4.2.2. Illumina sequencing and *de novo* assembly of the *C. gattii* strain 97/170 genome

The genome sequence of 97/170 was compiled by Dr Nandan Deshpande from the University of New South Wales, Australia.

Following extraction as outline above, DNA from strain 97/170 was purified of RNA using the moBIO UltraClean[®] microbial DNA isolation kit. Twenty micrograms of 97/170 DNA dissolved in 100 μL TE was mixed with 450 μL of MD3 buffer and centrifuged through the supplied column at 10,000 *g* for 30 sec. 300 μL of solution MD4 was then added to the column and the flow through discarded before centrifuging for 1 min at 10,000 *g*. The spin filter was then transferred into the supplied collection tube and the purified DNA was eluted through the column with 50 μL nuclease free water at 10,000 *g* for 30 sec.

The OD_{260/280} and OD_{260/230} ratios of the extracted 97/170 genomic DNA were assessed using a NanoDrop 1000 (ver. 3.6.0, Thermo Scientific). DNA quantity was assessed using a Qubit[®] dsDNA HS assay kit and Qubit[®] 2.0 fluorometer (ver. 2, Invitrogen) as specified by the manufacturer's instructions. The grade and purity of the DNA were checked on a 1% agarose gel. At least 5 μg of DNA in 25 μL of nuclease free water, with optical density (OD) ratios from 1.8 – 2, was sent to the Ramaciotti Centre, UNSW, Australia for Illumina genomic sequencing, using the MiSeq sequencing platform.

Genomic read-data were generated in a single lane on an Illumina MiSeq sequencing platform. DNA libraries were prepared with the TruSeq DNA LT Sample prep kit (Illumina), according to the manufacturer's instructions. Chromosomal DNA was chemically fragmented to generate blunt ended, double stranded sequences of less than 800 bp. 'A' bases were then attached to the 3' ends for ligation of index adapters, which contain sequencing primer hybridisation sites. As the genome DNA of 97/170 was sequenced along with 4 other strains (not included in this thesis), the DNA fragments were multiplexed, which involves adding 'barcode' sequences onto the fragments of each sample. This allows for faster sorting, sequencing and assembly of each sample. The library fragments were then attached to a flow cell channel, where 250 bp paired-end reads with inset sizes between 500 – 600 bp were enriched

by bridge amplification using 500 cycles of PCR and sequenced using the MiSeq Reagent Kit v2. PhiX Control v3 was spiked in the runs at 1% and the data were demultiplexed using Casava (ver. 1.8.3).

Prior to assembly, low quality bases in sequence reads were trimmed using SolexaQA (ver. 2.2). *De novo* assembly of reads was performed using the genome assembly tool Assembly By Short Sequences (ABYSS; ver. 1.3.4) [360], using the default parameters. ABYSS uses de Bruijn graphs, which breaks reads into smaller sequences of DNA called k-mers where k denotes the length in bases. Directed graphs are then constructed by connecting pairs of k-mers with overlapping nucleotides [361]. These parameters yielded an optimised genome assembly of 17.45 Mb with 364 contigs and a N50 parameter of 85,384 bp. N50 indicates the median contig size and gives an indication of the quality of assembly with respect to all the generated contigs [362]. A total of 7,315 genes were predicted from the assembly using Augustus (ver. 2.7), a tool for *ab initio* gene prediction in eukaryotic genomic sequences [363].

4.2.3. Transcriptome analysis

4.2.3.1. Characterising the effect of the AMB+LF combination in *S. cerevisiae* S288C and *C. neoformans* H99 for RNA isolation

To understand the mechanism of drug synergy, the transcriptome of cells treated with the synergistic combination AMB+LF was examined. The ID₂₀ time point (= the time taken for drug exposures to inhibit 20% of growth in drug treated versus untreated cells) was chosen to extract RNA for RNA-Seq, as at this point the effect of the drugs would be evident without a dominant apoptotic response.

C. neoformans strain H99 and *S. cerevisiae* strain S288C were streaked from glycerol stocks onto SDA as detailed previously (Section 2.2.1). For broth cultures, H99 was grown in YNB at 37 °C and S288C in RPMI-1640 at 30 °C in a shaking incubator at 180 rpm. S288C was incubated at 30 °C as it exhibited difficulty in budding at 37 °C, suggesting the yeast was under stress. (Note: Results from the AMB+LF checkerboard assay at 30 °C and 37 °C were identical; data not shown). 100 mL cultures of H99 and S288C were grown overnight and the exponential phase culture was subcultured into fresh media in a final volume of 150 mL at a starting concentration of 1×10^7 cells/mL and grown to the start of log phase (3 hrs).

To determine ID₂₀ for RNA isolation, the inoculum was divided into four cultures, with two cultures treated with AMB and AMB+LF, and the remaining two cultures serving as untreated controls for AMB treatment (CA) and AMB+LF treatment (CAL). AMB+LF treatment used the concentrations of AMB and

LF that achieved drug synergy in H99 and S288C, i.e. 0.06 µg/mL AMB + 2 µg/mL LF and 0.03 µg/mL AMB + 2 µg/mL LF, respectively. For AMB treatment, the concentration of AMB was 0.06 µg/mL for H99 and 0.03 µg/mL for S288C. Growth curves for AMB and AMB+LF-treated cultures were established by sampling 500 µL of the drug-treated and corresponding untreated cultures every 15 min following drug inoculation and performing serial dilutions from 10^{-1} to 10^{-6} in Milli Q water. Aliquots of 100 µL were plated in duplicate on Sabouraud dextrose agar (SDA) to obtain countable plates (30 – 300 cfu) following 48 hr of incubation at 30 °C.

4.2.3.2. Sample preparation for RNA isolation in AMB+LF synergy experiments

For RNA isolation, 300 mL overnight cultures of S288C and H99 were grown and subcultured into 700 mL fresh media as detailed previously (Section 4.2.3.1). To prevent RNA degradation during harvesting of the cells for RNA extraction, the cultures of each organism were divided into four 50 mL volumes for each drug treatment and corresponding controls, giving a total of twelve 50 mL cultures. The addition of drugs to the AMB and AMB+LF treatments were staggered by 10 min to allow time for harvesting the cells by centrifugation and back plating.

At the ID₂₀ timepoints determined above (1 hr for AMB and 50 min for AMB+LF, in S288C and H99), three 15 mL aliquots of each treatment and its corresponding control were harvested and pelleted in falcon tubes for 30 sec at 4,000 rpm at 4 °C. The supernatant was decanted and the cells were snap frozen in liquid nitrogen, lyophilised, and kept at – 80 °C until RNA extraction. Non-lyophilised samples were also kept in – 80 °C storage before freeze drying. To confirm ID₂₀ time points, 500 µL samples from drug treated and corresponding untreated control cultures were serially diluted and back plated onto SDA as detailed previously (Section 4.2.3.1).

For the AMB+LF synergy experiments, the entire RNA isolation procedure, beginning with the growth of cells, was repeated on three separate occasions to give three independent biological replicates. Three technical replicates were performed for each sample, so that for the four treatments there was a total number of 36 samples each for S288C and H99.

4.2.3.3. Characterising the effect of VRC+EDTA in *C. neoformans* H99 and *C. gattii* 97/170 and sample preparation for RNA isolation

Similar to characterising the effect of AMB+LF on the growth of S288C and H99, the effects of VRC and VRC+EDTA treatments were characterised in comparison to untreated controls (C). This was done in H99 (antagonistic; 4-fold increase in requirement for VRC in the presence of EDTA) and *C. gattii* 97/170 (additive; 16-fold decrease in requirement for VRC in combinations with EDTA; Appendix 3.1). Unlike AMB+LF synergy where an ID₂₀ between drug treated cells versus untreated cells was used to extract RNA, the timepoint where a 20% increase in growth of VRC+EDTA versus VRC treated cells in H99 was used to extract RNA. This timepoint was also used to extract RNA from H99 and 97/170 following C, VRC and VRC+EDTA treatments to provide a comparable analysis of the drug treatments and of antagonism and additivity between the two *Cryptococcus* strains.

Growth curves were performed as described in Section 4.2.3.1 but at a lower starting concentration of 1×10^6 cells/mL as preliminary analyses indicated the effect of VRC was cell concentration-dependant. H99 was treated with 0.03 µg/mL VRC alone and in combination with 8 µg/mL EDTA, while 97/170 was treated with 0.03 µg/mL VRC alone and in combination with 64 µg/mL EDTA (Appendix 3.1). Three independent biological replicates were performed for the three drug treatments, with three technical replicates performed for each sample. Altogether, H99 and 97/170 had a total 27 samples each for RNA isolation.

For RNA isolation, 100 mL overnight cultures of H99 and 97/170 were grown and the exponential phase cultures were subcultured into fresh media to a starting concentration of 1×10^6 cells/mL in a final volume of 200 mL and grown for 3 hours. These were then divided into three 50 mL volumes for C, VRC and VRC+EDTA treatments. The addition of the drugs to VRC and VRC+EDTA treatments were staggered at 3 min to allow time for harvesting the cells by centrifugation and back plating. Cell harvesting and lyophilisation were performed as detailed in Section 4.2.3.2.

4.2.3.4. RNA extraction from *S. cerevisiae* S288C and *C. neoformans* H99

To ensure uniformity across RNA extractions, lyophilised S288C, H99 and 97/170 samples were randomised to twelve isolations at a time. Labels were assigned by grouping the 12 samples numerically, with the twelve individual samples labelled alphabetically. This labelling was kept for Illumina sequencing and data sorting and is presented in Appendix 4.1.

Approximately 200 μ L of freeze-dried cells prepared above were transferred to a cryogenic storage tube and mechanically broken with \sim 200 – 250 μ L RNase Zap-treated 0.5 mm glass beads using a Minilys tissue homogeniser at 5,000 rpm. The cells were beaten for a total of 2 min and cooled on ice after every 1 min of beating.

Total RNA was extracted from the disrupted yeast cells using the Qiagen RNA isolation kit with some modifications. Firstly, 700 μ L of lysis buffer was added to each tube and the debris and beads were removed by centrifugation at maximum speed in a desktop centrifuge at 4 °C for 3 min. The supernatant was transferred to a new tube and mixed with an equal volume of 70% ethanol, and this was then centrifuged through the Qiagen RNA spin-through column for 30 sec at 10,000 g . The column was washed once with 700 μ L RW1 buffer and twice with 500 μ L of RPE buffer by centrifugation for 30 sec at 10,000 g for each wash, and the flow through was discarded. The column was then transferred to a new collection tube and spun dry for 2 min at 10,000 g before the RNA was eluted by centrifuging at 10,000 g for 1 min with 50 μ L of RNase free water (supplied in the Qiagen kit).

Aliquots of 10 μ L of the eluted RNA were used to assess quantity and quality. $OD_{260/280}$ and $OD_{260/230}$ were assessed using a NanoDrop 1000 (ver. 3.6.0, Thermo Scientific). RNA integrity number (RIN)/RNA quality index (RQI) was assessed using Experion std Sen RNA chips and reagents and Experion™ software (ver. 3.2, Bio-Rad). RNA quantity was assessed using a Qubit® RNA BR assay kit and Qubit® 2.0 fluorometer (ver. 2, Invitrogen). Total RNA with OD ratios between 1.8 – 2, a RIN/RQI of at least 8 and a yield of at least 5 μ g in a minimum concentration of 200 μ g/mL was sent to the Ramaciotti Centre, UNSW, Australia, for Illumina RNA sequencing.

4.2.4. Illumina RNA-Seq and data processing

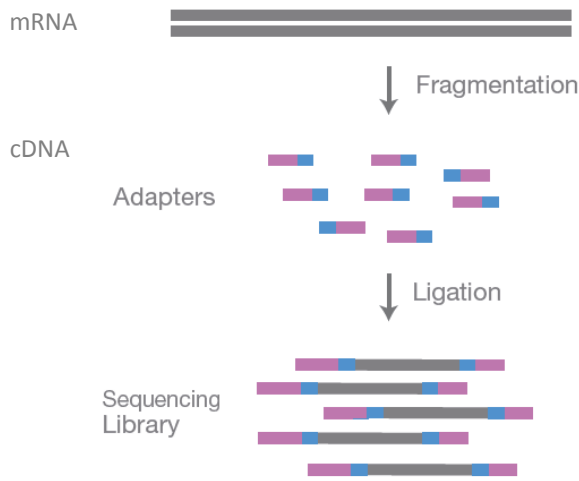
The following sections were undertaken with assistance from Dr Igy Pang, a bioinformatician employed on the grant that funded this work.

4.2.4.1. RNA-Seq library preparation and sequencing

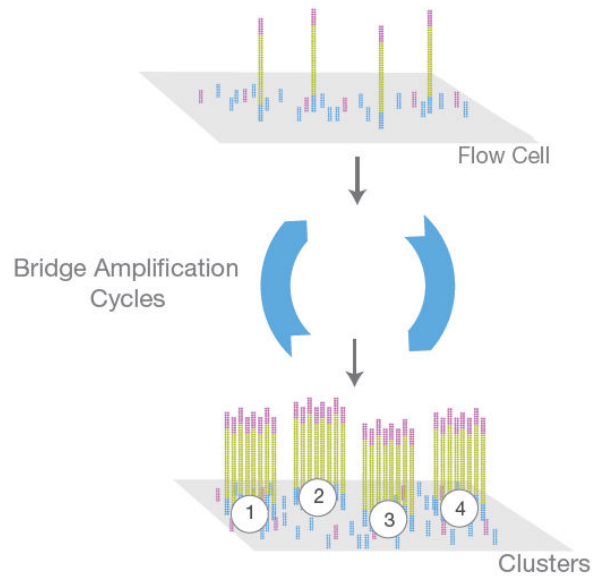
One technical replicate from each biological replicate was selected for RNA-sequencing, giving 12 samples each for S288C and H99 for synergy experiments, and 9 samples each for H99 and 97/170 for antagonism experiments. The RNA samples were prepared using an Illumina TruSeq RNA sample prep kit (ver. 2) to generate DNA libraries, according to manufacturer's instructions. Briefly, mRNA was purified from 2 µg of total RNA using polyA selection before the nucleic acids were chemically fragmented and converted into single-stranded cDNA by random hexamer priming. The second strand of cDNA was synthesised, and double-stranded cDNAs were created with blunt ends. 'A' bases were then attached to the blunt ends for the ligation of index adapters, which contain sequencing primer hybridisation sites for selected reads, such as single, paired-end or multiplexed reads [364]. Paired end reads were chosen to improve the discovery of novel transcripts and increases the total read length per library fragment. Multiplexing was also applied.

The library fragments were then attached to a flow cell channel, which is a planar surface fixed with complementary adapter sequences and primers that hybridise to the ends of the added DNA fragments. Libraries were constructed with insert sizes between 80 – 330 bp and were enriched by bridge amplification using 15 cycles of PCR. Complementary fragments were removed, and libraries were randomised onto two separate lanes for RNA-Seq using the HiSeq2000 platform to generate 100 bp paired-end reads. The TruSeq v3 SBS kit was used to fluorescently label nucleotides in each library for sequencing by capturing the emitted fluorescence of different bases. The data were demultiplexed using Casava (ver. 1.8.2). An overview of this process is shown in Figure 4.1.

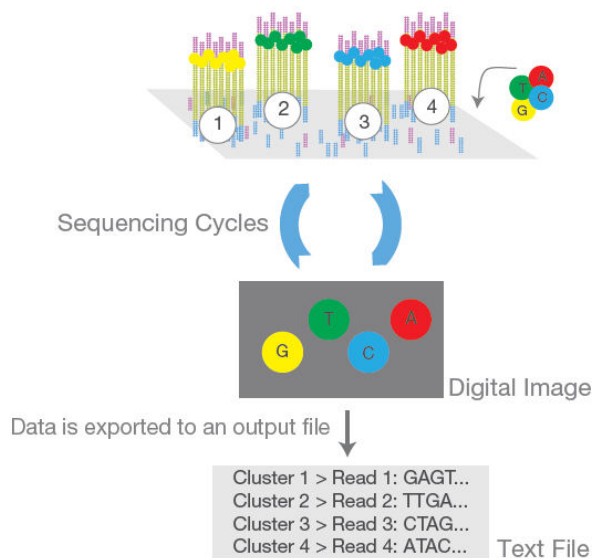
(a) Library preparation



(b) Cluster amplification



(c) Sequencing



(d) Alignment and data analysis

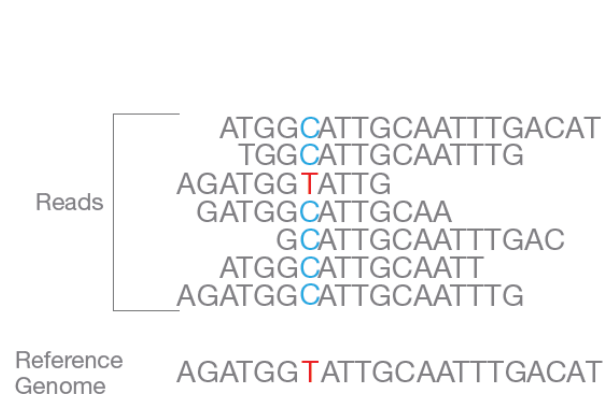


Figure 4.1. An overview of RNA-Seq library preparation and sequencing. **(a)** mRNA was chemically fragmented and converted to cDNA, where DNA libraries were prepared by ligating specialised adapters to both ends of DNA fragments. **(b)** Libraries were loaded to the surface of a flow cell channel and DNA fragments hybridised to complementary adapter sequences present on the channel. Each bound fragment was enriched through bridge amplification and complementary fragments were removed after amplification. **(c)** Amplified fragments were sequenced by adding fluorescently labelled nucleotides and sequencing reagents. The flow cell was imaged and sequence data were generated by capturing the emitted fluorescence of incorporated bases. **(d)** Sequenced reads were then aligned bioinformatically to a reference sequence. Taken from http://www.illumina.com/content/dam/illumina-marketing/documents/products/illumina_sequencing_introduction.pdf

4.2.4.2. Processing of RNA-Seq data

FastQC (ver. 0.10.1) was used to assess the accuracy of sequence reads. Phred quality scores (Q scores) are defined by the equation $Q = -10 \log_{10} P$ and indicate the accuracy of a sequencing platform by calculating the probability (P) of a given base being called incorrectly [365]. All RNA samples achieved an average Phred score of at least 30, indicating a base call accuracy of 99.9% where the probability of an incorrect base call was 1 in 1000 bp.

The quality of generated sequences was checked using SolexaQA (ver. 2.2). This program extracts the longest contiguous sequence where all bases have high Phred scores by trimming off bases with low Phred scores [366]. A median of 93.26% of high quality paired-end reads across all samples was achieved by trimming paired end sequences with the cut-off p-value of < 0.05 , and read lengths of at least 25 nucleotides was generated.

The reads were then mapped against the reference genomes using TopHat (ver. 2.0.4), a fast short read mapping program for RNA-Seq that aligns sequences to a reference genome and identifies exon-exon splice junctions [367]. The parameter '-N 3 -library-type-fr-unstranded' was selected to map reads from the left most end of the nucleotide fragment to the transcript strand and the right most end to the opposite strand. Aligned reads with three or more mismatches were discarded and S288C sequences were mapped to the genome reference R64-1-1 from the *Saccharomyces* genome database (SGD) [332]. H99 sequences were mapped to the *C. neoformans* var. *grubii* H99 CNA3 and mitochondrial reference genomes (Assembly 2, ver. 29/07/2013) from the Broad institute of Harvard and MIT (<http://www.broadinstitute.org/>). 97/170 sequences were mapped to the 97/170 genome, which was sequenced.

HTSeq (ver. 0.5.3p9) was used to count the number of reads that mapped to a gene on the reference genome. This program pre-processes RNA-Seq data for differential expression analysis by counting the overlap of aligned reads on exons of a gene [368]. The general feature format (GFF) that contains the coordinates of each gene on each chromosome of the *S. cerevisiae* genome was downloaded from SGD and converted to the gene transfer format (GTF) using a custom Perl scripts for HTSeq. For *Cryptococcus*, transcripts.fasta and transcripts.gtf files, which contain the position of the genes on each chromosome, were used. The parameters '-s no -m union -t CDS -i gene_id' were used, where reads were mapped to the coding sequence (CDS) regardless of the strand and only counted if they aligned unambiguously to a CDS. Genes with low raw read counts were removed and only genes with seven counts per million for at

least six samples were kept for analysis. For S288C, H99 and 97/170 sequences, a 99% median correlation was observed for counts per gene between biological triplicates, indicating high reproducibility. The counts were then used for gene level differential expression analysis using the Empirical analysis of digital gene expression data in R (EdgeR; ver. 3.2.8) software.

To correct for technical biases introduced during the RNA-Seq procedure and to allow for accurate estimation and detection of differential gene expressions and analysis, normalisation was applied. Each sample was first normalised to the size of the library with the statistical package in EdgeR using the 'cpm' (counts per million) function, such that the expected size of each count is the product of the library size and the relative abundance of that gene in an analysed sample. The RNA-Seq lane effect was normalised as part of the generalised linear model parameter. Negative binomial distribution was used to model transcript counts by distinguishing biological (due to expression levels between experimental samples) and technical (associated with sequencing technology) variance across the samples. This was then used to infer the biological coefficient variance (BCV), which is estimated by the square-root of the dispersion parameter for the negative binomial distribution [369]. The similarity of biological replicates for each treatment was analysed by multiple dimension scaling (MDS), where the distances between samples correspond to the average of the largest absolute log fold change between each pair of samples.

4.2.4.3. Generating differentially expressed transcripts from the effects of synergistic and antagonistic drug treatments

To determine the effect of drug synergy and antagonism on the yeast transcriptome, the averaged differential gene expression of untreated controls were subtracted from their respective drug treatments. These were labelled T_A (treatment with AMB only; AMB – CA) and T_{AL} (treatment with AMB+LF; AMB+LF – CAL) in synergy, and T_V (treatment with VRC only; VRC-C) and T_{VE} (treatment with VRC+EDTA; VRC+EDTA – C) in antagonism experiments. The Benjamini-Hochberg algorithm [370] was applied to filter out genes falsely differentially expressed, using the cut-off p-value of < 0.05.

4.2.4.4. Self-organising maps (SOMs)

The differentially expressed genes in T_A and T_{AL} were analysed independently using two SOMs, (Kohonen package, ver. 2.0.15) which uses an unsupervised learning algorithm to group similar data points from high dimensional data sets and visualises it in lower dimensional representations. This type of artificial neural network (also known as Kohonen maps or networks) clusters genes with close expression profiles

into individual cells, and then organises the cells across the map based on cell-to-cell similarity [371, 372].

The log normalised read counts from EdgeR were further scaled to log reads per kilobase per million (rpkm) by subtracting the log of the gene length. The log rpkm values across the 12 samples per gene were transformed to a mean of 0 and standard deviation of 1 across all samples with Pareto scaling from the 'genefilter' library (ver. 1.46.1). Each SOMs was generated using the R statistical computing environment (ver. 3.1.1) [373] and the normalised data were clustered into a 5 x 5 grid using the 'som' function. The groups converged after 100 iterations of the learning algorithm. The maps were then visualised using custom R scripts and the 'lattice' package, and the clusters were labelled numerically starting from the bottom left to the top right cluster. A heat map was generated for each SOMs to present the average expression pattern for each cluster to provide an overview of the SOMs.

4.2.4.5. Gene ontology (GO) enrichment analysis

Significantly up and down-regulated genes in each treatment and model were analysed for enrichment of GO terms. Co-expressed genes within each of the SOMs cells were likewise analysed. The analysis of differentially expressed S288C and H99 genes was performed with the GOstats package (ver. 2.30.0) from the R statistical computing software (ver. 3.1.1) [373]. The GO annotations used for S288C were from org.Sc.sgd.db (ver. 2.14.0) and GO.db (ver. 2.14.0) package. For H99, GO annotations were compiled from multiple sources to improve GO coverage and quality. 97/170 GO annotations were reciprocal blasted against the improved H99 GO annotations to identify homologous proteins with one-to-one sequence matches using custom scripts to run BLAST+ [374], using the Blastp option. Statistics for GO enrichments were calculated in R using a 'GOstats' library (ver. 2.29.2) [375]. GO terms for S288C were biased for child terms to enable detailed analyses, and were retrieved by Fisher's exact test at a p-value < 0.05. Significant child GO terms that appeared with their significant parent term were filtered out to ensure the significance of child terms was not biasing the parent GO terms. For H99 and 97/170, only the parent GO terms were used. The Benjamini-Hochberg algorithm [370] from the multtest package (ver. 2.19.2) [376] was then used to adjust for false discovery rates and significance of GO terms were considered at a p-value < 0.01. GO terms containing only one gene were removed from the analysis. GO analysis was also cross-checked with YeastMine [345] using Benjamini-Hochberg at a p-value of < 0.05.

To improve the coverage and quality of GO annotations from the *C. neoformans* genome, UNSW colleagues Igy Pang and Nandan Deshpande compiled GO annotations from Uniprot (accessed 09/02/2015) [377] and QuickGO [378] (unpublished). OrthoMCL [379] was used to find orthologous *C. neoformans* proteins with one-to-one sequence matches in other fungal species, including *S. cerevisiae*, *Aspergillus fumigatus*, *Schizosaccharomyces pombe* and *Agaricus bisporus*. Blast2GO (ver. 3, database ver. B2g_sept2014) [380] was also used to search for homologous *C. neoformans* proteins from the Broad Institute against the NCBI non redundant (NR) sequence database using the Blastp option [374]. GO terms that were not previously found in the databases of fungal species mentioned above, including *C. neoformans*, were removed from the Blast2GO output. All GO term annotations from Uniprot, QuickGO, OrthoMCL and Blast2GO were merged into a single table. Duplicated protein entries were removed and the resulting list was used for GO enrichment analysis. All analyses were performed using custom Python scripts. The databases used for each organism, websites and dates accessed are listed below:

- *C. neoformans* protein sequences (accessed 03/2014):
https://www.broadinstitute.org/annotation/genome/cryptococcus_neoformans/MultiDownloads.html
- Uniprot *C. neoformans* GO annotations (accessed 09/02/2015):
<http://www.uniprot.org/uniprot/?query=taxonomy:235443>
- QuickGO (accessed 07/05/2015):
QuickGO: <http://www.ebi.ac.uk/QuickGO/GAnnotation?tax=235443>
- *S. cerevisiae* GO annotations (accessed 06/05/2015):
http://downloads.yeastgenome.org/curation/literature/gene_association.sgd.gz
- *S. pombe* GO annotations (accessed 06/05/2015): <http://www.pombase.org/downloads/go-associations>
- *A. fumigatus* GO annotations (accessed 06/05/2015):
<http://www.aspergillusgenome.org/download/go/>
- *A. bisporus* GO annotations (accessed 06/05/2015): http://genome.jgi-psf.org/cgi-bin/ToGo?accession=all&species=Agabi_varbisH97_2&batchId=Agabi_varbisH97_2-159

Non-redundant (NR) protein sequences were from GenPept, Swissprot, PIR, PDF, PDB and NCBI RefSeq (accessed 21/01/2015): <ftp://ftp.ncbi.nlm.nih.gov/blast/db/>

4.2.4.6. Analysis of biological networks

For network analysis, selected pathways were mapped and visualised in the open source software Cytoscape (ver. 3.1.1) [381]. Regulatory data for transcription factors and target genes, which were identified from ChIP-Seq studies or from transcript changes in gene deletion studies, were downloaded from Yeasttract (accessed 27/09/2013) and the ranking of transcription factors based on their connectivity to differentially expressed genes was performed using TFRank with a heat diffusion coefficient of 0.25 [382]. Protein-protein interactions were obtained from Pang *et al.* (2012) [383] and genes in selected pathways were further curated with literature searches and in the Kyoto Encyclopedia of Gene and Genomes (KEGG) and YeastCyc biochemical pathway databases [332, 384]. Log fold-changes from the differential expression analysis were co-visualised as node colours.

4.2.5. Validation of transcriptomic data in *S. cerevisiae*

To validate the transcriptomic data in S288C, knock-out mutants of chosen genes were obtained from the Yeast Deletion Project collection [341], which was provided by the Wilkins Lab in UNSW. This collection contains a near complete set of deletion strains and allows the functions of characterised genes and many uncharacterised ORFs in the S288C genome to be analysed through phenotypic characterisation of the knock-out mutants. The knock-out collection was generated in the background strain BY4741 with the genotype *MAT α ura3 Δ 0 leu2 Δ 0 his3 Δ 1 met15 Δ 0*.

4.2.5.1. PCR confirmation of knock-out mutants

Knock-out mutants were confirmed with PCR primers using primer combinations A-B, A-KanB, A-NatB, KanC-D, NatC-D and A-D that were designed for each selected gene (Fig. 4.2; Appendix 4.2). KanB and KanC are primers designed from the kanamycin selection marker and NatC and NatD were designed from the nourseothricin marker. Amplification of bands using primers A-KanB and KanC-D was required for knock-out confirmation. Where bands were not amplified with either of primer A-KanB or KanC-D combinations, amplification of expected band sizes from primers A-D served as knock-out confirmation. Additionally, primers A-B were used to amplify DNA sequences from the wild type strain BY4741 to confirm gene identity [341]. PCR conditions were performed as specified in the Yeast Deletion Project, where reaction mixtures contained 10 x *Taq* reaction buffer, 2.5 U *Taq* polymerase, 0.2 mM of mixed dNTPs, and 5 μ L genomic DNA (1 ng – 1 μ g) in a final volume of 50 μ L. Forward (A, KanC or NatC) and reverse (B, KanB, NatB or D) primers were added at a final concentration of 1 μ M to the reaction mixture for the region of amplification desired. Amplifications were performed by an initial denaturation

of 94 °C for 3 min, followed by 35 cycles of 94 °C for 15 sec, 57 °C for 15 sec and 72 °C for 60 sec, with a final extension of 72 °C for 3 min. For *cch1Δ*, the annealing temperature in the 35 cycles was lowered to 50 °C, with an extension time of 7 min.

4.2.5.2. Knock-out cassette construction

As one of the chosen genes, *YOR387C*, was not present in the *Saccharomyces* gene deletion library, gene deletion was performed by homologous recombination in the wild type strain BY4741 using a modified protocol from Janke *et al.* (2004) [385]. A double deletion of *YOR387C* in the *vel1Δ* mutant was also created as *VEL1* shares 93% homology with *YOR387C*. The plasmid cassette pFA6a-natNT2 with a selection marker for nourseothricin was provided by the Wilkins Lab. PCR primers were designed to encompass 45-55 bp before and after the *YOR387C* ORF, inclusive of the start and stop codons. Each primer contained a sequence at the 3' end that was homologous to the selection marker cassette within the plasmid (see Fig. 4.3). The primers were designated *yor387c_S1* and *yor387c_S2*, with the sequences outlined in Appendix 4.2.

The *YOR387C* gene deletion construct was made in a 50 μL reaction mixture containing LongAmp™ *Taq* 2 X master mix, 10 μM of each *yor387c_S1* and *yor387c_S2* primer, and 1 μL (100 ng) of the selected plasmid cassette DNA. Amplification conditions were performed with an initial denaturation of 94 °C for 3 min, followed by 30 cycles of 94 °C for 30 sec, 54 °C for 30 sec and 65 °C for 4 min, with a final extension of 65 °C for 10 min.

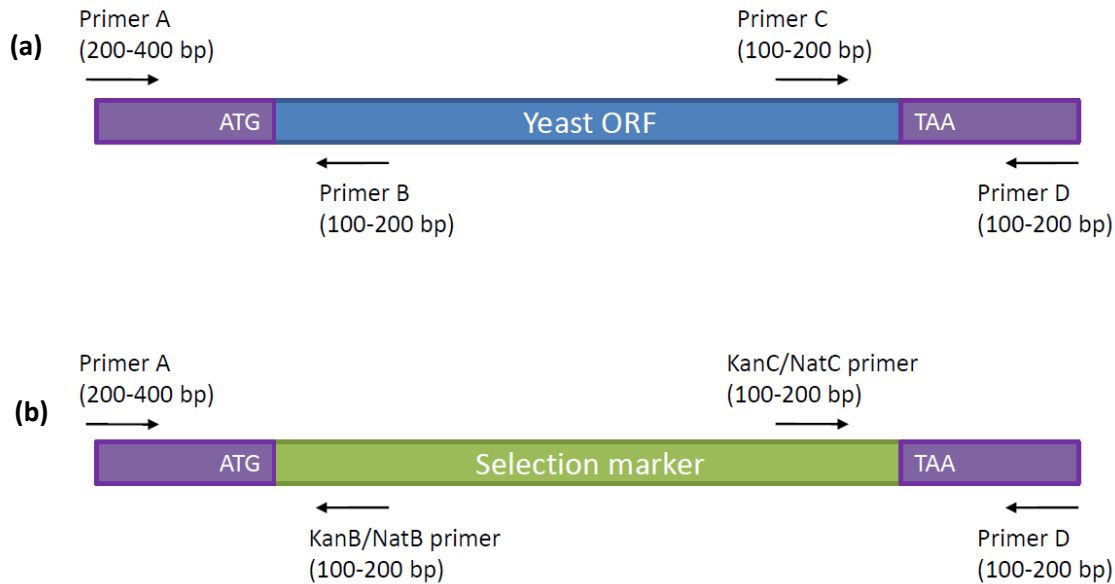


Figure 4.2. Primers designed to confirm gene deletions. Primers A and D were designed from sequences 200 – 400 bp before and after the yeast ORF or selection marker. Primers B, C, KanB, KanC, NatB and NatC were designed from sequences 100-200 bp from the ends of the yeast ORF and selection marker, to amplify with primers A and D. **(a)** Primer sets A-B, C-D and A-D will amplify bands in the DNA of wild-type cells while A-KanB/NatB and KanC/NatC-D will not. **(b)** DNA of mutants with successful gene deletions by replacement with the selection marker will have amplification bands from primer sets A-KanB/NatB and KanC/NatC-D, but not with A-B and C-D. Adapted from Kelly *et al.* (2001) [341].

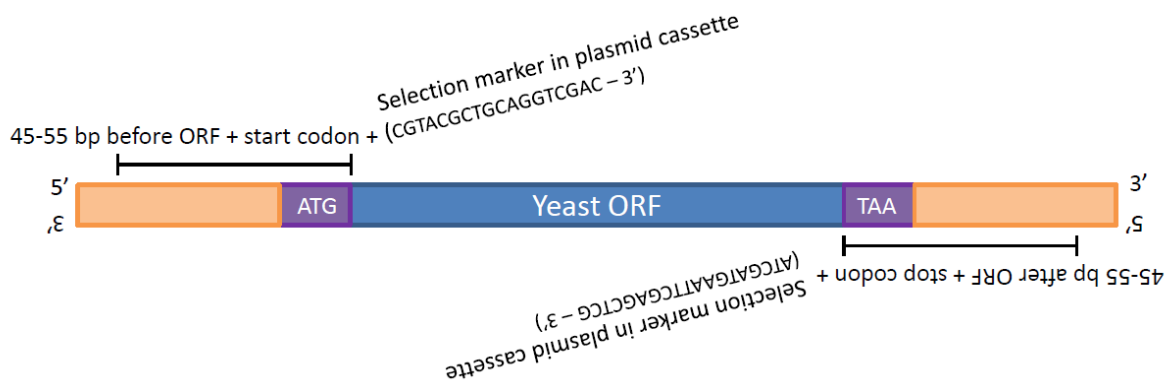


Figure 4.3. Primer design for cassette construction and gene deletion. Primers were designed to stitch the selection marker from the plasmid cassette with homologous sequences upstream and downstream from the ORF of interest. From 5' to 3' direction, primers included sequences 45-55 bp upstream of the start/stop codon, plus the start/stop codon and the sequence of the selection marker as indicated in the diagram. Adapted from Janke *et al.* (2004) [385].

4.2.5.3. Transformation of *S. cerevisiae* with knock-out constructs

Five microlitres of the constructed plasmid cassette DNA was transformed into the *S. cerevisiae* wild type BY4741 and *vel1Δ* (KanMX4 marker, BY4741 background) strains using a LiAc/SS-DNA transformation protocol [386] with slight modifications. Briefly, a 5 mL culture of BY4741 was grown overnight in Sabouraud dextrose broth (SDB) at 30 °C, with shaking at 180 rpm. The overnight yeast culture was used to inoculate 50 mL of pre-warmed SDB at a starting concentration of 5×10^6 cells/mL. The culture was grown at 30 °C, 200 rpm, until it reached 2×10^7 cells/mL indicating at least two rounds of cell division. 10 mL of the culture was pelleted at 4,000 rpm for 5 min, washed with 25 mL of sterile water and re-centrifuged. The pelleted cells were resuspended in 1 mL of sterile 100 mM LiAc, centrifuged again at top speed for 40 sec and resuspended in 100 mM LiAc, giving a final cell concentration of approximately 2×10^9 cells/mL in a final volume of 500 μ L. 50 μ L of the cell suspension was aliquoted into four separate eppendorf tubes (for the three replicates and one control), pelleted and the LiAc solution removed. Transformation reagents were then added in the following order to a total volume of 360 μ L: 240 μ L of PEG (50% w/v), 36 μ L of 1 M LiAc, 25 μ L of pre-boiled and chilled SS-DNA (4 mg/mL), plasmid DNA (100 ng – 1 μ g, volume not to exceed 10% of total volume) and sterile distilled water. Water was added in place of plasmid DNA as a negative control.

Each tube was vortexed until the cell pellets were resuspended, before incubation at 30 °C for 30 min. Cells were then heat shocked for 30 min at 42 °C and centrifuged at 7,000 rpm for 90 sec. The transformation mix was removed and transformed cells were incubated overnight at room temperature in 200 μ L SDB before selecting mutants on SDA plates supplemented with 100 μ g/mL nourseothricin. Plates were incubated at 30 °C for up to 5 days. Knock-out mutants were confirmed using the primers outlined above (Section 4.2.5.1; Fig. 4.2, Appendix 4.2).

4.2.6. Spot plate assays

To test the phenotype of the knock-out mutants, spot plate assays were performed on synthetic complete (SC) media with a variety of stressing agents. Overnight broth cultures of knock-out mutants were grown in 5 mL SC broth in a shaking incubator at 30 °C, 180 rpm. Cell concentrations were standardised at 1×10^6 cells/mL with a haemocytometer and dilutions were made from 10^6 to 10 cells/mL. Five microlitre aliquots of each dilution were spotted onto 25 mL SC plates supplemented with stressing agents at the following concentration ranges: AMB from 0.25 – 1 μ g/mL, FLC from 16 – 64 μ g/mL, calcofluor white from 100 – 200 μ g/mL, congo red from 100 – 300 μ g/mL, SDS from 0.005 –

0.02% (w/v), salt (NaCl) at 1 M, sodium nitrite (NaNO₂) from 1 – 3 mM, hydrogen peroxide (H₂O₂) from 1 – 3 mM, caffeine from 10 – 15 mM. Plates were left to dry and were incubated at 30 °C. Growth was checked every day until the 5th day.

4.2.7. Rescue assays

Rescue iron assays performed in Chapter 3 (3.2.6) showed that low concentrations of iron did not disrupt AMB+LF synergy and were unable to rescue cell growth (Fig. 3.4). To understand the effect of iron addition at higher concentrations, rescue assays were once again performed, along with zinc, calcium, and BAPTA, in the presence of different concentrations of AMB+LF. The concentrations tested were determined by preliminary screens, unless specified. Iron (III) chloride and iron (II) sulphate were tested from 0.3 – 80 µg/mL, zinc chloride from 0.25 – 64 µg/mL, calcium chloride from 1.5 – 400 µg/mL, BAPTA from 1.5 – 400 µg/mL. The concentrations of AMB and LF tested encompassed the FIC with the following combinations (AMB, LF): (0.015, 0.5), (0.015, 1), (0.03, 2; the FIC), (0.06, 4) and (0.06, 8) µg/mL. AMB+LF combinations were made together at 4 x the final concentration. Similarly, AMB and LF were prepared separately at 4 x their MIC, and each rescue agent was prepared at 4 x the final concentration.

Rescue assay plates were set up as follows: serial doubling dilutions of the rescue agent were aliquoted from columns 11 to 3 in 50 µL volumes. Column 12 was designated as the positive growth control and column 1 was the negative growth control. Row A tested the effect of the rescue agent alone on yeast growth, and included 50 µL of media in the place of 50 µL of AMB+LF. 50 µL of each of the AMB+LF concentrations was aliquoted into each well from row B to F, from column 11 to 2. Column 2 tested the individual effects of the different concentrations of AMB+LF as well as AMB and LF alone on growth and included 50 µL of media in place of rescue agents. Row G and H contained 50 µL of MIC levels of AMB alone and LF alone, respectively.

Cell inoculations were performed as outlined in the MIC protocols (Section 3.2.3). Assays were incubated for 48 hr and growth or no growth was recorded by visual observation.

4.3. Results

4.3.1 Effect of AMB, LF and AMB+LF on the growth of *S. cerevisiae* S288C and *C. neoformans* H99

Growth curves of S288C and H99 treated with AMB+LF at concentrations causing synergy, and with AMB or LF alone at their respective FIC concentrations, were performed to determine the ID₂₀ for RNA extraction and sequencing (Fig. 4.4). Growth curves clearly differed between the cultures treated with AMB+LF and AMB alone after three hours of drug exposure (Fig 4.4a and 4.4c). Treatment with LF at 2 µg/mL did not inhibit the growth of S288C or H99, and an ID₂₀ could not be determined even when LF treatment was extended to 24 hrs (Fig. 4.4b and 4.4d). Note that these assays were more favourable for fungal growth than the plates used for MIC testing as they were performed in large culture volumes with shaking, and the level of inhibition therefore differs somewhat to what was seen in the checkerboard assays.

In S288C, the ID₂₀ for AMB+LF occurred between 45 min and 1 hr, and the ID₂₀ for AMB was at 1 hr (Fig. 4.4a). With increasing time of exposure, the drug treatments progressively inhibited cell growth, with AMB+LF inhibiting growth to a significantly greater extent than AMB (Table 4.1, Fig. 4.4b). In H99, a similar ID₂₀ was seen in the AMB+LF and AMB treatments (Fig. 4.4.c), however, the extended growth curve was quite different with inhibition by AMB essentially lost at 24 hr (Table 4.1, Fig. 4.4d). AMB+LF continued to inhibit growth to a greater extent than AMB alone but did not inhibit H99 to the extent seen in S288C (Fig. 4.4b and 4.4d). For RNA-sequencing, RNA was extracted at 50 min for AMB+LF treatment (along with the untreated control at the same timepoint) and 1 hr for AMB treatment (with an untreated 1 hr control) for both S288C and H99.

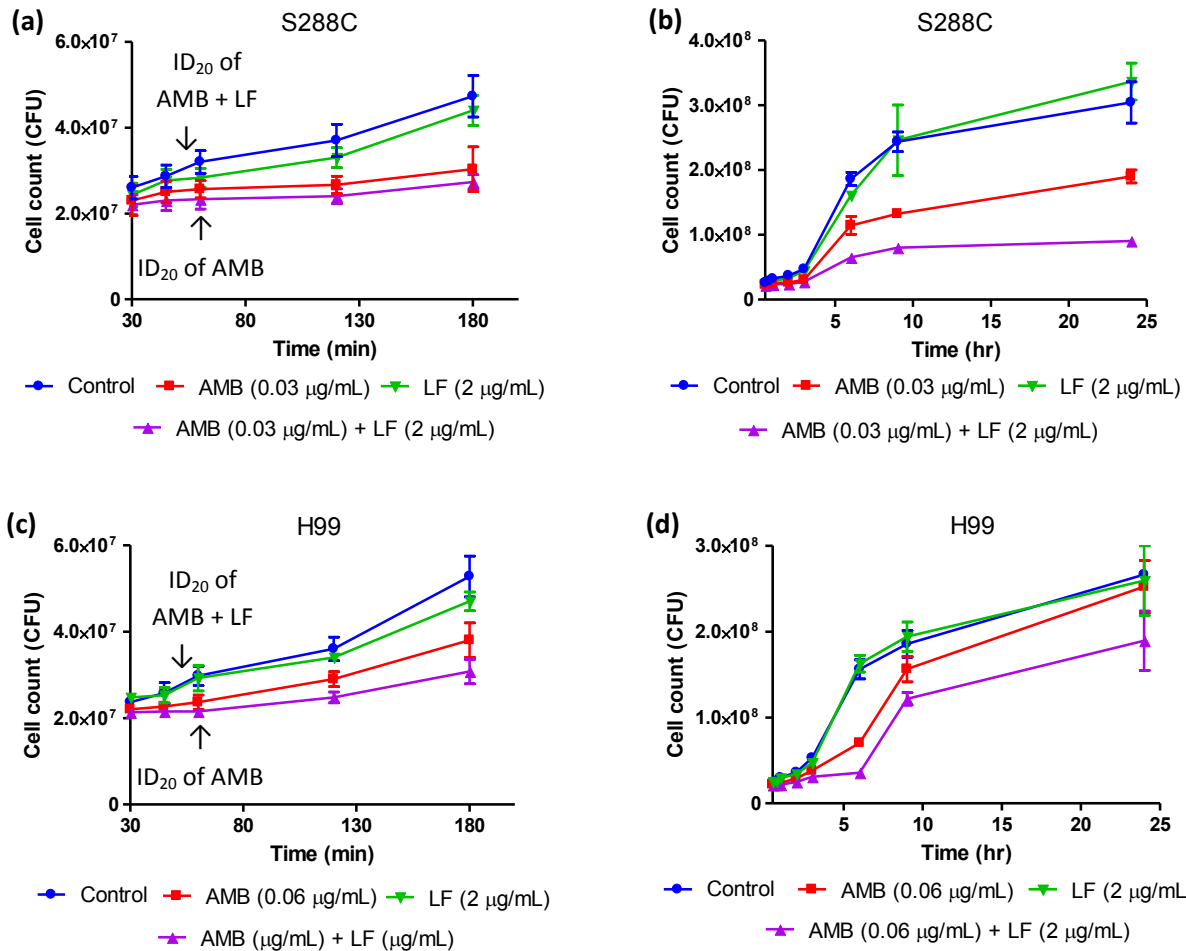


Figure 4.4. The effect of AMB+LF, AMB, and LF on the growth of *S. cerevisiae* S288C and *C. neoformans* H99. **(a)** and **(c)** First 3 hours of drug treatment. ID₂₀ occurred at 50 min for AMB+LF and 1 hr for AMB treatment. **(b)** and **(d)** Growth curves extended for 24 hr. LF at 2 μg/mL did not inhibit S288C or H99 growth throughout 24 hr of treatment, while AMB and AMB+LF provided sustained inhibition, particularly of S288C. Data is shown as mean +/- standard error of the mean (SEM).

Table 4.1. Percent reduction in growth relative to untreated controls at selected timepoints for AMB and AMB+LF treatment in *S. cerevisiae* S288C and *C. neoformans* H99

| Organism | Treatments | 30 min | 45 min | 1 hr | 2 hr | 3 hr | 6 hr | 9 hr |
|--------------|---------------|--------|--------|------|------|------|------|------|
| S288C | AMB | 11% | 12% | 20% | 28% | 36% | 38% | 46% |
| | AMB+LF | 15% | 18% | 26% | 35% | 40% | 65% | 67% |
| H99 | AMB | 7% | 12% | 20% | 27% | 24% | 26% | 24% |
| | AMB+LF | 10% | 17% | 28% | 37% | 47% | 36% | 47% |

4.3.2. Analysis of RNA-Seq data

4.3.2.1. Data quality control for RNA-Seq analysis

The accuracy and quality of RNA-Seq reads were analysed with FastQC (ver. 0.10.1) and SolexaQA (ver. 2.2). There were on average 9.95 million reads per sample with a coverage of approximately 80x. Sequences had a median Spearman correlation of 0.99 for raw gene counts between biological replicates, indicating high experimental reproducibility. A total of 5,456 transcripts were identified in S288C, while 6,810 transcripts were identified in H99.

For S288C samples in synergy experiments, the average biological coefficient variance (BCV) was 0.0987 (about 10%) (Fig. 4.5b), indicating low variability between biological replicates, which is normally observed in model organisms [387]. Biological replicates of each drug treatment grouped together in MDS, indicating similar gene expression profiles (Fig. 4.5a). However, sample 1B from the AMB control (CA) clustered with the AMB+LF control (CAL) samples, and vice versa for sample 8A. To determine if samples 1B and 8A should be swapped to where they should cluster, i.e. corrected, kept without swapping, or deleted, a list of differentially expressed transcripts was first generated to then compare the number of differentially expressed genes for each drug treatment (detailed in Section 4.3.2.2). Not swapping the positions of 1B and 8A caused a drastic reduction in the gene counts for both drug treatments, while deletion of both samples caused a minor increase in the gene counts in AMB treated cells and a decrease in AMB+LF treated cells (Table 4.2). Based on these results it was assumed that these samples had been inadvertently mixed up and they were swapped to be where they clustered by MDS.

For AMB and AMB+LF treatment, the log-fold changes of individual genes relative to their expression in their respective controls (CA and CAL) were plotted against their log-concentrations, to give a ratio of expression levels against the overall averaged expression level (Fig. 4.5c – d). Genes with low counts are shown in black and differentially expressed genes are in red. Comparison of genes expressed following AMB (Fig. 4.5c) and AMB+LF treatment (Fig. 4.5d) shows that differential expression was greater following AMB+LF treatment.

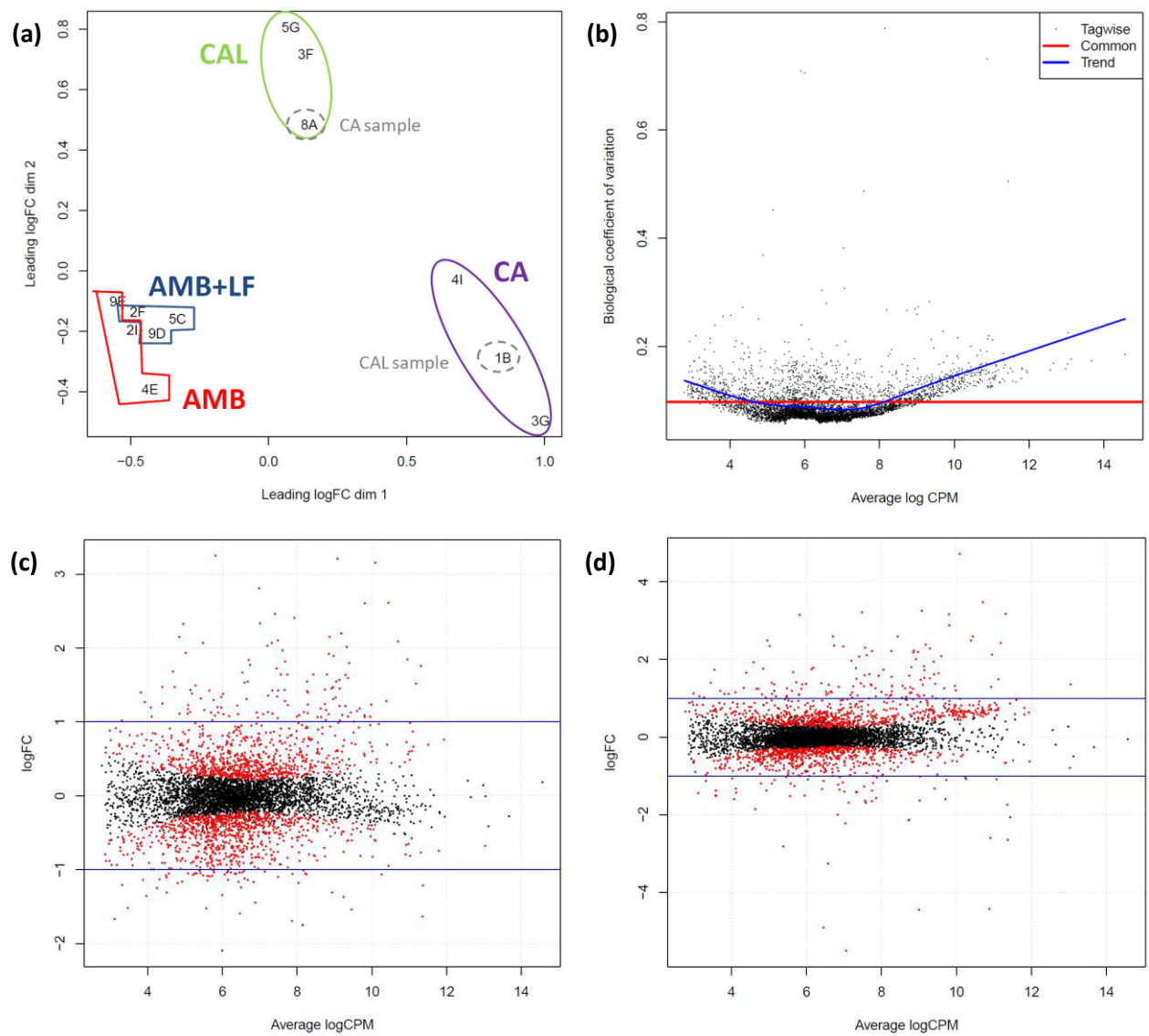


Figure 4.5. RNA-Seq analyses of *S. cerevisiae* S288C samples. **(a)** MDS plot of all RNA-Seq samples after normalisation with EdgeR. Biological replicates of each drug treatment have similar gene expression profiles and cluster together as outlined, except for samples 1B and 8A. **(b)** BCV versus average \log_2 counts per million (CPM) of RNA-Seq samples. The red line represents the common dispersion of all genes while the blue line represents the trended dispersion of all genes. Each dot is a data point that represents the tag-wise dispersion of each gene. **(c)** Smear plot of \log_2 fold change (FC) versus the average \log_2 CPM values of genes in the AMB treatment. **(d)** Smear plot of \log_2 FC versus the average \log_2 CPM values of genes in the AMB+LF treatment. For **(c)** and **(d)**, differentially expressed genes are represented in red and the blue lines are drawn at 2-fold changes in expression.

Table 4.2. Comparison of gene counts when *S. cerevisiae* S288C RNA samples 1B and 8A were swapped, not swapped or deleted

| | Gene expression | 1B and 8A with swapping | 1B and 8A with no swapping | 1B and 8A deletion |
|----------|-----------------|-------------------------|----------------------------|--------------------|
| T_A | Up-regulated | 907 | 474 | 946 |
| | No fold change | 3628 | 4613 | 3600 |
| | Down-regulated | 921 | 369 | 897 |
| T_{AL} | Up-regulated | 748 | 302 | 675 |
| | No fold change | 4019 | 4961 | 4308 |
| | Down-regulated | 689 | 193 | 460 |

Although treatment with LF alone did not cause growth inhibition (Fig. 4.4), RNA-Seq analysis was subsequently performed to investigate whether the FIC of LF caused changes to the yeast transcriptome (Fig. 4.6). Three separate clusters are seen in the MDS plot (Fig. 4.6a), which represent the three biological replicates of LF treatment and the untreated control. The smear plot in Figure 4.6b shows that no genes were differentially expressed between LF and the untreated control. The BCV of LF samples are presented in Appendix 4.3. As there was no apparent transcriptional response to LF alone, the analysis of synergy between AMB+LF was restricted to the comparison between AMB and AMB+LF treatment.

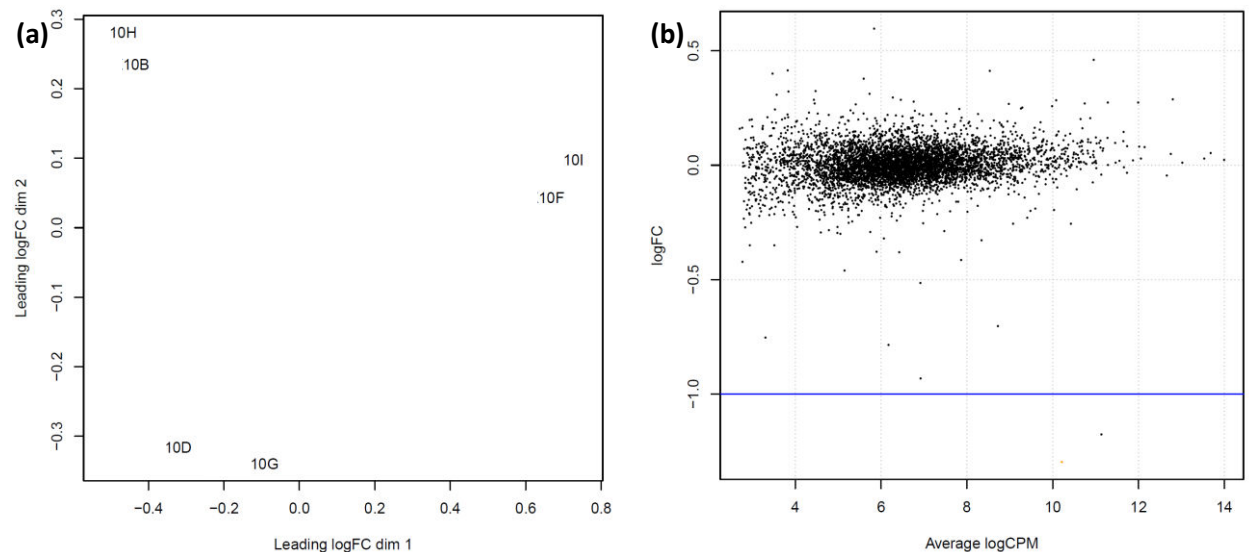


Figure 4.6. RNA-Seq analysis of LF treatment only. **(a)** MDS plot of LF treatment and its untreated control. Biological replicates of treatments and control samples grouped together. **(b)** Smear plot of \log_2 fold change (FC) versus the average \log_2 CPM values of genes in the LF treatment. An absence of red dots indicates there was no change in log-fold expression of any genes.

For H99, PCA plots clustered the samples better than MDS and identified sample 5A as an outlier (Fig. 4.7a). The effects of deleting 5A on the counts of differentially expressed genes in AMB and AMB+LF treatment was investigated. Deletion of this sample increased the number of genes in AMB treatment, while little change was observed in AMB+LF treatment (Table 4.3). The averaged BCV improved from 0.2179 to 0.1511 with 5A deletion (Fig. 4.7b, Appendix 4.4) and subsequent analyses were performed without this sample. The plots of gene fold-changes of AMB and AMB+LF treatment were highly similar, with AMB+LF treatment having more differentially expressed genes at log fold changes above six (Fig. 4.7c and d).

4.3.2.2. Comparison of differentially expressed genes in *S. cerevisiae* S288C and *C. neoformans* H99

AMB and AMB+LF treatment affected the growth of cells differently and cultures reached ID₂₀ at different timepoints (Fig. 4.4). As ID₂₀ was used for RNA-Seq, the differences in the time of RNA isolation is likely to result in changes in the transcriptomes between AMB and AMB+LF treatment that are due to factors other than drug treatment. Each single and combined drug treatment therefore needed its own control, i.e., CA and CAL, respectively, to allow a comparable analysis. A list of transcripts that were differentially regulated due to AMB and AMB+LF treatment was then generated by subtracting genes that were expressed under AMB with those expressed in its control CA (defined as T_A, where T stands for transcripts), and AMB+LF with CAL (defined as T_{AL}).

A comparison of the number of differentially expressed genes from the two yeast species is shown in Table 4.4. In S288C, T_A had 906 and 921 up- and down-regulated genes, respectively, while T_{AL} had 748 up-regulated genes and 689 down-regulated genes. In H99, T_A had 1677 and 1615 up- and down-regulated genes, respectively and T_{AL} had 1678 up-regulated genes and 1474 down-regulated genes. In S288C around 15% of genes encoded putative proteins or proteins with unknown function, whereas about a third of the transcripts in H99 encoded uncharacterised proteins, even when annotations were taken from other fungal species. This likely reflects differences in annotation between the two yeast genomes. Approximately 50% and 60% of genes were differentially expressed from the total number of transcripts identified for S288C and H99, respectively.

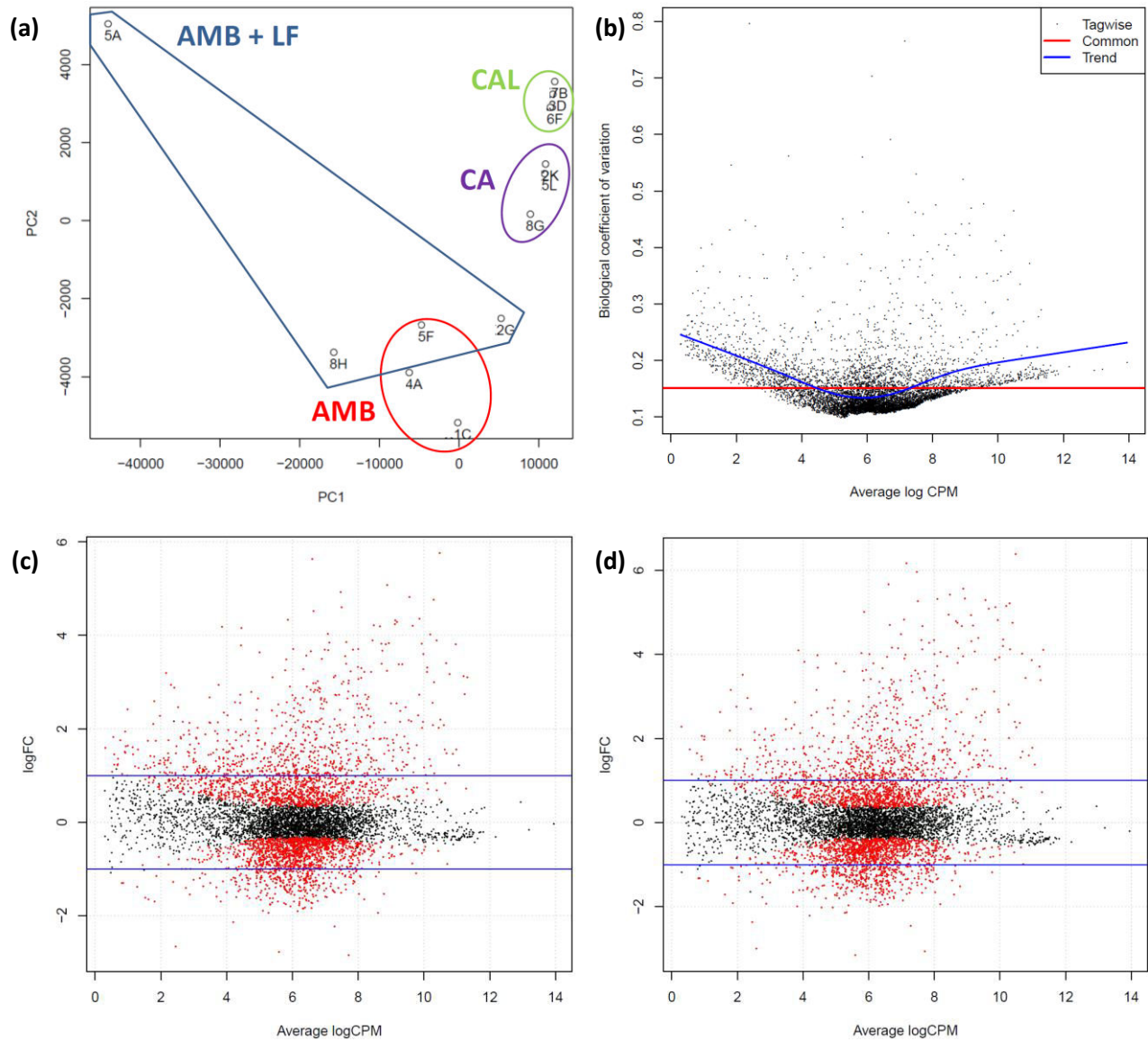


Figure 4.7. RNA-Seq analyses of *C. neoformans* H99 samples. **(a)** PCA plot of all RNA-Seq samples after normalisation with EdgeR. Biological replicates clustered together as circled, showing 5A as an outlier. **(b)** BCV versus average log₂ CPM with 5A deletion. The red line represents the common dispersion of all genes while the blue line represents the trended dispersion of all genes. Each dot is a data point that represents the tag-wise dispersion of each gene. **(c)** Smear plot of log₂ fold change (FC) versus the average log₂ CPM values of genes in AMB treatment with 5A deletion. **(d)** Smear plot of log₂ FC versus the average log₂ CPM values of genes in AMB+LF treatment with 5A deletion. For **(c)** and **(d)**, differentially expressed genes are represented in red and the blue lines are drawn at 2-fold changes in expression.

Table 4.3. *C. neoformans* H99 gene count comparison with and without RNA sample 5A

| | Gene expression | With 5A | Without 5A |
|-----------------------|------------------------|----------------|-------------------|
| T_A | Up-regulated | 1103 | 1677 |
| | No fold change | 4894 | 3517 |
| | Down-regulated | 819 | 1615 |
| T_{AL} | Up-regulated | 1694 | 1678 |
| | No fold change | 3576 | 3658 |
| | Down-regulated | 1546 | 1474 |

Table 4.4. Comparison of differentially expressed genes in *S. cerevisiae* S288C and *C. neoformans* H99 in response to the two drug treatments

| Differentially expressed genes | T_A | | T_{AL} | |
|---|----------------------|------------|-----------------------|------------|
| | S288C | H99 | S288C | H99 |
| Total number | 1828 | 3293 | 1437 | 3152 |
| Up-regulated | 907 | 1677 | 748 | 1678 |
| Down-regulated | 921 | 1615 | 689 | 1474 |
| Protein of unknown function | 97 | – | 63 | – |
| Putative protein | 192 | – | 163 | – |
| Uncharacterised protein | – | 1430 | – | 1350 |
| Unique to treatment – Up-regulated | 532 | 244 | 320 | 241 |
| Unique to treatment – Down-regulated | 630 | 331 | 451 | 192 |

4.4. Results – Analysis of the transcriptome of drug synergy in *S. cerevisiae* S288C

4.4.1. GO enrichments of differentially expressed S288C genes in T_A and T_{AL}

GO enrichment was performed to analyse the changes in transcript expression induced in synergy by comparing the expressions caused by AMB+LF treatment to the expressions observed in AMB treatment alone. As seen in Table 4.5, the GO enrichments between the two drug treatments were distinctly different. Treatment with AMB down-regulated GO terms related to DNA synthesis, RNA processes and cellular component biogenesis, and up-regulated GO terms involved energy production-related processes such as the tricarboxylic acid (TCA) cycle, electron transport and redox. Other up-regulated GO terms include degradation processes including mitophagy and the cytoplasm to vacuole transport (CVT) pathway, processes related to metal ion homeostasis, especially iron homeostasis, and stress such as trehalose biosynthesis [388] and hydrogen peroxide catabolism. These enrichments suggest a reduction in DNA replication and protein production, and an increased requirement for energy, possibly for the degradation of intracellular organelles to survive AMB treatment [389].

For T_{AL}, down-regulated GO terms were related to post-translational modifications like ubiquitination and lipid biosynthesis. Stress related processes such as endoplasmic reticulum (ER) and oxidative stress were also down-regulated, in contrast to T_A. Amino acid synthesis, translation and ribosome biogenesis GO terms were up-regulated in AMB+LF treatment, suggesting the cells are not sensing and responding to the toxic stress of AMB when LF is present and are continuing to switch on growth-related terms. Despite the chelating properties of LF, terms related to metal ion homeostasis were not enriched.

Table 4.5. Selected gene ontology term enrichments of differentially expressed transcripts in *S. cerevisiae* S288C for T_A and T_{AL}

| GO Terms | Transcriptome responses to drug treatments and odds ratio ^a | | | |
|---|--|---|-----------------|---|
| | T _A | Genes in enrichment | T _{AL} | Genes in enrichment |
| DNA synthesis related | | | | |
| Nucleobase metabolic process | 5.68 | AAH1, ADE2, ADE4, ADE5,7, ADE8, APT1, MTD1, URA1, URA3, URA4, URA5, URA6, URA7, URA8, XPT1 | | |
| Positive regulation of transcription from RNA polymerase I promoter | 4.38 | CDC37, NAN1, UTP10, UTP15, UTP4, UTP5, UTP8, UTP9 | | |
| Purine ribonucleoside monophosphate biosynthetic process | 3.18 | AAH1, ADE1, ADE17, ADE2, ADE4, ADE5,7, ADE6, ADE8, ADK2, PMA1, XPT1 | | |
| Pyrimidine ribonucleoside monophosphate biosynthetic process | 9.02 | DAS2, FUR1, URA1, URA3, URA4, URA5 | | |
| Amino acid related | | | | |
| Cellular amino acid metabolic process | 3.69 | 69 genes | 8.44 | 51 genes |
| Positive regulation of cellular amino acid metabolic process | | | 10.32 | DAL81, LEU3, LYS14, PUT3 |
| Amino acid transmembrane transport | 6.25 | AGP1, AGP2, ALP1, ATG22, AVT4, AVT6, BAP2, BAP3, BIO5, CAN1, DIP5, GAP1, GNP1, PUT4, RTC2, TAT2 | 11.83 | AGP1, ALP1, AVT1, BAP2, BAP3, CAN1, DIP5, GAP1, GNP1, HNM1, LYP1, PUT4, TAT1, TAT2, UGA4 |
| Protein related | | | | |
| Regulation of translation fidelity | | | 7.81 | CDC60, ILS1, RPL31A, RPL31B, RPS23A, RPS23B, RPS5, VAS2, YHR202W |
| Regulation of translation initiation | 4.83 | FUN12, GCD1, GCD10, GCN3, MPT5, NIP1, PAB1, TIF1, TIF2, TIF34, TIF35, TIF5 | | |
| Cytoplasmic translation | | | 19.11 | 116 genes |
| Negative regulation of protein modification process | 3.24 | BMH2, CDC20, CDH1, LAG2, LRE1, LSP1, NCE102, PIL1, PTP2, SDP1, SPL2, STP22 | | |
| Ribosome biogenesis | 5.36 | BCD1, RPA12, RPA135, RPA190, RPA34, RPA43, RPA49, RPB5, RPB8, RPC10, RPC40, RPO26, RPS26B, TMA20 | 3.88 | BRX1, RPA12, RPA14, RPA49, RPC10, RPC40, RPL10, RPL11A, RPL11B, RPL12A, RPL12B, RPL25, RPL3, RPL34A, RPL5, RPL6A, RPL6B, RPP0, TOR1, TOR2 |
| Protein folding | 2.18 | AHA1, CCT2, CCT3, CCT5, CIN4, CNE5, CNS1, CPR7, CUR1, EMC5, FLC1, FPR4, GIM4, GIM5, GSF2, HCH1, HSP26, HSP82, PAC2, SIS1, SLP1, SSA2, SSA4, SSB1, SSB2, | 3.77 | AHA1, BTN2, CNE1, CPR1, CPR2, CUR1, ERJ5, EUG1, FLC1, FMO1, FPR1, FPR2, GSF2, HCH1, HSP26, JAC1, MPD1, MPD2, PDI1, PLP1, SIS1, SSA4, STI1, TAH1 |

| | | | | |
|---|--------------|---|--------------|--|
| | | <i>SSE1, STI1, TAH1, YDJ1</i> | | |
| Post-translational protein targeting to membrane | | | 16.65 | <i>KAR2, LHS1, SBH1, SEC61, SEC62, SEC72</i> |
| SRP-dependant co-translational protein targeting to membrane, translocation | | | 10.39 | <i>KAR2, SBH1, SEC61, SIL1, SSA4</i> |
| Retrograde protein transport, ER to cytosol | | | 24.98 | <i>DER1, HRD1, HRD3, NPL4, SEC61, UFD1</i> |
| ER associated misfolded protein catabolic process | | | 32.21 | <i>NPL4, PMT1, PMT2, UFD1</i> |
| ER associated ubiquitin dependent protein catabolic process | | | 6.65 | <i>ADD37, ATG19, CNE1, DER1, DFM1, HRD1, HRD3, JEM1, KAR2, LCL2, MNS1, POF1, SCI1, SEC61, UBC7, UBX2, UBX4, YDJ1</i> |
| Lipid related | | | | |
| Ergosterol biosynthesis | 4.03 | <i>ERG11, ERG2, ERG24, ERG26, ERG27, ERG3, ERG5, ERG6, ERG7, ERG8, MOT3, NCP1</i> | 4.84 | <i>ERG10, ERG12, ERG20, ERG26, ERG27, ERG28, ERG5, ERG6, ERG8, MCR1, NCP1</i> |
| Steroid biosynthetic process | 3.25 | <i>CYB5, ERG11, ERG2, ERG24, ERG26, ERG27, ERG3, ERG5, ERG6, ERG7, ERG8, MOT3, MVD2, NCP1</i> | 4.03 | <i>CYB5, ERG10, ERG12, ERG20, ERG26, ERG27, ERG28, ERG5, ERG6, ERG8, MCR1, MVD1, NCP1</i> |
| Phospholipid biosynthetic process | | | 2.52 | <i>CKI1, CSR1, DPM1, EPT1, ERG12, ERG20, ERG8, GAB1, GPI16, GPI17, GPI2, GWT1, ICT1, MCD4, MVD1, OPI3, PIK1, SCS22, SCS3, SEC14, URA8, YDR018C, YFT2</i> |
| Energy generation related | | | | |
| ATP synthesis coupled electron transport | 3.8 | <i>COX5B, CYC7, CYT1, NDI1, QCR10, QCR2, QCR6, RIP1, SDH1, SDH2, YLR164W</i> | | |
| Energy reserve metabolic process | 7.05 | <i>AAP1, BMH2, GAC1, GDB1, GIP2, GLC3, GLG1, GLG2, GPH1, GSY1, GSY2, IDG1, PCL8, PGM2, PIG2, PSK1, SGA1, UGP1</i> | | |
| Glycogen biosynthetic process | 10.14 | <i>GAC1, GDB1, GLC3, GLG1, GLG2, GSY1, GSY2, IGD1, PCL8, PGM2, PIG2, PSK1, UGP1</i> | | |
| Mitochondrial electron transport | 7.43 | <i>CYC7, CYT1, QCR10, QCR2, QCR6, RIP1</i> | | |
| Oxidation reduction process | 2.31 | 101 genes | 2.09 | 84 genes |
| TCA cycle | 3.27 | <i>ACO2, CIT1, DAL7, FUM1, IDP1, IDP2, LSC2, SDH1, SDH2, YMR31</i> | | |
| Degradation and recycling related | | | | |
| CVT pathway | 3.11 | <i>ATG1, ATG13, ATG14, ATG19, ATG2, ATG20, ATG4, ATG7, ATG8, COG1, COG6, TLG2, VSP30</i> | | |
| Eisosome assembly | 10.32 | <i>EIS1, NCE102, PIL1, SLM1, YPK2</i> | | |

| | | |
|---------------------------------------|-------|---|
| Mitochondrion degradation | 5.86 | ATG1, ATG13, ATG2, ATG20, ATG29, ATG32, ATG33, ATG4, ATG7, ATG8, ICY2, RTG3, WHI2, YIL165C, YOR019W |
| Stress related | | |
| Hydrogen peroxide catabolic process | Inf* | CCP1, CTA1, CTT1 |
| Trehalose biosynthetic process | 37.19 | PGM2, TPS1, TPS2, TPS3, TSL1, UGP1 |
| Trehalose catabolism | Inf* | NTH1, NTH2, ATH1 |
| Cellular response to oxidative stress | 2.26 | AHP1, GCY1, GPX1, GRE3, GRX1, GRX3, GRX7, HSP12, HYR1, LOT6, MCR1, MHR1, MXR1, MXR2, PRX1, SNT2, TSA1, TSA2, YDL124W, YJR096W, YKL069W |
| Response to misfolded protein | 9.99 | FES1, NPL4, PMT1, PMT2, SIS1, UFD1 |
| Others | | |
| Cellular metal ion homeostasis | 2.48 | ARN2, COT1, CTH1, CTR2, ERV1, FET3, FRE3, GGC1, GRX4, ISU1, IZH3, MDM38, PGM2, PHO80, PIC2, PPZ1, SCO1, SCO2, SIT1, SMF3, SOD1, SSQ1, TIS11 |
| Cellular iron ion homeostasis | 3.24 | ARN2, CTH1, ERV1, FET3, FRE3, GGC1, GRX4, ISU1, SIT1, SMF3, SSQ1, TIS1 |
| Siderophore transport | 18.59 | ARN1, ARN2, FIT2, FIT3, FRE3 |
| Iron-sulphur cluster assembly | 5 | CFD1, DRE2, ISA1, IBA57, ISU1, NAR1, TAH18, YAH1, YHR122W |

^aOdds ratios for each GO term are included, with regulation of GO terms colour coded. Red: up-regulated. Green: down-regulated. *Inf = all genes contributing to enrichment of this GO term are present.

4.4.2. SOMs analyses of T_A and T_{AL} in *S. cerevisiae* S288C

Independent SOMs analyses were performed on the genes differentially expressed in T_A and T_{AL}. SOMs groups together genes with a similar pattern of expression across the different treatments with the assumption that these are co-expressed or co-regulated, to allow a visual analysis of trends in the regulation of a group of genes. This provides more interpretive power to what and how transcripts change in response to different conditions. The SOMs maps are generated from the read counts of all experimental conditions (AMB, CA, AMB+LF, CAL), with a focus on genes differentially expressed in either T_A or T_{AL}, where T_A and T_{AL} each have different sets of genes. Each gene is represented by a line and their log fold changes are normalised to reach a maximum expression level of +/- 3 in each SOMs cell. The overall SOMs results are presented in Figures 4.8a and 4.8b along with their associated heat maps in Figures 4.8c and d. The heat maps were generated from the SOMs clusters and show the averaged expressions of genes present in each cluster for each drug treatment. The dendrogram on the left of each heat map separates the clusters into two groups based on up or down-regulation of co-expressed genes. In T_A (Fig. 4.8c), more SOMs clusters were down-regulated as indicated in blue in the AMB experiments (clusters 1 – 15), whereas the converse was observed for T_{AL} in the AMB+LF experiments (clusters 11 – 25) (Fig. 4.8d). GO enrichments for each SOMs cluster for T_A and T_{AL} were analysed and clusters of interest are presented in the following sections.

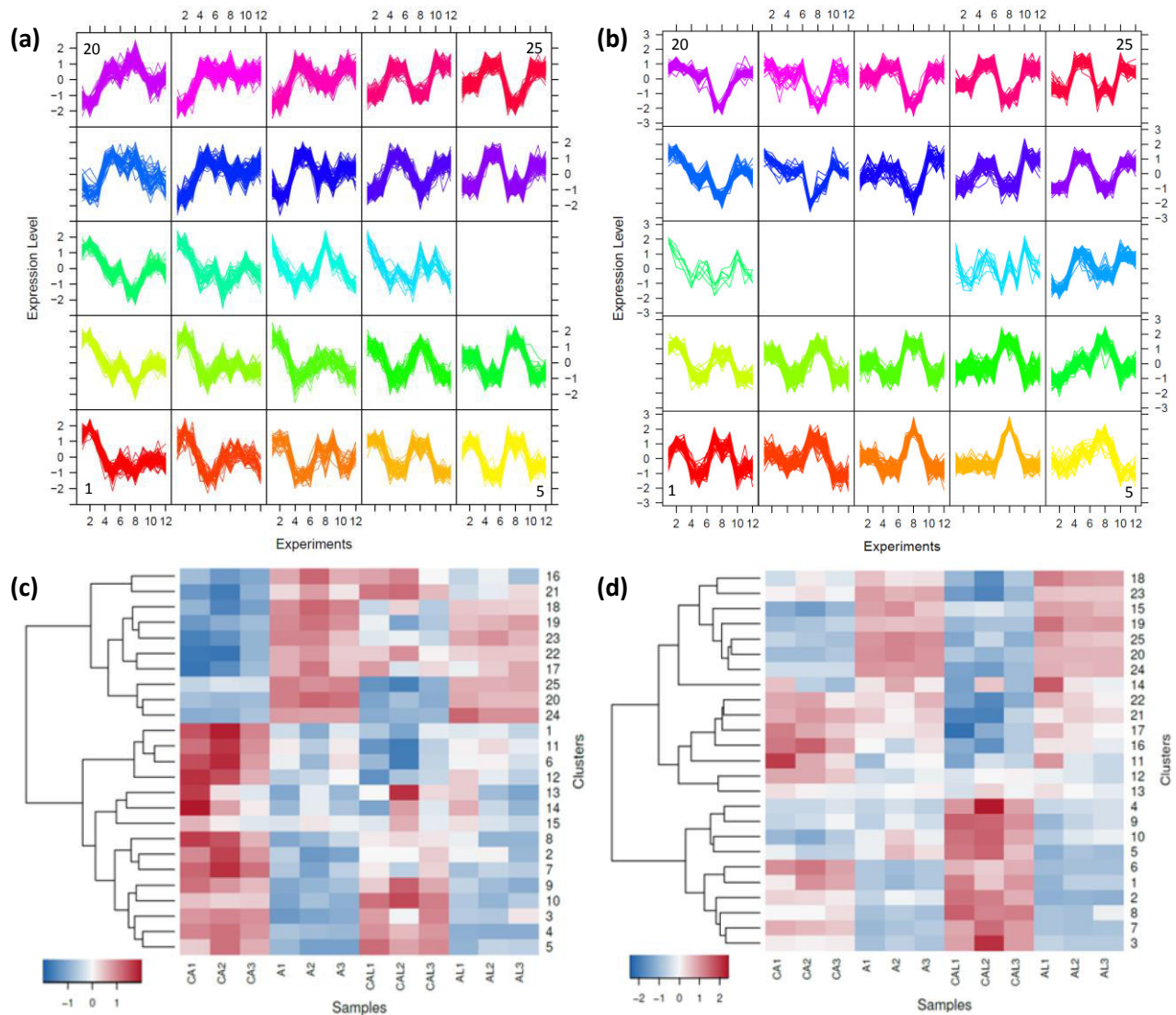


Figure 4.8. Independent SOMs of differentially expressed genes in *S. cerevisiae* S288C **(a)** T_A and **(b)** T_{AL} and the heat maps of averaged gene expressions of each SOMs cluster for **(c)** T_A and **(d)** T_{AL} . In the SOMs clusters, each gene is represented by a line and the y-axis denotes scaled expression levels across the 12 experimental samples along the x-axis. These are: Experiments 1-3: the three biological replicates of the control for AMB treatment (CA1 – CA3); Experiments 4-6: AMB treatment (A1 – A3, where A is AMB); Experiments 7-9: the control for AMB+LF treatment (CAL1 – CAL3); and Experiments 10-12: AMB+LF treatment (AL1 – AL3, where A is AMB and L is LF). The clusters are numbered from bottom left to top right. Empty clusters have no genes. The heat maps of average gene expressions **(c)** and **(d)** are represented by rpk values scaled to standard normal per gene using Pareto scaling. The x-axis represents the 12 experimental samples with each biological replicate numbered 1 – 3. The y-axis shows the 25 SOMs clusters and the dendrogram on the left separates the SOMs clusters into up- or down-regulated groups, exclusively. For T_A **(c)**, up-regulated genes were found in clusters 16 – 25 while clusters 1 – 15 mapped down-regulated genes. In T_{AL} **(d)**, up-regulated genes were found in clusters 11 – 25 and down-regulated genes in clusters 1 – 10.

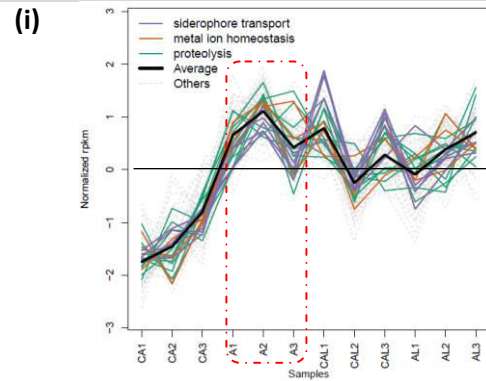
4.4.2.1. Metal ion transport and homeostasis are enriched but oppositely regulated in T_A and T_{AL}

In T_A, GO enrichments for metal ion homeostasis and siderophore transport were up-regulated in cluster 17 (Fig. 4.9a(i)). The genes contributing to these enrichments are mainly related to iron homeostasis and encode siderophore uptake proteins Arn1, Arn2, Fit2, and Fit3 and the cell wall ferric reductases Fre2, and Fre3 [390], similar to what was seen under metal ion homeostasis and siderophore transport in the overall GO terms in Table 4.5. Other co-regulated metal-related proteins in the same cluster were Cot1, encoding vacuolar zinc transport, and Sco2, encoding thioredoxin like copper binding protein involved in cytochrome c oxidase activity (Fig. 4.9a(i)) [391, 392]. Enrichment for copper ion homeostasis was seen in cluster 22 and consisted of the genes encoding Sco1, a homologue of Sco2, a vacuolar transporter Ctr2, and a mitochondrial copper transporter Pic2 (Fig. 4.9a(ii)) [392-394].

As the enrichment of metal ion homeostasis in Table 4.5 lists metal-related genes that were not observed in the T_A SOMs enrichments, a manual search was performed to observe where these genes clustered. Metal-related genes, including iron-related genes, were found in cluster 24 and included *SIT1*, *FET3* and *PHO80*, in cluster 21 with *TIS11*, in cluster 22 with *PGM2*, in cluster 25 with *CTH1*, *IZH3*, *MDM38* and *SOD1*, and in cluster 19 with *SSQ1* and *ENB1* (not shown). Cluster 20 was enriched for iron-sulphur (Fe-S) cluster assembly proteins Isa1, Isu1, Nar1, Cia2, and Erv1, Ggc1 and Grx4 (not shown), and the iron-regulating transcription factor Aft1 mapped to cluster 19 (not shown) [395]. The presence of iron-related genes in different SOMs clusters suggests different levels of gene regulation and differing co-expression.

In T_{AL}, genes encoding zinc ion transport were enriched and down-regulated in cluster 9 (Fig. 4.9b(i)). These included genes encoding Fet4, a low affinity plasma membrane iron transporter, Msc2, a transporter located in the ER, and Zrt3, a vacuolar membrane zinc transporter [396]. The zinc-regulating transcription factor Zap1 was also co-expressed in this cluster (not shown) [397]. Similar to the overall GO enrichments seen in Table 4.5, Fe-S cluster assembly was enriched and up-regulated, and was induced in cluster 23 with the assembly proteins Dre2, Tah18 and Yah1 (Fig. 4.9b(ii)).

(a) SOMs clusters in T_A



Details

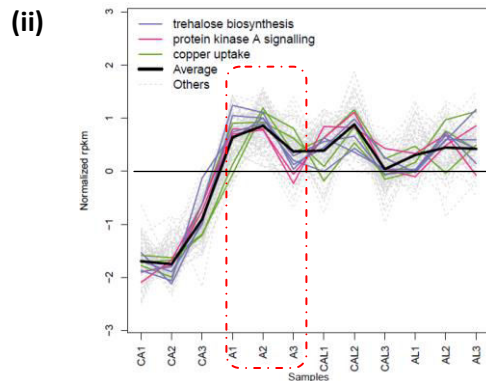
Cluster: 17

Gene expression: Up-regulated

Siderophore transport: *ARN1, ARN2, FIT2, FIT3, FRE3*

Metal ion homeostasis: *ARN1, ARN2, FIT2, FIT3, FRE3, FRE2, COT1, SCO2*

Proteolysis: *ASI2, CUE5, HUL5, NAR2, UBP11, UBP15, UBP2, UBX5, YKL100C, VID28, VID30*



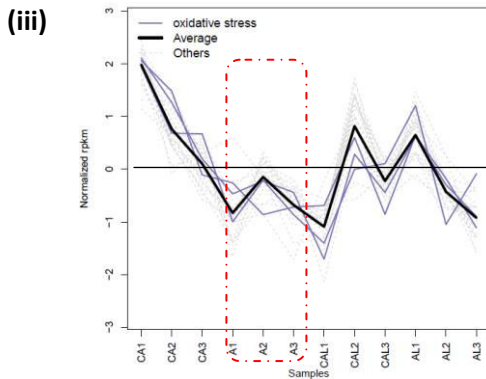
Cluster: 22

Gene expression: Up-regulated

Trehalose biosynthesis: *PGM2, TPS1, TPS2, UGP1*

Protein kinase A signalling: *TPK1, TPK2*

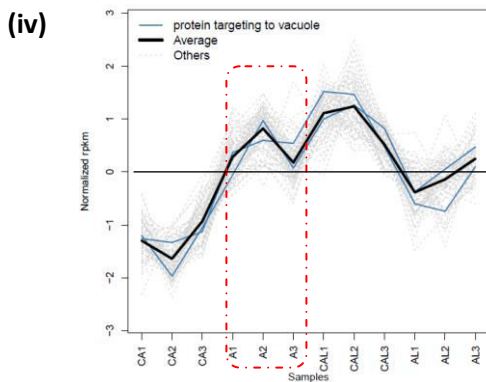
Copper uptake: *CTR2, PIC2, SCO1*



Cluster: 14

Gene expression: Down-regulated

Oxidative stress: *GPX2, TMA19, URM1*

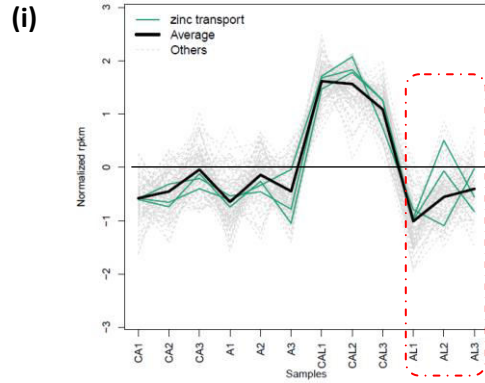


Cluster: 21

Gene expression: Up-regulated

Protein targeting to vacuole: *ATG34, ATG8*

(b) SOMs cluster in T_{AL}



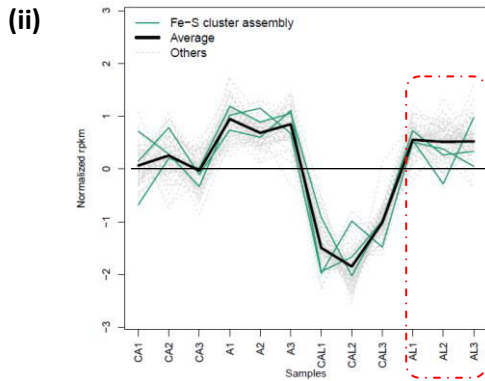
Details

Cluster: 9

Expression level: Down-regulated

Zinc transport: *FET4, MSC2, ZRT3*

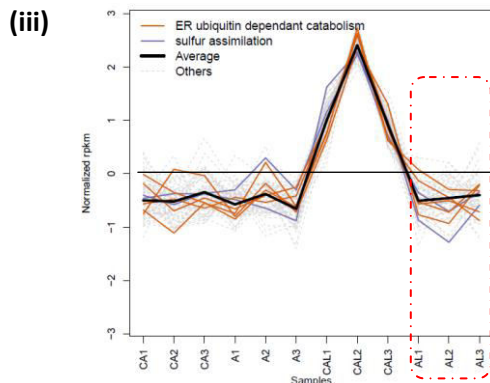
ZAP1 co-expressed in cluster 9 (not shown)



Cluster: 23

Expression level: Up-regulated

Iron-sulphur assembly: *DRE2, TAH18, YAH1*



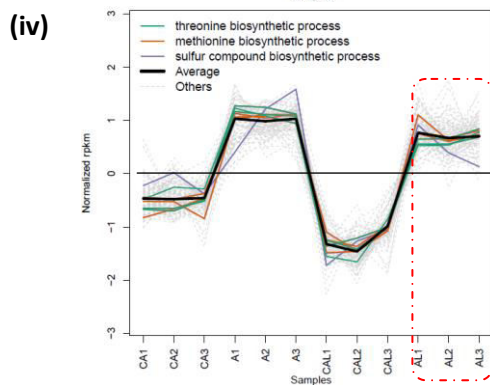
Cluster: 4

Expression level: Down-regulated

ER ubiquitin dependant catabolism: *DER1, DFM1, JEM1, LCL2, UBC7*

Sulphur assimilation: *MET16, MET3*

MET2 and *MET32* also mapped to cluster 4 (not shown)



Cluster: 24

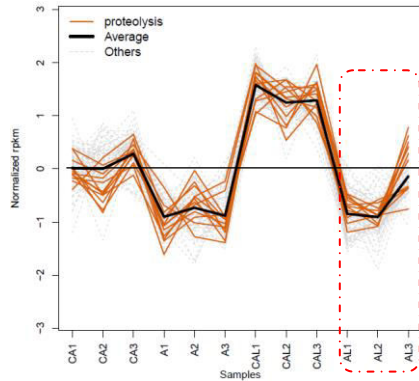
Expression level: Up-regulated

Threonine biosynthetic process: *HOM2, HOM3, THR4*

Methionine biosynthetic process: *ARO8, ARO9, HOM2, HOM3, SAM4*

Sulphur compound biosynthetic process: *ARO8, ARO9, BIO4, HOM2, HOM3, SAM4*

(v)

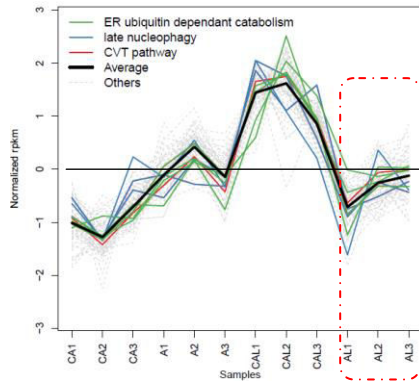


Cluster: 8

Expression level: Down-regulated

Proteolysis: *DDI1, FIN1, PRE1, RPN10, RPN12, RPT3, RPT6, UBC4, UBP16, UBX4, VPS25, CUZ1*

(vi)



Cluster: 10

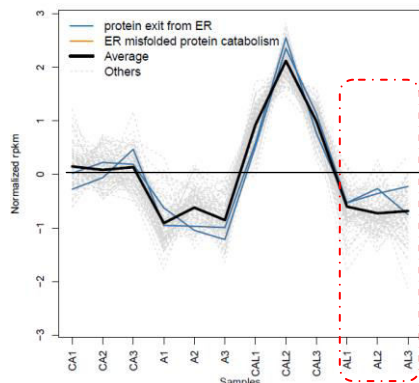
Expression level: Down-regulated

ER ubiquitin dependent catabolism: *ADD37, ATG19, HRD1, HRD3*

Late nucleophagy: *ATG23, ATG31, ATG9*

CVT pathway: *ATG19, ATG23, ATG9, SNX4*

(vii)



Cluster: 3

Expression level: Down-regulated

Protein exit from ER: *PMT1* and *PMT2*

ER misfolded protein catabolism: *PMT1* and *PMT2*

Figure 4.9. SOMs of interest and their enriched GO terms in *S. cerevisiae* S288C T_A (a) and T_{AL} (b). The average expression level of all co-expressed genes in each cluster is indicated by a black line, with each coloured line representing a single gene. Genes included in a GO enrichment are labelled with the same colour. The y-axis gives the normalised expression levels of genes in response to AMB and AMB+LF treatment. Drug treatments are boxed for visual clarity. Genes that make up the GO enrichments in each cluster are listed, along with other genes of interest.

4.4.2.2. Addition of LF causes changes to the regulation of cellular stress responses

In the overall enrichments for T_A , hydrogen peroxide catabolism and trehalose biosynthesis and catabolism were up-regulated (Table 4.5). In SOMs, enrichments related to stress were expressed in cluster 22, involving genes encoding for protein kinase A (PKA) signalling *TPK1* and *TPK2*, and trehalose biosynthesis processes *PGM2*, *TPS1*, *TPS2* and *UGP1* (Fig. 4.9a(ii)). Activation of the protein kinase signalling pathway increases the production of reactive oxygen species (ROS) in the mitochondria [398, 399]. Transcriptional evidence of mitochondrial ROS production is supported by the enrichment of mitophagy in the overall GO enrichments (Table 4.5), which is a selective autophagic process that prevents cellular damage from defective mitochondria [400]. Trehalose, peroxidases and catalases are most likely induced to protect the cell from ROS damage [401]. However, cellular responses to oxidative stress were down-regulated in cluster 14, which includes the genes *GPX2*, *TMA19* and *URM1* (Fig. 4.9a(iii)). As the proteins translated from these genes are localised to the cytosol (www.yeastgenome.org/), this suggests stress responses may be regulated by intracellular location.

While stress related enrichments were up-regulated in T_A , a down-regulation in these terms was observed in T_{AL} (Table 4.5). Although stress-related terms were not enriched in SOMs in T_{AL} , enrichments relating to sulphur metabolism were observed, which are required for many cellular functions including stress responses, where sulphur in amino acids like cysteine is required for the secondary structure of antioxidants like peroxiredoxins and glutathione [402]. Sulphur metabolising pathways were mapped to different clusters and included sulphate assimilation, which has been shown by Wu *et al.* (2009) to be involved in oxidative stress [403]. Sulphate assimilation mapped to cluster 4, which was down-regulated with *Met3*, an ATP sulfurylase that reduces assimilated sulphate into sulphide [404], and *Met16*, an enzyme that reduces 3'-phosphoadenylylsulfate to produce free sulphites for downstream sulphur processes [405] (Fig. 4.9b(iii)). Other sulphur related genes in the same cluster but not under an enriched GO term include *Met2*, a L-homoserine-O-acetyltransferase that acts as the first step of the methionine biosynthesis pathway [406], and *Met32*, a transcription factor that regulates methionine biosynthetic genes [407] (not shown).

In contrast to the down-regulation of *Met32* in cluster 4, methionine and sulphur compound biosynthesis were up-regulated in T_{AL} and enriched in cluster 24, which includes *ARO8*, *ARO9*, *HOM2*, *HOM3*, *SAM4* and *BIO4* (Fig. 4.9b(iv)). *ARO8* and *ARO9* encode aromatic aminotransferases that catabolise amino acids that can then be used to synthesise methionine via an alternative route from the sulphur assimilation pathway [408]. *HOM2* and *HOM3* are part of the threonine biosynthesis pathway

that can branch into the methionine biosynthetic pathway via *MET2*. However, while threonine biosynthesis was induced and also enriched in SOMs cluster 24 (Fig. 4.9b(iv)), the conversion of homoserine to homocysteine by *MET2* was shut down.

To understand the regulation of sulphur metabolism in T_{AL} , all of the pathways mentioned above, as well as downstream sulphur metabolising pathways including the S-adenosylmethionine (SAM) cycle and glutathione biosynthesis, were mapped along with the expression of their constituent genes. Figure 4.10 shows the control of sulphur metabolism in T_{AL} , where the regulation of sulphur-related pathways indicates that the generation and supply of precursors leading to the production of homocysteine is limited. This involves the expression of *Ssu1*, which exports sulphites out of the cell [409], the down-regulation of *MET17*, which converts sulphides into homocysteine at later steps in the sulphur assimilation pathway (blue-coloured pathway) and the repression of *MET2* from the threonine biosynthetic pathway (purple-coloured pathway). Pathways that use homocysteine as a starting substrate such as the SAM cycle (pink-coloured pathway) and the glutathione biosynthetic pathway (yellow-coloured pathway), which is involved in stress responses, were also repressed.

The down-regulation of glutathione biosynthesis also affects the production of cysteine, which is a precursor to many proteins and enzymes including Fe-S clusters and antioxidants like superoxide dismutases, and this in turn affects the cellular response to oxidative stress [77, 410]. However, cysteine can be acquired by the degradation of glutathione, through the induction of *ECM38*, or by importing extracellular cysteine using the transport protein *Yct1* [411], which were induced (Fig. 4.10). The overall regulation of sulphur metabolic pathways in T_{AL} points to the limitation of homocysteine production, which in turn affects cysteine and glutathione synthesis that is required for stress responses.

Sulphur metabolism is indirectly regulated by *Met32*, an auxiliary transcription factor that targets the transcriptional activator *Met4* to the promoters of sulphur metabolic genes [412]. It is interesting to note that *Met32* is also regulated by *Zap1*, which mapped to SOMs cluster 9 (not shown), hence, zinc homeostasis is important for stress responses through the regulation of sulphur metabolism as reported by Wu *et al.* (2009) [403].

Together, the transcriptome results for *S. cerevisiae* S288C suggest that AMB treatment induces stress in the mitochondria, and mitophagy is activated to avoid cellular damage. In contrast to T_A , the addition of LF to AMB treatment causes a down-regulation of stress responses. This may occur by the repression of sulphur assimilation, which is affected by zinc homeostasis that is also repressed in T_{AL} . Repressing

sulphur assimilation may in turn down-regulate the expression of genes in downstream pathways, including the production of glutathione and cysteine that are needed for detoxification of stress-inducing oxidants.

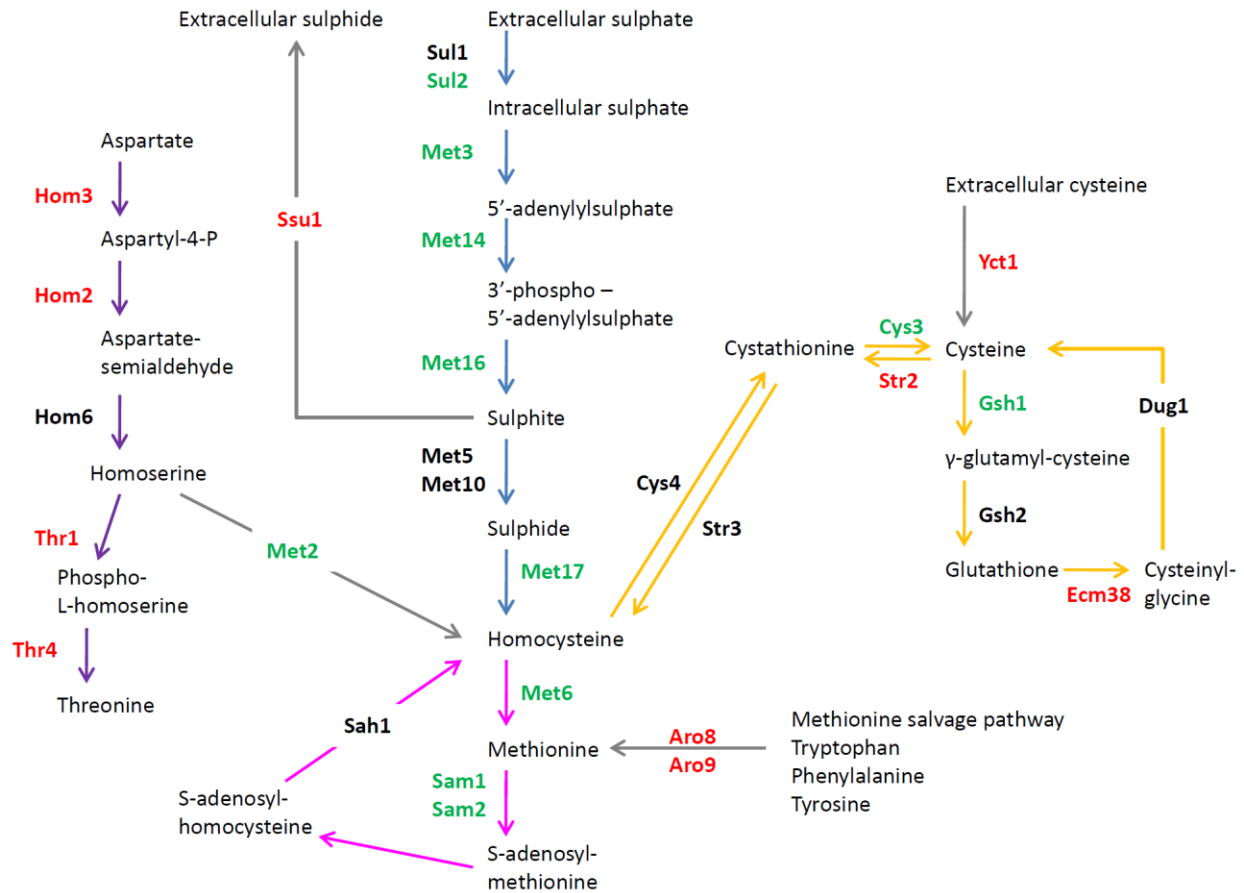


Figure 4.10. Mapping of sulphur metabolism pathways suggests in AMB+LF synergy there is a shutdown of homocysteine production by alterations in sulphur assimilation, threonine biosynthesis and glutathione biosynthesis pathways. Blue arrows indicate steps in the sulphur assimilation pathway, yellow arrows the glutathione biosynthetic pathway, purple arrows the threonine biosynthetic pathway, pink arrows the S-adenosylmethionine cycle and grey arrows indicate the substrates that feed into or out of the pathways. Genes induced in T_{AL} are shown in red, genes down-regulated are in green and those with no change in expression are black. Diagram based on pathway.yeastgenome.org

4.4.2.3. Protein degradation is regulated differently in T_A and T_{AL}

In T_A , proteolysis-related terms were enriched and induced in SOMs cluster 17, including vacuolar import and degradation with Vid28 and Vid30, and ubiquitin related processes Ubx5, Ubp2, Ubp11, Upb15, Hul5, and Cue5 (Fig. 4.9a(i)). Protein targeting to the vacuole was enriched in cluster 21 with Atg34 and Atg8, which are part of the cytoplasm to vacuole targeting (CVT) pathway that delivers hydrolases to the vacuole (Fig. 4.9a(iv)) [413]. Proteasome-related enrichments were not seen in either the overall GO terms in Table 4.5 or SOMs, implying that protein degradation occurred through the vacuole in T_A .

In T_{AL} , proteolysis was repressed and mapped to cluster 8 with genes mostly associated with ubiquitination (*UBC4*, *UFD1*, *VPS25*, *UBX4*, *CUZ1*, *UBP16*) and the proteasome (*PRE1*, *RPN10*, *RPN12*, *RPT3*, *RPT6*, *CUZ1*) (Fig. 4.9b(v)). Other enrichments mapped to cluster 8 included the SNARE complex assembly involved in vesicle fusion with Sly1 and Vsp45 (not shown) [414]. While the CVT pathway was not observed in the overall T_{AL} GO enrichments (Table 4.5), transcripts making up this enrichment were down-regulated in cluster 10 and included *ATG19*, *ATG23*, *ATG9* and *SNX4*. *ATG23* and *ATG9* also contributed to the enrichment of nucleophagy, the selective degradation of the nucleus [415], in the same cluster (Fig. 4.9b(vi)). Other enrichments involving protein degradation include endoplasmic reticulum (ER)-associated terms encompassing the ER-associated protein degradation (ERAD) process, which is an ER stress response involving the ubiquitination of misfolded proteins and their retrotranslocation to the cytosol for proteasomal degradation [416]. The terms that were enriched involved misfolded protein catabolism and exit from the ER in cluster 3 with protein O-mannosyltransferases Pmt1 and Pmt2, which are involved in glycosylation [417] (Fig. 4.9b(vii)), and ubiquitin-dependant catabolism which was mapped to clusters 4 and 10. The transcripts present in these clusters have functions in protein folding, ubiquitin tagging and lumen-to-cytosol signalling, with *DER1*, *DFM1*, *JEM1*, *LCL2* and *UBC7* mapping to cluster 4 (Fig. 4.9b(iii)), and *ADD37*, *HRD3*, *HRD1* and *ATG19* mapping to cluster 10 (Fig. 4.9b(vi)). Overall, this suggests the additional of LF in T_{AL} suppresses selective proteolytic pathways.

Interestingly, while co-translation translocation and retrograde transport from ER to the cytosol were repressed in T_{AL} , the expression of ribosome biogenesis and cytoplasmic translation were induced (Table 4.5). Another interesting finding was the co-expression of ER-associated ubiquitin protein catabolism with sulphate assimilation in cluster 4 (Fig. 4.9b(iii)). Eug1, Mpd1 and Ero1, which are protein disulfide isomerases and ER oxidoreductases involved in protein folding, also mapped to SOMs cluster 4 (not

shown), which altogether suggests ER function is repressed and that there is a dependency of ER function on sulphur metabolism.

In summary, vacuole mediated proteolysis was induced in T_A , while this was repressed in T_{AL} . Although protein synthesis was induced in T_{AL} , protein processing, which occurs in the ER, was repressed, suggesting disruptions in ER function.

4.4.3. Network analysis reveals metal ion regulation differs in T_A and T_{AL}

GO enrichments associated with iron and zinc import were observed in SOMs (Fig. 4.9a(i) and 4.9b(i)), but the up-regulation of iron uptake genes in T_A and down-regulation of zinc uptake genes in T_{AL} were unexpected in the context of the metal ion-chelating ability of LF. The expression of transcription factors Aft1, which regulates iron, and Zap1, which regulates zinc, were identified in T_A and T_{AL} respectively. Networks were drawn to investigate how these transcription factors interact with their target genes under the two drug treatments (Fig. 4.11). These have been co-visualised with the log fold-changes for each gene, with gene targets grouped according to biological functions for better interpretation.

To construct the regulatory network for Aft1 and iron homeostasis, binding targets of Aft1 and known iron uptake genes were curated from Yeastract and from Philpott and Protchenko (2008) [82]. The iron-related networks for T_A and T_{AL} are shown in Figures 4.11a and b. The localisation of Aft1 is controlled by the Grx3/Grx4/Fra1/Fra2 complex, which binds to Aft1 and prevents its entry into the nucleus to activate the iron regulon [91, 418]. In T_A , transcripts of *GRX3* and *FRA2* were down-regulated, while *AFT1*, *FRA1*, *GRX4* and *YAP5* (which induces *GRX4* expression) were up-regulated [90]. Twelve out of nineteen iron-associated genes with functions in iron uptake, storage and transport were also induced, which together suggest nuclear localisation of Aft1 and active transcription of the iron regulon. Two transcription factors regulated by Aft1, Cad1 and Yap5, share iron uptake-related gene targets with Aft1 and were also induced. In addition to iron transport, Aft1 also induces the expression of zinc and copper transport genes, showing that it can regulate other metals. Other processes unrelated to metal ion homeostasis but requiring metal ions were also seen and mostly induced, including vitamin and amino acid metabolism, response to stress and protein processing and degradation (Fig. 4.11a).

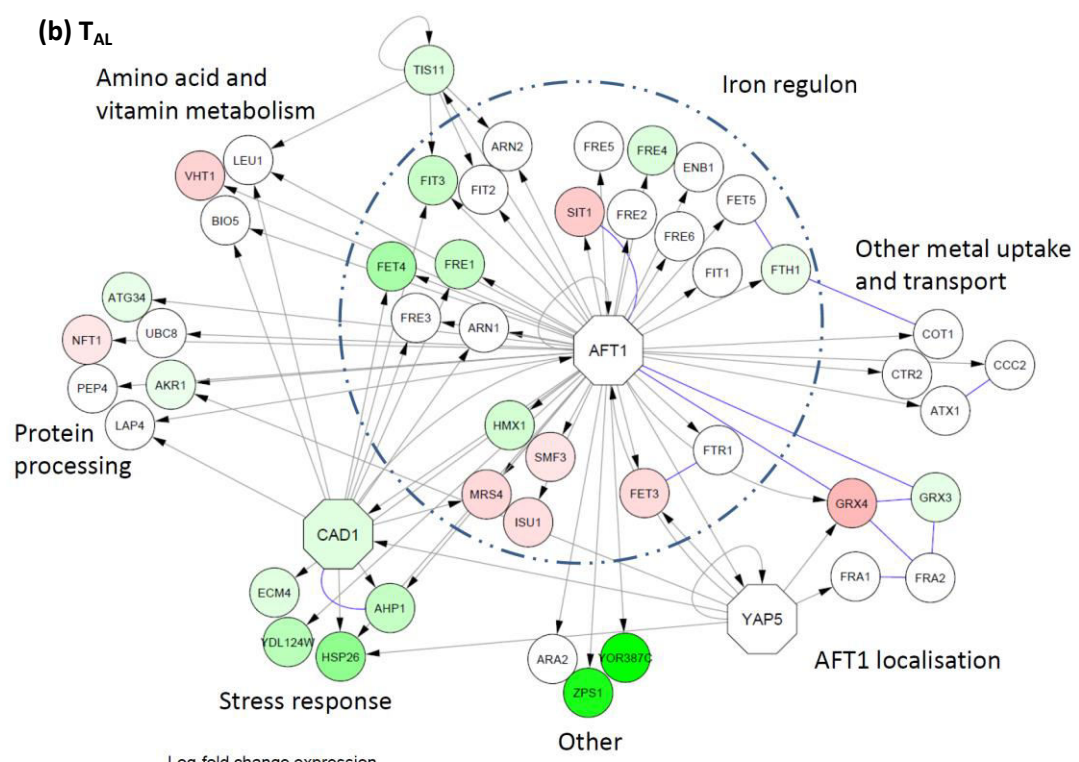
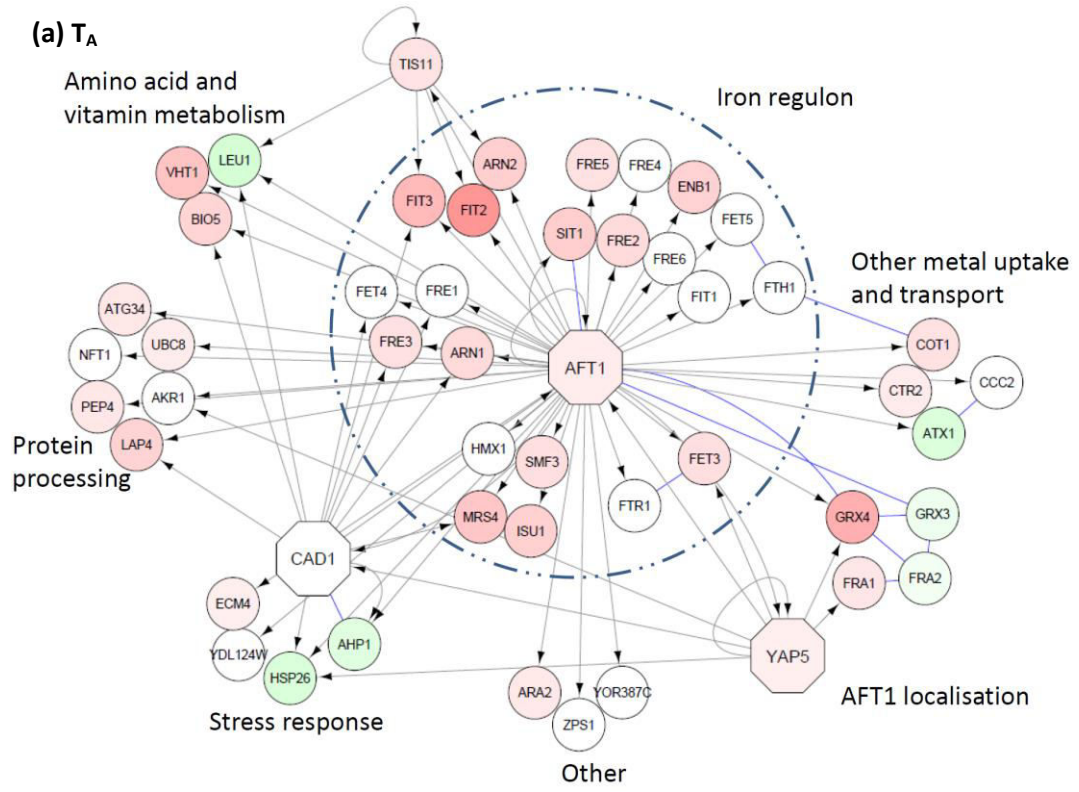
In T_{AL} , *AFT1* was not differentially regulated compared to the untreated control and expression fold-changes for genes controlling Aft1 localisation were only observed for *GRX3* and *GRX4*, which were down- and up-regulated, respectively. Only a subset of iron uptake transcripts in the iron regulon were significantly expressed, including the up-regulation of *FET3*, *SIT1*, *MRS4* and *SMF3*, and down-regulation

of *FIT3*, *FRE1*, *FRE4*, *FET4*, and *FTH1*. This implies that the addition of LF to the AMB treatment shuts down the iron regulon. Disrupting iron homeostasis also affects the uptake and storage of other metals, stress responses and protein processing, the transcripts of which were mostly repressed or not significantly expressed (Fig. 4.11b).

Zap1 regulates zinc homeostasis and metabolic responses to zinc deficiency [397, 419] and its target genes were curated from Wu *et al.* (2008), Wu *et al.* (2009) and Eide (2009) [403, 419, 420] and Yeasttract. As Yeasttract found more than 70 Zap1 target genes, only a subset of these were used to build the regulatory networks, based on their biological functions in YeastMine (yeastmine.yeastgenome.org/). The networks for T_A and T_{AL} are presented in Figures 4.11c and d, respectively. In T_A , the *ZAP1* transcript was not differentially expressed and direct Zap1 targets involved in zinc homeostasis and other processes were also not expressed (Fig. 4.11c). Genes that were differentially regulated are possibly under the control of other regulatory factors, such as the iron uptake genes that are under the control of Aft1 (Fig. 4.11a).

In contrast to T_A , *ZAP1* was repressed in T_{AL} . The expression of genes involved in zinc uptake (*FET4*), ER import (*MSC2* and *ZRG17*), and storage (*ZRT3*) were all repressed, which is consistent with observations in zinc-replete conditions (Fig. 4.11d) [419, 421]. Alcohol dehydrogenases, which are abundant zinc binding enzymes, are differentially regulated by Zap1 during zinc limitation to conserve zinc, with *ADH1* and *ADH3* repressed by Zap1 while *ADH4* is induced [93]. However, an opposite expression of these genes in the Figure 4.11d network suggests the cell senses an abundance of intracellular zinc in T_{AL} . Similar to Aft1, the network shows that Zap1 regulates the homeostasis of other metal ions and its repression down-regulates iron and copper related genes. Additionally, genes involved in stress responses, sulphur metabolism, cell wall function, lipid synthesis and protein processing are repressed, corresponding to the regulation of similar GO enrichments in Table 4.5 and the SOMs analyses (Fig. 4.9). Overall, the networks show that LF dysregulates zinc homeostasis, which in turn affects a broad range of cellular functions.

In summary, these networks show that, contrary to expected cellular responses in the presence of a metal ion chelator, the addition of LF causes an overall decrease in the transcription of iron and zinc regulatory elements, including gene targets that are involved in other cellular processes. This is in contrast to treatment with AMB alone, where the iron regulon was induced and the zinc network was largely unaffected.



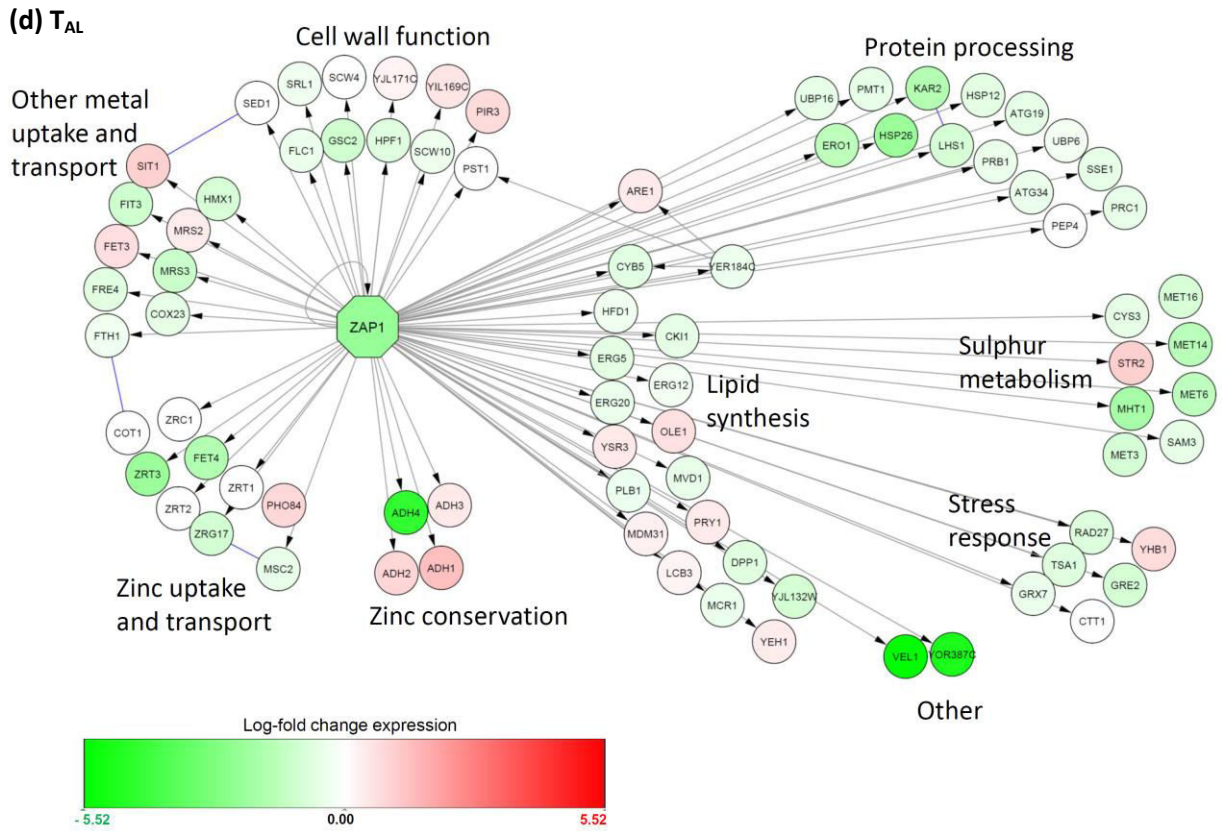
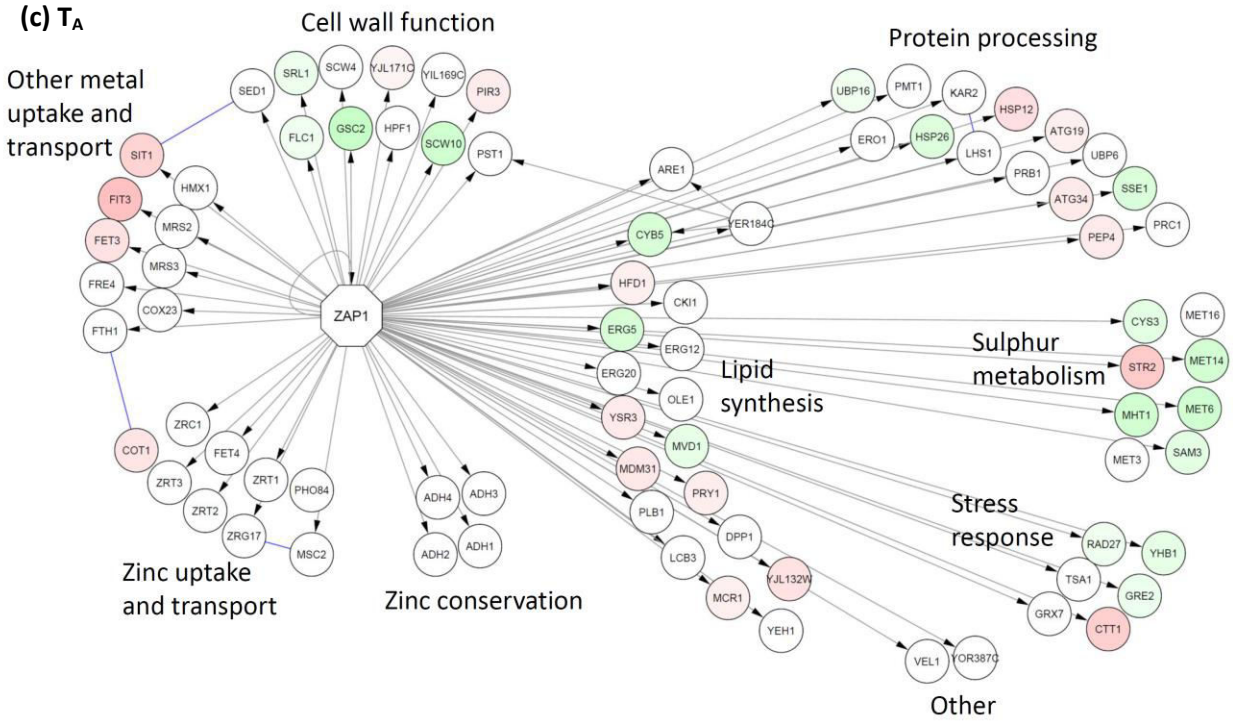


Figure legend on the next page.

Figure 4.11. Regulatory networks of the transcription factors Aft1 and its gene targets in **(a)** T_A and **(b)** T_{AL} , and Zap1 and its gene targets in **(c)** T_A and **(d)** T_{AL} . Each node represents a gene and the arrows show the direction of regulation. Transcription factors are shown in octagonal nodes. Log fold-changes of genes are coloured red for up-regulation, green for down-regulation and white for no expression relative to the control, with intensity of change indicated by the scale bar. Blue lines indicate direct protein-protein interactions.

4.4.4. Biological validation of transcriptome analysis

4.4.4.1. Rescue assays

As detailed in the previous chapter, LF is a metal ion chelator with the greatest binding affinity to iron (Section 3.1.3.2). However, LF did not cause synergy with AMB via iron chelation, as supplementation with iron at levels calculated to saturate the binding sites of LF neutralised growth inhibition in cells treated with LF alone but not when LF was combined with AMB (Fig. 3.4). In addition, the network analyses showed that the iron regulon was induced in T_A and repressed in the presence of LF, that zinc homeostasis was repressed in T_{AL} , and that Aft1 and Zap1 regulate the homeostasis of other metals (Fig. 4.11). Rescue assays were therefore performed, testing broad concentrations of selected rescue agents in the presence of different AMB+LF concentrations, to determine if and at what concentrations these might disrupt drug synergy.

Iron, zinc, calcium and the calcium chelator BAPTA were used. A summary detailing why these rescue agents were chosen and how they were hypothesised to rescue AMB+LF synergy is presented in Table 4.6. Iron rescue assays were first performed in this chapter to determine the concentration of iron required to rescue cells from AMB+LF synergy, before a modified version using lower concentrations of iron was tested in Chapter 3 (Section 3.2.6).

The following results are preliminary observations, as there was insufficient time to refine the rescue experiments using more appropriate levels of rescue agents as had been done for iron in Chapter 3. In addition batch-to-batch variation in LF sometimes changed the AMB+LF FIC between biological replicates, and toward the end of this study LF was discontinued from the original supplier (MP Biomedical) and LF from a new supplier, although still synergistic with AMB, gave quite different FIC results.

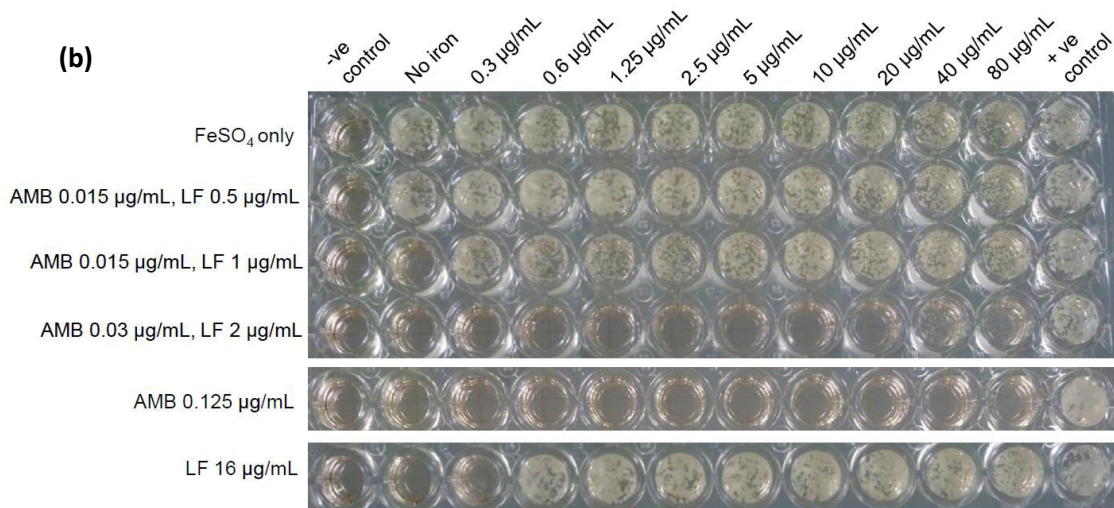
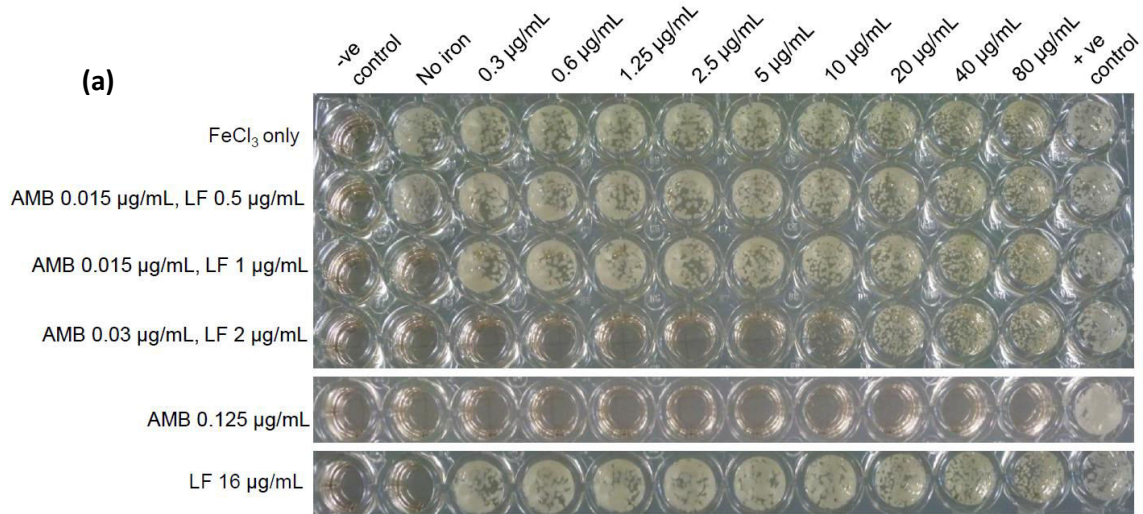
Table 4.6. Agents used for rescue assays in *S. cerevisiae* S288C

| Rescue agent | Observations/Reasons | Hypothesis |
|---------------------------------|---|--|
| Iron | Strongly chelated by LF (Fig. 3.4). Iron homeostasis and iron responsive genes in various biological pathways were altered in T _{AL} (Fig. 4.11.b) | Saturating iron binding by LF will prevent antifungal action caused by iron limitation and disrupt AMB+LF synergy. |
| Zinc | Can be chelated by LF [219]. Zinc homeostasis and zinc responsive genes in various biological pathways were altered in T _{AL} (Fig. 4.11.d). | Saturating zinc binding by LF will prevent antifungal action caused by zinc limitation and this will partially disrupt AMB+LF synergy. |
| Calcium | Weakly chelated by LF [219]. Calcium is essential for signalling, membrane fusion and ER regulation [422-424], and ER function was observed to be disrupted in T _{AL} (Fig. 4.11.d). | Addition will over-ride any limitation caused by LF chelation and will partially disrupt AMB+LF synergy |
| BAPTA (Calcium chelator) | Calcium is essential for signalling and regulation of cellular responses [422]. Test the effect of intracellular calcium depletion in AMB+LF synergy. | Chelation of calcium will do the opposite of calcium addition and enhance AMB+LF synergy |

AMB+LF was previously found to be synergistic at 0.03 µg/mL AMB and 2 µg/mL LF (Fig. 3.3, Appendix 3.1). At this concentration, none of the agents apart from iron were able to rescue growth (Fig. 4.12a and b). Iron supplementation was only able to rescue growth when supplied at excess levels; more appropriate lower iron concentrations that were sufficient to saturate iron binding by LF did not rescue synergy (Fig. 3.4). Only iron rescued the inhibition caused by LF alone at its MIC (Fig. 4.12a and b) and none of the agents were able to rescue inhibition by AMB alone at its MIC. As suggested in the previous iron rescue assay in Chapter 3, iron is not critical for synergy between AMB+LF, however iron is important for the inhibitory effect of LF alone. Growth at high concentrations of iron suggests oversaturation causes exuberant growth and interferes with the synergistic effect of AMB+LF. Over-supplementation with the other rescue agents was toxic to the cells and growth was inhibited at the highest concentrations (Fig. 4.12c – e).

Surprisingly, growth inhibition was observed at concentrations of the antifungal drug and iron chelator that were lower than the usual FIC levels (0.015 µg/mL AMB + 1 µg/mL LF), which may be due to the batch-to-batch variation in LF as noted above. At this concentration, all agents interfered with growth

inhibition as shown by the presence of growth in wells where rescue agents were added, even at the lowest concentrations tested. It is possible that at this very low FIC level synergy was borderline and rescue was more achievable. These experiments need to be repeated to fully understand the role of metal ions in synergy, however based on the inability to rescue synergy with iron supplementation seen in Chapter 3, and the general down-regulation of metal ion homeostasis seen in this chapter, it seems unlikely that chelation plays a primary role in AMB+LF synergy.



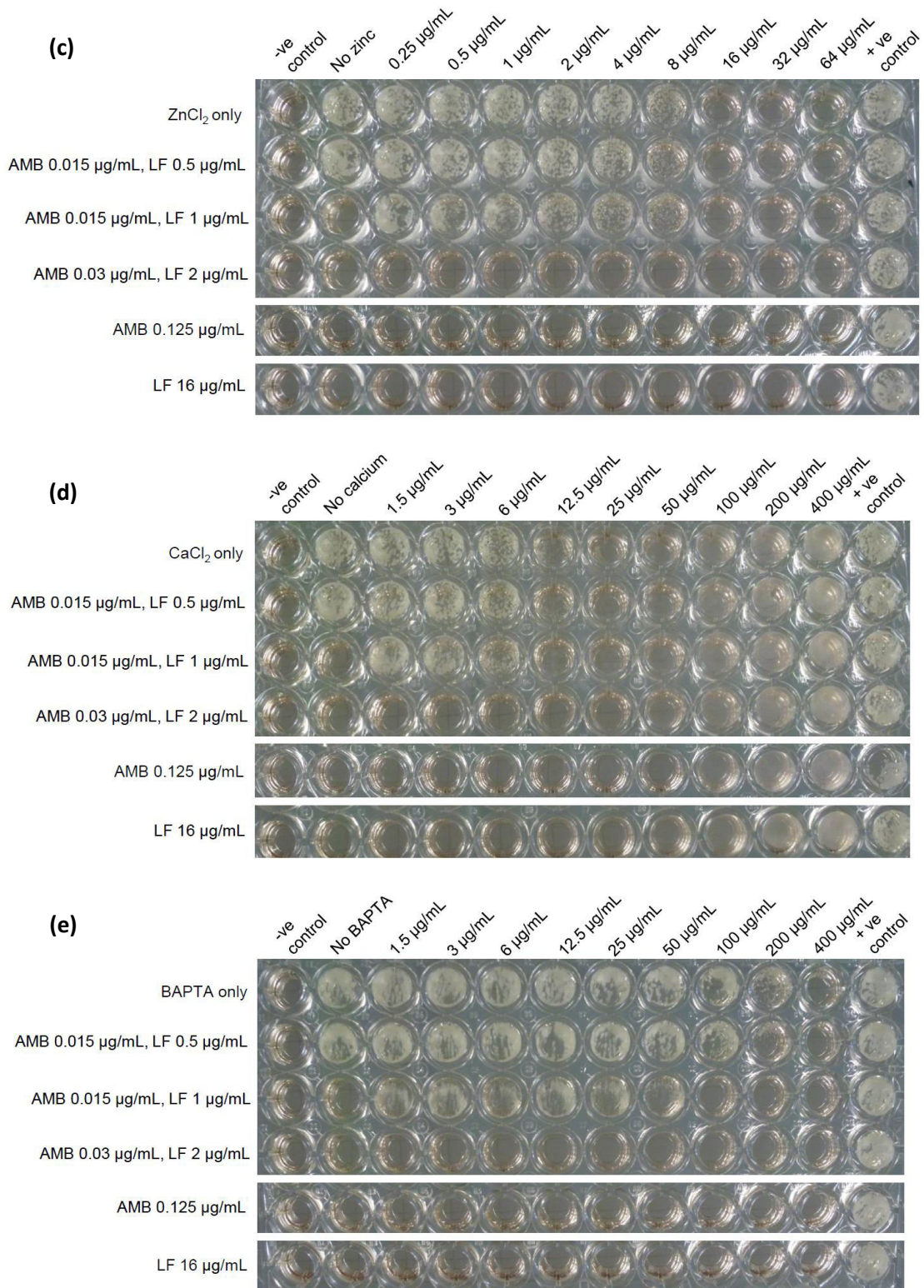


Figure legend on the next page.

Figure 4.12. *Saccharomyces* rescue assays in RPMI-1640 medium supplemented with **(a)** Iron (III) **(b)** Iron (II) **(c)** Zinc **(d)** Calcium and **(e)** BAPTA. Rescue agents were added to AMB and LF alone at their MICs, and to different concentrations of AMB+LF, including the established FIC concentration of AMB 0.03 µg/mL + LF 2 µg/mL. Yeast growth in the wells indicates rescue from the antifungal agents. Note that only iron could rescue cells from LF, and no agents rescued cells from AMB. In **(d)**, high concentrations of calcium have precipitated out into the medium.

4.4.4.2. Validation of selected target genes using spot plate assays of gene knock-out mutants

To validate the GO terms and network analyses obtained from the transcriptomic data, and to further investigate the roles of differentially regulated proteins in the response to AMB and other stressors, a list of criteria was drawn to select genes of interest for mutant generation and phenotype characterisation. The aim of testing each mutant was to determine if disruption would increase susceptibility to AMB without the addition of LF, and to determine if this was due to alterations in cell or membrane integrity or due to oxidative or nitrosative stress. The criteria selected the genes based on their:

- log fold expression
- co-expression with other genes
- involvement in a significant pathway
- type of protein when translated and effects on other proteins, i.e., kinases, transcription factors, part of a protein complex
- fungal orthologues
- mutant phenotypes compiled in SGD (www.yeastgenome.org/)

A summary of the list of potential and chosen genes using the above criteria is presented in Table 4.7 and the genes of interest and their hypothesised phenotypes in relation to AMB sensitivity are discussed below.

AFT1: encodes the iron regulating transcription factor Aft1 that also plays a role in chromosome maintenance [395, 425]. *aft1Δ* mutants have decreased accumulation and use of iron, decreased resistance to DFP, DFO, oxidative stress and a decreased rate of respiratory growth. Mutants also have

abnormal vacuole morphologies. In T_{A_v} but not T_{AL} , biological networks predict the nucleolar localisation of Aft1 and its activation of the iron regulon (Fig. 4.11a). Iron is important for many cellular processes and supplementation with ferrous and ferric iron at high concentrations was able to rescue AMB+LF synergy (Fig. 4.12a and b), although this was not seen at lower concentrations, even though there was enough iron to saturate the binding sites of LF and prevent its antifungal activity (Fig. 3.4). The deletion of *AFT1* was hypothesised to increase inhibition by AMB through inactivation of the iron regulon, as was seen in T_{AL} (Fig. 4.11b).

ATG1: encodes a protein serine/threonine kinase and is part of the core machinery of autophagy and the CVT pathway [426]. Atg1 forms the first signal that activates autophagy and the CVT pathway and mutants are defective in progression of these processes. This is because activation becomes a cascade, where Atg1 binds to Atg13 and Atg17 and this complex then interacts with other proteins and targets them to the phagophore assembly site (PAS). The PAS isolates the cargo for degradation in a membrane vesicle, which is then delivered to the vacuole [427]. Autophagy and related processes are important to the cell as they serve to degrade old and defective organelles that can damage the cell; mutants defective in autophagy and the CVT pathway have decreased lifespans and increased ROS accumulation. *ATG1* was induced in T_A (not shown) and deletion of *ATG1* is hypothesised to increase AMB susceptibility through the impaired delivery of cargo to the vacuole for degradation, as this process is repressed in T_{AL} (Fig. 4.9b(vi)).

CCH1: encodes a voltage gated calcium channel that associates with the transmembrane proteins Mid1 and Ecm7 [93]. This complex imports extracellular calcium with high affinity but at low capacity under environmental stresses and perturbations to the membrane [428, 429]. Other stresses that induce *CCH1* expression include compromised vesicle mediated transport in the protein secretory pathway and ER stress from the accumulation of unfolded proteins [430, 431]. The influx of extracellular calcium activates calcineurin-dependent signalling [430, 432], which exerts control on many cellular functions including ion homeostasis, cell wall and lipid synthesis, autophagy, vesicle transport and protein degradation [422, 433]. However, while *CCH1* was induced in T_{AL} , possibly from the disrupting effect of AMB and LF on the cell membrane, the majority of genes involved in the calcineurin pathway were not significantly expressed. Additionally, ER protein processing and response to misfolded proteins, which are also regulated by calcineurin signalling and induce *CCH1* expression, were repressed (Table 4.5). Targeting extracellular calcium uptake by knocking out *CCH1* may increase sensitivity to AMB and may be a potential antifungal drug target, as suggested by other studies [434].

TPK2: encodes a subunit of the Ras/cAMP-dependent PKA [435]. PKA regulates cell metabolism and growth according to available carbon sources, and Tpk2 is involved in the negative regulation of iron uptake as well as the induction of trehalose degradation [436]. PKA also negatively regulates autophagy by directly modifying Atg1 and alters its intracellular localisation such that it is not targeted to the PAS and halts the delivery of cargo to the vacuole for degradation [426]. *TPK2* was induced in T_A (Fig. 4.9a(ii)), which has also been reported by Belenky *et al.* (2013) [398]. Knock-out mutants were predicted to de-repress the iron regulon, reduce trehalose degradation needed to counter ROS production [401], dysregulate autophagy and increase susceptibility to AMB.

YAP5: is a basic leucine zipper iron-sensing transcription factor that controls iron overload [89]. It directly regulates *GRX4* that forms a complex with Grx3, Fra1 and Fra2 and controls the localisation of Aft1 [90]. Yap5 also regulates vacuolar iron storage through activation of *CCC1*, which sequesters cytosolic iron into the vacuole [89]. Knock-out mutants of this transcription factor have abnormal vacuoles. *YAP5* was induced in T_A along with the iron regulon (Fig. 4.11a), and the deletion of this gene was predicted to increase susceptibility to AMB by an unregulated importation of iron, resulting in increased oxidative damage in the cell.

YCT1: encodes a high affinity cysteine-specific transporter that is fungal-specific and localised to the ER [411]. Cysteines can be used for glutathione biosynthesis or broken down to homocysteine to generate amino acids. Cells may prefer to import extracellular cysteine as this takes less energy than its biosynthesis, and cysteine may be required in T_A where energy production is induced, possibly for the induction of stress responses, or alternatively in T_{AL} where energy needs to be conserved as its production is not induced (Table 4.5). *YCT1* was induced in T_A, where the need for extracellular cysteine was suggested by the activation of the iron regulon (Fig. 4.11a), an observation also reported by Philpott *et al.* (2012) who found that amino acid transporters were induced in iron starvation conditions [92]. *YCT1* was also induced in T_{AL} where the glutathione biosynthetic pathway was repressed, suggesting they may have an increased need for cysteine as a precursor for glutathione (Fig. 4.10). Deletion of this transporter is hypothesised to decrease the levels of cysteine available for glutathione biosynthesis and detoxification, leading to an increased susceptibility to AMB due to an inability to mount a full stress response to AMB exposure.

YOR387C and **VEL1:** encode uncharacterised proteins that are paralogous and have 93% similarity in gene sequence. *YOR387C* is located on chromosome XV, in proximity to *FIT2*, *FIT3* and *FRE3* that are regulated by *AFT1* in the iron regulon (SGD; www.yeastgenome.org/). In T_{AL}, *VEL1* is the most highly

repressed gene and is controlled by *ZAP1* and *IZH2* [437], while *YOR387C* is the next most repressed gene and is controlled by both *AFT1* and *ZAP1* (Fig. 4.11). Both *VEL1* and *YOR387C* are highly induced in zinc-depleted conditions [438] and encode soluble putative glycoproteins [439, 440]. Knock-out mutants of either or both genes are hypothesised to be disrupted in iron and zinc regulation and to have increased cell stress in response to AMB, leading to increased AMB susceptibility.

ZAP1: encodes transcription factor Zap1 that controls zinc homeostasis as well a range of other biological processes. These include response to stress, lipid biosynthesis, amino acid metabolism and protein processing [403, 419, 420, 441]. *zap1Δ* mutants have decreased resistance to oxidative stress, BAPTA, EDTA, decreased use of iron and abnormal vacuole morphologies. *ZAP1* transcription was repressed in T_{AL} but not differentially expressed in T_A. As Zap1 target genes were also repressed in T_{AL} (Fig. 4.11d), its deletion is predicted to mimic the AMB susceptibility seen following AMB+LF treatment.

The following genes were potential candidates for knock-out testing based on the selected criteria, but were not tested as they have been tested in other studies in *Saccharomyces* and/or *Cryptococcus*:

FET3: encodes a multicopper oxidase that oxidises ferrous iron to ferric iron for import by the transmembrane permease Ftr1 [442]. Orthologues of Fet3 have been identified in other fungi [116, 443] and *fet3Δ* mutants are defective in iron accumulation, respiration, and resistance to transition metals. *FET3* was a knock-out candidate as the protein imports iron with high affinity and was induced in both T_A and T_{AL} (Fig. 4.11), even though the iron regulon was differentially expressed in the two treatments. There has been evidence that some fungi are able to utilise transferrin and/or LF as a source of iron via the Fet3/Ftr1 iron uptake system [94, 444]. Therefore, this gene was chosen for deletion to rule out the possibility of LF acting as a siderophore with the prediction that the mutant will become more susceptible to AMB. However, literature searches found knock-outs of Fet3 orthologues were reported to be sensitive to AMB in *Cryptococcus* and *Candida* and Fet3 was therefore removed from the candidate list [116, 445].

IZH2: encodes a plasma membrane receptor homologous to mammalian adiponectin receptors that regulate sugar and lipid metabolism [446]. *Izh2* has been proposed as a potential antifungal drug target as its binding to the antifungal plant protein osmotin mediates apoptosis [446, 447]. Osmotin-bound *Izh2* also activates PKA via the cAMP pathway and suppresses stress responses by modulating the expression of transcription factors *NRG1/NRG2* and *MSN2/MSN4* [448, 449]. Additionally, *Izh2* is involved in iron homeostasis, through the repression of *FET3* via *TPK2*, and zinc homeostasis, by the

repression of *ZAP1* and *ZRT1* [437, 450, 451]. Overexpression of *IZH2* has been shown to increase levels of phytosphingosine (PHS) [450], which is a bioactive lipid required for sphingolipid biosynthesis, and PHS play important roles in cell signalling, regulation and intracellular trafficking [452]. Sphingolipids, together with ergosterol, constitute lipid rafts that deliver secretory proteins to their correct locations and have been observed to deliver virulence factors like phospholipase B and Cu/Zn superoxide dismutase in *Cryptococcus* [452, 453]. This suggests a possible mechanism of AMB+LF synergy through *Izh2*-mediated membrane disruption. Although *IZH2* was repressed in T_A (Table 4.7) and its deletion was hypothesised to cause an increased sensitivity to AMB by disrupting sphingolipid production, mutants have been observed to be resistant to AMB [447, 451] and *IZH2* was removed from the candidate list.

THR1: is a homoserine kinase that is required for threonine biosynthesis [454]. Disruption of *THR1* causes threonine auxotrophy as well as decreased resistance to oxidative stress, fluconazole, ionic stress and changes in pH. Knock-out mutants also accumulate homoserine from the threonine pathway, which replaces threonine as a toxic analogue and disrupts protein degradation [455]. *THR1* was up-regulated in T_A and the knock-out mutant was predicted to become more susceptible to AMB from defective proteolytic pathways that are induced in T_A (Table 4.5). Alternatively, aspartate metabolism would be directed into the sulphur assimilation pathway through *MET6* and lead to an overaccumulation of homocysteine (Fig. 4.10), and increased susceptibility to AMB might occur via dual oxidative damage from homocysteine and AMB. *THR1* has been suggested as an antifungal drug target, however, as *thr1Δ* mutants have already been reported to be sensitive to AMB in *Saccharomyces* and lethal in *Cryptococcus* [456-458], the gene was removed from the candidate gene list.

Table 4.7. Candidate genes for knock-out mutant generation and their selection criteria

| Gene name | T _A log ₂ FC ^a | T _{AL} log ₂ FC | Orthologues in fungal pathogens ^b | Pathway | Knock-out Phenotypes ^c | Description of gene type |
|---------------|---|-------------------------------------|--|--|---|---|
| <i>AFT1</i> * | 0.34 | | <i>C. glabrata</i> (CAGL0H03487g) | Iron homeostasis | Decreased iron accumulation Decreased resistance to DFO and DFP Increased protein accumulation | Transcription factor involved in regulation of iron homeostasis |
| <i>ATG1</i> * | 1.30 | 0.43 | <i>C. neoformans</i> (CNAG_05005) <i>C. albicans</i> (orf19.3841) <i>C. glabrata</i> (CAGL0L06006g) <i>A. fumigatus</i> (Afu4g09050) | Autophagy and CVT | Absence of autophagy and mitophagy Increased accumulation of ROS Decreased respiratory growth | Protein serine/threonine kinase required for vesicle formation in autophagy and CVT pathway |
| <i>CCH1</i> * | | 0.31 | <i>C. neoformans</i> (CNAG_01208) <i>C. albicans</i> (orf19.3298) <i>C. glabrata</i> (CAGL0B02211g) <i>A. fumigatus</i> (Afu1g11110) | Calcium homeostasis Cell signalling | Decreased resistance to iron Abnormal vacuole morphology Decreased stress resistance Decreased calcium accumulation | Regulation of transmembrane transport |
| <i>FET3</i> | 0.60 | 0.69 | <i>C. neoformans</i> (CNAG_02958/ CNAG_06241) <i>C. albicans</i> (Orf19.4211/Orf19.4212/ Orf19.4213/Orf19.4215/ Orf19.943) <i>C. glabrata</i> (CAGL0F06413g) <i>A. fumigatus</i> (Afu4g14490/Afu5g03790) | Iron regulon | Decreased oxidative stress resistance Decreased resistance to CPO and DSX Abnormal vacuole morphology Decreased respiratory growth Decreased resistance to metals | Complex with Ftr1 involved in high affinity iron uptake |
| <i>IZH2</i> | -0.36 | | <i>C. neoformans</i> (CNAG_05370) <i>C. glabrata</i> (CAGL0G04631g) <i>A. fumigatus</i> (Afu3g10570) | Zinc/lipid homeostasis | Absence of apoptosis Decreased accumulation of ROS Decreased resistance to CPO Abnormal vacuole morphology Increased resistance to polyenes [447] | Plasma membrane receptor for plant antifungal osmotin |
| <i>THR1</i> | 0.32 | 0.55 | <i>C. neoformans</i> (CNAG_04156) <i>C. albicans</i> (orf19.923) <i>C. glabrata</i> (CAGL0J00649g) <i>A. fumigatus</i> (Afu5g05820) | Threonine synthesis | Auxotrophy Decreased resistance to FLC Decreased resistance to oxidative stress Susceptible to AMB [457] | Homoserine kinase required for threonine biosynthesis |
| <i>TPK2</i> * | 0.43 | | <i>C. neoformans</i> (CNAG_00396/CNAG_04162) <i>C. albicans</i> (orf19.2277/orf19.4892) | cAMP pathway | Abnormal vacuole morphology | Protein kinase A subunit involved in repression of iron uptake genes |

| | | | <i>C. glabrata</i> (CAGL0G09020g/ CAGL0M08404g) <i>A. fumigatus</i> (Afu2g12200/Afu5g08570) | | | |
|----------------------------|-------|------|---|---------------------------------------|---|--|
| <i>VEL1</i> * [#] | -5.51 | None | | Iron/zinc homeostasis | Decreased invasive growth | Putative cell surface glycoprotein [439] |
| <i>YAP5</i> * | 0.31 | | <i>C. glabrata</i> (CAGL0K08756g) | Iron homeostasis | Abnormal vacuole morphology | Transcription factor involved in regulation of iron homeostasis |
| <i>YCT1</i> * | 0.66 | 0.65 | <i>A. fumigatus</i> (Afu7g06790) | Sulphur assimilation, stress response | Absent utilisation of sulphur source Abnormal vacuole morphology | Transporter involved in cysteine import and sulphur assimilation |
| <i>YOR387C</i> * | -4.91 | None | | Iron/zinc homeostasis | Decreased invasive growth | Putative cell surface glycoprotein [439] |
| <i>ZAP1</i> * | -2.22 | | <i>C. neoformans</i> (CNAG_05392) <i>C. albicans</i> (orf19.3794) <i>C. glabrata</i> (CAGL0J05060g) | Zinc homeostasis | Decreased oxidative stress resistance Decreased resistance to BAPTA, EDTA Decreased use of iron source Abnormal vacuole morphology | Transcription factor involved in regulation of zinc homeostasis |

*Genes selected for knock-out mutant analysis. [#] Used for double knock-out with *YOR387C*

^aFold-change

^bWhether an orthologue of the *S. cerevisiae* gene is present in the genomes of *C. neoformans*, *C. albicans* and *A. fumigatus* using OrthoMCL [379]

^cPhenotypes were according to SGD unless referenced with specific study (www.yeastgenome.org/)

Knock-out mutants obtained from the Yeast Deletion Project collection [341] were screened by PCR using the primers listed in Appendix 4.2 to confirm that the genes of interest were deleted. Each primer set used to confirm gene deletions amplified the expected band sizes from the DNA of wild type strains and knock-out mutants (Appendix 4.6 and 4.7). The knock-out mutants were tested for susceptibility to AMB, FLC, heat (37 °C), cell wall inhibitors (calcofluor white (CW), salt (NaCl), caffeine, and SDS), oxidative stress (hydrogen peroxide; H₂O₂) and nitrosative stress; NaNO₂). With the exception of *zap1Δ*, all knock-out mutants grew to a similar extent as the wild type strain on the control plates. Of the knock-out mutants tested (Fig. 4.13), only *aft1Δ* was susceptible to AMB and all other stressing agents. *zap1Δ* had increased susceptibility to AMB and other stressors except NaCl, NaNO₂ and 0.005% SDS; and was susceptible to 0.01% SDS (not shown). These results confirm the importance of Aft1 and Zap1 in cell wall and membrane maintenance, and for AMB and general stress survival, as predicted by the regulatory networks (Fig. 4.11). The lack of susceptibility to stressors by other mutants suggests that the yeast cell has redundant pathways that compensate for the deletion of the other target genes.

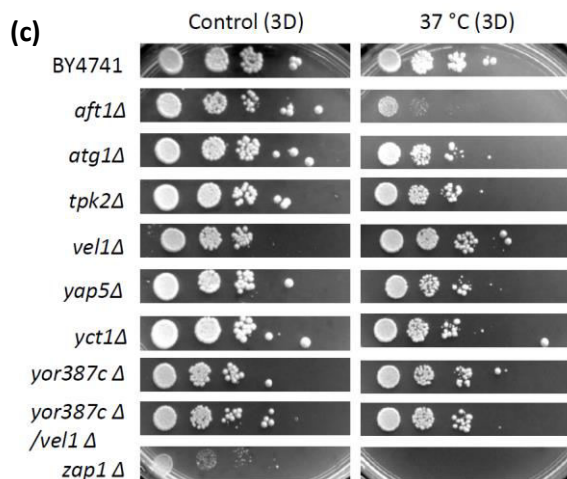
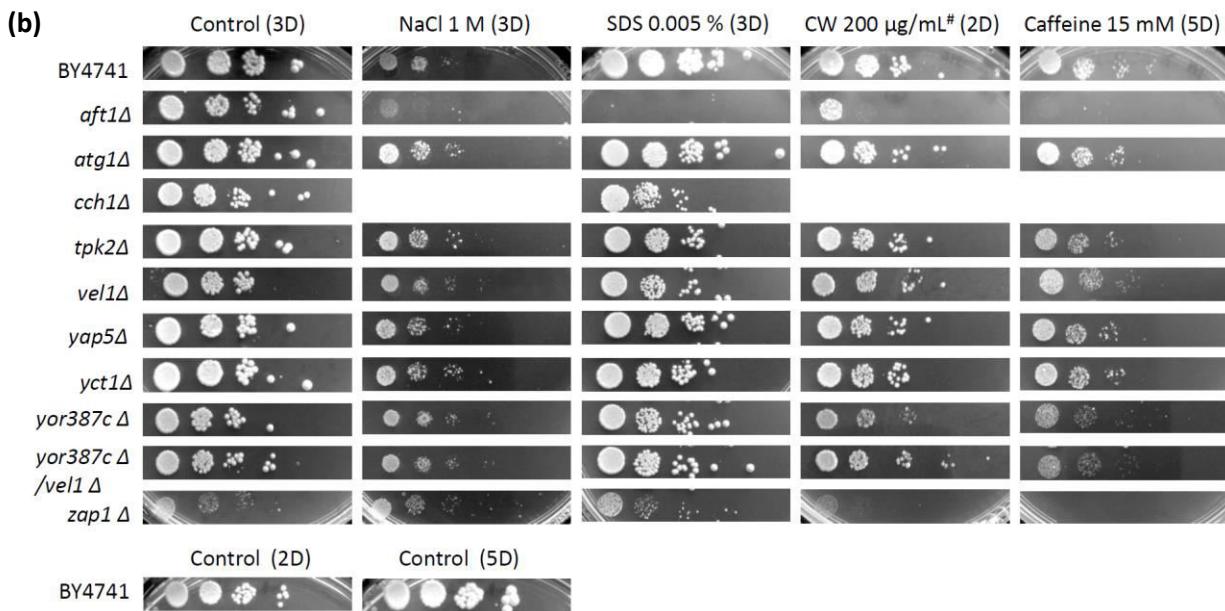
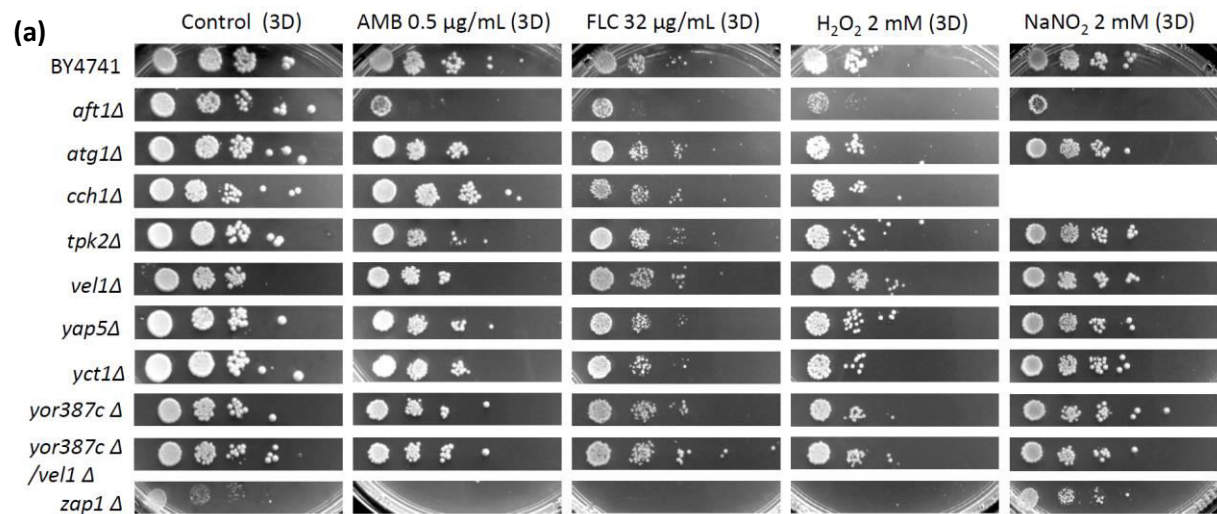


Figure 4.13. Spot plate assays of knock-out mutants grown **(a)** on plates containing antifungal agents, oxidative and nitrosative stressors; **(b)** on plates containing cell wall stressing agents; and **(c)** at 37 °C. 10-fold serial dilutions of cultures were plated on synthetic complete agar from left to right starting at 10⁶ cells/mL. 'D' indicates the days of growth. #Calcofluor white (CW) was tested at 200 $\mu\text{g}/\text{mL}$ except with *vel1* Δ , *yor387c* Δ and *vel1* Δ /*yor387c* Δ where it was accidentally tested at 300 $\mu\text{g}/\text{mL}$. In **(a)** and **(b)** *cch1* Δ was tested later with only selected stressing agents.

4.4.4.3. Testing downstream binding targets of Aft1 and Zap1 as possible drug targets

Iron and zinc are essential trace elements and the direct disruption of their regulation through *AFT1* and *ZAP1* deletion confirms their necessity in cellular functions (Fig. 4.13). While targeting zinc and iron homeostasis through disrupting *AFT1* and *ZAP1* might be considered a promising approach for enhancing current antifungal drugs (AMB and FLC), *AFT1* is not widely conserved across pathogenic fungal species, while *ZAP1* is conserved between fungi and mammals, although it does have druggable domains (from OrthoMCL [92, 379]). Given that iron and zinc are important in humans, any disruption to their regulation in the human host could cause the same problems with side effects as the iron chelating drugs (Sections 3.1.3.1 – 3.1.3.6), hence less conserved targets were sought.

Targets that require metal ions but are not involved in their uptake may be better choices as potential antifungal targets. To investigate this, mutants with disruptions to genes encoding mutual targets of Aft1 and Zap1 were targeted. As above, a set of criteria was implemented to choose the best candidate genes. The genes selected were:

- binding targets of Zap1 and Aft1 transcription factors
- differentially expressed in T_A or T_{AL}
- associated with a list of manually curated enriched GO terms from SOMs analysis
- not homologous with human genes, based on the OrthoMCL database [379]
- homologous to genes in *C. neoformans*, *C. albicans*, *C. glabrata* and *A. fumigatus* based on the OrthoMCL database [379]
- ‘druggable’ based on DrugBank (ver. 4.1) (<http://www.drugbank.ca/>) [459], from common domains in their protein sequences based on Pfam (ver. 27.0) [460]

These criteria narrowed down the target to two genes: *MET32* and *MTD1*. *Met32* is an auxiliary transcription factor involved in targeting Met4 to sulphur metabolism genes as previously mentioned (4.4.2.2). *MTD1* is an NAD-dependant methylenetetrahydrofolate dehydrogenase involved in folate biosynthesis [461] and was down-regulated in T_A and up-regulated in T_{AL} (not shown). Knock-outs of these genes were tested for their response to AMB, FLC, oxidative and cell wall stress. Unfortunately, neither of the knock-out mutants were susceptible to any of the stressing agents tested and grew to the

same extent as the wild type strain (Fig.4.14). This suggests that direct disruption of iron and zinc regulation at the level of overall control, i.e., Aft1 and Zap1 as seen in Figure 4.13, is needed to increase susceptibility to antifungal drugs.

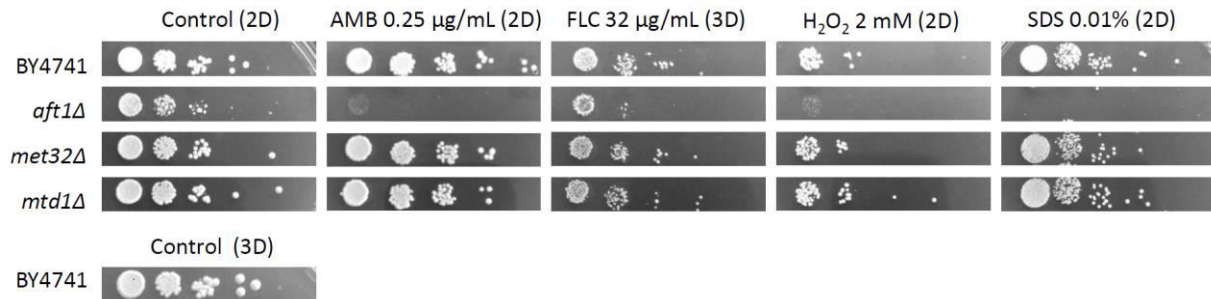


Figure 4.14. Knock-out mutants of ‘druggable’ targets tested on various stressors. *aft1* Δ was included as a susceptible control. 10-fold serial dilutions of cells starting at 10^6 cell/mL from left to right were plated onto synthetic complete agar. ‘D’ indicates the number of days grown at 30 °C.

4.5. Discussion – AMB+LF synergy in *S. cerevisiae* S288C

4.5.1. Exploring the molecular mechanisms of synergy between antifungals and iron chelators for novel antifungal therapies

There is increased interest in synergising compounds that potentiate current antifungal drugs [69, 70, 462]. The use of iron chelators as synergents is rationalised by the fact that iron is a critical growth factor for fungal pathogens during host infection. *In vitro*, some iron chelators have been found to synergise the activity of antifungal drugs against fungal pathogens [9, 10], and in animal infection studies iron chelation has been seen to potentiate antifungal treatment, reducing fungal dissemination and organ burden and increasing survival [73, 74].

A range of iron chelating agents and antifungal drugs were screened in *Saccharomyces* and *Cryptococcus* (in Chapter 3) with the expectation of finding a number of synergistic combinations for transcriptomic analysis. However, the only synergistic combination was AMB and LF, and the focus then became understanding this synergy. As supplementation with iron did not rescue AMB+LF synergy (Fig. 3.4) and other iron chelating agents were not synergistic, it appeared that iron chelation was not the primary cause of synergy with AMB.

To understand how LF potentiates AMB, yeast cells were treated at the fractional inhibitory concentrations (FIC) of each agent alone and in combination to find the ID₂₀ timepoint, when cells were harvested for RNA-sequencing. LF is only weakly antifungal toward *Cryptococcus* and *Saccharomyces* (Table 3.2), and at the FIC (2 µg/mL) it did not inhibit growth or produce an ID₂₀ (Fig. 4.4). Furthermore, the transcriptome of *S. cerevisiae* treated with 2 µg/mL LF had no changes in gene expression compared to the untreated control (Fig. 4.6). Hence, this chapter focuses on understanding the response to AMB+LF treatment by analysing the yeast transcriptome when treated with AMB treatment alone and comparing this to the response to AMB+LF.

4.5.2. The addition of LF to AMB caused unexpected changes in the transcriptomic response by *S. cerevisiae* that appear contrary to enhanced growth inhibition

With AMB treatment, *Saccharomyces* cells mounted a response fairly typical to the environmental stress response (ESR), which is a set of differentially regulated responses that are common to a variety of suboptimal environmental conditions including heat and osmotic shock, oxidative stress and nutrient starvation [347]. Responses seen in the analysis of T_A that were similar to the ESR included the up-

regulation of the cellular responses to stress, mitochondrial processes and carbohydrate metabolism for the generation of energy, metabolite and metal ion transport and autophagy (Table 4.5). Responses that were down-regulated were associated with cell growth, such as DNA, ribosome and protein synthesis (Table 4.5). Exceptions to the ESR were the down-regulation of ergosterol biosynthesis and protein folding, which have been reported in microarray studies in AMB-treated *Saccharomyces* and *Candida* cells (Table 4.5) [346, 463].

In contrast, gene expression in T_{AL} was more indicative of an absence of cellular stress. In addition, and contrary to expectations in the presence of an iron chelator, cells did not appear to have an increased requirement for iron and other trace metals as there was an absence of enrichments relating to iron homeostasis and down-regulation in zinc uptake (Table 4.5 and Fig. 4.9b(i)). Finally, an up-regulation of transcripts related to amino acid and protein synthesis suggested active growth. Given the more rapid and severe growth inhibition caused by AMB+LF compared to AMB treatment (Fig. 4.4), the observed responses were surprising and contrary to expected cell stress and death responses. Down-regulation of responses associated with stress does not correspond to the growth inhibition mechanism reported for AMB and LF when used independently, which both involve an increased production of endogenous ROS [303]. LF also inhibits growth through the chelation of iron and other metals and through perturbations to the cell membrane and cell wall [464-467]. While it was established in Chapter 3 that iron chelation by LF was not the cause of synergy when combined with AMB (Fig. 3.4), LF is nonetheless a chelator, and the down-regulation of metal uptake genes (Fig. 4.11b and d) is difficult to explain.

The cellular response to AMB and AMB+LF are summarised in the model presented in Figure 4.15 and are discussed in the following sections.

4.5.2.1. The presence of LF down-regulated stress-associated responses that were induced by AMB

T_A showed an up-regulation of antioxidant responses related to hydrogen peroxide catabolism and trehalose metabolism [401] (Table 4.5), which suggested the induction of oxidative stress. This is consistent with many studies that have shown that AMB induces the accumulation of ROS in fungi and that antioxidants are produced as a mechanism to protect cells from ROS damage [303, 468-471]. In the current study, SOMs analysis suggested an increase in mitochondrial stress with the induction of PKA signalling (Fig. 4.9a(ii)), which increases the production of ROS in the mitochondria through increased respiratory function [398]. Additionally, mitophagy, which prevents apoptosis by degrading damaged

mitochondria [400], was up-regulated (Table 4.5) and suggested oxidative stress was induced following AMB treatment.

In contrast to T_A , the synergistic response seen in T_{AL} was characterised by a down-regulation in responses associated with stress (Fig. 4.15). This was seen by the down-regulation of transcripts involved in glutathione biosynthesis and the shutdown of GO terms related to ER processes that are typical of ERAD, which suggests either the cells fail to sense oxidative damage or are unable to mount an appropriate response. Glutathione is a major antioxidant involved in oxidative stress responses [472]. Down-regulation of glutathione biosynthesis may be a secondary effect resulting from the down-regulation of sulphur metabolic pathways that in turn limit homocysteine production (Fig. 4.10). Although contrary to an expected increase in antioxidant production in response to AMB+LF, the down-regulation of homocysteine production may be a mechanism to avoid homocysteine toxicity as this can cause oxidative stress, alter purine biosynthesis, and inhibit transmethylation reactions [473, 474].

In T_{AL} , there was a down-regulation of protein sorting processes while enrichments for protein synthesis were up-regulated, suggesting disruption to protein turnover (Table 4.5), which would be expected to activate ERAD. Contrary to this, however, the processes involved in ERAD were down-regulated in T_{AL} (Fig. 4.9b(iii), (v) – (vii)), which may be linked to the decrease in glutathione production noted above (Fig. 4.15). The ER lumen is highly oxidising as the process of protein folding generates ROS [475] and glutathiones are present in the ER as a net reductant to maintain redox balance [476]. Protein folding activities in the ER have been shown to be suppressed when glutathione is depleted, indicating a dependency between these processes [477]. In T_{AL} , down-regulation of ERAD processes and the repression of glutathione production from the down-regulation of sulphur metabolising pathways may be a response to minimise oxidative damage in the ER, which can induce apoptosis. The ER stores calcium, which has a major role in signalling and is maintained at low cytosolic concentrations [93]. One of the consequences of oxidative stress in the ER is the leakage of calcium ions into the cytosol where they can come into contact with the mitochondria and induce apoptosis [424].

4.5.2.2. The addition of LF decreased the need for trace metals that was required with AMB treatment

In T_A , network analysis suggested activation of the iron regulon through the up-regulation of *AFT1* and increased iron uptake processes (Fig. 4.11a). A similar response was reported by Zhang *et al.* (2002) and Agarwal *et al.* (2003) with up-regulation of genes involved in metal uptake and transport seen in their microarray analysis of AMB-treated *Saccharomyces* and *Candida* cells [346, 463]. Iron is required for

many cellular processes and is co-regulated with processes involved in oxygen metabolism, such as respiration and lipid biosynthesis [109]. Iron is also required as a catalytic cofactor in catalases and peroxidases that are part of the response to oxidative stress [77]. Up-regulation of iron homeostasis by AMB correlates with the induction of mitochondrial stress that was suggested by SOMs analysis (Fig. 4.9a(ii)). The importance of iron regulation to AMB susceptibility was further shown by the increased susceptibility of the *aft1Δ* strain to AMB and other stressors (Fig. 4.13).

In contrast to this, the addition of LF shut down the activated iron regulon in T_A and caused a repression of genes involved in iron uptake (Fig. 4.11b and 4.15). This was unexpected as iron should be limited by LF chelation. Furthermore, the enrichment for Fe-S assembly, which requires iron and sulphur, was induced (Fig. 4.9b(ii)). Repression of the iron regulon may be associated with the down-regulation of stress responses as these are co-regulated, as mentioned previously. The presence of LF also caused zinc transport and the expression of the zinc-controlling transcription factor Zap1 to be down-regulated (Fig. 4.9b(i)), suggesting the cell was either not sensing or not responding appropriately to zinc depletion. Zinc is another essential metal that is needed as a structural and catalytic cofactor in many proteins and its depletion induces the production of oxidants [478]. Zinc deficiency usually up-regulates the expression of oxidative stress response genes through the activity of Zap1 [419], and the repression of oxidative stress responses observed in T_{AL} is consistent with *ZAP1* down-regulation. Interestingly, network analysis suggested that the down-regulation of *ZAP1* in T_{AL} was also associated with the repression of genes involved in protein processing and sulphur metabolism (Fig. 4.11d). This finding suggests that the down-regulation of oxidative stress and ER function may be linked to zinc regulation. Similar to iron, *zap1Δ* showed increased susceptibility to AMB (Fig. 4.13), which suggests zinc regulation is also important for AMB susceptibility.

In summary, the transcriptome analysis suggests the addition of LF caused a dysregulation of responses to stress and metal regulation (Fig. 4.15). AMB alone caused up-regulation of oxidative stress responses and increased stress in the mitochondria as suggested by the activation of PKA signalling, along with an increased need for iron through the activation of the iron regulon. In the synergistic response to AMB+LF, however, the coordinated stress responses of glutathione biosynthesis and ERAD were down-regulated, along with metal ion regulation. These stress-associated responses may be linked to the regulation of zinc via *ZAP1*, which is important in AMB susceptibility, but was repressed with the addition of LF.

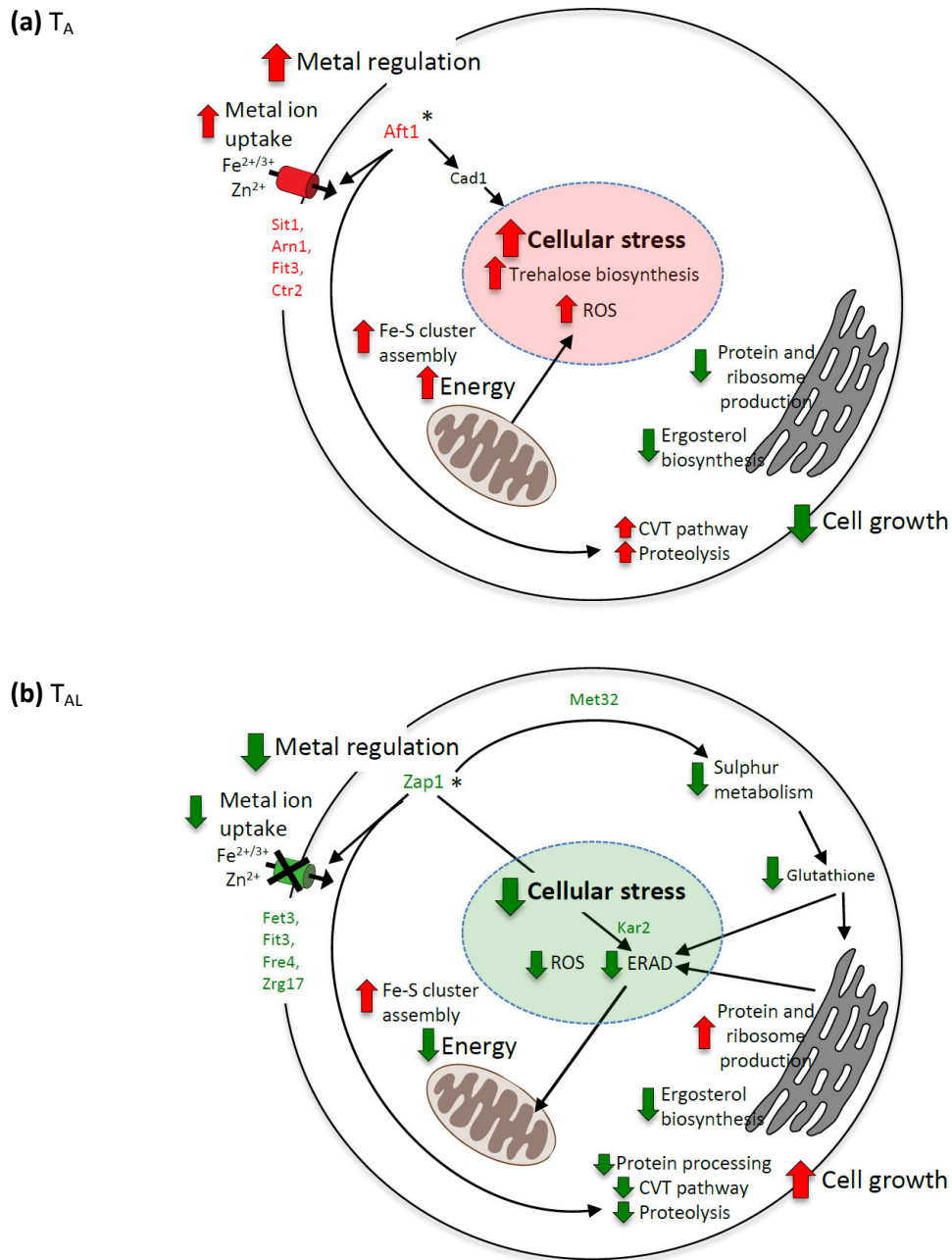


Figure 4.15. Model of the transcriptome response to AMB+LF synergy in *S. cerevisiae* S288C. **(a)** In T_A , a range of stress responses were induced, metal transport was up-regulated via the transcription factor *AFT1* and cell growth was shut down. **(b)** In T_{AL} , there was down-regulation of stress responses and of iron and zinc metal ion uptake mediated by *AFT1* and *ZAP1*. Proteolysis was repressed while protein and ribosome production, which are indicative of cell growth, were induced. This paradoxical response suggests a general dysfunction of the appropriate cellular stress response and metal ion homeostasis, resulting in enhanced cell death. Red arrows and text: up-regulated processes; green arrows and text: down-regulated processes. Black arrows: observed effect of processes on other cellular functions in drug treatments. Asterisks: gene knock-out mutants that have increased susceptibility to AMB treatment.

4.5.3. Appropriate regulation of stress responses is required for survival against combinatorial stresses

Although the down-regulation of stress-associated responses seen in T_{AL} appeared paradoxical, other studies examining the enhanced antifungal activity of combined drug treatments or chemical stressors have reported similar effects. Proteomic analysis of synergy between FLC and the BBR derivative B-7b in *Candida albicans* also found GO enrichments related to protein folding and regulation of stress defences were down-regulated by FLC+B-7b compared to FLC treatment alone. Interaction network analysis of the differentially expressed proteins found those regulating stress were highly connected, indicating that the regulation of stress responses had a major role in FLC+B-7b synergy. Interestingly, FLC+B-7b treatment did not augment ROS production and was only synergistic in FLC-resistant *C. albicans* strains, suggesting FLC+B-7b inhibits cellular mechanisms that cause resistance to FLC [321].

A combined exposure to cationic and oxidative stresses has also been seen to reduce stress responses but enhance cell death in *Candida* [479, 480]. Comparison of the transcriptome response to NaCl and H₂O₂ treatments alone and in combination found stress responses were up-regulated with each individual agent, but were not enriched in NaCl+H₂O₂. Cationic and oxidative stresses activate Hog1 and Cap1, which are regulatory proteins involved in different stress signalling pathways that mediate osmo-adaptative responses and antioxidant gene expressions in *Candida*. Expression analysis of Hog1 and Cap1 and their respective gene targets following NaCl+H₂O₂ treatment found that while Hog1 was activated, some of its downstream cationic stress targets were not expressed. Cap1 was not activated following NaCl+H₂O₂ treatment, and Cap1-dependent genes, such as catalases and thioredoxin reductases, were not up-regulated. This reduced activity of catalase was correlated with an increased accumulation of ROS and increased anti-*Candida* activity by NaCl+H₂O₂ treatment. Overall, this showed that the stress response to NaCl impaired the appropriate response to oxidative stress by disrupting the expression of catalase, which was required to neutralise ROS induced by H₂O₂ [479]. The disruption of one stress signalling pathway by the activity of another was termed 'stress pathway interference' and was suggested as a new target for antifungal development.

While stress pathway interference cannot be deduced in the current study as stress pathways were not activated by LF alone, this does illustrate how a paradoxical down-regulation of stress responses can contribute to enhanced cell death. Cross talk exists between the many stress signalling pathways in a cell, such as between calcineurin and Rim101 signalling pathways, which both mediate adaptive responses to pH and cell wall perturbations [481]. In response to combinatorial stresses, stress signalling pathways can either act cooperatively or antagonistically with one another, resulting in either stress

adaptation and survival, or cell death [480]. Therefore, while the down-regulation of stress responses during AMB+LF synergy suggested an avoidance of oxidative stress, this may instead imply a disruption to the appropriate regulation or activation of stress-associated responses.

4.5.3.1. Dysregulation of stress responses in AMB+LF synergy is associated with metal ion homeostasis

Aft1 and Zap1 were suggested to play critical roles in AMB+LF synergy. Network analysis suggested Aft1 was involved in various cellular functions in T_A including stress responses and nutrient metabolism (Fig. 4.11a and 4.11b), which is consistent with iron being essential for various homeostatic processes [77, 307]. In contrast, absence of *AFT1* expression and shut down of the iron regulon in T_{AL} were associated with down-regulation of cellular stress responses (Fig. 4.11b), which together with the increased susceptibility of *aft1Δ* to AMB (Fig. 4.13) suggested *AFT1* is needed to maintain an appropriate regulation of stress responses to survive AMB+LF inhibition.

Zap1 had a profound effect in AMB+LF synergy. Analysis of differential expression in T_{AL} suggested down-regulation of many genes regulated by *Zap1*. A subset of Zap1-regulated genes is shown in the network analysis, which illustrates the central role of *ZAP1* in functions performed in the ER, sulphur metabolic pathways and response to stress (Fig. 4.11d). This, together with the increased susceptibility of the *zap1Δ* mutant to AMB and other stressors, suggests that *ZAP1* may have a central role in LF-mediated drug synergy (Fig. 4.13).

Sulphur metabolism is involved in glutathione biosynthesis and is coordinated with zinc homeostasis through the activity of Zap1. Under zinc deficiency, Zap1 is activated and down-regulates sulphur metabolism by increasing the expression of the *MET30* [403]. Met30 is associated with a SCF ubiquitin ligase complex and binds to and inhibits the activity of transcriptional activator Met4 [482]. This prevents the interaction of Met4, which does not have DNA binding activity, with DNA binding cofactors Met31 and/or Met32 that then regulate sulphur metabolic genes [412]. As Zap1 activity and sulphur metabolism are normally negatively correlated, the down-regulation of both processes seen in T_{AL} suggests that cross talk between them was disrupted. This in turn may have affected stress responses, such as by decreasing production of the antioxidant glutathione. Zap1 also controls the activity of *MET32*, which was the only gene encoding a transcription factor involved in sulphur metabolism to be differentially regulated in T_{AL} (Fig. 4.9b(iii)). However, knocking out *MET32* did not increase susceptibility to AMB (Fig. 4.14), which suggests that cross-communication between zinc homeostasis and the regulation of sulphur pathways is complex and that redundant processes probably occur.

Similar to sulphur metabolism, Zap1 regulates the expression of genes involved in ER function and homeostasis, such as protein sorting and degradation and lipid metabolism [420]. In T_{AL} , network analysis of suggested Zap1 caused the regulation of ER-related stress responses to be suppressed (Fig. 4.11d). Among the genes under the regulation of Zap1, *KAR2*, which encodes an ATPase/chaperone and is integral to ER stress tolerance [483, 484], was down-regulated (Fig. 4.11d). Kar2 is an essential protein that has a basal level of expression and is usually bound to Ire1 under normal ER conditions [485, 486]. Ire1 is a kinase/endoribonuclease that is required for the synthesis of the ER stress-specific transcription factor Hac1 [487]. Under ER stress, Kar2 disassociates from Ire1, which in turn induces the ER stress response through the synthesis and activity of Hac1 [486, 487]. As both *IRE1* and *HAC1* were not observed in T_{AL} (not shown) and *KAR2*, which is normally constitutively expressed, was down-regulated by Zap1 (Fig. 4.11d), this suggests that Zap1 affects the regulation of the ER stress response.

The ER requires zinc ions for function and homeostasis, and disruption to ER zinc concentration, such as through deletion of ER zinc transporters *Zrg17* and *Msc2*, induces ER stress [421, 488]. However, the induction of ER stress responses including ERAD also requires cytosolic zinc as *msc2Δ* mutants are defective in ERAD induction under zinc deficient conditions [488]. In T_{AL} , where ERAD processes were down-regulated (Fig. 4.9b(iii), (v) – (vii)), network analysis indicated that Zap1 suppressed extracellular and ER zinc uptake by down-regulating *MSC2* and *ZRG17* (Fig. 4.11d). This suggested that the down-regulation of overall zinc homeostasis by Zap1 repression also affected induction of ERAD due to lack of ER zinc that is required for this stress response.

Zap1 also plays a role in oxidative stress responses as it controls the expression of antioxidants like *TSA1* and *CTT1* [420, 489]. Down-regulation of target genes involved in oxidative stress in the Zap1 regulatory network (Fig. 4.11d) and the susceptibility of *zap1Δ* to hydrogen peroxide showed the importance of Zap1 for surviving oxidative stress (Fig. 4.13).

Overall in T_{AL} , Zap1 and Aft1 are suggested to be important for cellular stress responses as these metal-controlling transcription factors directly and indirectly affected stress regulation. Compared to Aft1, Zap1 appeared to have a more pronounced impact on the dysregulation of stress responses in AMB+LF synergy. This included the disrupted cross talk between Zap1 and sulphur metabolism, where regulation by Zap1 on sulphur metabolic pathways affected the expression of stress defence responses such as glutathione biosynthesis. Additionally, the repression of Zap1 seen in T_{AL} may have disrupted the induction of ER stress responses such as ERAD through down-regulation of *KAR2*, which is needed to express the ER stress transcription factor Hac1. As zinc ions are required for ER homeostasis, down-

regulation of Zap1 may have also disrupted ER stress tolerance through an overall decrease in zinc ion uptake. Together, this suggests that disruption of stress-associated responses via metal regulation and homeostasis may be a mechanism of synergy in AMB+LF.

4.5.4. LF enhances disruption in membrane-mediated trafficking that is associated with AMB treatment

Enriched processes that were not related to the dysregulation of stress-associated responses were also seen. These included down-regulation of ergosterol biosynthesis over that seen in response to AMB treatment (Table 4.5), and repression of vacuole-mediated degradation processes like the CVT pathway and nucleophagy (Fig. 4.9b(vi)). Disruptions to ergosterol biosynthesis affect vacuole function and membrane fusion and trafficking [490, 491], which were down-regulated in T_{AL} (Fig. 4.9b(vi – vii)). While these processes were not observed when AMB was used alone at sub-inhibitory concentrations, lethal concentrations of AMB have been shown to disrupt membrane-mediated trafficking such as cargo delivery to the vacuole [492]. As the addition of LF to sub-inhibitory concentrations of AMB caused a similar disruption in membrane-mediated trafficking that is seen at higher concentrations of AMB, this suggests that LF may enhance activities of AMB that would normally be sub-inhibitory. This may therefore be another mechanism whereby LF mediates synergy with AMB, in addition to the dysregulation of stress responses.

4.6. Results – Analysis of AMB+LF synergy in *C. neoformans* H99

4.6.1. GO enrichments of differentially expressed H99 genes in T_A and T_{AL}

GO enrichments analyses in T_A and T_{AL} for *C. neoformans* H99 are shown in Table 4.8. This also includes the GO terms enriched in response to each drug treatment in *S. cerevisiae* S288C for comparison. Enriched GO terms in T_A and T_{AL} had the same direction of expression in H99, which is unlike S288C where the regulation of some GO enrichments changed in direction with the addition of LF. Overall, the transcriptional responses between T_A and T_{AL} in H99 were similar: nucleic acid metabolism, replication, cell organisation, transcription, translation and lipid biosynthesis were suppressed, and terms related to energy production and lipid catabolism were induced. GO enrichments unique to either drug treatment include protein folding, which was suppressed in T_A, and actin polymerisation, responses to oxidative stress and autophagy, which were induced in T_{AL}. Overall, AMB inhibited all aspects of cell function in H99, except for processes required for the production of energy, and lipid catabolism. The addition of LF to AMB treatment caused similar dysfunctions to the cell, but additionally induced autophagy and cell stress.

Table 4.8. Major GO enrichments in T_A and T_{AL} for *C. neoformans* H99 and *S. cerevisiae* S288C

| GO term enrichments | GO ID | H99 | | S288C | |
|---|------------|----------------|-----------------|----------------|-----------------|
| | | T _A | T _{AL} | T _A | T _{AL} |
| Nucleic acid and amino acid related | | | | | |
| Nitrogen compound metabolic process | GO:0006807 | 1.65 | 1.71 | | 4.88 |
| Nucleic acid metabolic process | GO:0090304 | 2.07 | 2.07 | 2.01 | |
| Nucleobase-containing compound catabolic process | GO:0034655 | | | 1.88 | |
| Purine-containing compound metabolic process | GO:0072521 | | | 1.86 | |
| Pyridine-containing compound metabolic process | GO:0072524 | 2.76 | | 2.47 | |
| Cellular amino acid metabolic process | GO:0006520 | | | 3.69 | 8.44 |
| Cell organisation and replication related | | | | | |
| Cellular component biogenesis | GO:0044085 | 2.55 | 2.65 | 2.69 | |
| DNA replication | GO:0006260 | 4.09 | 4.91 | | |
| Cell division | GO:0051301 | 2.26 | 2.6 | | |
| Microtubule-based process | GO:0007017 | 5.53 | 6.33 | | |
| Actin polymerisation or depolymerisation | GO:0008154 | | 4.44 | | |
| Energy related | | | | | |
| Tricarboxylic acid cycle | GO:0006099 | 9.69 | 11.67 | 3.27 | |
| Mitochondrial electron transport, ubiquinol to cytochrome c | GO:0006122 | | | 7.43 | |
| Generation of precursor metabolites and energy | GO:0006091 | | | 2.06 | |

| | | | | | |
|---|------------|------|-------|-------|-------|
| Oxidation-reduction process | GO:0055114 | 2.23 | 1.98 | 2.31 | 2.09 |
| Carbohydrate catabolic process | GO:0016052 | 3.2 | 2.45 | | |
| Transcription and translation related | | | | | |
| Ribonucleoprotein complex biogenesis | GO:0022613 | 4.57 | 4.36 | | |
| Ribosome biogenesis | GO:0042254 | 6.61 | 6.96 | 5.36 | 3.88 |
| RNA processing | GO:0006396 | 2.05 | 1.51 | 2.71 | |
| Translational initiation | GO:0006413 | 1.92 | | | |
| Regulation of translational initiation | GO:0006446 | | | 4.83 | |
| Transcription of nuclear large rRNA transcript from RNA polymerase I promoter | GO:0042790 | 8.43 | 6.63 | 5.42 | |
| Protein related | | | | | |
| Cellular protein metabolic process | GO:0044267 | 1.38 | | | |
| Protein folding | GO:0006457 | 2.54 | | 2.18 | 3.77 |
| Post-translational protein targeting to membrane, translocation | GO:0031204 | | | | 16.65 |
| Ubiquitin-dependent protein catabolic process | GO:0006511 | | | | 2.51 |
| ER-associated ubiquitin-dependent protein catabolic process | GO:0030433 | | | | 6.65 |
| Lipid related | | | | | |
| Ergosterol biosynthetic process | GO:0006696 | 3.03 | 4.16 | 4.03 | 4.84 |
| Cellular lipid catabolic process | GO:0044242 | 4.22 | 3.41 | | |
| Phospholipid biosynthetic process | GO:0008654 | | | | 2.52 |
| Fatty acid catabolic process | GO:0009062 | 5.77 | | | |
| Stress related | | | | | |
| Hydrogen peroxide catabolic process | GO:0042744 | | 16.98 | Inf* | |
| Response to oxidative stress | GO:0006979 | | 2.04 | | |
| Cellular response to oxidative stress | GO:0034599 | | | | 2.26 |
| Cellular response to DNA damage stimulus | GO:0006974 | 1.9 | 2.39 | | |
| Response to misfolded protein | GO:0051788 | | | | 9.99 |
| ER-associated misfolded protein catabolic process | GO:0071712 | | | | 33.21 |
| Metal related | | | | | |
| Cellular iron ion homeostasis | GO:0006879 | | | 3.24 | |
| Iron-sulphur cluster assembly | GO:0016226 | | | | 5 |
| Siderophore transport | GO:0015891 | | | 18.59 | |
| Cellular metal ion homeostasis | GO:0006875 | | | 2.48 | |
| Autophagy related | | | | | |
| CVT pathway | GO:0032258 | | | 3.11 | |
| Autophagy | GO:0006914 | | 2.13 | | |
| Mitochondrion degradation | GO:0000422 | | | 5.86 | |

Odds ratios for each GO term are included, with regulation of GO terms colour coded. Red: up-regulated. Green: down-regulated. *Inf = all genes contributing to enrichment of this GO term are present.

4.6.2. SOMs enrichment analyses of *C. neoformans* H99 transcripts in T_A and T_{AL}

SOMs analyses were performed on the H99 transcriptomic data, with the results presented in Figure 4.16. As one outlier from the AMB+LF treatment had been removed (Fig. 4.7), transcript expressions in each SOMs cluster (Fig. 4.16a and b) and the heat maps showing the averaged gene expressions for each SOMs cluster (Fig. 4.16c and d) were mapped across a total of 11 experiments along the x-axis. Dendrograms from the heat maps once again separated the SOMs clusters for T_A and T_{AL} by the differential expression of co-regulated genes mapped to each cluster. In T_A, transcripts with up-regulated expression were mapped to clusters 1 – 3, 6 – 8, 11 – 12, 16 – 17 and 21 – 22, while clusters 4 – 5, 9 – 10, 14 – 15, 20, 24 – 25 mapped down-regulated genes. In T_{AL}, up-regulated genes were found in clusters 11 – 25 and down-regulated genes in clusters 1 – 10. SOMs of interest are presented in Figure 4.17 and are discussed in the following sections. As in Table 4.8, similar GO enrichments in some of the SOMs clusters were observed between the drug treatments and these SOMs clusters are placed adjacent to each other in Figure 4.17 (a(i) – (iii) and b(i) – (iii)) for comparison. Other SOMs clusters of interest are presented in Figures 4.17c(i) – (iv).

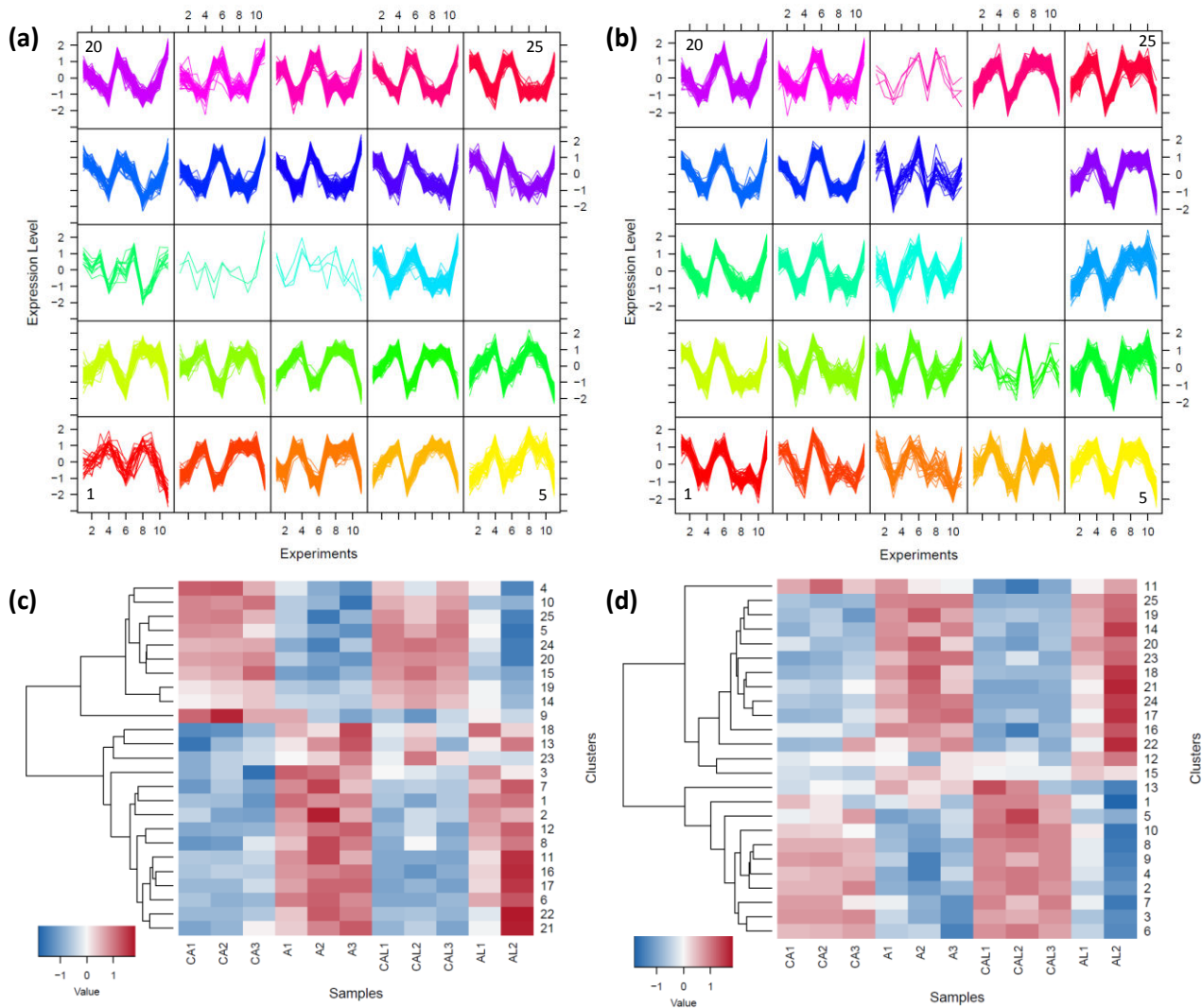


Figure 4.16. Independent SOMs of *C. neoformans* H99 genes differentially expressed in **(a)** T_A and **(b)** T_{AL} , and the heat maps of average gene expressions of each SOMs cluster for **(c)** T_A and **(d)** T_{AL} . For each SOMs cluster shown in **(a)** and **(b)**, the y-axis denotes the scaled gene expression levels and the x-axis represents the 11 experimental samples, arranged from left to right. These are the three biological replicates of the control for AMB treatment (CA1 – CA3), AMB treatment (A4 – A6), the control for AMB+LF treatment (CAL7 – CAL9), and AMB+LF treatment (with one biological replicate removed; AL10 – AL11). The clusters are numbered from bottom left to top right. Empty clusters have no genes. The heat maps for average gene expressions **(c)** and **(d)** are represented by rpk values scaled to standard normal per gene using Pareto scaling. The x-axis represents the 11 experimental samples with each biological replicate numbered. The y-axis shows the 25 SOMs clusters and the dendrogram on the left separates the SOMs clusters into up- or down-regulated groups, exclusively. For T_A **(c)**, down-regulated genes were found in clusters 4 – 5, 9 – 10, 14 – 15, 20, 24 – 25 while the remaining clusters mapped up-regulated genes. In T_{AL} **(d)**, up-regulated genes were found in clusters 11 – 25 and down-regulated genes in clusters 1 – 10.

4.6.2.1. Metal homeostasis is affected in AMB and AMB+LF drug treatments

No enrichment of metal ion homeostasis was observed in the overall H99 transcripts presented in Table 4.8. However, the analysis of gene co-expressions by SOMs mapped enrichments associated with copper transport to cluster 1 in T_A with CNAG_05626, Ctr4 and Ctr1 (CNAG_07701, formally named Ctr2 [493]), which were induced (Fig. 4.17a(i)). Iron transporters including Cft1, Cfo1, CNAG_05640 and CNAG_05154 were also enriched in T_A , but were repressed and mapped to cluster 5 (Fig. 4.17a(ii)). CNAG_05640 and CNAG_05154 also contribute to the enrichment for manganese transport. However, the functions of CNAG_05640 and CNAG_05154 as iron and manganese transporters are tentative as they were based on homology and have not been experimentally validated.

In T_{AL} , SOMs analysis found metal homeostasis enriched and up-regulated in cluster 14, with genes related to iron, manganese, zinc, and copper transport and homeostasis (Fig. 4.17b(i)). For iron, these included the Fe-S cluster assembly proteins Isa1, CNAG_03589, CNAG_03395 and CNAG_03226, and a copper exporting ATPase Ccc2 [494]. For zinc, the transporters CNAG_02993 and CNAG_02806, which are homologous to the *Saccharomyces* zinc transporters Yke4 and Zrc1 (from FungiDB; <http://fungidb.org/fungidb/>), respectively, were identified. For copper transport, Ccc2, Ctr1 and the cytochrome c oxidase assembly protein subunit CNAG_05573 [495] contributed to metal homeostasis enrichment.

As was done for S288C transcripts, a manual search for other iron, copper and zinc related transcripts was performed. All metal-related genes, including those mentioned previously, are listed in Table 4.9 with the SOMs clusters they were mapped to and their differential expression levels. In addition to ferric reductases and siderophore transporters, a haem transporter Cig1 [100] was induced in both T_A and T_{AL} , which implies that under drug exposure H99 sequesters inorganic (e.g. iron chloride) and organic (e.g. haem) sources of iron. While iron and manganese uptake were down-regulated in T_A , the expression of mitochondrial manganese superoxide dismutase (Sod2), which detoxifies superoxides [496], was up-regulated. A similar finding was observed in T_{AL} where transcripts for zinc and copper uptake were induced, but the chaperone that transfers copper ions to Sod1 (CNAG_02292) was repressed and the expression of Sod1 itself was absent.

Transcription factors regulating iron, copper and zinc were also observed in SOMs, but these had different expression patterns as each mapped to different clusters, as summarised in Table 4.10. The copper transcription factor Cuf1 was expressed in T_{AL} only (cluster 21), while the zinc regulatory factor

Zap104 mapped to clusters 6 in T_A and 20 in T_{AL}. Iron homeostasis in *Cryptococcus* is mainly regulated by Cir1 and HapX, however, other regulatory factors also play a part (reviewed in Ding *et al.* (2014)) [106]. *CIR1* is constitutively regulated [107] and its transcript was not detected in T_A or T_{AL}. HapX is part of a CCAAT motif binding complex that associates with other Hap proteins [497] and induces siderophore transport while suppressing mitochondrial functions such as respiratory and TCA functions in low iron conditions [103]. However, while HapX mapped to cluster 2 in T_A and 20 in T_{AL}, Hap2 and Hap3 mapped to different clusters suggesting differences in the regulation of the Hap complex under the different experimental conditions (Table 4.9 and 4.10). Other iron-regulating transcription factors included the pH-responsive transcription factor Rim101 [111], which was induced in clusters 1 and 19 in T_A and T_{AL}, respectively, and Nrg1, which is involved in the cAMP signalling pathway [110] and was repressed in clusters 15 in T_A and 2 in T_{AL} (not shown).

Table 4.9. Iron-, copper- and zinc-related transcripts identified in SOMs analysis of *C. neoformans* H99 in T_A and T_{AL}

| <i>C. neoformans</i> gene name (ID)* | Description | SOMs cluster in T _A | SOMs cluster in T _{AL} | <i>S. cerevisiae</i> homologue | Description |
|--------------------------------------|---|--------------------------------|---------------------------------|---|--|
| Iron related genes | | | | | |
| <i>HAP3 (CNAG_02215)</i> | CCAAT-binding transcription factor | 3 | - | <i>HAP3 (YBL021C)</i> | Subunit of the haem activated, glucose repressed Hap2/3/4/5 CCAAT-binding complex |
| <i>SRE1 (CNAG_04804)</i> | Sterol regulatory element binding protein | 22 | - | - | - |
| <i>CCC2 (CNAG_06415)</i> | Copper-exporting P-type ATPase | - | 14 | <i>CCC2 (YDR270W)</i> | Copper transporting P-type ATPase |
| <i>CNAG_03589</i> | Adrenodoxin-type ferredoxin | 1 | 14 | <i>YAH1 (YPL252C)</i> | Ferredoxin of the mitochondrial matrix required for cellular Fe-S protein formation |
| <i>CNAG_06524</i> | Uncharacterised protein | 1 | 14 | <i>FRE2 (YKL220C)</i> <i>FRE3 (YOR381W)</i> <i>FRE4 (YNR060W)</i> <i>FRE5 (YOR384W)</i> <i>FRE6 (YLL051C)</i> | Metalloreductase |
| <i>ISA1 (CNAG_02131)</i> | Fe-S cluster assembly protein | 17 | 14 | <i>ISA1 (YLL027W)</i> | Protein required for maturation of mitochondrial Fe-S proteins |
| <i>CNAG_03395</i> | NifU-like protein c | - | 14 | <i>NFU1 (YKLO40C)</i> | Protein required for maturation of Fe-S clusters |
| <i>CNAG_03226</i> | Succinate dehydrogenase [ubiquinone] Fe-S subunit, mitochondria | - | 14 | <i>SDH2 (YLL041C)</i> | Fe-S protein subunit of succinate dehydrogenases |
| <i>CNAG_04202</i> | Cytosolic Fe-S cluster assembly factor <i>NAR1</i> | 21 | 17 | <i>NAR1 (YNL240C)</i> | Component of cytosolic Fe-S protein assembly machinery, required for normal resistance to oxidative stress |
| <i>HAP2 (CNAG_07435)</i> | CCAAT-binding transcription factor | 11 | 18 | <i>HAP2 (YGL237C)</i> | Subunit of the haem activated, glucose repressed Hap2/3/4/5/ CCAAT binding complex |
| <i>CNAG_00491</i> | Uncharacterised protein | - | 18 | <i>ISA2 (YPR067W)</i> | Required for maturation of mitochondrial Fe-S proteins, functions in a complex with Isa1 |
| <i>CNAG_05058</i> | GTPase | - | 18 | <i>MTG2 (YHR168W)</i> | Putative GTPase, peripheral protein of the mitochondrial inner membrane |
| <i>RIM101 (CNAG_05431)</i> | pH-response transcription factor | 1 | 19 | <i>RIM101 (YHL027W)</i> | Transcription repressor involved in adaptation to alkaline conditions |
| <i>FRE7 (CNAG_00876)</i> | Ferric reductase | 12 | 19 | <i>FRE7 (YOL152W)</i> | Putative ferric reductase |
| <i>HAPX (CNAG_01242)</i> | CCAAT-binding transcription factor | 2 | 20 | - | - |

| | | | | | |
|--------------------------|---|----|----|---|---|
| <i>CIG1 (CNAG_01653)</i> | Cytokine inducing-glycoprotein | 2 | 20 | - | - |
| <i>CNAG_00727</i> | Mitochondrial protein with role in iron accumulation | 21 | 22 | <i>MMT2 (YPL224C)</i> <i>MMT1(YMR177W)</i> | Putative metal transporter involved in mitochondrial iron accumulation |
| <i>CNAG_07316</i> | Hydroxyacid-oxoacid transhydrogenase | 6 | 24 | <i>ADH4 (YGL256W)</i> | Alcohol dehydrogenase |
| <i>CNAG_05737</i> | Oligopeptide transporter 8 | 11 | 24 | <i>YGL114W</i> | Oligopeptide transporter |
| <i>SOD2 (CNAG_04388)</i> | Mitochondrial manganese superoxide dismutase | 16 | 24 | <i>SOD2 (YHR008C)</i> | Mitochondrial manganese superoxide dismutase |
| <i>CNAG_00638</i> | GTPase | 17 | 24 | <i>MSS1 (YMR023C)</i> | Mitochondrial protein; involved in the modification of mitochondrial tRNAs |
| <i>CNAG_04039</i> | Fe-S cluster assembly protein 2, mitochondrial | 17 | 24 | <i>ISU1 (YPL135W)</i> <i>ISU2 (YOR226C)</i> | Protein required for synthesis of Fe-S proteins |
| <i>ZIP2 (CNAG_03398)</i> | Solute carrier family 39 (Zinc transporter), member 1/2/3 | 6 | 25 | <i>ZRT1 (YGL255W)</i> <i>ZRT2 (YLR130C)</i> | High affinity zinc transporter (Zrt1), Low affinity zinc transporter (Zrt2) |
| <i>FRE4 (CNAG_07334)</i> | Ferric reductase | 6 | 25 | <i>FRE5 (YOR384W)</i> | Putative ferric reductase with similarity to Fre2 |
| <i>SIT1 (CNAG_00815)</i> | Siderophore iron transporter | 12 | 25 | <i>SIT1 (YEL065W)</i> <i>ARN1 (YHL040C)</i> <i>ARN2 (YHL047C)</i> <i>GEX1 (YCL073C)</i> <i>GEX2 (YKR106W)</i> | Glutathione antiporter (Gex1, Gex2), ferrioxamine B transporter (Sit1), ARN family transporter for siderophore iron chelates (Arn1, Arn2) |
| <i>SIT2 (CNAG_02083)</i> | Siderochrome iron transporter | - | 1 | - | - |
| <i>NRG1 (CNAG_05222)</i> | Transcriptional regulator | 15 | 2 | <i>NRG1 (YDR043C)</i> | Transcriptional repressor involved in glucose, filamentation and alkaline adaptation |
| <i>CNAG_01608</i> | Nuclear GTP-binding protein | 15 | 2 | <i>NUG1 (YER006W)</i> | GTPase that associates with nuclear 60S pre-ribosomes |
| <i>CNAG_04872</i> | Mitochondrial protein | 24 | 2 | <i>FSF1 (YOR271C)</i> | Predicted alpha-isopropylmalate carrier, likely to play a role in iron homeostasis |
| <i>CNAG_01634</i> | Large subunit GTPase 1 | 24 | 4 | <i>LSG1 (YGL099W)</i> | Putative GTPase involved in 60S ribosomal subunit biogenesis |
| <i>CFT1 (CNAG_06242)</i> | Major iron permease | 5 | 7 | <i>FTR1 (YER145C)</i> | High affinity iron permease (Ftr1) |
| <i>CFO1 (CNAG_06241)</i> | Ferroxidase/lacase | 5 | 7 | <i>FET3 (YMR058W)</i> | Multicopper oxidase |
| <i>CNAG_05640</i> | Metal iron and manganese transporter | 5 | 7 | <i>SMF1 (YOL122C)</i> <i>SMF3 (YLR034C)</i> | Putative divalent metal ion transporter (Smf3), divalent metal ion transporter (Smf1) |
| <i>CNAG_05154</i> | Membrane fraction protein. Transports iron and manganese ions | 5 | 9 | <i>CCC1 (YLR220W)</i> | Putative vacuolar iron/manganese transporter |

| | | | | | |
|-----------------------------|---|----|----|--|--|
| <i>CFO2 (CNAG_02958)</i> | Ferrioxidase | - | 8 | <i>FET5 (YFLO41W)</i> | Multicopper oxidase |
| <i>FRE201 (CNAG_03498)</i> | Ferric reductase | - | 10 | - | - |
| Copper related genes | | | | | |
| <i>CUF1 (CNAG_07724)</i> | Ligand-regulated, copper-sensing transcription factor | - | 21 | <i>HAA1 (YPR008W)</i> | Transcriptional activator involved in adaptation to weak acid stress |
| <i>CNAG_05626</i> | Uncharacterised | 1 | 25 | <i>SCO1 (YBR037C)</i> <i>SCO2 (YBR024W)</i> | Copper binding protein, required for cytochrome c oxidase activity and respiration |
| <i>CTR4 (CNAG_00979)</i> | High affinity copper uptake transporter | 1 | 25 | <i>CTR2 (YHR175W)</i> | Low affinity vacuolar copper transporter |
| <i>CCC2 (CNAG_06415)</i> | Copper-exporting P-type ATPase | - | 14 | <i>CCC2 (YDR270W)</i> | Copper transporter P-type ATPase |
| <i>CTR1 (CNAG_07701)</i> | Copper transporter (formerly named <i>CTR2</i> [493]) | 1 | 14 | <i>CTR1 (YPR124W)</i> | - |
| <i>CNAG_05573</i> | Cytochrome c oxidase assembly protein subunit 17 | 12 | 14 | <i>COX17 (YLL009C)</i> | Copper metallochaperone, transfers copper to Sco1 and Cox1, to cytochrome c oxidase |
| <i>CMT2 (CNAG_00306)</i> | Copper metallothionein | 10 | 3 | - | - |
| <i>CNAG_02292</i> | Superoxide dismutase copper chaperone | 20 | 3 | <i>CCS1 (YMR038C)</i> | Copper chaperone for superoxide dismutase Sod1 |
| <i>CNAG_06414</i> | Cytochrome c oxidase-assembly factor COX23, mitochondrial | 24 | 4 | <i>COX23 (YHR116W)</i> | Cytochrome oxidase function |
| <i>LAC2 (CNAG_03464)</i> | Cu-oxidase, laccase | 20 | 6 | <i>FET3 (YMR058W)</i> <i>FET5 (YFLO41W)</i> | Multicopper oxidase |
| <i>CNAG_02157</i> | Hypothetical protein | 20 | 6 | - | - |
| <i>CFO1 (CNAG_06241)</i> | Ferrioxidase/laccase | 5 | 7 | <i>FET5 (YFLO41W)</i> <i>FET3 (YMR058W)</i> | Multicopper oxidase |
| <i>CFO2 (CNAG_02958)</i> | Ferrioxidase | - | 8 | <i>FET5 (YFLO41W)</i> <i>FET3 (YMR058W)</i> | Iron transporter |
| <i>CTR2 (CNAG_01872)</i> | Solute carrier family 31 (copper vacuole transporter) | 4 | - | <i>CTR2 (YHR175W)</i> <i>CTR3 (YLR411W)</i> | Putative low affinity copper transporter (Ctr2), High affinity copper transporter (Ctr3) |
| Zinc related genes | | | | | |
| <i>CNAG_02993</i> | Solute carrier family 39 (zinc transporter), member 7 | 16 | 14 | <i>YKE4 (YIL023C)</i> | ER zinc transporter |
| <i>CNAG_02806</i> | Solute carrier family 30 (zinc transporter), member 1 | 16 | 14 | <i>COT1 (YOR316C)</i> <i>ZRC1 (YMR243C)</i> | Vacuole membrane zinc transporter |
| <i>CNAG_07728</i> | Solute carrier family 39 (zinc | 3 | 19 | - | - |

| transporter), member 1/2/3 | | | | | |
|----------------------------|---|----|----|--|---|
| <i>ZAP104 (CNAG_05392)</i> | Putative zinc finger transcription factor | 6 | 20 | <i>ZAP1 (YJL056C)</i> | Zinc regulating transcription factor |
| <i>ZIP2 (CNAG_03398)</i> | Zinc ion transporter | 6 | 25 | <i>ZRT1 (YGL255W)</i> <i>ZRT2 (YLR130C)</i> | High affinity zinc transporter (Zrt1), low affinity zinc transporter (Zrt2) |
| <i>CNAG_04524</i> | Zinc metalloprotease | 16 | 14 | - | - |
| <i>CNAG_01969</i> | Zinc metalloprotease | - | 17 | - | - |
| <i>CNAG_01016</i> | Vacuolar membrane protein | 11 | 18 | <i>MTC5 (YDR128W)</i> | Subunit of SEA (Seh1-associated) complex |
| <i>CNAG_00505</i> | Uncharacterised protein | 1 | 25 | - | - |
| <i>CNAG_05394</i> | Cation:cation antiporter | 24 | 8 | <i>MSC2 (YDR205W)</i> | ER zinc transporter |
| <i>CNAG_00837</i> | Uncharacterised protein | - | 7 | <i>ZRG17 (YNR039C)</i> | ER zinc transporter |

*Expression of genes colour-coded red = up-regulated; green = down-regulated. - = not present.

4.6.2.2. Co-expression of stress and ER-related enrichments suggests that ER stress is repressed in T_A and induced in T_{AL}

Stress responses were enriched in different SOMs clusters for both T_A and T_{AL}, suggesting stress terms were related to co-expressed GO enrichments present in the different clusters. In T_A, response to oxidative stress was up-regulated and enriched in cluster 17, along with genes encoding antioxidants such as catalases (Cat1 and Cat4), sulfiredoxins (Srx1) and flavoproteins (CNAG_01846). Oxidative stress was co-enriched with protein maturation by Fe-S cluster transfer, with the Fe-S assembly proteins Isa1 and CNAG_04039 (Fig. 4.17a(iii)). These co-enrichments reflect the requirement of Fe-S clusters for the catalytic activity of antioxidant proteins [77]. Although these transcripts can be associated with mitochondrial processes, enrichments of cellular components in cluster 17 did not return any terms associated with the mitochondrion. cAMP signalling, which causes mitochondrial stress by stimulating ROS production when induced [399] was down-regulated (cluster 15; Fig. 4.17c(i)). Together these results suggest that oxidative stress was not occurring in mitochondria.

Response to stress was also enriched in cluster 9 in T_A but was down-regulated. Many of the transcripts in this GO term encode for chaperones and heat shock proteins and contribute to the enrichments associated with protein folding (CNAG_00305, CNAG_03892), response to topologically incorrect proteins (CNAG_01185, CNAG_02500) and apoptosis (CNAG_06150, CNAG_02500) (Fig. 4.17c(ii)). Most of these terms relate to functions of the ER and suggest that within the ER there is a repression of stress responses, possibly by repressing functions that increase ROS production like protein folding [475] to avoid apoptosis. Other stress-related enrichments were found in cluster 24 with cell cycle regulation and transcription (not shown), which was also repressed.

In T_{AL}, stress-related enrichments were all induced. In cluster 24, oxidative stress was co-enriched with membrane fusion and trehalose biosynthesis, where genes with functions in oxidative stress were also involved in membrane fusion and trehalose biosyntheses. These include CNAG_00816, CNAG_03796, and CNAG_02895 for membrane fusion, and Tps2 for trehalose biosynthesis (Fig. 4.17b(iii)). Enrichments of cellular components in cluster 24 returned lipid, ER and vacuole terms (not shown), suggesting that oxidative stress could be occurring in the ER through the protein secretory process. The induction of oxidative stress promotes membrane fusion via actin polymerisation [498] and although actin-related enrichments were not co-expressed in cluster 24, they were enriched in SOMs clusters 16 (not shown) and 21 (Fig. 4.17c(iv)), and were also observed in the overall enrichments for T_{AL} (Table 4.8).

In T_{AL} , stress responses were co-enriched with protein folding as was seen in T_A (Fig. 4.17c(ii)), however, these terms were up-regulated and mapped to cluster 11 (Fig. 4.17c(iii)), further suggesting that the ER is under stress in AMB+LF treatment. Other enrichments for stress and related terms mapped to clusters 4 and 10 with cell cycle and maintenance-related processes (not shown), and cluster 18 with mitochondrion degradation (i.e. mitophagy) and nucleophagy (Fig. 4.17c(v)).

4.6.2.3. Repression of protein sorting and lipid biosynthesis in T_A and T_{AL} suggests disruptions in ER functions such as transport protein synthesis

In T_A , protein retention in the ER and glycosylphosphatidylinositol (GPI) anchor biosynthesis were repressed and co-regulated with iron and manganese transport in cluster 5 (Fig. 4.17a(ii)). Lipid biosynthesis was also enriched in this cluster. Protein retention in the ER describes the transport of correctly synthesised and folded proteins in the ER to the Golgi apparatus (<http://www.yeastgenome.org/go/GO:0006621/overview>). GPI anchors are synthesised in the ER lumen and are required for the localisation of proteins processed through the ER [499]. As transport proteins like iron transporters are made in the ER, all the enriched terms in cluster 5 suggest the down-regulation of protein sorting in the ER.

Protein-, lipid- and transport-related enrichments were also observed in T_{AL} . These were repressed and co-enriched in SOMs cluster 7, with a wider range of transport proteins affected by repression of ER function (Fig. 4.17b(ii)). These included transport proteins for iron (CNAG_05640 and Cft1), zinc (CNAG_00837, homologous to Zrg17 in *Saccharomyces*), carbohydrates (Hxs1, Itr4, CNAG_05867 and CNAG_05387), salts (CNAG_04038 and CNAG_04142), vitamins (CNAG_00598), and multidrug resistance transporters (Fnx1). Interestingly, while ER processes were repressed in T_{AL} , protein targeting to the ER was induced in cluster 11 (Fig. 4.17c(iii)), as were terms related to protein exit through the Golgi apparatus in cluster 21 (discussed below, Section 4.6.2.4).

4.6.2.4. Enrichments related to vesicle-mediated transport are induced in T_{AL}

The addition of LF to AMB treatment induced transcripts involved with the SNARE complex assembly, which mediates membrane fusion [500], endocytosis, Golgi to endosome transport, endosome to vacuole transport, and ubiquitin-dependent protein catabolism. These terms were all co-enriched in cluster 21 (Fig. 4.17c(iv)) and describe the journey of cargo from the Golgi apparatus to the vacuole, possibly for degradation or storage. Actin polymerisation, which is required to aid membrane fusion and trafficking [501], was also enriched in this cluster. Similar to this process, autophagy, which requires

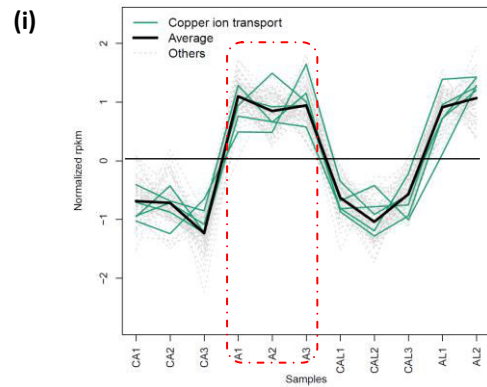
membrane organisation and mediates protein degradation through the vacuole [426], was observed in the overall GO enrichments in T_{AL} (Table 4.8). Apart from vesicle fusion, where enrichments were repressed in T_A in cluster 4 (not shown), the enrichments related to vesicle-mediated transport were unique to T_{AL} . This suggests that one of the ways through which LF causes synergy with AMB in H99 could be by affecting processes related to membrane fusion and trafficking.

4.6.2.5. Addition of LF to AMB treatment may repress cellular processes regulated by the activity of kinases

The regulation of kinase activity was enriched and repressed in T_{AL} in clusters 3, 5 and 8 (not shown) but was absent in T_A . Kinase activity is important for many cellular functions, ranging from metabolism, signalling and transport. The GO terms co-enriched with kinase regulation in clusters 3, 5 and 8 included processes related to cell cycle and replication, signal transduction, RNA metabolism and protein modification, suggesting the repression of kinase activity may have down-regulated these processes.

SOMs clusters with similar profiles and enrichments in (a) T_A and (b) T_{AL}

(a) T_A SOMs clusters



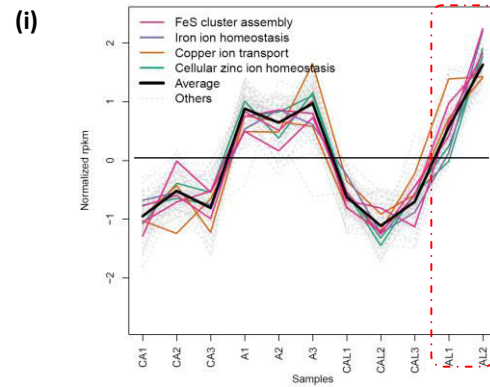
Cluster: 1

Gene expression: Up-regulated

Copper ion transport: *CTR4* (CNAG_00979), *CTR1* (CNAG_07701), *CNAG_05626*

RIM101 (CNAG_05431) expressed in this cluster (not shown)

(b) T_{AL} SOMs clusters



Cluster: 14

Gene expression: Up-regulated

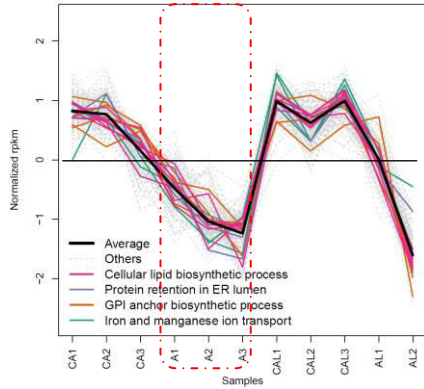
Fe-S assembly: *ISA1* (CNAG_02131), *CNAG_03395*, *CNAG_03589*

Iron ion homeostasis: *CCC2* (CNAG_06415), *CNAG_03589*, *CNAG_02131*, *CNAG_03395*, *CNAG_03226*

Copper ion transport: *CCC2* (CNAG_06415), *CTR1* (CNAG_07701), *CNAG_05573*

Cellular zinc ion homeostasis: *YKE4* (CNAG_02993), *ZRC1* (CNAG_02806)

(ii)



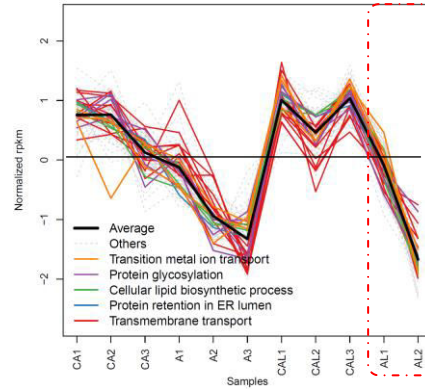
Cluster: 5

Gene expression: Down-regulated

Cellular lipid biosynthetic process: *ERG20* (CNAG_02084), *ERG28* (CNAG_03009), *ERG26* (CNAG_04605), *CNAG_05125*, *ERG27* (CNAG_07437), *CNAG_07510*
Protein retention in ER lumen: *CNAG_00319*, *CNAG_04671*
GPI anchor biosynthetic process: *CNAG_00420*, *CNAG_03753*, *CNAG_03855*, *CNAG_06647*
Iron ion transport: *CFT1* (CNAG_06242), *CFO1* (CNAG_06241), *CNAG_05640*, *CNAG_05154*
Manganese ion transport: *SMF1/SMF3* (CNAG_05640), *CCC1* (CNAG_05154)

Post-translational modifications enriched (not shown)

(ii)



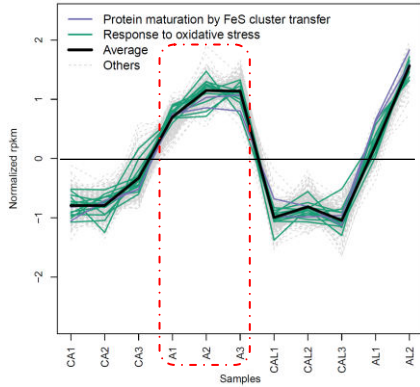
Cluster: 7

Gene expression: Down-regulated

Transition metal ion transport: *CNAG_05640*, *CFT1* (CNAG_06242), *ZRG17* (CNAG_00837)
Protein glycosylation: *CNAG_00473*, *CNAG_03014*, *CNAG_03855*, *CNAG_04671*
Cellular lipid biosynthetic process: *ERG20* (CNAG_02084), *ERG26* (CNAG_04605), *ERG27* (CNAG_07437)
Protein retention in ER lumen: *CNAG_00319*, *CNAG_04671*
Transmembrane transport: *CNAG_05640*, *CFT1* (CNAG_06242), *ZRG17* (CNAG_00837), *HXS1* (CNAG_03772), *ITR4* (CNAG_05662), *CNAG_05867*, *CNAG_05387*, *CNAG_04038*, *CNAG_04142*, *CNAG_00598*, *CNAG_06186*, *CNAG_07869*, *CNAG_03605*, *FNX1* (CNAG_03845)

Continued on the next page.

(iii)



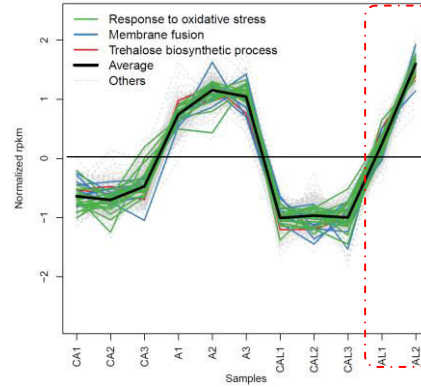
Cluster: 17

Gene expression: Up-regulated

Protein maturation by Fe-S cluster transfer: *ISA1* (CNAG_02131), *CNAG_04039*

Response to oxidative stress: *AOX1* (CNAG_00162), *RCK2* (CNAG_00130), *SRX1* (CNAG_00654), *CNAG_01686*, *CNAG_01846*, *CNAG_03143*, *ATF1* (CNAG_04090), *CNAG_04268*, *CNAG_04466*, *CAT1* (CNAG_04981), *CAT4* (CNAG_05015), *CNAG_05260*, *PIM1* (CNAG_01266), *TPS2* (CNAG_03765)

(iii)



Cluster: 24

Gene expression: Up-regulated

Response to oxidative stress: *RCK2* (CNAG_00130), *SRX1* (CNAG_00654), *CNAG_00816*, *PIM1* (CNAG_01266), *CNAG_01686*, *CNAG_01846*, *CNAG_02431*, *CNAG_02895*, *ZWF1* (CNAG_03245), *TPS2* (CNAG_03765), *CNAG_03796*, *ATF1* (CNAG_04090), *CNAG_04268*, *SOD2* (CNAG_04388), *CNAG_04466*, *CAT1* (CNAG_04981), *CNAG_05260*, *YPD1* (CNAG_06151), *CNAG_07032*

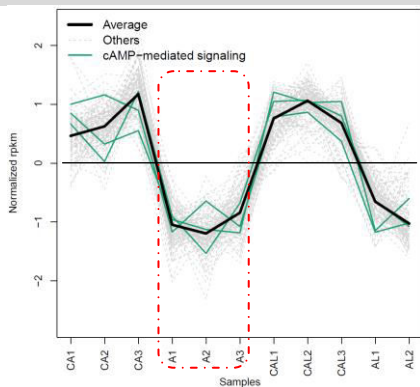
Membrane fusion: *CNAG_00582*, *CNAG_00816*, *CNAG_01412*, *CNAG_02895*, *CNAG_03796*, *CNAG_04270*, *CNAG_04401*, *CNAG_04959*, *CNAG_05410*, *CNAG_06021*, *CNAG_06625*, *CNAG_06737*

Trehalose biosynthetic process: *TPS2* (CNAG_03765), *CNAG_05292*, *CNAG_06313*

ER-, lipid- and vacuole- associated enrichments were observed in cellular component analysis (not shown)

(c) SOMs clusters with no similarity in T_A and T_{AL}

(i)



Experiment: T_A

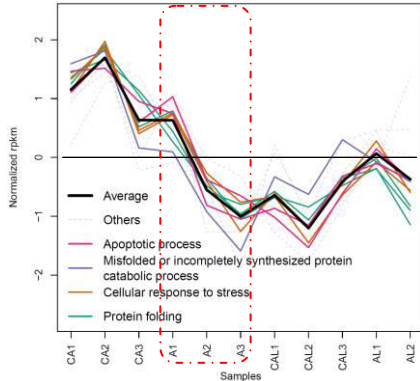
Cluster: 15

Gene expression: Down-regulated

cAMP-mediated signalling: *CNAG_01203*, *PDE1* (CNAG_05081), *CNAG_06401*

NRG1 (CNAG_05222) expressed in this cluster (not shown)

(ii)



Experiment: T_A

Cluster: 9

Differential expression: Down-regulated

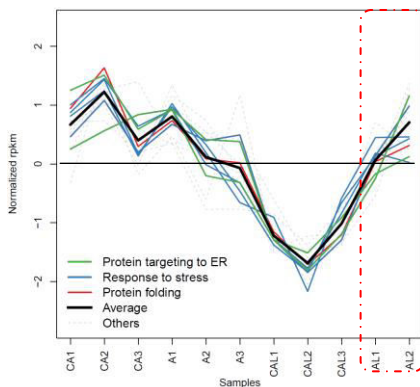
Apoptotic process: CNAG_02500, CNAG_06150

Misfolded or incompletely synthesized protein catabolic process: CNAG_01185, CNAG_02500

Cellular response to stress: CNAG_00305, CNAG_01185, CNAG_01391, CNAG_01727, CNAG_02500, CNAG_03892, CNAG_06150

Protein folding: CNAG_00100, CNAG_00305, CNAG_01391, CNAG_02500, CNAG_03176, CNAG_03892, CNAG_06150

(iii)



Experiment: T_{AL}

Cluster: 11

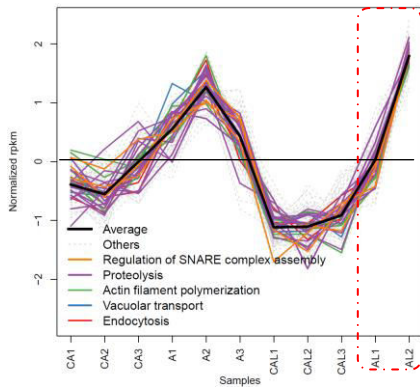
Gene expression: Up-regulated

Protein targeting to ER: CNAG_00287, CNAG_03899

Response to stress: CNAG_00287, CNAG_01727, CNAG_02674, CNAG_03347, CNAG_03899, CNAG_06106

Protein folding: CNAG_03899, CNAG_06106, CNAG_07558

(iv)



Experiment: T_{AL}

Cluster: 21

Gene expression: Up-regulated

Regulation of SNARE complex assembly: CNAG_01610, CNAG_03628, CNAG_06376

Proteolysis: DOA4 (CNAG_00757), UFD4 (CNAG_01251), CNAG_01561, CNAG_01732, CNAG_02167, CNAG_02543, ATG4 (CNAG_02662), CNAG_02873, CNAG_03376, CNAG_04636, CNAG_05195, CNAG_05308, HSE102 (CNAG_05882), CNAG_06423

Actin filament polymerisation: WSP1 (CNAG_02029), CNAG_02201, CNAG_03900, CNAG_04765, CNAG_05878

Vacuolar transport: CNAG_00787, CNAG_01610, CNAG_02167, ATG4 (CNAG_02662), CNAG_03628, VTA1 (CNAG_05747), HSE102 (CNAG_05882), CNAG_06376

Endocytosis: DOA4 (CNAG_00757), CNAG_00787, WSP1 (CNAG_02029), CNAG_02167, CNAG_02201, CNAG_02568, CNAG_03155, CNAG_04765, CNAG_05878, CNAG_06423, CNAG_07571

Golgi to endosome transport, endosome to vacuole transport and ubiquitin dependant protein catabolism were also enriched in this cluster (not shown)

CUF1 (CNAG_07724) mapped to this cluster (not shown)

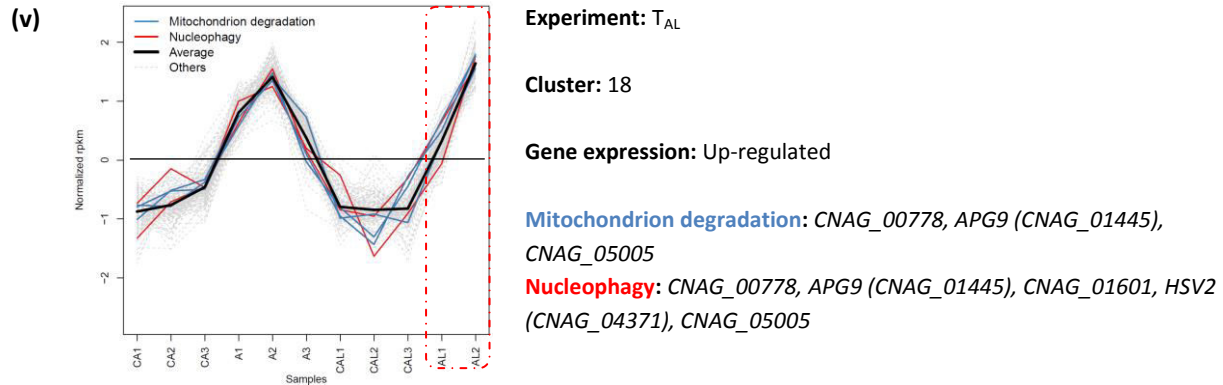


Figure 4.17. SOMs of interest and their enriched GO terms in *C. neoformans* H99. Adjacent clusters (ai – iii) and (bi – iii) have similar GO term enrichments and differential expression profiles in T_A and T_{AL}. SOMs clusters (ci – v) contain GO terms in T_A or T_{AL} that are not present in the other treatment. Each coloured line represents a gene, with colour determined by the associated GO term. The averaged expression level of all co-expressed genes in each cluster is drawn in black. Normalised expression levels of genes in response to AMB and AMB+LF treatment (boxed for visual clarity) are depicted by the y-axis. Genes that make up the GO enrichments in each cluster are listed.

In summary, both treatments repressed the transcription of genes related to protein processing and metal transport proteins. The presence of LF in AMB treatment repressed the synthesis of additional transport proteins that mobilise substrates like sugars, salts and drugs. While protein transfer between the ER and Golgi appeared to be down-regulated in AMB treatment, LF with AMB induced the expression of genes related to membrane fusion and transport, through the up-regulation of terms related to the protein secretory pathway in the ER and Golgi apparatus, and autophagy-related processes. Responses to stress were enriched in both drug treatments. However, terms related to ER stress were down-regulated in T_A while mitophagy was induced in T_{AL}. Finally, the addition of LF to AMB appeared to down-regulate the regulation of kinase activity.

4.6.3. Comparison of the response to AMB and AMB+LF treatment by *S. cerevisiae* S288C and *C. neoformans* H99

Similarities and differences in the transcriptional response to AMB and AMB+LF treatments by S288C and H99 are summarised in this section.

The overall GO enrichments indicated that the FIC concentration of AMB repressed cellular metabolism in both S288C and H99. These terms included nucleic acid metabolism, RNA and protein processing, ergosterol biosynthesis and the response to DNA damage. Conversely, processes involved in energy

generation like the TCA cycle and redox were induced (Table 4.8). Additional GO enrichments induced in S288C were hydrogen peroxide catabolism, autophagy and metal ion homeostasis, while in H99 fatty acid catabolism was induced. The differential expression of these GO enrichments, apart from protein folding which is part of protein processing, response to DNA damage and metal ion homeostasis, are typical of an environmental stress response [347].

In T_{AL} , a stark contrast between the transcriptomes of S288C and H99 was observed. In H99 GO enrichments continued to resemble the environmental stress response seen with AMB treatment, while in S288C the reverse was seen, with amino acid metabolism and ribosome biogenesis induced and redox processes and oxidative stress repressed following the addition of LF (Table 4.8).

SOMs analyses further highlighted similarities and differences between the transcriptomes of H99 and S288C cells treated with AMB and AMB+LF. These involved metal ion homeostasis, responses to stress, protein translation, and disruption of the protein secretory pathway and membrane-mediated processes.

Metal ion homeostasis was enriched in both drug treatments in S288C and H99. However, the regulation of iron and zinc differed between the drug treatments and the two yeasts. While iron homeostasis was induced in T_A in S288C (Fig. 4.9a(i)), iron uptake transcripts were repressed in H99 (Fig. 4.17a(ii)). Similarly in T_{AL} , zinc homeostasis was repressed in S288C (Fig. 4.9b(i)) but induced in H99 (Fig. 4.17b(i)). Copper was the only metal that was commonly regulated, with copper transport genes induced in T_A in both S288C and H99 (Fig. 4.9a(ii) and Fig. 4.17a(i)). However, while copper transport was enriched and up-regulated in T_{AL} in H99 (Fig. 4.17b(i)), it was not enriched in S288C.

The SOMs analysis suggested that responses to stress localised to different organelles in S288C and H99. In T_A , mitochondrial stress was observed in S288C (Fig. 4.9a(ii)) while ER stress was repressed in H99 (Fig. 4.17c(ii)). Oxidative stress was enriched in both species, but this was repressed in S288C (Fig. 4.9a(iii)) and induced in H99 (Fig. 4.17a(iii)). There were no clear indications of where oxidative stress was located in both organisms. In T_{AL} , oxidative stress was down-regulated and was associated with the repression of sulphur assimilation and ER function in S288C (Fig. 4.9b(iii)). In contrast, ER stress was induced in H99 (Fig. 4.17b(iii)).

Protein translation was affected by the addition of LF. AMB treatment repressed terms related to cytoplasmic translation in S288C and H99 (not shown), while AMB+LF treatment induced this process in

S288C (Table 4.5). With LF addition, protein targeting to the ER showed opposite differential regulation, where it was down- and up-regulated in S288C (Table 4.5) and H99 (Fig. 4.17c(iii)), respectively.

One common effect of AMB and AMB+LF treatment was the disruption of the protein secretory pathway, which was seen in both H99 and S288C. This was observed through the repression of GO terms related to ER function, which involved protein processing and lipid biosynthesis (Table 4.8). An exception was protein folding in H99, which was induced in AMB+LF treatment (Fig. 4.17c(iii)). With LF, the GO term relating to protein exit from the ER was repressed in S288C (Fig. 4.9b(vii)), whereas protein transfer from the Golgi to the endosome was induced in H99 (Fig. 4.17c(iv)).

AMB and AMB+LF treatment disrupted terms related to vesicle-mediated processes in both organisms, including membrane fusion, endocytosis, vacuole mediated proteolysis and transport. In T_A , the CVT pathway was induced in S288C (Table 4.5), while membrane fusion was repressed in H99 (not shown). In T_{AL} , membrane fusion and autophagy-related processes were repressed in S288C (Fig. 4.9b(vi)) and induced in H99 (Fig. 4.17b(iii) and c(iv)).

4.6.4. Dysregulation of metal homeostasis increases susceptibility to stress and antifungal drugs in *C. neoformans* H99

Disruptions to metal ion homeostasis were seen in both S288C and H99 T_A and T_{AL} transcripts. However, as noted above transcripts for iron uptake proteins were induced in T_A in S288C but repressed in H99. Similarly, transcripts for zinc uptake were repressed in S288C T_{AL} but induced in H99.

Disruption of iron and zinc homeostasis in S288C increased susceptibility to AMB and other cell stressors (Fig. 4.13), indicating the importance of metal regulation and its requirement to mount an appropriate stress response against antifungal exposure. Knock-out mutants in H99 with phenotypic characterisations have been reported by Jung *et al.* (2006), Jung *et al.* (2015), Kim *et al.* (2012) and Geddes (2015) [104, 293, 353, 502]. These data were used to assess the phenotypes of metal ion transcription factors present in T_A and T_{AL} and are summarised in Table 4.10. Cir1 was also included as it is the main regulator of iron homeostasis in *C. neoformans*, even though it was not differentially expressed in the drug treatments.

Where the phenotypes were known, a majority of iron controlling transcription factors exhibited increased susceptibility to AMB, except for *hap2Δ* and *sre1Δ*. Hap2 is a subunit of the CCAAT motif binding Hap complex that, together with HapX, controls iron dependant pathways like haem

biosynthesis [503]. Sre1 senses oxygen and regulates sterol homeostasis and iron uptake proteins [109]. The knock-out mutants *sre1Δ* and *rim101Δ* additionally had increased susceptibility to FLC. Knock-out mutants of iron-controlling transcription factors were defective in response to various stressors.

Dysregulation of copper and zinc homeostasis by knocking out *CUF1* and *ZAP104* also increased susceptibility to AMB, but caused a decrease and no change in susceptibility to FLC, respectively. Proper copper regulation was required for survival against cell wall and oxidative stressors, whereas disrupting zinc homeostasis did not appear to affect the cellular response to the various stressors. Overall, these results indicate that disrupting the homeostasis of different metals affects cell responses and survival against antifungal agents in *C. neoformans* in different ways.

Table 4.10. Phenotypes of *C. neoformans* mutants with disrupted iron, copper and zinc transcription factors that were differentially expressed in T_A and T_{AL}

| Transcription factor knock-out mutants | | | Transcript data* | | | | | | Susceptibility to stressors [#] | | | | | | |
|--|------------------------------|------------|------------------|-----------------|---------------------|-----------------|------------------|-----|--|-----------|-----|-------------------------------|----|------|-------|
| | | | Log Fold Change | | SOMs cluster number | | Antifungal drugs | | Oxidative stress | ER stress | | Cell wall and membrane stress | | | °C |
| Metal | Gene name | Gene ID | T _A | T _{AL} | T _A | T _{AL} | AMB | FLC | H ₂ O ₂ | DTT | TUN | SDS | CW | NaCl | 37 °C |
| Iron | <i>cir1Δ</i> [104, 502, 504] | CNAG_04864 | - | - | NA | NA | + | - | ND | ND | ND | + | ND | ND | + |
| | <i>hapXΔ</i> [293] | CNAG_01242 | 0.77 | 0.76 | 2 | 20 | ND | - | ND | ND | ND | ND | ND | ND | ND |
| | <i>hap3Δ</i> [293] | CNAG_02215 | 0.57 | - | 3 | - | ND | - | ND | ND | ND | ND | ND | ND | ND |
| | <i>hap2Δ</i> [353] | CNAG_07435 | 0.79 | 0.92 | 11 | 18 | 0 | - | 0 | + | - | + | + | 0 | 0 |
| | <i>nrg1Δ</i> [353] | CNAG_05222 | -0.34 | -0.48 | 15 | 2 | + | - | + | 0 | - | + | + | 0 | + |
| | <i>rim101Δ</i> [353] | CNAG_05431 | 1.12 | 1.07 | 1 | 19 | + | + | + | 0 | + | 0 | + | + | 0 |
| | <i>sre1Δ</i> [353] | CNAG_04804 | 0.92 | - | 22 | - | - | + | + | 0 | + | 0 | 0 | 0 | 0 |
| Copper | <i>cuf1Δ</i> [353] | CNAG_07724 | - | 0.48 | - | 21 | + | - | + | + | - | + | 0 | 0 | + |
| Zinc | <i>zap104Δ</i> [353] | CNAG_05392 | 0.35 | 0.65 | 6 | 20 | + | 0 | 0 | 0 | 0 | 0 | 0 | 0 | 0 |

*- = No change in expression. NA = not applicable

[#] DTT = dithiothreitol. TUN = tunicamycin. + = increased susceptibility, 0 = no difference to wild type, - = decreased susceptibility, ND = not done.

4.7. Discussion –AMB+LF synergy in *C. neoformans* H99

4.7.1. Transcriptomic analysis of synergy in *C. neoformans* H99 revealed a completely different response to AMB+LF compared to *S. cerevisiae* S288C

The transcriptome response to AMB treatment was similar overall in H99 and S288C, apart from an absence of enrichments relating to stress response and metal homeostasis in H99 (Table 4.8), which suggests that *Cryptococcus* may tolerate the stress induced by AMB better than *Saccharomyces* (discussed Section 4.7.2). However, the addition of LF to AMB elicited responses in H99 that were completely different to the responses seen in S288C (Table 4.8). A schematic model of the overall responses to AMB and AMB+LF synergy in H99 is presented in Figure 4.18 (see Figure 4.15 for a direct comparison of these in S288C). While T_{AL} in S288C indicated an up-regulation of responses such as protein synthesis and nucleic acid metabolism that indicated cell growth, repression of these responses indicating a decrease in cell growth was seen in H99. Additionally, response to stress and metal ion uptake that were down-regulated in S288C were up-regulated in H99, including up-regulation of oxidative stress (Fig. 4.17b(iii) and Table 4.8) and iron, copper and zinc transport (Fig. 4.17b(i)). Unlike in S288C, the responses in H99 are more in line with what might be expected following AMB+LF treatment as they are consistent with the increased inhibition of H99 growth (Fig. 4.4), the ROS-inducing properties of AMB and LF, and the metal chelating activity of LF [219, 303, 465].

The different responses seen in T_{AL} in H99 and S288C suggest that the mechanisms responsible for synergy are different in H99, and that despite a similar outcome to treatment, diverse cellular responses may be elicited in different fungi. However, analysis of differential gene expression patterns and validation by gene deletion revealed metal ion homeostasis as a critical point in AMB+LF synergy in both S288C and H99. These results suggest transcription factors controlling metal ions may be putative targets to enhance susceptibility to AMB.

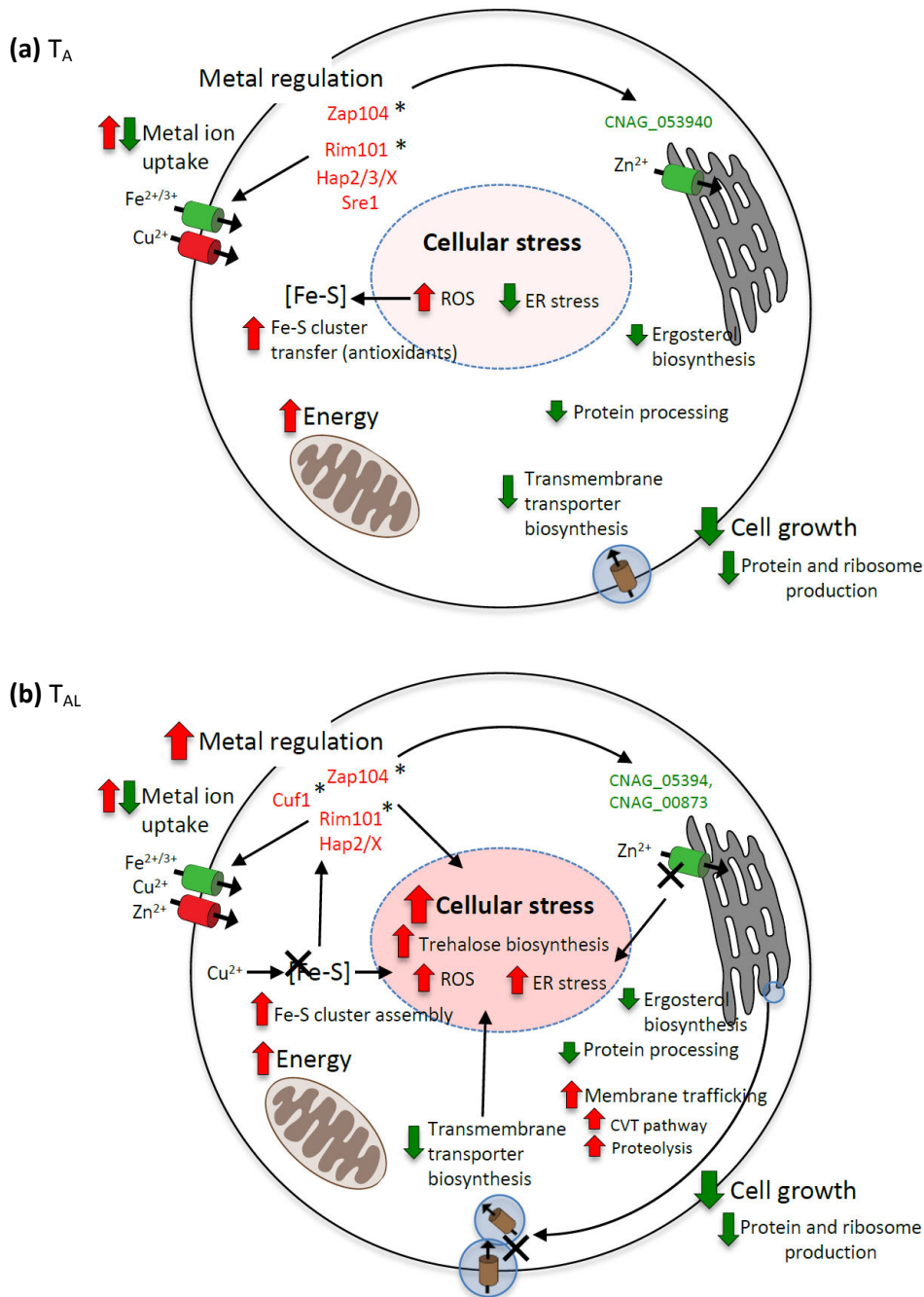


Figure 4.18. A model of the transcriptome response to AMB+LF synergy in *C. neoformans* H99. Cellular responses to AMB and AMB+LF treatments had many similarities including down-regulation of cell growth processes and up-regulation of stress responses, which may be associated with disruption to metal regulation and transmembrane transport synthesis. **(a)** T_A showed minimal induction in stress responses, which may be due to the up-regulation of antioxidants that rapidly neutralise ROS induced by AMB. **(b)** T_{AL} indicated that the cell experienced similar but higher levels of stress in the presence of AMB+LF, which may be due to stress in the ER and an increased dysregulation of metal homeostasis from the destabilisation of Fe-S clusters. This accumulation of cell stress then resulted in enhanced cell death. Red arrows and text: up-regulated processes; green arrows and text: down-regulated processes. Black arrows: observed effect of processes on other cellular functions in drug treatments. Asterisks: gene knock-out mutants that have increased susceptibility to AMB treatment.

4.7.2. Up-regulation of antioxidant genes may lower the overall stress response to AMB in *C. neoformans* H99

In H99, an absence of stress defence responses in the overall enrichments in T_A (Table 4.8) suggested it had a higher capacity to tolerate and adapt to the stresses induced by AMB treatment than S288C. In the SOMs analysis, up-regulation of the response to oxidative stress also encompassed antioxidant genes including catalases Cat1 and Cat4, and sulfiredoxin (CNAG_00654) (Fig. 4.17a(iii)), which suggested the presence of ROS that is consistent with AMB exposure [303, 469]. In T_A , *CAT1*, *CAT4* and sulfiredoxin were highly induced with 3.6, 1.3 and 2.29 log fold-changes in expression, respectively (not shown). This is consistent with studies in *Candida tropicalis*, which found increased activity of catalases and minimal ROS accumulation correlated with the increased capacity for AMB tolerance in AMB-resistant strains [303]. Similarly, analysis of the transcriptomic response to H_2O_2 -induced oxidative stress in *Cryptococcus* found the expression of catalases and sulfiredoxin to be highly induced, and this was associated with the ability to rapidly detoxify H_2O_2 [505]. Altogether, the minimal induction of stress responses in T_A suggested minimal oxidative damage following AMB treatment due to highly induced expression of antioxidants that contributed to rapid clearance of oxidants (Fig. 4.18).

4.7.3. Disruption to transmembrane transport synthesis may be associated with ER stress and enhanced growth inhibition in AMB+LF synergy

The most significant responses that were seen in AMB+LF synergy in H99 were the up-regulation of stress in the ER and vesicle mediated trafficking (Fig. 4.17b(iii), c(iii) and c(iv)), which were down-regulated and absent in T_A , respectively (Fig. 4.17c(ii)). A more pronounced disruption to transmembrane transport synthesis was also seen in T_{AL} compared to T_A (Section 4.6.2.3), which suggested that this and ER stress may have worked together to enhance cell inhibition following AMB+LF treatment (Fig. 4.18).

ER stress induces the unfolded protein response (UPR) which regulates a number of cellular responses to restore the folding capacity of the ER and maintain homeostasis. These include a decrease in translation activity to limit protein synthesis, an increase in ER protein folding and proteolysis, and the retrotranslocation of unfolded and misfolded proteins from the ER into the cytoplasm for degradation via ERAD [506]. These responses were observed in T_{AL} (Fig. 4.17b(iii), c(iii), c(iv) and Table 4.8). The exceptions were down-regulation of ER functions relating to the biosynthesis of lipids and protein processing activities like glycosylation. These were co-regulated

with transmembrane transporters, suggesting a disruption in the synthesis of transporter proteins (Fig. 4.17b(ii)).

Transmembrane transport proteins are post-translationally modified in order to traverse through the secretory pathway and localise to their required cellular destinations [507, 508]. Inadequate processing, such as by disrupted glycosylation, causes the proteins to be retained or mobilised back into the ER where they are either degraded or accumulate and cause ER stress [507, 509]. Disruptions to transmembrane transporters also cause stress as they serve important functions in cellular homeostasis by maintaining the balance of ions in the cytosol, which are involved in osmoregulation (K^+/Na^+), signalling (Ca^{2+}) and act as enzyme cofactors (Fe^{3+}/Fe^{2+} and Zn^{2+}) [93, 510]. Transporters also enable the fast mobilisation of specific substrates like vitamins and amino acids to meet cellular requirements [511]. Additionally, they control the transport of ions and substrates into cellular organelles, such as the transport of calcium and iron into the mitochondria, which helps prevent organelle damage [512, 513]. Ions and substrates can also play a role in maintaining organelle homeostasis, and disruption of their transport affects organelle function.

Disruptions to processes involving transmembrane transporters may also cause alterations in ER function. In T_{AL} , the expression of cryptococcal orthologues of *MSC2* (*CNAG_05394*) and *ZRG17* (*CNAG_00873*), which encode ER zinc transporters, was down-regulated and *ZRG17* was observed in the enrichment for transmembrane transport (Table 4.9 and Fig. 4.17b(ii)). As mentioned in Section 4.5.3.1, zinc is needed for the protein-sorting and secretory processes performed in the ER, and disruption of ER zinc uptake induces ER stress [421, 488]. Repression of *MSC2* and *ZRG17* would be expected to cause a decrease in zinc uptake and influence the down-regulation of ER protein and lipid processing that was seen in T_{AL} (Fig. 4.17b(ii)). Down-regulation of ER zinc uptake and transport proteins was also seen in T_A (Table 4.9 and Fig. 4.17a(ii)) but to a lesser extent (Fig. 4.17b(ii)). This suggested that AMB disrupts the synthesis of transmembrane proteins in *Cryptococcus* and that the addition of LF enhances these disruptions that possibly resulted in ER stress.

In summary, it is suggested that in H99 the addition of LF to AMB enhanced disruption of transmembrane transport synthesis in the ER with subsequent disruption of the ionic balance, and these caused an accumulation of stress resulting in an increase in cell inhibition (Fig. 4.18).

4.7.4. Increased dysregulation of metal homeostasis in AMB+LF synergy may be mediated by destabilisation of Fe-S clusters and contribute to cell stress

Analysis of T_A and T_{AL} showed that enrichments involved in metal ion uptake were both up and down-regulated despite the induction of the metal ion-controlling transcription factors (HapX, Hap2, Rim101 and Zap104) in both treatments (Fig. 4.17a(i – ii), b(i – ii) and Table 4.10)). Although metal regulation in *Cryptococcus* is less well characterised than in *Saccharomyces*, the opposing enrichments of metal uptake seen in both T_A and T_{AL} suggested that the way the metal ion-controlling transcription factors control their gene targets was disrupted. This may be associated with the disrupted synthesis of transmembrane transport proteins in the ER (Section 4.7.3), which included down-regulated iron (Cft1 and CNAG_05640) and zinc (CNAG_00837) transporters (Fig. 4.17a(ii) and b(ii)).

In addition to the disrupted synthesis of metal transporters, the dysregulation of metal ions in AMB+LF synergy may also be mediated by the destabilisation of Fe-S clusters, which can contribute to increased stress. Fe-S cluster assembly was co-regulated with iron, zinc and copper transport (Fig. 4.17b(i)), but while iron and zinc are required for the synthesis and structural stability of Fe-S clusters [514], copper has been shown to target and destabilise Fe-S clusters [515]. Iron homeostasis, especially iron uptake, is regulated by sensing the level of Fe-S clusters, and in *Saccharomyces* decreased Fe-S clusters levels activate the iron regulon through Aft1 [86, 88]. Fe-S clusters are also present in proteins and their destabilisation causes a loss in their activity, which can be detrimental to the cell as they have functions in important cellular homeostatic processes as well as stress responses like oxidation-reduction and catalase activity [77, 516].

Copper mediated destabilisation of Fe-S structures in proteins is an antimicrobial mechanism of the ionophore zinc pyrithione, which causes an increase in copper influx across the cell membrane [517]. Additionally, in *Saccharomyces* zinc pyrithione has been found to induce metal starvation, increasing iron uptake through *AFT1* up-regulation and zinc uptake through Zap1 activation [517, 518]. LF has not been shown to have ionophoric activity. However, the up-regulation of metal ion-controlling transcription factors and co-enrichment of Fe-S cluster synthesis and copper transport during AMB+LF treatment suggest the inappropriate induction of metal ion-regulating transcription factors may occur through a mechanism similar to that seen in zinc pyrithione. Disrupted regulation of metal ions can catalyse the formation of oxidants and cause cell stress [93]. This, together with the induction of stress responses associated with the disruption in ER functions described previously, suggest that in H99 LF produces an increase in cellular stress that overwhelms the capacity of the cell to cope, resulting in inhibition and death.

4.7.5. Avenues for future work

Transcriptome analysis of AMB+LF treatment and knock-out data in both *Saccharomyces* and *Cryptococcus* suggested that disruptions to metal regulation involving iron and zinc homeostasis via Aft1, Zap1, Cir1 and Zap104 were critical to AMB+LF synergy (Fig. 4.13 and Table 4.10). In *Cryptococcus*, the copper regulating transcription factor Cuf1 was also important for AMB survival (Table 4.10). Additionally, the disruption of metal homeostasis was suggested to cause either a dysregulated stress responses (in S288C) or an accumulation of stress (in H99), in each case resulting in drug synergy (Fig. 4.15 and Fig. 4.18). However, transcriptomic data can only provide indirect evidence of cellular responses and validation and future work are needed to confirm these observations.

Of most interest is validating the differential expressions of *AFT1* and *ZAP1* in S288C and *HAPX* and *ZAP104* in H99, and the effects of their regulatory activities on stress responses. This can be confirmed by qPCR on the transcription factors and their gene targets, including Zap1 targets *ZRG17*, *YHB1*, *KAR2* and Aft1 targets *FIT3*, *GRX4* and *CAD1* in S288C (Fig. 4.11). In H99, HapX targets *SIT1* and *RIM101* [103], and Zap104 target *ZIP2* [519] could be tested. The expression of genes that are not targets of these transcription factors but encode functions related to stress responses should also be confirmed, such as *TPK2*, which encodes a subunit of the Ras/cAMP-dependant PKA in S288C, and the copper regulating transcription factor *CUF1*, which was expressed only in H99.

In addition to confirming their differential expression, the dynamic response of these genes during treatment can be monitored by qPCR. Chong *et al.* (2012) assessed the response of *Cryptococcus* to FLC over 6 hrs and revealed substantial changes in the level of various proteins [356]. In the current study, RNA samples from AMB and AMB+LF treatments were extracted before and after the ID₂₀, which will enable this analysis. Examining the expression dynamics of the chosen genes at these additional time points will help unravel how the changes in cellular function that occur in response to AMB+LF eventually lead to enhanced cell death.

Other avenues for understanding AMB+LF synergy include assessing the physical interaction of LF with the cell and determining the intracellular concentrations of metal ions during treatment. While LF has been shown to bind to and cause alterations to the cell surface [464-467], it is not known if LF can enter the cell. AMB create pores in the cell membrane and can enter the cell [520], and it is possible that this facilitates LF entry and subsequent disruption of intracellular targets. To assess this, LF could be tagged with a fluorescent protein or radiolabel and tracked during AMB+LF treatment [521].

The transcriptomic observations and the results of the iron rescue assay in Chapter 3 (Fig. 3.4) suggested that the dysregulation of metal homeostasis was not a direct result of metal chelation by LF but was due to the shutdown of Aft1 activity and repression of Zap1. However, Aft1 and Zap1 expression is normally regulated by internal metal concentrations [87, 522] and it is not known if LF directly disrupts intracellular metal concentrations, which then affect the regulation of metal-controlling transcription factors, as has been observed for zinc pyrithione [517]. Inductively coupled plasma mass spectrometry (ICP-MS) is a sensitive technique that detects elements at low concentrations by converting the atoms of elements into ions and separating them for detection by mass spectrometry, and was used by Chillappagari *et al.* (2010) to show that cells treated with zinc pyrithione had an increased concentration of copper compared to untreated controls [515]. This method could similarly be employed in AMB+LF treated H99 and S288C cells to establish if changes in intracellular metal ion concentrations affect the regulation of metal-regulating transcription factors.

The effect of synergy on oxidative stress could also be further explored. The inability to clear ROS could be confirmed via fluorescence using fluorogenic dye 2', 7'-dichlorofluorescein diacetate, which is oxidised in the presence of ROS and converts into a fluorescent substrate. Glutathione, a major antioxidant, has previously been found to rescue *C. albicans* from BBR+FLC synergy by neutralising the accumulation of ROS [6], and was down-regulated in S288C by AMB+LF (Fig. 4.10). Supplementing AMB+LF treated S288C with glutathione would determine whether the disruption of glutathione biosynthesis or if the inhibition of other antioxidants contributes to enhanced cell death. Although the response to AMB+LF synergy in S288C differed to H99, it might be applicable to other more closely related ascomycete pathogens. Additionally, developing drug strategies aimed at inhibiting appropriate stress responses would be a novel and beneficial approach to therapy as this should be less likely to induce toxic damage to the host cells than agents that induce stress.

4.8. Results – Analysis of VRC+EDTA antagonism and additivity in *C. neoformans* H99 and *C. gattii* 97/170

4.8.1. Effect of VRC and VRC+EDTA on the growth of *C. neoformans* H99 and *C. gattii* 97/170

Growth curves were established to choose the optimal time point for RNA extraction from *C. neoformans* H99 and *C. gattii* 97/170 cells, where treatment with VRC+EDTA resulted in antagonism and additivity, respectively (Fig. 4.19). Both strains were treated at the FIC for VRC+EDTA, which was 0.03 µg/mL VRC + 8 µg/mL EDTA for H99, and 0.03 µg/mL VRC + 64 µg/mL EDTA for 97/170. Growth curves were also established for both strains with VRC alone at the FIC (0.03 µg/mL). For 97/170, the additive effect of EDTA to the activity of VRC was evident from the 5th hr of treatment, where growth decreased compared to treatment with VRC alone. Significant inhibition of growth by VRC was not seen until 8 hrs, which was three hours later than was observed for VRC+EDTA (Fig. 4.19a). In contrast, in H99 the addition of EDTA antagonised the inhibitory activity of VRC, which was evident from the 5th hr and persisted throughout treatment (Fig. 4.19b). Note that VRC inhibited the growth of H99 to a greater extent than 97/170 as the concentration of VRC used was 4-fold higher than the MIC for H99 (MIC = 0.007 µg/mL) but 16-fold lower than the MIC for 97/170 (MIC = 0.5 µg/mL; Table 3.2). In H99, VRC+EDTA caused a 20% increase in growth compared to VRC at the 7th hour of treatment, and this timepoint was chosen for RNA-Seq. The same timepoint was used to extract RNA from 97/170 treated with VRC and VRC+EDTA (shown by arrows on Fig. 4.19).

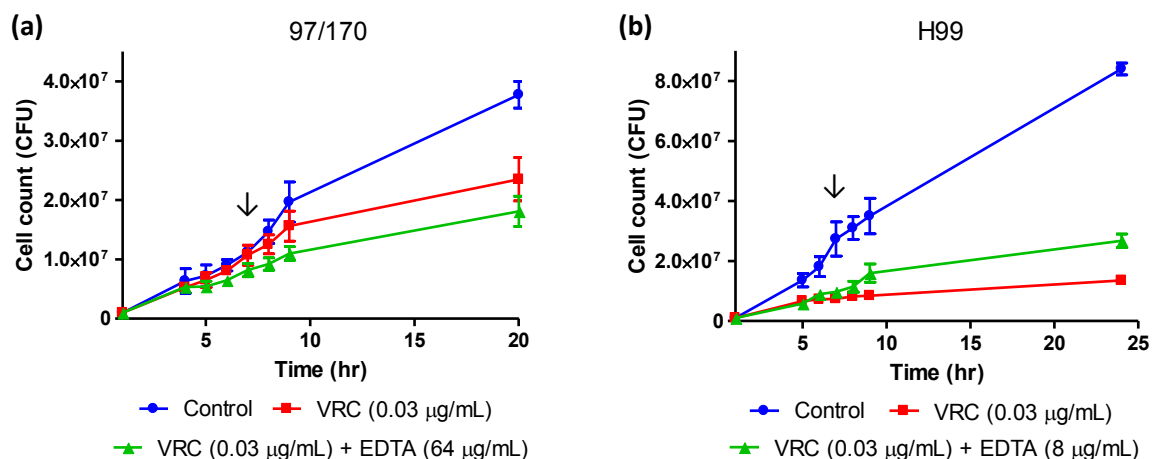


Figure 4.19. The effect of VRC and VRC+EDTA on the growth of *C. gattii* 97/170 and *C. neoformans* H99. **(a)** Treatment of *C. gattii* 97/170 with 0.03 µg/mL VRC had a limited effect on growth, and activity was enhanced by the addition of 64 µg/mL EDTA. **(b)** In contrast, 0.03 µg/mL VRC inhibited the growth of *C. neoformans* H99, and the addition of EDTA was antagonistic to this treatment. Arrows indicate the timepoints chosen for RNA-Seq, based on a 20% increase in growth of H99 with VRC+EDTA compared to VRC only treatment at 7 hrs. Data are shown as mean +/- SEM.

4.8.2. Analysis of RNA-Seq data from VRC and VRC+EDTA treatments

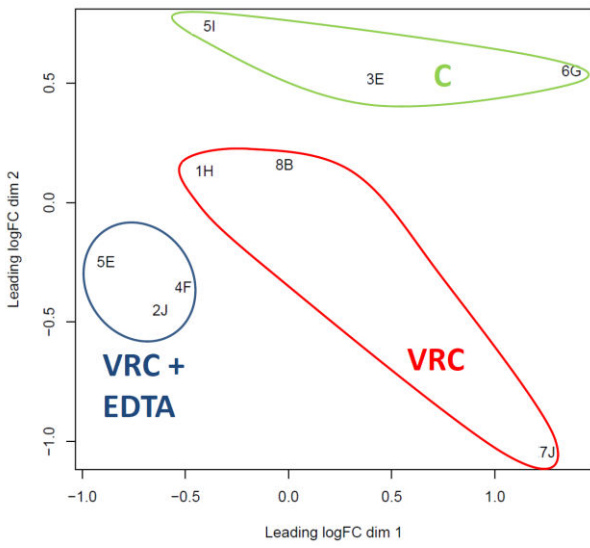
4.8.2.1. RNA-Seq data quality

As all RNA samples were sequenced together, the drug antagonism experiments had the same number of reads per sample and coverage as the synergy experiments (Section 4.3.2.1). Similarity between the biological replicates of H99 and 97/170 RNA samples was examined on MDS plots (Fig. 4.20). In H99, sample 7J was an outlier in the VRC treatment (Fig. 4.20a) while all biological replicates of the same drug treatments clustered together in 97/170 (Fig. 4.20e). To determine whether or not to delete 7J, a list of differentially expressed transcripts induced or repressed in H99 due to VRC and VRC+EDTA treatment was generated by subtracting the fold-change expressions of genes under the drug treatments with those expressed in the control, i.e. T_V and T_{VE} , where 'T' stands for transcripts. Deletion of 7J from the H99 dataset improved the BCV from 0.267 to 0.237 (Fig. 4.20b; Appendix 4.8), and mostly increased the counts of differentially expressed genes in both VRC and VRC+EDTA treatment (Table 4.11). Subsequent analyses of H99 transcripts for antagonism experiments were therefore performed without sample 7J.

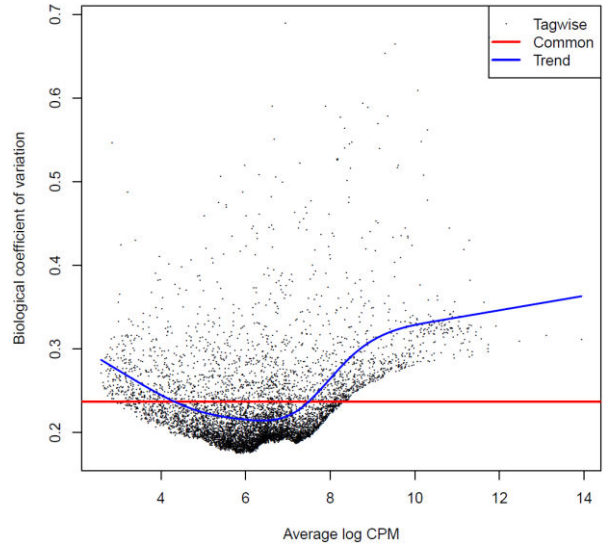
Table 4.11. *C. neoformans* H99 gene count comparison with and without RNA sample 7J

| | Gene fold expression | With 7J | Without 7J |
|----------------------------|-----------------------------|----------------|-------------------|
| T_V | Up-regulated | 79 | 62 |
| | No fold change | 6391 | 6909 |
| | Down-regulated | 1 | 4 |
| T_{VE} | Up-regulated | 148 | 208 |
| | No fold change | 6240 | 6632 |
| | Down-regulated | 83 | 135 |

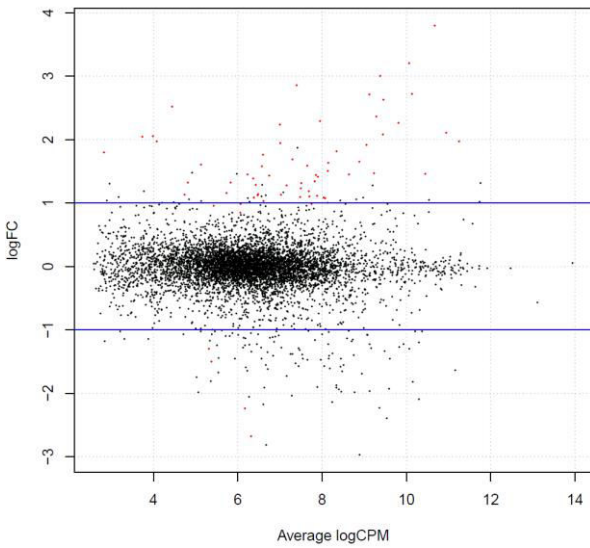
(a) MDS plot of H99 RNA samples



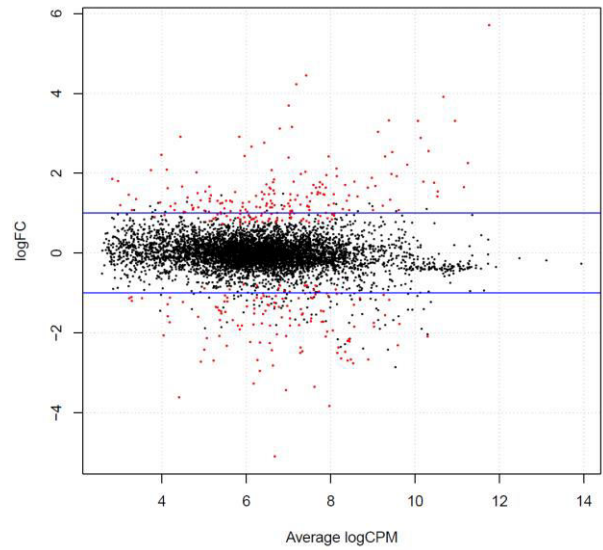
(b) BCV for H99



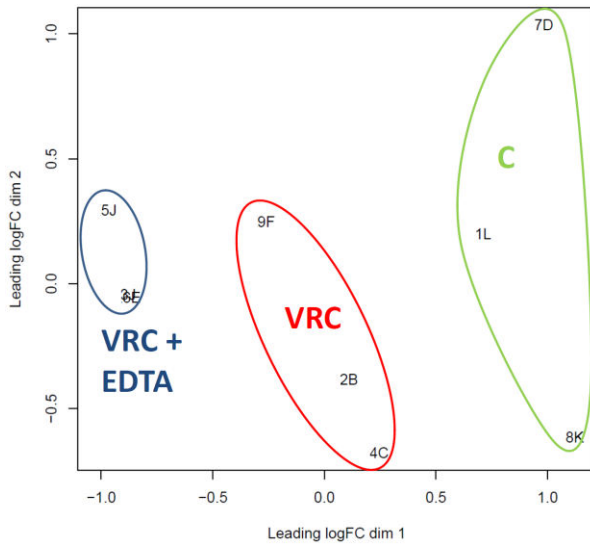
(c) Log₂ FC of H99 transcripts in VRC



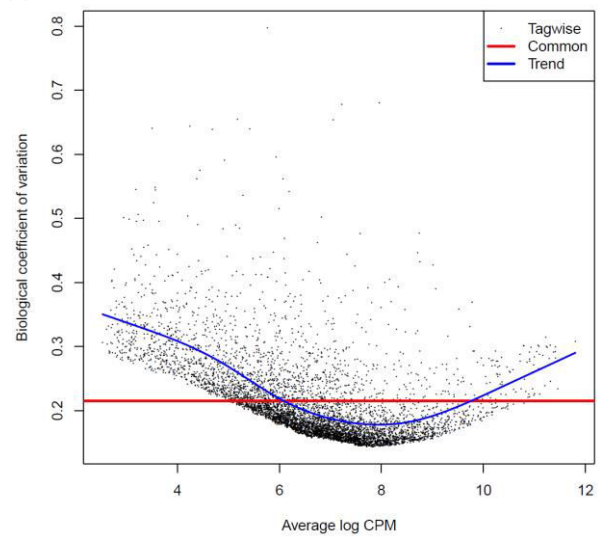
(d) Log₂ FC of H99 transcripts in VRC+EDTA



(e) MDS plot of 97/170 RNA samples



(f) BCV for 97/170



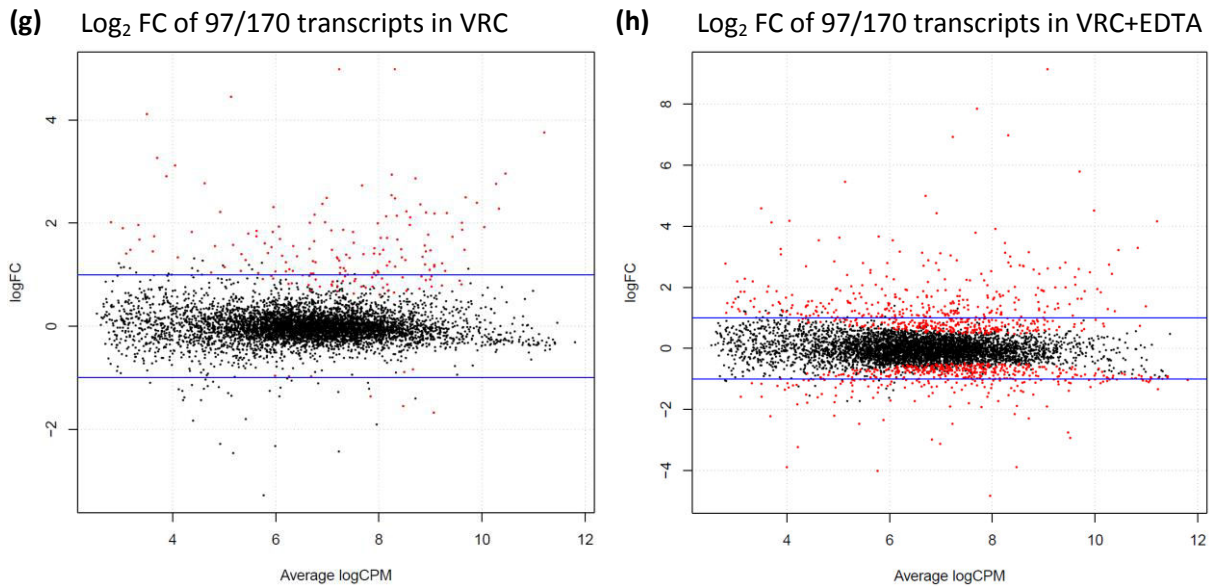


Figure 4.20. Quality analysis of RNA-Seq data from drug antagonism experiments in *C. neoformans* H99 (a) – (d) and *C. gattii* 97/170 (e) – (h). (a) and (e) MDS plot of RNA-Seq samples after normalisation with EdgeR. In H99, biological replicates clustered together except for H99 sample 7J, which was excluded from all subsequent analyses. (b) and (f) BCV versus average log₂ CPM. The red line represents the common dispersion of all genes and the blue line represents their trended dispersion. Each dot is a data point that represents tag-wise dispersion of each gene. (c) and (g) Smear plot of log₂ FC versus the average log₂ CPM values of genes in response to VRC treatment. (d) and (h) Smear plot of log₂ FC versus the average log₂ CPM values of genes in response to VRC+EDTA treatment. Differentially expressed genes in (c) – (d) and (g) – (h) are represented in red. Blue lines are drawn at 2-fold changes in expression. Black dots above the blue lines are genes not counted in the analysis due to high a signal-to-noise ratio between biological replicates.

4.8.3. Analysis of gene expression in *C. neoformans* H99 and *C. gattii* 97/170 in response to VRC and VRC+EDTA

Due to time constraints, the following section is a preliminary analysis of the transcriptome data and awaits further validation.

4.8.3.1. Analysis of orthology between genes expressed in *C. neoformans* H99 and *C. gattii* 97/170

RNA-Seq results identified transcripts for a total of 6,975 genes in H99 and 6,932 genes in 97/170 that were expressed in response to the single or the combined drug treatment or were in the untreated controls. Although *C. neoformans* and *C. gattii* are closely related they are different species estimated to have diverged between 16 – 160 million years ago [28]. Therefore, in order to compare their response to the drug treatments, genes that were common to the transcriptomes of both were first identified by reciprocal BLAST to find orthologues. BLAST returned 5,935 orthologous

genes between H99 and 97/170, and 1,040 and 977 non-orthologous genes in H99 and 97/170, respectively.

4.8.3.2. Analysis of differentially expressed genes in response to drug treatments

A list of transcripts that were differentially expressed in response to VRC and VRC+EDTA treatment were generated as described in Section 4.3.2.2. Two datasets are presented for subsequent comparison: the total number of genes differentially expressed in each organism, and the total number of orthologous genes differentially expressed in each organism.

For clarity, the number of orthologous and non-orthologous transcripts identified from BLAST (Section 4.8.3.1) and the gene sets that were used to analyse the two datasets of differentially expressed genes are presented in the Venn diagram shown in Figure 4.21. The yellow circle includes all 6,975 genes expressed in H99, including genes with orthologues in 97/170 that were either expressed only in H99 (A) or were also expressed in 97/170 (B), and genes without orthologues in 97/170 (D: 1,040 genes). Similarly, the purple circle includes the 6,932 genes expressed in 97/170, which comprises (B) as above, along with genes with orthologues that were not expressed in H99 (C) and genes without orthologues in H99 (E). The blue circle (A+B+C) comprises all 5,935 transcribed genes in H99 and 97/170 with orthologues in both strains. The total set of differentially expressed genes was analysed from A+B+D for H99, where 138, 171 and 37 genes were differentially expressed, respectively. Similarly in 97/170, the total set of differentially expressed genes was analysed from B+C+E, where C and E contained 825 and 46 differentially expressed genes, respectively. The differentially expressed orthologous genes were analysed from A+B for H99 and B+C for 97/170.

Table 4.12 shows the gene counts for the total number of genes differentially expressed in each organism (Fig. 4.21; A+B+D for H99, B+C+E for 97/170) and the total number of orthologous genes differentially expressed in each organism (Fig. 4.21; A+B for H99, C+B for 97/170). Of the total genes differentially expressed in H99 in T_V , 62 were up-regulated while 4 were down-regulated. In T_{VE} , 208 and 124 genes were up and down-regulated, respectively. Substantially more genes were differentially expressed in 97/170, with 168 genes up-regulated and 8 genes down-regulated in T_V , and 560 genes up-regulated and 473 down-regulated in T_{VE} (Table 4.12). The majority of genes that were differentially expressed in both H99 and 97/170 were orthologous. Overall, the combined drug treatment resulted in more genes being differentially expressed and up-regulated in both species compared to VRC treatment only. About 5% and 15% of genes were differentially expressed from the total number of transcripts identified for H99 and 97/170, respectively.

Among the orthologous gene set, H99 had 58 up-regulated and 4 down-regulated genes in T_V , and 184 and 124 up and down-regulated genes in T_{VE} . In 97/170, there were 161 up-regulated and 8 down-regulated genes in T_V and 531 up-regulated and 458 genes down-regulated in T_{VE} (Table 4.12). There were 171 orthologous genes that were expressed in both in H99 and 97/170, (represented by B in Fig. 4.21). The direction of fold-change of these genes in H99 and 97/170 were plotted against each other for T_V and T_{VE} (Fig. 4.22), which revealed that all but five genes in T_{VE} presented in Table 4.12 had the same direction of fold-change. These five genes are listed in Table 4.13.

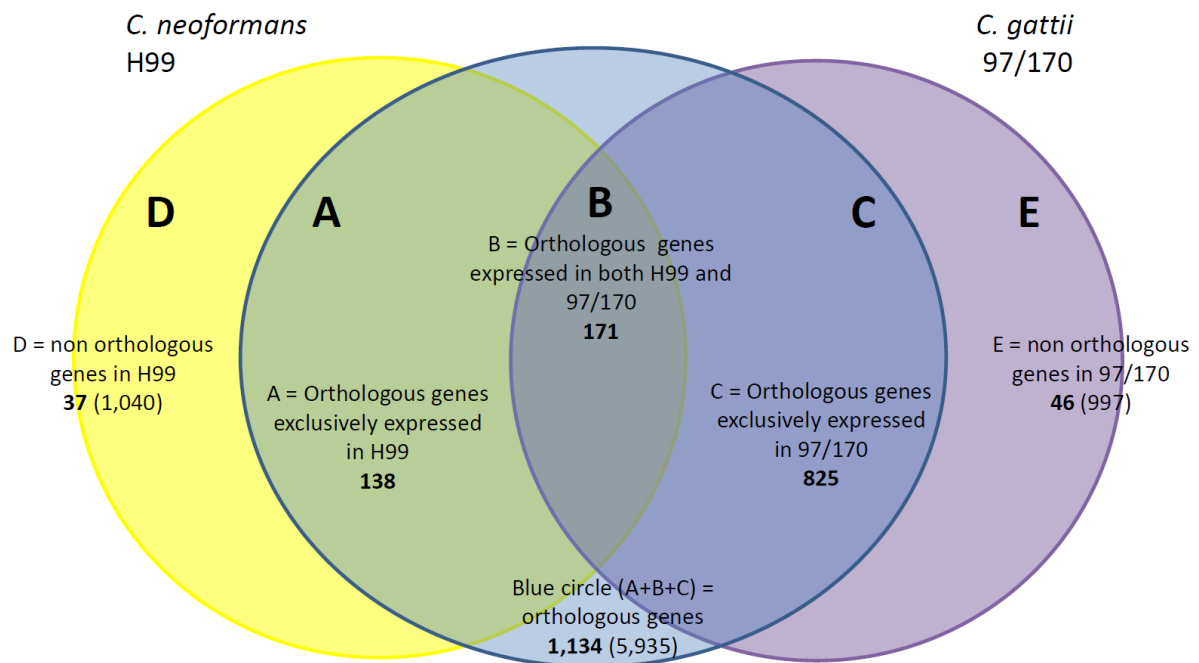


Figure 4.21. Venn diagram of differentially genes in *C. neoformans* H99 and *C. gattii* 97/170 divided according to whether or not orthologues were identified in one or both strains. The total number of differentially expressed genes for H99 is A+B+D (346) and for 97/170 is B+C+E (1,042). The blue circle (A+B+C) encompasses reciprocally orthologous genes expressed in both H99 and 97/170 (1,134 genes). B includes orthologous genes that were expressed in both H99 and 97/170 (171 genes); A and C include orthologous genes that were exclusively expressed in H99 (138 genes) or 97/170 (825 genes), respectively; D and E include non-orthologous genes that were expressed in H99 (37 genes) and 97/170 (46 genes), respectively. Bolded numbers indicate differentially expressed genes relative to the untreated controls; bracketed numbers indicate identified transcripts.

Table 4.12. Number of genes differentially expressed in *C. neoformans* H99 and *C. gattii* 97/170 in each drug treatment compared to untreated controls: orthologous genes* (total gene count#)

| Differentially expressed genes | T _V | | T _{VE} | |
|---|----------------|-----------|-----------------|-------------|
| | H99 | 97/170 | H99 | 97/170 |
| Total number | 62 (66) | 169 (176) | 308 (343) | 989 (1,033) |
| Up-regulated | 58 (62) | 161 (168) | 184 (208) | 531 (560) |
| Down-regulated | 4 (4) | 8 (8) | 124 (135) | 458 (473) |
| Uncharacterised/hypothetical | 24 (28) | 53 (77) | 115 (139) | 350 (393) |
| Unique to treatment – Up-regulated | 1 (2) | 1 (1) | 129 (148) | 371 (393) |
| Unique to treatment – Down-regulated | 0 (1) | 2 (2) | 121 (132) | 452 (467) |

*Gene set A+B for H99 and B+C for 97/170 in Figure 4.21.

Gene set A+B+D for H99 and B+C+E for 97/170 in Figure 4.21.

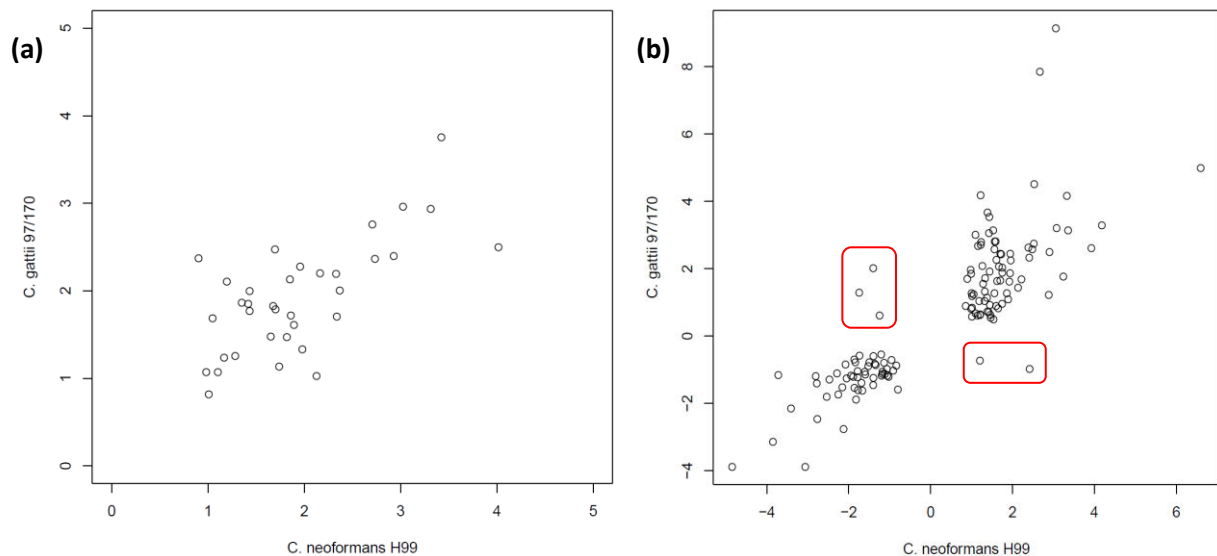


Figure 4.22. Comparison of the direction of expression of orthologous genes (B in Fig. 4.21) in *C. neoformans* H99 and *C. gattii* 97/170 following (a) VRC treatment and (b) VRC+EDTA treatment. Axes show fold-change in expression of genes present in H99 (x-axis) and 97/170 (y-axis) compared to untreated controls. Five orthologous genes had opposing fold change expression following VRC+EDTA treatment and are boxed in red. These genes and their functions are presented in Table 4.13.

Table 4.13. Orthologous genes in *C. neoformans* H99 and *C. gattii* 97/170 with opposing directions of expression

| 97/170 contig | T _V * | T _{VE} | H99 Gene ID | T _V | T _{VE} | Gene description |
|---------------|------------------|-----------------|-------------|----------------|-----------------|-------------------------------|
| g1778 | – | -0.98 | CNAG_01980 | – | 2.42 | Uncharacterised protein |
| g2974 | 1.07 | 1.28 | CNAG_02000 | – | -1.74 | Short-chain dehydrogenase |
| g3042 | – | -0.73 | CNAG_00537 | – | 1.20 | Carnitine O-acetyltransferase |
| g3228 | – | 0.62 | CNAG_02387 | – | -1.24 | Uncharacterised protein |
| g4485 | – | 2.02 | CNAG_03663 | – | -1.40 | L-lactate dehydrogenase |

* Fold-change in expression relative to untreated control; – = No change

4.8.4. GO term enrichments for *C. neoformans* H99 and *C. gattii* 97/170 in T_V and T_{VE}

GO terms were enriched from the total set of differentially expressed genes to investigate the overall response by H99 and 97/170 to VRC and VRC+EDTA (Table 4.14; genes included in A, B, C, D and E in Fig. 4.21). These results are presented below in Section 4.8.4.1. The analysis was then restricted to just orthologous transcripts that were exclusively expressed in one or other organism to compare the antagonism produced by VRC+EDTA in H99 with the additive interaction seen in 97/170 (Table 4.15; A and C in Fig. 4.21); presented in Section 4.8.4.2.

4.8.4.1. GO term analysis of total differentially expressed genes to assess the individual responses by H99 and 97/170 to treatment

Among the GO terms enriched from the total transcripts in H99 (Table 4.14) only ergosterol biosynthesis, which is targeted by azoles including VRC, was enriched and up-regulated in T_V, with thirteen genes present under this term (not shown). There were no enrichments that were down-regulated in T_V as only four unrelated genes, an oxidoreductase (CNAG_01878), nitric oxide dioxygenase (CNAG_01464) and two uncharacterised proteins (CNAG_03454 and CNAG_07765) were present. With the addition of EDTA to VRC treatment, ergosterol biosynthesis remained enriched and up-regulated in T_{VE} and included fourteen genes (not shown). However, the odds ratio for ergosterol biosynthesis was much higher in T_V than in T_{VE} as it represents a greater proportion of all expressed genes (Table 4.12). EDTA+VRC in H99 affected additional cellular processes with GO enrichments involved in mitochondrial ATP synthesis, redox, energy generation and purine metabolism, which were all repressed.

Genes where log-fold changes in differential expression exceeded 2 were examined further. As expected with VRC treatment in H99, the majority of up-regulated genes were involved in lipid biosynthesis and energy generation, with the most up-regulated gene encoding a methylsterol

monooxygenase (CNAG_01737) involved in steroid biosynthesis. Other highly expressed transcripts that are not involved in lipid synthesis or energy generation and have known functions included a sodium dependant phosphate transporter (CNAG_05075) and β -glucan synthesis-associated protein (CNAG_06031).

The most highly induced transcript in T_{VE} in H99 encodes a cytokine-inducing glycoprotein (CNAG_01653). Other induced transcripts encode a number of transporters, including zinc transporters (CNAG_03398, CNAG_00895 and CNAG_07728) and an ATP binding cassette transporter (CNAG_00869). The same β -glucan synthesis-associated protein (CNAG_06031) noted above was also highly induced. Highly repressed genes included antioxidants including catalases (CNAG_00575 and CNAG_04981), flavoprotein (CNAG_01846) and a nitric oxide dioxygenase (CNAG_01464). 3-isopropylmalate dehydratase, which is involved in leucine biosynthesis, was also repressed (CNAG_00237).

In 97/170, transcripts involved in ergosterol biosynthesis were enriched and up-regulated with VRC treatment as was seen in H99. Unlike H99, however, protein insertion into membrane rafts was also induced. There were no down-regulated enrichments as the eight genes that were repressed in T_V were involved in a variety of functions including redox, stress, assembly of the nuclear pore complex and copper transport. The addition of EDTA to VRC, which produces an additive effect in 97/170, also affected DNA, amino acid and mitochondrial-related processes as was seen in H99. Other enrichments in T_{VE} in 97/170 included translation, and protein folding and localisation, which were repressed, while metal and vacuolar transport were induced.

The most up-regulated transcript in 97/170 with VRC treatment was a hypothetical protein (g1817) at a fold change of 6.36. Most of the up-regulated genes with more than 2-log fold changes in differential expression in T_V were hypothetical proteins, genes related to lipid biosynthesis and genes involved in mitochondrial processes. The exceptions were transport-related proteins, such as a vacuolar iron transporter (g3364), an ATP binding cassette transporter (g6492), a membrane transporter (g5603) and Grg1, a regulator of G protein signalling (g2446).

The most down-regulated 97/170 transcripts following VRC+EDTA treatment had log fold changes less than 2 and were involved in cell stress, including a heat shock protein (g141) and a flavohemoprotein (g6989). The most highly up-regulated gene was a hypothetical protein (g7205) with a log fold change of 9.14. Other genes up-regulated more than 2-log fold with predicted functions were involved in signalling and included Crg1 (g2446), a cytokine inducing glycoprotein (g3268) and a receptor (g6793). Transporters mobilising zinc (g4019 and g762), iron (g1505, g2180,

g3364 and g1996), dityrosine (g822), oligopeptide (g564), and ATP binding cassette transporters (g6492 and Pdr11; g5852) were also induced. A metalloreductase (g3415) and a homologue of Zap104 (g3530), which is a zinc-controlling transcription factor, were also highly up-regulated in 97/170.

In summary, relatively few GO terms were enriched in response to VRC and VRC+EDTA treatments in both *Cryptococcus* species when all differentially expressed genes were considered. Ergosterol biosynthesis was induced by both drug treatments in both organisms, as would be expected in response to azole drugs. Little changes to cellular processes were observed with VRC treatment, while the addition of EDTA to VRC treatment turned off transcripts involved in mitochondrial functions in both organisms. In 97/170, however, protein-related processes were additionally repressed by VRC+EDTA treatment.

4.8.4.2. GO analysis of differentially expressed orthologous genes to compare the antagonistic (H99) versus additive (97/170) interaction of VRC+EDTA

Orthologous genes that were expressed in both H99 and 97/170 (Fig. 4.21, set B) were removed to focus on the genes unique to each organism. Most of the genes in this set that were up-regulated in both H99 and 97/170 compared to the untreated controls encode functions involved in lipid biosynthesis, including ergosterol biosynthesis, and these were seen in both VRC and VRC+EDTA treatments. Genes involved in metal transport were also up-regulated by VRC+EDTA, while genes involved in energy generation, oxidation-reduction, TCA cycle and Fe-S cluster assembly were down-regulated (not shown).

Restricting the analysis to orthologous genes expressed only in one organism (Fig. 4.21; A and C) changed the types of GO terms enriched by VRC and VRC+EDTA treatment in H99 (Table 4.15). In *T.*, proteolysis and oxidation-reduction processes were enriched and up-regulated, as were phospholipid and phosphatidylinositol biosynthesis. In the H99 response to VRC+EDTA, oxidation-reduction was shut down and GO enrichments including transmembrane and transition metal ion transporters were induced. More than half of the genes involved in transmembrane transport encode proteins that are involved in transporting drugs (CNAG_06348, CNAG_04616, CNAG_04546, CNAG_02336), which have been observed in response to azole drugs in other studies [523], while other transporters mobilise substrates such as sugar (CNAG_02586) and inorganic phosphate (CNAG_02777). The transition metal transporters transport iron (Cft3; CNAG_03694) and copper (Ctr4; CNAG_00970).

C. gattii strain 97/170 had substantially more differentially expressed genes in response to both VRC and VRC+EDTA than *C. neoformans* H99. In T_V , GO enrichments for redox, lipid metabolism, transport including transmembrane and metal ion transporters, and cell stress responses such as response to hydrogen peroxide and osmotic stress were up-regulated. Genes that were enriched in transmembrane transport encode proteins that mobilise drugs (g4255, g6793, g3132, g3248). Other up-regulated GO enrichments included amino acid import, regulation of actin organisation, and osmosensory signalling.

A more dynamic response was seen in 97/170 upon the addition of EDTA to VRC treatment, where enrichments related to translation, protein folding and the regulation of translation in response to stress were repressed. Mitochondrial functions were also repressed, and redox, which was induced in VRC treatment, was shut down. GO enrichments that were induced included amino acid import, lipid metabolism, vesicle mediated transport and signalling. The enrichment of GO terms related to drug mobilisation found in T_V was no longer seen in T_{VE} . Stress responses differed between the single and combined drug treatments in 97/170. While autophagy and cellular responses to pH were also induced, the response to hydrogen peroxide that was observed in T_V was no longer seen.

To understand how EDTA represses the inhibitory action of VRC in H99, the response to treatment was compared to that seen for 97/170. The most striking difference in enrichment in T_{VE} was the induced expression of transmembrane transport genes, most of which were drug transporters (CNAG_06348, CNAG_04616, CNAG_04546, CNAG_02336), which occurred in H99 but not in 97/170. Transition metal ion transporters were also induced in H99 but not in 97/170 and included Cft3 and Ctr4, which transport iron and copper, respectively. Additional GO terms in 97/170 that were not enriched in H99 included the induction of lipid metabolism, response to pH, mitophagy and cytolysis. Protein-related processes such as translation and folding, and terms associated with transport such as tubulin complex assembly and protein localisation to the mitochondria were repressed in 97/170, suggesting a decrease in active growth. The only enrichment common to the two species was the shutdown of oxidation-reduction, and DNA metabolism was generally repressed in both organisms.

Table 4.14. Selected GO term enrichments for all differentially expressed transcripts in *C. neoformans* H99 and *C. gattii* 97/170 in T_V and T_{VE}

| GO term | GO ID | H99 | | 97/170 | |
|--|------------|----------------|-----------------|----------------|-----------------|
| | | T _V | T _{VE} | T _V | T _{VE} |
| DNA and amino acid related | | | | | |
| Cellular amino acid metabolic process | GO:0006520 | | | | 2.46 |
| Purine nucleoside triphosphate metabolic process | GO:0009144 | | 11.82 | | 11.5 |
| Mitochondria and energy related | | | | | |
| Haem biosynthetic process | GO:0006783 | | | | 9.9 |
| Mitochondrial ATP synthesis coupled electron transport | GO:0042775 | | 41.19 | | 142.54 |
| Oxidation-reduction process | GO:0055114 | | 7.16 | | 2.46 |
| Generation of precursor metabolites and energy | GO:0006091 | | 9.66 | | 5.69 |
| Mitochondrial membrane organisation | GO:0007006 | | | | 4.66 |
| Lipid related[#] | | | | | |
| Cellular lipid biosynthetic process | GO:0097384 | 176.2 | 40.35 | 97.69 | 26.14 |
| Ergosterol biosynthetic process | GO:0006696 | 176.2 | 40.35 | 97.69 | 26.14 |
| Protein related | | | | | |
| Protein insertion into membrane raft | GO:0071210 | | | Inf* | |
| Protein folding | GO:0006457 | | | | 3.87 |
| Translation related | | | | | |
| Translation | GO:0006412 | | | | 4.46 |
| Cytoplasmic translation | GO:0002181 | | | | 5.56 |
| Transport, cell organisation and regulation related | | | | | |
| Metal ion transport | GO:0030001 | | | | 3 |
| Vacuolar transport | GO:0007034 | | | | 2.8 |
| Tubulin complex assembly | GO:0007021 | | | | 7.02 |
| Protein localisation to mitochondrion | GO:0070585 | | | | 7.08 |

Odds ratios for each GO term are included, with regulation of GO terms colour coded. Red: up-regulated. Green: down-regulated. *Inf = all genes contributing to enrichment of this GO term are present. [#] Ergosterol biosynthesis is a child GO term of lipid biosynthesis and both terms have the same odds ratios.

Table 4.15. Selected GO term enrichments for transcripts of orthologous genes in *C. neoformans* H99 and *C. gattii* 97/170 in T_V and T_{VE}

| GO term | GO ID | H99 | | 97/170 | |
|--|------------|----------------|-----------------|----------------|-----------------|
| | | T _V | T _{VE} | T _V | T _{VE} |
| DNA and amino acid related | | | | | |
| Cellular amino acid metabolic process | GO:0006520 | | | | 2.44 |
| Purine nucleobase biosynthetic process | GO:0009113 | | | | 5.71 |
| Pyridine nucleotide biosynthetic process | GO:0019363 | | 19.46 | | |
| Pyrimidine nucleobase metabolic process | GO:0006206 | | | | 17.15 |
| Amino acid import | GO:0043090 | | | 22.01 | 13.78 |
| Mitochondria and energy related | | | | | |
| Haem biosynthetic process | GO:0006783 | | | | 4.58 |
| Mitochondrial ATP synthesis coupled electron transport | GO:0042775 | | | | 10.15 |
| Oxidation-reduction process | GO:0055114 | Inf* | 2.99 | 2.13 | 1.62 |
| Generation of precursor metabolites and energy | GO:0006091 | | | | 3.01 |
| Mitochondrial membrane organisation | GO:0007006 | | | | 4.49 |
| Lipid related | | | | | |
| Phosphatidylinositol biosynthetic process | GO:0006661 | 20.51 | | | |
| Phospholipid biosynthetic process | GO:0008654 | 8.94 | | | |
| Lipid metabolic process | GO:0006629 | | | 3.10 | 1.75 |
| Fatty acid biosynthetic process | GO:0006633 | | | 10.63 | |
| Protein related | | | | | |
| Proteolysis | GO:0006508 | 5.23 | | | |
| Protein folding | GO:0006457 | | | | 4.23 |
| Translation related | | | | | |
| Posttranscriptional regulation of gene expression | GO:0010608 | | | | 2.32 |
| Translation | GO:0006412 | | | | 5.18 |
| Cytoplasmic translation | GO:0002181 | | | | 6.21 |
| Response to stress | | | | | |
| Regulation of translation in response to stress | GO:0043555 | | | | 8.57 |
| Positive regulation of autophagy | GO:0010508 | | | | 13.72 |
| Response to hydrogen peroxide | GO:0042542 | | | 8.78 | |
| Cellular response to hydrogen peroxide | GO:0070301 | | | 10.99 | |
| Cellular response to osmotic stress | GO:0071470 | | | 4.02 | |
| Cellular response to pH | GO:0071467 | | | | 3.67 |
| Cytolysis | GO:0019835 | | | | Inf* |
| Mitochondrion degradation | GO:0000422 | | | | 5.89 |
| Transport, cell organisation and regulation related | | | | | |
| Transmembrane transport | GO:0055085 | | 2.14 | 2.47 | |
| Regulation of actin cytoskeleton organisation | GO:0032956 | | | 4.58 | |
| Tubulin complex assembly | GO:0007021 | | | | 8.22 |
| Protein localisation to mitochondrion | GO:0070585 | | | | 7.33 |
| Golgi vesicle transport | GO:0048193 | | | | 2.14 |

| | | | |
|--|------------|-------|-------|
| Endosomal transport | GO:0016197 | | 3.30 |
| Activation of MAPKKK activity | GO:0000185 | | 27.45 |
| Signal transduction by phosphorylation | GO:0023014 | | 3.14 |
| Osmosensory signalling pathway | GO:0007231 | 12.56 | 6.88 |
| Metal related[#] | | | |
| Transition metal ion transport | GO:0000041 | 6.59 | |
| Metal ion transport | GO:0030001 | | 3.50 |

Odds ratios for each GO term are included, with regulation of GO terms colour coded. Red: up-regulated. Green: down-regulated. *Inf = all genes in this GO enrichment are present. [#]Metal ion transport also includes transition metal ion transport.

4.9. Discussion – VRC+EDTA antagonism and additivity in *C. neoformans* H99 and *C. gattii* 97/170

Antagonistic drug interactions occur when the efficacy of the drugs when combined is less than the most effective drug when used alone [148]. Drug prediction databases can identify some antagonistic drug pairs but investigations into the mechanistic understanding of antagonistic drug combinations have not garnered as much attention as drug synergy.

Certain iron chelators can act as antagonists in combination with antifungal treatments. An *in vivo* study of *Rhizopus*-infected guinea pigs found the addition of DFO to AMB treatment abolished the prolonged survival produced by the antifungal alone. It appeared that DFO antagonised AMB activity by behaving as a siderophore and stimulating *Rhizopus* growth by providing iron [294]. Antagonistic interactions between antifungals and iron chelators have also been observed *in vitro* in other fungi, with AMB+DFP and FLC+LF producing antagonism in *A. fumigatus*, and FLC+LF in *C. albicans* [9, 235]. Minor antagonism was also seen when LF was combined with FLC, AMB and 5-FC in *Candida* species but only at the lower range of concentrations tested for both agents [10]. None of these studies investigated or discussed how the tested iron chelators might antagonise the activity of antifungal drugs. In the current study AMB+DFP and FLC+LF produced an additive interaction in *Saccharomyces* and *Cryptococcus* while AMB+LF was synergistic (Fig. 3.3a), indicating the complexity and species-specific nature of drug interactions.

In this thesis, antagonism occurred when FLC, ITC and VRC were combined with DFP, DSX and EDTA, but this occurred in *C. neoformans* var. *grubii* only and was not seen in closely related *C. neoformans* var. *neoformans* and *C. gattii* strains (Fig. 3.3a). The most extreme difference was where VRC+EDTA was antagonistic in H99, raising the requirement for VRC 4-fold yet, this same combination was almost synergistic in 97/170 and reduced the requirement for VRC 16-fold (Section 3.4.2; Appendix 3.1). Understanding how this difference occurred became the focus of the analysis presented in this chapter.

As using cells that are inhibited but not killed is essential for transcriptomic analysis of drug inhibition, considerable effort went into determining a suitable timepoint to analyse the transcriptome of VRC+EDTA antagonism in H99 and additivity in 97/170. In the synergy experiments (Section 4.2.3.1), RNA-Seq was performed when AMB and AMB+LF treatments caused a 20% decrease in growth compared to the untreated control (i.e. at ID_{20}). It was therefore decided to use the point where VRC+EDTA treatment caused a 20% increase in the growth of H99 compared to VRC treatment alone, which was at the 7th hour of treatment (Fig. 4.19), to extract RNA across all VRC+EDTA experiments in H99 and 97/170. This caused some challenges in choosing a comparable

time for RNA-Seq during treatment with VRC alone. Most importantly, the concentrations of VRC and EDTA used to treat H99 and 97/170, which was included to investigate how VRC+EDTA could be additive in one species but antagonistic in another, caused different effects on the growth of both organisms (Fig. 4.19) as the MICs of VRC and EDTA were different in the two strains (Table 3.2). At the 7th hour of treatment, H99 was significantly inhibited by the FIC for VRC treatment (which was four times higher than its MIC), while the growth of VRC-treated 97/170 cells resembled that of its untreated control (Fig. 4.19). Therefore, the transcriptome analysis of VRC treatment in H99 may be confounded by the presence of apoptotic responses, while 97/170 may lack a sufficiently strong response to VRC.

In 97/170 at the 7th hour of drug treatment, VRC+EDTA had inhibited growth by 27% relative to the untreated control, while VRC had only inhibited growth by 4% (Fig. 4.19a). This may affect the comparison between the two treatments by RNA-Seq, compared to performing it at a common inhibitory point like ID₂₀, as used in Section 4.2.3.1. In addition, due to cost the transcriptome responses to EDTA alone in H99 and 97/170 was not assessed and this is therefore not available for comparison. These issues need to be considered in the comparative analysis of VRC and VRC+EDTA treatments in H99 and 97/170, which are also limited by a lack of validation. Nevertheless, the transcriptomic data revealed interesting insights into antagonism and highlight species-specific differences in how cells respond to the same drug combination.

4.9.1. Up-regulation of efflux pumps as a mechanism of VRC+EDTA antagonism in *C. neoformans* H99

In H99, ergosterol biosynthesis and oxidation-reduction processes, which were up-regulated in T_v, (Table 4.14 and 4.15) reflect a subset of cellular responses that have been reported in FLC-treated *Cryptococcus* cells. In contrast the up-regulation in proteolysis (Table 4.15) has not been previously observed as a response to azole treatment [137, 356]. This may be due to the high concentration of VRC used here, which was 4 x MIC for VRC compared to 0.5 and 2 x MIC of FLC used in the two other *Cryptococcus* studies [137, 356]. Alternatively, it may be due to different effects of VRC on the cell compared to FLC.

With the addition of EDTA, the most striking enrichment in H99 was the induction of transmembrane transport, where genes encoding drug efflux pumps were observed (Table 4.15). These included the ATP-binding cassette (ABC) transporter Pmr5 (CNAG_06348), major facilitator superfamily (MFS) transporters (CNAG_04616 and CNAG_00433), a multidrug transporter (CNAG_04546) and a multidrug resistance protein (CNAG_02336). Of these, only *PMR5* was up-regulated following VRC

treatment in H99 (not shown). While some genes encoding drug transporters were also seen in T_{VE} in 97/170, none of drug transporter genes listed above were seen.

The expression of efflux transporters that remove drugs from the cell is a major mechanism of decreasing azole susceptibility in fungi and has been extensively reviewed [523, 524]. ABC and MFS transporters are the main classes of drug translocators that cause multidrug resistance. ABC transporters hydrolyse ATP to move substrates across membranes and include pleiotropic drug resistance (PDR), multidrug resistance (MDR) and multidrug resistance-associated proteins (MRP). MFS transporters use proton motive force and include drug:H⁺ antiporters, symporters and uniporters [523]. Up-regulation of these suggested that EDTA may antagonise the inhibitory effect of VRC in H99 by enhancing the removal of VRC from the cell. This would explain the substantially lower transcriptomic response to VRC+EDTA treatment seen in H99 compared to 97/170, as the intracellular concentration of VRC may not be harmful enough to elicit changes in cellular homeostasis and cause cell stress. This is in contrast to 97/170, where efflux genes were seen T_V but became absent in T_{VE}, and suggests that the lack of differentially expressed drug efflux genes may be one of the mechanisms that augmented the inhibitory activity of VRC in 97/170 (Table 4.15).

Interestingly, *MDR1* and *AFR1*, which encode the most characterised drug efflux transporters in *C. neoformans* [523], were not observed in H99 in T_V or T_{VE}. However, *PDR11*, a *C. gattii* orthologue of *AFR1* [525], was up-regulated by both drug treatments in 97/170 with fold changes of 1.69 in response to VRC, and 2.69 in response to VRC+EDTA (Section 4.8.4.1, not shown). *AFR1* overexpression is associated with FLC resistance and increased virulence [523]. In *C. neoformans*, azole treatment can cause heteroresistance, which appears in part due to duplication of the chromosome containing the *AFR1* locus [185]. *MDR1* overexpression is also associated with decreased FLC susceptibility and heteroresistance, but this is not as well characterised as the *Afr1* response [523, 526]. The absence of *AFR1* and *MDR1* expression in *C. neoformans* strain H99 suggests that these transporters may not have a major role in VRC efflux and that other drug transporters may have higher specificity for VRC. In contrast to H99, up-regulation of *PDR11* in *C. gattii* strain 97/170 suggests that *PDR11* may have a role in VRC survival. However, *PDR11* expression may not contribute to VRC+EDTA survival, even at a higher fold-change in expression, as this drug combination may have caused cellular damage that was irreversible by drug efflux.

The induction of efflux proteins has been implicated as a mechanism of antagonism in other organisms. In gram negative bacteria, addition of the analgesic salicylate to chloramphenicol or tetracycline induced antagonism through the induction of the *marRAB* operon, which encodes transcriptional activators that increase the production of various drug efflux mechanisms [527]. The

role of drug efflux proteins in drug antagonism was clearly demonstrated when the deletion of a central efflux protein, TolC, abolished antagonism between salicylate combinations with chloramphenicol and tetracycline in *E. coli* [528]. This suggests that non-antimicrobial medicines, which are not thought to induce drug resistance mechanisms, can have unexpected consequences on the activities of antimicrobial drugs.

Increased expression of drug efflux pumps has also been observed in *Candida* petite mutants, which are deficient in mitochondrial DNA and have decreased susceptibility to azole drugs [529-531]. In *Cryptococcus*, mutants that are disrupted in mitochondrial function have decreased susceptibility to azoles, which suggests azole sensitivity can be dependent on mitochondrial function [532]. This may be relevant to the antagonistic effect of VRC+EDTA on H99, as the addition of EDTA had a suppressive effect on enrichments relevant to mitochondrial activity and to the targeting of protein to the mitochondrion (Table 4.14). Additionally, transition metal ion transport was enriched and up-regulated in T_{VE} in H99 (Table 4.15) but not in T_V . While this coincides with the metal chelating ability of EDTA, it also corresponds to the accumulation of metals and the activation of metal uptake responses exhibited by cells with dysfunctional mitochondria [533, 534]. Therefore, an additional way in which EDTA is antagonistic to VRC in H99 may be by causing mitochondria to mis-function in ways similar to those seen in petite mutants, which may in turn cause the up-regulation of drug efflux genes and decrease susceptibility to azole drugs.

Interestingly, certain disruptions of mitochondrial functions including electron transport chain complexes and mitochondrial biogenesis can increase susceptibility to azoles [534, 535], and this may have occurred in 97/170, where EDTA increased VRC inhibition and enrichments for mitochondrial processes were suppressed (Table 4.14).

4.9.2. EDTA may potentiate VRC activity in *C. gattii* 97/170 by alterations to the stress response

With VRC treatment, 97/170 exhibited responses that are commonly seen in response to azole drugs, with up-regulation of enrichments relating to ergosterol biosynthesis, mitochondrial and energy generation, response to stress and transmembrane transport that included some drug efflux transporters (Table 4.14 and 4.15) [137, 356, 359, 463]. Additional responses that have been reported in other azole-treated yeast cells included the up-regulation of metal transport, signal transduction and cell wall maintenance (Table 4.15) [137, 359, 463]. Altogether, this suggested that the effect of VRC on 97/170 was typical for azoles.

EDTA altered the stress responses seen in T_V , where the enrichments for oxidative and osmotic stress responses became absent. Additionally, the GO term transmembrane transport, which was

induced in T_V , became absent with the addition of EDTA. In contrast, activation of mitogen protein kinase kinase kinase (MAPKKK), mitophagy, response to pH and cytolysis, which were not observed in T_V , were induced (Table 4.15).

These enrichments suggest that EDTA may have potentiated the effect of VRC in 97/170 by disrupting antioxidant production and inducing more rapid cytolysis. EDTA disrupts membrane integrity by binding to the membrane and increases its permeability [536], which can lead to cellular osmotic imbalance. The high-osmolarity glycerol (HOG) response pathway may be activated in response, as *SSK2*, an upstream MAPKKK activator in the HOG pathway that is the main regulator of stress responses, cell differentiation and virulence factor production, was up-regulated in T_{VE} [537]. However, target genes of *Ssk1* were not differentially expressed (not shown). This suggests an incomplete activation of the stress adaptation response and inability of the cells to respond appropriately.

EDTA causes Mg^{2+} efflux from the mitochondrial matrix, which can disrupt mitochondrial function by affecting mitochondrial RNA metabolism and ATP synthesis [538]. This effect, in addition to the antifungal activity of VRC, may lead to increased mitochondrial stress and mitophagy in 97/170 (Table 4.15). Additionally, EDTA has been shown to affect vesicle mediated trafficking, which is required for the localisation of transport proteins [283]. Interestingly, mitochondrial dysfunction also disrupts HOG stress signalling and affects the localisation of drug efflux transporters [534], which were all suggested in T_{VE} in 97/170. This may explain why in 97/170 the enrichments for metal ion and transmembrane transport, which included drug efflux transporters, were seen in VRC treatment but became absent in the presence of EDTA (Table 4.15).

A comparison of the transcriptomic data produced by H99 and 97/170 showed a number of differences that may determine their responses to VRC+EDTA. Up-regulation of transmembrane transporters including drug efflux proteins was implicated as a mechanism of VRC+EDTA antagonism in H99 (Table 4.15). However, although some genes associated with drug transporters were up-regulated, the absence of enrichments related to drug efflux proteins in 97/170 suggested that the expression of more drug transport encoding genes may be associated with increased survival to VRC+EDTA. This was because enrichments for drug efflux were up-regulated in VRC where growth was less inhibited than VRC+EDTA treatment (Fig. 4.19 and Table 4.15). Dysregulation of mitochondrial responses was also observed in both H99 and 97/170, however in 97/170 many more mitochondrial-related enrichments were observed, including haem and ATP synthesis and mitophagy, suggesting a more severe disruption to mitochondrial function (Table 4.15). Finally, dysregulation of stress responses was implicated in 97/170 but not in H99, suggesting that the

disruption in mitochondrial function caused by the addition of EDTA to VRC in 97/710 may have affected the appropriate induction of stress responses. Interestingly, this dysregulation of stress responses was similar to that seen in the synergistic interaction of AMB+LF in S288C (Section 4.5.3.1) and to the synergy of FLC+B-7b and NaCl+H₂O₂ reported in *C. albicans* [321, 479], suggesting a common mechanism of synergy is the disruption of stress related responses. This will be further discussed in Section 5.2.

4.9.3. Species-specific responses to drugs and to drug combinations

Transcriptome analyses of EDTA+VRC treatment in *C. neoformans* H99 and *C. gattii* 97/170 revealed species-specific differences in their cellular response. Different fungal organisms can vary substantially in their intrinsic susceptibility to antifungal drugs; for example, FLC is active against a range of fungal organisms but has no activity against *Aspergillus* and some species of *Candida* [181]. Differences in drug susceptibility are also seen between closely related fungal species. In *Cryptococcus*, *C. gattii* isolates are generally less susceptible to azoles than *C. neoformans* isolates and between cryptococcal genotypes, *C. gattii* VGII strains have been shown to be less susceptible to FLC than VGI and VGIII strains [21]. Additionally, the development of heteroresistance is more prevalent in *C. gattii* than *C. neoformans* strains [32]. However, how and why closely related fungal species respond differently to drug treatments is often poorly understood.

The response to drug combinations can also differ substantially among closely related species, as seen in Chapter 3 in this thesis. Azole combinations with EDTA, DFP and DSX were antagonistic only in *C. neoformans* var. *grubii* strains (genotypes VNI and VNII) and not in *C. neoformans* var. *neoformans* (VNIV) or *C. gattii* strains (Fig. 3.3a). However, while VRC was consistently antagonistic with EDTA, DFP and DSX in all *C. neoformans* var. *grubii* strains, other azole-chelator combinations like FLC+EDTA were not (Fig. 3.3a). In the *C. gattii* strains tested most of the additive and synergistic drug combinations produced consistent 2- to 4-fold reductions in the requirement for the antifungal, however for strain R272 treated with AMB+LF, and strain 97/170 treated with VRC+EDTA, the presence of chelators caused a 16-fold reduction in antifungal requirement (Appendix 3.1).

C. gattii strain 97/170 has been of interest to our laboratory as it is a VGII isolate with no apparent previous exposure to FLC, yet it is inherently very resistant to FLC with an MIC of 64 µg/mL (Table 3.2). Of the VGII strains tested, 97/170 exhibited the highest MIC to VRC and other azoles and it also had the greatest reduction for VRC in presence of EDTA (Table 3.2, Appendix 3.1). Based on its highly resistant phenotype, our laboratory undertook a comparative analysis of the genomic sequence of 97/170 and other *C. gattii* VGII strains with wild-type and elevated resistance but found minimal

differences (not shown) and none appeared to account for how the strains differed in their responses to azoles. Similarly, comparative studies of the genomes of *C. neoformans* and *C. gattii* strains did not find a genetic basis for the difference in drug susceptibilities between the two species [141, 539].

97/170 is closely related to H99 and shares 83% genome identity, which is consistent with the genomic differences reported between *C. gattii* and *C. neoformans* [539]. In hindsight, however, investigating the antagonistic interaction of VRC+EDTA in H99 may have been better with a more closely related strain where VRC+EDTA was not antagonistic, such as *C. neoformans* var. *neoformans* strain JEC21 α (Fig. 3.3a). Strains within the same species generally have higher synteny and orthology [141, 539] making it easier to find specific differences in genome content that cause differences in drug responses. However, as only the variety *grubii* in *C. neoformans* exhibited antagonism in Chapter 3, this suggested that the different drug interactions seen between the varieties and species of *Cryptococcus* may be influenced by other factors that make these organisms distinct.

C. neoformans var. *grubii* is the most common *Cryptococcus* species isolated from HIV/AIDS and other immunosuppressed patients [540] and latent clinical isolates may be exposed to azoles during prophylactic treatment prior to being isolated during active infection. *C. gattii*, on the other hand, is a primary pathogen and exposure to clinical azoles is unlikely. Such prior exposure could increase the expression resistance mechanisms like drug transporters [541], and this may contribute to the difference in drug interactions observed between H99 and 97/170. Adaptive responses to host infection may also contribute to differences in drug response. Analysis of the transcriptome profiles of *C. neoformans* var. *grubii* strains isolated from the cerebral spinal fluid of AIDS patients before antifungal treatment showed that genes encoding drug efflux transporters were commonly up-regulated during host infection [542]. While transcriptome profiles of host adaptation during infection by other varieties have yet to be reported, it is possible that extended infection during latency and HIV/AIDS and/or a greater exposure to azoles may cause *C. neoformans* var. *grubii* strains to have a higher propensity for drug efflux expression during stress, which may influence responses to drug interactions in a different manner to other cryptococcal varieties.

Overall, this study shows that a drug combination that inhibits the growth of one fungal organism may not always be suitable to inhibit the growth of another due to potential differences in their responses to the drug combination, which can be difficult to predict, and extensive testing across a wide variety of different strains is advisable.

4.9.4. Future avenues for understanding the mechanisms of azole-chelator interactions

Drug efflux transporters and disruption of stress responses were strongly implied by the transcriptomic data as mechanisms of VRC+EDTA antagonism in H99 and additivity in 97/170. In order to validate these, qPCR using primers specific for the H99 multidrug transporter *CNAG_004546* and the 97/170 MAPKKK associated kinase *STE11 (g3399)*, which were only expressed in T_{VE} , can be monitored during VRC+EDTA treatment, as previously mentioned for AMB+LF synergy experiments (Section 4.7.5). Monitoring of genes expressed in both T_V and T_{VE} , such as the H99 β -glycan associated protein *CNAG_00869* and the 97/170 ABC transporter *PDR11 (g8582)*, should also be done. As well as validating the current data, qPCR of efflux transporter genes would also be useful for understanding the species-specific nature of drug interactions with VRC+EDTA and other antagonistic azole-chelator combinations like ITC+DFP and FLC+DSX (Fig. 3.3) in different *Cryptococcus* species and strains.

Due to time constraints, SOMs analyses of the transcriptome data produced by H99 and 97/170 were not performed. As SOMs analysis in the synergy experiments provided a more detailed understanding of AMB+LF mechanisms in S288C and H99. SOMs should also be applied to the antagonism experiments. This would enable further understanding of the functional processes that are co-regulated following VRC+EDTA treatment and contribute to antagonism in H99 and additivity in 97/170.

As noted above, disruption of mitochondrial function can cause increased expression of drug efflux pumps [529-531]. However, while enrichment analysis of T_{VE} in H99 and 97/170 both suggested alterations in the mitochondria (Table 4.15), the increased expression of efflux transporters seen only in H99 suggested that the disruptive effect of VRC+EDTA on the mitochondria may differ between H99 and 97/170. Disruptions to the mitochondria can range from changes in physiological functions such as ATP synthesis, to apoptotic processes, changes mitochondrial ion homeostasis and the generation and neutralisation of ROS [543]. These could be assessed in VRC+EDTA-treated H99 and 97/170 cells such as by assaying changes in mitochondrial membrane potential, ATPase activity and intracellular ATP and ROS concentrations, as were performed in the study of BBR+FLC synergy [6]. Release of cytochrome *c*, which is a pre-apoptotic indicator and is indicative of disruptions in the electron transport chain and the generation of superoxides [544], could also be tested. Differences in how mitochondria were disrupted in H99 and 97/170 may indicate how VRC+EDTA disrupted stress responses in 97/170 but up-regulated drug efflux proteins in H99.

4.10. Additional observations in the transcriptomes of drug synergy and antagonism

4.10.1. Differences in RNA-Seq data between synergy and antagonism experiments reflect the different cellular effects of polyenes and azoles

One of the intriguing observations in this analysis was the difference in the number of genes differentially expressed in response to azole treatments (T_V and T_{VE}) compared to polyene treatments (T_A and T_{AL}), as well as the difference in the number of genes differentially expressed in H99 AMB+LF synergy versus those expressed in 97/170 VRC+EDTA additivity/H99 VRC+EDTA antagonism. Previous microarray studies have reported more differentially regulated genes in response to polyenes than azoles. In *Saccharomyces*, 44 genes were up-regulated and 7 were down-regulated in response to ketaconazole treatment compared to 185 up- and 80 down-regulated genes with AMB treatment [463]. Similarly in *Candida*, 60 genes were up-regulated and 22 were down-regulated in response to ketaconazole, while 87 were up- and 169 genes were down-regulated in response to AMB [359, 463]. These differences may reflect different inhibitory mechanisms and a wider range of effects exerted on cells by polyenes compared to azoles. The higher percentage of genes differentially expressed from the total number of identified transcripts in AMB+LF experiments (50% in S288C and 60% in H99) compared to VRC+EDTA experiments (5% in H99 and 15% in 97/170) appears to reflect this.

The fewer number of genes in both T_V and T_{VE} in H99 compared to 97/170 (Table 4.12) is surprising given that level of inhibition of H99 caused by both drug treatments in relation to the untreated controls was greater at the time of RNA-sequencing (Fig. 4.19). In H99, the minimal changes in the transcriptome during VRC+EDTA treatment may be due to the negating effect of EDTA inducing VRC efflux out of the cell. However, the lack of differentially expressed genes in H99 during treatment with VRC alone, which was used at 4 x MIC and caused significant growth inhibition of H99, is difficult to explain. It is possible that at the concentration used, VRC overwhelmed the cell making it unable to mount an appropriate transcriptional response, or that by the time of extraction (7 hr), the response had been missed. Conversely, the higher number of genes that were differentially expressed by H99 and S288C during AMB+LF synergy and by 97/170 during VRC+EDTA additivity (Table 4.4 and 4.12) may be a result of the cell rewiring its metabolic pathways and processes to survive the drug treatments that were at a more sub-lethal level.

4.10.2. Problems and limitations in transcriptome analyses of drug synergy and antagonism

A major limitation to the transcriptome analysis of synergy and antagonism was the level of genome annotation available for *Cryptococcus* strains H99 and 97/170, which affected the depth of analysis of the drug interactions. Although genome annotations were improved by pooling functional annotations of orthologous genes from other fungal species such as *Saccharomyces*, *Aspergillus*, *Candida* and *Agaricus*, about 30% of the genes differentially expressed in AMB+LF synergy and 40% of those seen in VRC+EDTA antagonism were uncharacterised with no known functions (Tables 4.4 and 4.12). This in turn affected network analysis, as the mapping of cellular processes and pathways relies on genes or proteins that have been characterised in terms of functions and interactions or have orthology to *Saccharomcyes*.

Another problem observed in the RNA-Seq analysis was the presence of outlier RNA samples (Fig. 4.7a and 4.20a). As RNA-Seq is a sensitive technique that can detect low abundance transcripts [127], drug synergy and antagonism treatments and sequencing of RNA samples were performed in a way to minimise technical and biological variations. This involved performing drug treatments and RNA harvesting in the same way, randomising the extraction of RNA from all samples across different drug treatments and their placements across sequencing lanes, and normalising the generated data. Outliers in RNA-Seq data are more often found in studies that process and analyse many RNA samples [545] and the current drug synergy and antagonism transcriptome studies had a total of 42 RNA samples that were sequenced together. The presence of outliers suggested that variation in stages of the RNA processing may have occurred, which can invariably occur with larger RNA sample sizes. Additionally, biological variation between *Cryptococcus* RNA samples was higher than between *Saccharomcyes* RNA samples (Fig. 4.5b, 4.7b, 4.20b and 4.20f). However, this is consistent with the low variability of biological replicates observed in model organisms such as *Saccharomcyes* versus non model organisms like *Cryptococcus* [387].

CHAPTER 5: Final discussion and conclusions

5.1. The value of holistic analysis

Significant advances in next generation sequencing technologies and reducing costs have led to their increased application in systems biology, which adopts a holistic approach to understanding cellular responses. This contrasts with the reductionist approach of molecular biology, which studies complex systems by analysing their simpler components. Systems biology also differs from molecular biology and other more traditional sciences where hypotheses are formed from observations and/or prior knowledge, which is then proven or refuted from the generation and analysis of experimental results. In contrast, systems biology uses a reverse hypothesis approach, where the analysis of experimental data is used to generate hypotheses. This type of unbiased approach has been advantageous in understanding poorly characterised and complex events. An example is understanding the process of pathogenicity in host-pathogen interactions, which involves the expression of gene sets with distinct functions at different stages of infection, which would have been challenging to decipher using molecular biological approaches alone [546].

Holistic analyses have also unveiled additional functions of characterised proteins, such as the collagen tyrosine kinase receptor *Drd2*, which besides regulating cell proliferation, adhesion, migration and extracellular collagen remodelling, has an unexpected role in regulating ovarian function [547]. Sometimes unexpected or contrary findings have been observed via holistic studies. For example, transcriptomics has been used to study how calcification and skeletal formation in corals is disrupted by ocean acidification. One proposed mechanism of coral calcification involves the uptake and transport of extracellular ions involved in the chemical production of calcium carbonate in the space where skeletal formation occurs. Acidification was thought to disturb this process, but contrary to expectations, transcriptomic analysis found the expression of ion transporters was relatively unaffected by the decrease in pH. Instead, genes associated with the skeletal organic matrix, which mediates the controlled deposition of the calcium carbonate skeleton, were shown to be enriched and up-regulated following acidification [548].

In this thesis, the transcriptomic analysis of antifungal-iron chelator interactions revealed unexpected mechanisms of synergy and antagonism. The comparison of transcriptome data produced by different yeast species further revealed complex and diverse species-specific responses to the same synergistic and antagonistic drug pair. Visualisation of the dynamic changes to cellular pathways caused by the presence of iron chelators aided the discovery of targets that, when disrupted, perpetuated synergy with AMB.

5.2. Disruption of stress-related responses as an antifungal strategy

Stress is an adaptive response that is activated to survive changes in the external and internal cellular environment. An inability to adapt to change inhibits the restoration of cellular homeostasis and eventually results in cell death. The transcriptomic analysis of AMB+LF and VRC+EDTA presented in this thesis, and the proteomic analyses of synergy induced by NaCl+H₂O₂ and FLC+B-7b in *C. albicans* by Kaloriti *et al.* (2014) and Li *et al.* (2015) [321, 479] suggest that alteration in stress-related responses is a common mechanism of enhanced fungal death.

Stress related responses can be perturbed in a number of ways. In the synergy experiments with AMB+LF, AMB alone caused a relatively typical toxin-induced ESR in S288C and H99 (Sections 4.5.2 and 4.7.2). However, the addition of LF disrupted this response differently in the two species. In H99, LF caused an increase in cell stress that was suggested to overwhelm the ESR and prevent the restoration of cellular homeostasis (Section 4.7.3 and 4.7.4, Fig. 4.18). In S288C, however, LF disrupted the stress response to AMB causing the inappropriate sensing of stress and/or dysregulation of stress-related pathways, which were repressed (Section 4.5.3.1, Fig. 4.15). This disruption appeared paradoxical and contrary to expectations but is similar to the mechanism of synergy between FLC+B-7b, where regulation of stress defences were down-regulated compared to FLC alone, which weakened the cell defence response to drugs and inhibited growth [321].

In the additive interaction between VRC+EDTA in 97/170, dysregulation of stress responses were also observed, but this was mediated via a disrupted activation of stress-related pathways. With VRC alone, oxidative and osmotic stress responses were induced, but these became absent with the addition of EDTA. Interestingly, *SSK1*, an upstream activator and regulator of stress responses in the HOG signalling pathway was up-regulated by VRC+EDTA. However, *Ssk1* target genes were not differentially expressed, suggesting that EDTA caused an incomplete activation of the HOG pathway and impaired the appropriate cellular response to stress (Section 4.9.2). Impairment of stress signalling pathways was also observed in the synergy induced by NaCl+H₂O₂, where target genes of *Cap1* and *Hog1*, which are activated in response to cationic and oxidative stresses, respectively, were not differentially expressed by the combined treatment, resulting in cell death via ROS accumulation [479].

Stress adaptation responses are crucial for survival and are ideal sources of antifungal targets. Examples include calcineurin and the heat shock protein Hsp90, which are inhibited by the drugs FK506 and geldanamycin, respectively. Interestingly, while these drugs inhibit fungi on their own they also induce synergy with some antifungal drugs [170, 549, 550]. In this thesis, the different

alterations of stress responses observed in synergistic and additive antifungal-chelator combinations suggest different avenues for targeting fungal stress responses as an antifungal strategy that warrant further investigation.

5.3. The potential of metal homeostasis as an antifungal target

Although the regulation of copper, iron and zinc in response to AMB and AMB+LF treatments differed in *S. cerevisiae* and *C. neoformans* (Section 4.6.3), disruption of metal ion homeostasis by knocking out controlling transcription factors increased the susceptibility to AMB in both fungal species. For Zap1, Aft1, Rim101 and Sre1, antifungal susceptibility extended to FLC, suggesting metal homeostasis could be targeted as an antifungal strategy (Fig. 4.13 and Table 4.10).

Metal ions have important functions in biological systems as they take part in many catalytic, homeostatic and signalling roles. While important for cellular functions, metal ions are tightly regulated as they can also cause the production of ROS and mediate apoptosis [93]. Additionally, the dysregulation of the homeostasis of one metal often affects the regulation of another; for example high zinc levels decrease the intracellular content of iron [551] and elevated concentrations of cytosolic calcium cause zinc release from storage organelles [552]. Due to its importance, metal homeostasis has been explored as a potential source of antifungal targets [553-555]. Furthermore, disruption of metal homeostasis has been suggested as an inhibitory mechanism for existing antifungal drugs and bioactive compounds, including amiodorane, an anti-arrhythmic drug that causes the hyper-accumulation of cytosolic calcium and has a broad spectrum of antifungal activity, and zinc pyrithione, which inhibits the scalp fungus *Malassezia globosa* [517, 556].

In *S. cerevisiae*, disrupting iron homeostasis by deleting *AFT1*, which is the dominant iron-controlling transcription factor, rendered the cell susceptible to a range of oxidative, nitrosative, cell wall and membrane stressors (Fig. 4.13). Similarly, disrupting zinc homeostasis by deleting *ZAP1* increased susceptibility to most of the tested stressors (Fig. 4.13), suggesting that the regulation of iron and zinc are required for various cellular functions and processes including stress response and maintenance of the cell wall and membrane.

To narrow down potential drug targets involved in metal homeostasis, knock-out mutants of known upstream regulators of Aft1 and Zap1 and their downstream gene targets were investigated for increased susceptibility to antifungal drugs. However, knock-out mutants of the kinase Tpk2 and the transcription factor Yap5, which control Aft1 activity and Aft1 localisation to the nucleus, respectively, did not result in altered susceptibility to AMB compared to wild type cells (Fig. 4.13). For zinc homeostasis, a knock-out mutant of *Izh2*, which influences Zap1 activity, was previously

shown to have decreased susceptibility to AMB [447, 451]. Knock-out mutants of *YOR387C* and *VEL1*, which are downstream targets of both Aft1 and Zap1, also had no change in susceptibility to AMB compared to the wild type strain (Fig. 4.13). Mutants of two other Aft1 and Zap1 targets, *MET32* and *MTD1*, which are regulated by both Aft1 and Zap1 and encode proteins with 'druggable' domains, did not exhibit increased susceptibility to AMB or FLC (Fig. 4.14). From this it appeared that only targeting the transcription factors that directly regulate iron and zinc homeostasis, i.e. Aft1 and Zap1, would augment antifungal activity in *S. cerevisiae*.

Similarly in *Cryptococcus*, knock-out mutants of metal-controlling transcription factors generated by Kim *et al.* (2015), including *cir1Δ*, *nrg1Δ*, *rim101Δ*, *zap104Δ* and *cuf1Δ*, showed increased susceptibility to AMB ([353]; Table 4.10), which suggested that iron-, zinc- and copper-regulating transcription factors might be potential antifungal targets. In contrast to *S. cerevisiae*, however, disruption of the cryptococcal iron uptake proteins Cfo1 and Cft1 has been observed to increase susceptibility to AMB and FLC [94, 116, 557], suggesting these may also be potential antifungal targets. In *Cryptococcus*, zinc uptake genes under the control of transcription factors Zap103 and Zap104 have been identified [558] but have not been tested as potential antifungal targets. It would be interesting to test whether these, like Cfo1 and Cft1, increase susceptibility to AMB and FLC.

5.4. Potential of Zap1 and Zap104 transcription factors as antifungal drug targets

Transcription factors have been suggested as antifungal drug targets as their disruption can render mutants avirulent in infection models, dysregulate cellular stress responses and increase antifungal drug susceptibility [353]. One transcription factor from the analysis of AMB+LF synergy in S288C and H99 that emerged as a potential, broad-spectrum antifungal target was Zap1. While Aft1 was also a potential target, it is only conserved in the pathogen *C. glabrata* [92]. In contrast, Zap1 is widely conserved and orthologues in *Cryptococcus* and *Aspergillus* have been identified [353, 555], with an increase in AMB susceptibility of the *C. neoformans* Zap104 knock-out mutant already reported [353].

One difference observed following Zap1 and Zap104 deletion was that *zap1Δ* (in *S. cerevisiae*) had a sickly phenotype and was susceptible to many stressors (Fig. 4.13), whereas *zap104Δ* (in *Cryptococcus*) grew robustly and was only susceptible to AMB (Table 4.10). *C. neoformans* has a paralogue of Zap104 named Zap103, however deletion of *ZAP103* does not confer susceptibility to antifungal drugs [353]. This suggests that the different phenotypes observed between *zap1Δ* and *zap104Δ* are not due to functional redundancy and rewiring of Zap103/Zap104-controlling pathways in *C. neoformans*, and points to a difference in functions governed by Zap1 in *S. cerevisiae* and

Zap104 in *C. neoformans*. Despite potentially different functions, both Zap1 and Zap104 contain a C₂H₂ zinc finger domain that is druggable [459] and can be inhibited by small molecules that are designed or modified to bind to it. However, Zap1 is also conserved in humans and drugs targeting fungal Zap1 could inadvertently cause toxicity in humans. Further study of the structural similarities between yeast and human Zap1 is required to determine if there are drug binding sites that are either specific to fungal Zap1 or will not affect the function of the human orthologue.

5.5. Iron chelators as therapeutic agents for antifungal treatment

In Chapter 3, the search for iron chelators that synergised with antifungal drugs found that only LF potentiated AMB activity (Fig. 3.3). Unlike the general metal chelator EDTA, or the clinically approved iron chelators DFO, DFP, DSX and CPO, LF is a natural and multifunctional glycoprotein that increases in concentration during host infection and inflammation. The activities of LF, its peptides and derivatives have been investigated in various fields of research, as has their therapeutic potential as adjuvants in chemotherapies and treatments of severe and chronic infections such as sepsis and hepatitis C infection [559-561].

Interestingly, besides the prophylactic use of LF to prevent invasive fungal infections in neonates [562], there are no studies that have investigated its use as a therapeutic agent for invasive fungal diseases. This contrasts with DSX which is employed in last resort adjuvant therapies against mucormycoses [57, 154]. Although the aim of this thesis was to understand the molecular basis of synergy to discover alternative antifungal strategies, the therapeutic potential of LF in treating invasive fungal diseases is worth exploring as LF appears to have broad-spectrum synergistic activity against fungal pathogens when combined with AMB. To date, AMB+LF has been tested and reported to produce synergy in *Cryptococcus*, *Saccharomyces*, *Candida* and *Aspergillus* [9, 10, 72]. Further work is required to determine the spectrum of synergistic activity in a wider range of pathogenic fungi, and to test whether interactions other than synergy can occur.

Published studies on the effects of iron chelators on fungi are limited, and most are pilot studies that have used a small number of fungal strains (see Table 3.1). It is possible that chelators possess additional properties that cause unknown outcomes in fungi, especially when combined with antifungal drugs, which can be complicated by species-specific responses. Caution should therefore be observed when using iron chelating agents during antifungal therapy.

5.6. Diversity of fungal responses to drug treatment and implications for studying drug responses in model organisms

Although the combination of AMB+LF was synergistic in both S288C and H99, their different transcriptional responses demonstrate that diverse responses can be elicited by the same drug combination (Fig. 4.15 and 4.18). This may be due to the physiological differences between *Saccharomyces* and *Cryptococcus*, which may in turn be influenced by the transcription factors present in their genomes.

S. cerevisiae and *C. neoformans* belong to different phyla where the former is ascomycete and the latter is a basidiomycete. Analysis of transcription factors in sequenced genomes of ascomycetes and basidiomycetes found different classes dominated in the two phyla, with Zn₂Cys₆ regulators more abundant in ascomycetes, and C₂H₂ dominating in basidiomycetes. Basidiomycetes also had fewer transcription factors for which an ascomycete orthologue could be found, compared to the number of ascomycete transcription factors that had orthologues in basidiomycetes. This suggests that some components of the regulatory systems in the two phyla evolved after their divergence [563]. Additionally, orthologous transcription factors between the phyla may not always have conserved functions; for example Nrg1 plays an important role in filamentation in *Saccharomyces* but does not in *Cryptococcus*, where it mediates pathogenesis, capsule formation and stress responses [110].

Fungal species are also known to exhibit different susceptibility to different types of stresses, such as oxidative, osmotic and cell wall stress. A comparative bioinformatic analysis of regulatory proteins involved in stress-related pathways across the genomes of fungi from different environmental niches, including *Cryptococcus* and *Saccharomyces*, showed that the upstream sensory proteins and downstream transcription factors in stress signalling pathways were generally less evolutionarily conserved compared to those that were central to a pathway. This study also found a correlation between susceptibility to stressors and environmental niche. For example, *Debaryomyces hansenii* is isolated from saline environments and was resistant to NaCl, and the human pathogens *A. fumigatus*, *C. albicans* and *C. glabrata* were highly resistant to oxidative stress compared to plant pathogens *Magnaporthe grisea*, *Fusarium graminearum*, *Ashbya gossypii* and *Ustilago maydis*, which may have evolved to survive encounters with phagocytes and phagocytic microbes like amoeba that kill cells using oxidative bursts. This suggests that up- and downstream transcriptional regulators in stress signalling pathways are diverse to enable fungi to adapt to their different environmental niches [564].

While the specific niche of *S. cerevisiae* is unknown, it is mostly found in controlled or stable environments with limited exposure to stresses and it has a long history of domestication in the production of fermented foods and beverages [565]. In addition, as a laboratory strain used for biochemical studies, S288C was developed to have minimal nutritional requirements [337]. Furthermore, although it can grow at 37 °C *S. cerevisiae* cannot naturally infect mammals except in cases of extreme immunocompromise. In contrast, *C. neoformans* is a cosmopolitan yeast that has to adapt to a range of stresses including changes in temperature and nutrient availability. Pathogenic strains such as H99 are exposed to harsh stresses including elevated temperature, oxidative stress and nutrient limitation. These different environmental pressures influence how *Saccharomyces* and *Cryptococcus* have evolved to respond to stress, which may explain their divergent responses to AMB+LF synergy (Fig. 4.15 and 4.18).

S. cerevisiae is a widely used model organism as its genome is well annotated and many of its genes and pathways are highly conserved [332]. However, the different transcriptomic response seen for S288C and H99 under AMB and AMB+LF treatment suggest that *S. cerevisiae* may not be a good platform for modelling drug responses in *Cryptococcus* as initially intended. It may, however, still be suitable for modelling and understanding fungal responses in ascomycete pathogens such as *Candida* and *Aspergillus*.

5.7. Implications of drug antagonism for antifungal therapy

Up-regulation of drug efflux pumps as a mechanism of drug antagonism is unusual compared to the inhibition of metabolic and homeostatic functions that have been found to be associated with many other antagonistic drug combinations. In fungi, azoles are thought to be antagonistic with polyenes as they both target ergosterol but in ways that reduces the efficacy of the other, i.e. azoles inhibit the biosynthesis of ergosterol which is required for polyenes to bind to in order to exert their fungicidal activity. In other drug combinations, antagonism can occur by the competitive binding of drugs to the same target, which inhibits the effects of one of the agents [320]. Drugs that impede cellular metabolism, such as bromopyruvate which inhibits glycolysis, have also been found to act as antagonists and prevent the optimal activity of a second drug [320]. Additionally, drugs can interact directly with each other and cause a reduction in their efficacies, such as the antileishmania drug miltefosine, which binds to AMB and decreases the uptake of both drugs into the cell [566].

An aspect of drug efflux as a mode of antagonism is its role in drug resistance, as combination therapies are often employed to reduce the rate of development of drug resistance. In fitness trade-off studies in bacteria, synergistic drug pairs are thought to inhibit drug-resistant strains by

exploiting the fitness costs associated with drug resistance and associated changes in cellular functions, resulting in metabolic burden. For example, resistance to aminoglycosides is mediated by decreased proton motive force activity, which is required for aminoglycoside uptake and the activities of drug efflux pumps. However, this change in function reduces cellular fitness in aminoglycoside-resistant bacteria when exposed to other antibiotics that require active efflux pumps to expel drugs from the cell [567]. In fungi, acquired resistance to drug pairs such as FLC combined with the Hsp90 inhibitor GdA, and FLC with the calcineurin inhibitor FK506, were also resistant to FLC alone but imposed a fitness costs in the absence of both drugs or when exposed to different types of stresses. These experiments implied that the cost of resistance that developed to the drug combination during therapy would reduce the population of drug-resistant pathogens in the host once drug selection was removed [568].

However, fitness trade-offs associated with increased drug efflux transport in response to VRC+EDTA are not obvious in H99, as resistance to VRC+EDTA was not induced in this strain and it grew better with no inhibition in the absence of both agents (Fig. 4.19b). Additionally, in the absence of antifungal selection, induced expression of drug efflux transporters is commonly observed in human infections and has been shown to contribute to fungal virulence in mice [542, 569]. This questions whether a fitness cost is involved with efflux transporters as a mechanism of resistance to drug combinations and as a mechanism of antagonism. In contrast, inhibition of drug efflux has an obvious effect on fitness cost and is considered a potential antifungal strategy [523]. It has also been proposed to be a mechanism of synergy in FLC resistant *Candida* strains, where FLC combined with thyme oil extracts thymol and carvacrol caused a decrease in efflux pump activity compared to FLC treatment alone [570].

Overall, drug antagonism via induction of efflux pumps has significant implications for combination therapies. A better understanding of what drugs and agents can induce the expression of efflux pumps and how this occurs is needed in order to consider what drugs and other agents can be co-administered and which combinations should be avoided.

5.8. Conclusions

In summary, the major findings of this study are that antifungal-iron chelator combinations exhibit a diverse range of interactions in *Cryptococcus* species, where synergy was observed with AMB+LF and antagonism was seen between azoles and EDTA, DFP and DSX. Iron rescue assays with AMB+LF showed that synergy is not due to iron chelation and that additional properties of LF enhanced the activity of AMB.

Transcriptomic analysis of AMB+LF synergy in *S. cerevisiae* S288C and *C. neoformans* H99 showed that LF caused complex changes in the transcriptomic response to AMB, which differed between S288C and H99. As S288C was included to guide the understanding and validation of AMB+LF synergy in H99 and find potential antifungal targets, the different transcriptome responses to AMB+LF highlighted issues with using S288C to model drug responses for distantly related organisms. Nevertheless, metal regulation was found to be important in AMB+LF synergy as knock-out mutants of iron- and zinc-controlling transcription factors in both yeasts showed similar susceptibilities to AMB

The comparative analysis of how VRC+EDTA is antagonistic in *C. neoformans* H99 but additive in *C. gattii* 97/170 revealed an unexpected but simple mechanism of antagonism, which involved the up-regulation of drug efflux transporters. Although VRC+EDTA caused similar disruptions to mitochondrial function in both *Cryptococcus* species, the different outcomes to VRC+EDTA, with antagonism in *C. neoformans* and additivity in *C. gattii*, highlighted the complexity of species-specific responses to the same drug combination, which requires further analysis.

The analysis of AMB+LF synergy and VRC+EDTA additivity suggested that the dysregulation of metal ions by iron chelators enhances cell inhibition by disrupting stress-related responses and stress signalling pathways. Stress responses can be disrupted by overwhelming the stress adaptation response, or by dysregulating appropriate stress associated responses via inactivation or down-regulation of stress-associated pathways. Metal homeostasis and its importance for proper stress regulation provide multiple avenues for developing antifungal strategies. A potential antifungal target that disrupts stress responses and perpetuates synergy with antifungal drugs is the zinc controlling transcription factor Zap1, which is conserved across fungal species and contains domains that can be targeted by drugs.

APPENDICES

Chapter 3 Appendix

Appendix 3.1. MIC of antifungal drugs (A) and iron chelators (IC) alone and in combination ($\mu\text{g}/\text{mL}$), with fold changes (FC)

| | | | Iron chelating agent (IC) | | | | | | | | | | | | | | | | | | | |
|---|-----------------------|----------------|---------------------------------|-----------|---------------------------------|------|---------------------------------|-----------|---------------------------------|-------|---------------------------------|-----------|---------------------------------|-------|---------------------------------|-----------|---------------------------------|-------|---------------------------------|-----------|---------------------------------|------|
| | | | LACTOFERRIN | | | | EDTA | | | | DFP | | | | DSX | | | | CPO | | | |
| Species | Strain / Genotype | MIC of A | MIC of A in presence of IC (FC) | | MIC of IC in presence of A (FC) | | MIC of A in presence of IC (FC) | | MIC of IC in presence of A (FC) | | MIC of A in presence of IC (FC) | | MIC of IC in presence of A (FC) | | MIC of A in presence of IC (FC) | | MIC of IC in presence of A (FC) | | MIC of A in presence of IC (FC) | | MIC of IC in presence of A (FC) | |
| | | | IC | MIC of IC | FC | FICI | IC | MIC of IC | FC | FICI | IC | MIC of IC | FC | FICI | IC | MIC of IC | FC | FICI | IC | MIC of IC | FC | FICI |
| AMPHOTERICIN B | | | | | | | | | | | | | | | | | | | | | | |
| | | AMB MIC | | | | | | | | | | | | | | | | | | | | |
| <i>C. neoformans</i> var. <i>grubii</i> | KN99 α / VNI | 0.5 | 0.125 (- 4) | 64 | 4 (-16) | 0.31 | 0.125 (- 4) | 64 | 32 (-2) | 1 | 0.25 (- 2) | 8 | 8 (0) | 1 | 0.25 (- 2) | 2 | 2 (0) | 0.625 | 0.5 (0) | 1 | 1 | 0.84 |
| | H99 / VNI | 0.25 | 0.06 (- 4) | 64 | 2 (-32) | 0.28 | - | 64 | - | - | - | 16 | - | - | - | 4 | - | - | - | 2 | - | - |
| | WM148 / VNI | 0.5 | 0.125 (- 4) | 64 | 4 (-16) | 0.31 | - | 64 | - | - | - | 8 | - | - | - | 4 | - | - | - | 1 | - | - |
| | WM626 / VNII | 0.5 | 0.125 (- 4) | 64 | 2 (-32) | 0.31 | - | 64 | - | - | - | 8 | - | - | - | 8 | - | - | - | 1 | - | - |
| <i>C. neoformans</i> var. <i>neoformans</i> | WM629 / VNIV | 0.25 | 0.06 (- 4) | 64 | 2 (-32) | 0.28 | - | 128 | - | - | - | 4 | - | - | - | 4 | - | - | - | 1 | - | - |
| | JEC21 α / VNIV | 0.125 | 0.03 (- 4) | 64 | 2 (-32) | 0.31 | - | 64 | - | - | - | 8 | - | - | - | 2 | - | - | - | 0.5 | - | - |
| <i>C. gattii</i> | R265 / VGIIa | 0.5 | 0.125 (- 4) | 64 | 4 (-16) | 0.25 | 0.25 (- 2) | 128 | 32 (-4) | 0.75 | 0.25 (- 2) | 32 | 4 (-8) | 0.56 | 0.125 (- 4) | 4 | 4 (0) | 0.56 | 0.25 (- 2) | 2 | 0.25 (-8) | 0.78 |
| | R272 / VGIIb | 0.5 | 0.03 (-16) | 64 | 4 (-16) | 0.29 | 0.25 (- 2) | 128 | 32 (-4) | 0.75 | 0.25 (- 2) | 8 | 4 (-2) | 1 | 0.25 (- 2) | 2 | 4 (+2) | 0.75 | 0.25 (- 2) | 1 | 0.5 (-2) | 0.87 |
| | 97/170 / VGII | 0.5 | 0.125 (- 4) | 64 | 2 (-32) | 0.41 | 0.25 (- 2) | 128 | 32 (-4) | 1 | 0.25 (- 2) | 4 | 4 (0) | 1.75 | 0.25 (- 2) | 4 | 4 (0) | 0.81 | 0.25 (- 2) | 1 | 0.25 (-4) | 0.87 |
| <i>S. cerevisiae</i> | S288C | 0.125 | 0.03 (- 4) | 16 | 2 (-8) | 0.37 | 0.06 (- 2) | 16 | 4 (-4) | 0.625 | 0.125 (0) | 64 | 64 (0) | 2 | 0.06 (- 2) | 4 | 4 (0) | 1 | 0.06 (- 2) | 1 | 0.125(-8) | 0.75 |
| FLUCONAZOLE | | | | | | | | | | | | | | | | | | | | | | |
| | | FLC MIC | | | | | | | | | | | | | | | | | | | | |
| <i>C. neoformans</i> var. <i>grubii</i> | KN99 α / VNI | 0.25 | 0.25 (0) | 64 | 64 (0) | 2 | 0.25 (0) | 128 | 64 (-2) | 1.12 | 0.25 (0) | 8 | 4 (-2) | 1.625 | 0.25 (0) | 8 | 4 (-2) | 1.75 | 0.25 (0) | 2 | 2 (0) | 1.5 |
| | H99 / VNI | 1 | - | - | - | - | 1 (0) | 64 | 64 (0) | 2 | 4 (+ 4) | 4 | 1 (-4) | 3.25 | 4 (+ 4) | 2 | 0.5 (-4) | 3.25 | - | - | - | - |
| | WM148 / VNI | 4 | - | - | - | - | 16 (+ 4) | 64 | 8 (-8) | 4.125 | 16 (+ 4) | 8 | 2 (-4) | 4.19 | 16 (+ 4) | 8 | 1 (-8) | 4.31 | - | - | - | - |
| | WM626 / VNII | 4 | - | - | - | - | 8 (+ 2) | 64 | 8 (-8) | 2.125 | 16 (+ 4) | 8 | 4 (-2) | 4.19 | 16 (+ 4) | 4 | 1 (-4) | 4.25 | - | - | - | - |
| <i>C. neoformans</i> var. <i>neoformans</i> | WM629 / VNIV | 1 | - | - | - | - | 1 (0) | 64 | 4 (-16) | 0.84 | 2 (+ 2) | 4 | 1 (-4) | 2.25 | 1 (0) | 4 | 4 (0) | 2.125 | - | - | - | - |
| | JEC21 α / VNIV | 0.5 | - | - | - | - | 0.5 (0) | 64 | 16 (-4) | 1.125 | 0.5 (0) | 8 | 4 (-2) | 1.5 | 0.5 (0) | 2 | 1 (-2) | 1.75 | - | - | - | - |
| <i>C. gattii</i> | R265 / VGIIa | 2 | 1 (- 2) | 128 | 128 (0) | 1.5 | 2 (0) | 128 | 64 (-2) | 1.5 | 1 (- 2) | 32 | 16 (-2) | 1 | 2 (0) | 4 | 4 (0) | 2 | 1 (- 2) | 2 | 1 (-2) | 1 |
| | R272 / VGIIb | 2 | 2 (0) | 64 | 16 (-4) | 1.12 | 2 (0) | 128 | 128 (0) | 1.5 | 1 (- 2) | 8 | 4 (-2) | 1.25 | 2 (0) | 2 | 1 (-2) | 1 | 2 (0) | 1 | 0.5 (-2) | 1.25 |
| | 97/170 / VGII | 64 | 64 (0) | 128 | 128 (0) | 1 | 16 (- 4) | 128 | 64 (-2) | 0.75 | 32 (- 2) | 4 | 2 (-2) | 1.5 | 64 (0) | 4 | 2 (-2) | 2 | 64 (0) | 2 | 1 (-2) | 1.5 |
| <i>S. cerevisiae</i> | S288C | 4 | 2 (-2) | 16 | 8 (-2) | 1 | 2 (-2) | 16 | 16 (0) | 1.5 | 2 (-2) | 64 | 32 (-2) | 1.5 | 2 (-2) | 4 | 2 (-2) | 1 | 4 (0) | 1 | 0.5 (-2) | 1.5 |
| ITRACONAZOLE | | | | | | | | | | | | | | | | | | | | | | |
| | | ITR MIC | | | | | | | | | | | | | | | | | | | | |
| <i>C. neoformans</i> var. <i>grubii</i> | KN99 α / VNI | 0.015 | 0.007 (- 2) | 64 | 32 (-2) | 1 | 0.06 (+ 4) | 64 | 8 (-8) | 4.38 | 0.06 (+ 4) | 16 | 4 (-4) | 4.25 | 0.06 (+ 4) | 4 | 0.5 (-8) | 4.25 | 0.007 (- 2) | 2 | 1 (-2) | 1 |
| | H99 / VNI | 0.03 | - | - | - | - | 0.25 (+ 8) | 64 | 16 (-4) | 4.125 | 0.125 (+ 4) | 8 | 1 (-8) | 4.125 | 0.125 (+ 4) | 2 | 0.5 (-4) | 4.25 | - | - | - | - |
| | WM148 / VNI | 0.25 | - | - | - | - | 0.25 (0) | 64 | 8 (-8) | 1.08 | 0.25 (0) | 8 | 4 (-2) | 1.25 | 0.25 (0) | 4 | 1 (-4) | 1.5 | - | - | - | - |
| | WM626 / VNII | 0.125 | - | - | - | - | 0.5 (+ 4) | 64 | 8 (-8) | 4.06 | 0.25 (+ 2) | 8 | 4 (-2) | 2.81 | 0.25 (+ 2) | 4 | 2 (-2) | 2.25 | - | - | - | - |
| <i>C. neoformans</i> var. <i>neoformans</i> | WM629 / VNIV | 0.03 | - | - | - | - | 0.015 (- 2) | 128 | 32 (-4) | 0.75 | 0.03 (0) | 4 | 0.5 (-8) | 1.88 | 0.03 (0) | 4 | 2 (-2) | 1.81 | - | - | - | - |
| | JEC21 α / VNIV | 0.03 | - | - | - | - | 0.015 (- 2) | 64 | 16 (-4) | 0.64 | 0.015 (- 2) | 64 | 16 (-4) | 0.88 | 0.03 (0) | 4 | 1 (-4) | 0.81 | - | - | - | - |

| | | | | | | | | | | | | | | | | | | | | | | |
|--|---------------|----------------|------------|-----|---------|------|-------------|-----|---------|--------------|-------------|----|---------|--------------|------------|---|-----------|--------------|------------|-----|----------|-------|
| <i>C. gattii</i> | R265 / VGIIa | 0.125 | 0.06 (-2) | 128 | 32 (-4) | 0.75 | 0.06 (-2) | 128 | 32 (-4) | 0.625 | 0.06 (-2) | 32 | 8 (-4) | 0.625 | 0.06 (-2) | 2 | 1 (-2) | 1 | 0.06 (-2) | 2 | 1 (-2) | 1 |
| | R272 / VGIIb | 0.06 | 0.03 (-2) | 64 | 32 (-2) | 1 | 0.03 (-2) | 128 | 32 (-4) | 0.75 | 0.015 (-4) | 8 | 4 (-2) | 0.75 | 0.015 (-4) | 2 | 1 (-2) | 0.75 | 0.015 (-4) | 2 | 1 (-2) | 0.75 |
| | 97/170 / VGII | 0.5 | 0.5 (0) | 64 | 32 (-2) | 1.5 | 0.25 (-2) | 128 | 32 (-4) | 0.75 | 0.5 (0) | 4 | 4 (0) | 2 | 0.5 (0) | 2 | 1 (-2) | 1.5 | 0.5 (0) | 2 | 2 (0) | 2 |
| <i>S. cerevisiae</i> | S288C | 2 | 1 (-2) | 16 | 8 (-2) | 1 | 0.5 (-4) | 8 | 4 (-2) | 0.66 | 1 (-2) | 64 | 16 (-4) | 0.81 | 1 (-2) | 1 | 1 (0) | 1 | 1 (-2) | 1 | 0.5 (-2) | 0.88 |
| VORICONAZOLE | | VRC MIC | | | | | | | | | | | | | | | | | | | | |
| <i>C. neoformans</i> var. <i>grubii</i> | KN99α / VNI | 0.0035 | 0.0035 (0) | 64 | 32 (-2) | 1.56 | 0.015 (+4) | 64 | 16 (-4) | 4.5 | 0.015 (+4) | 16 | 2 (-8) | 4.25 | 0.015 (+4) | 4 | 0.5 (-8) | 4.25 | 0.0035 (0) | 2 | 2 (0) | 2 |
| | H99 / VNI | 0.007 | - | - | - | - | 0.03 (+4) | 64 | 8 (-8) | 4.125 | 0.03 (+4) | 8 | 1 (-8) | 4.25 | 0.03 (+4) | 4 | 1 (-4) | 4.25 | - | - | - | - |
| | WM148 / VNI | 0.03 | - | - | - | - | 0.125 (+4) | 64 | 8 (-8) | 4.125 | 0.125 (+4) | 8 | 2 (-4) | 4.25 | 0.125 (+4) | 8 | 2 (-4) | 4.19 | - | - | - | - |
| | WM626 / VNII | 0.03 | - | - | - | - | 0.125 (+4) | 32 | 8 (-4) | 4.16 | 0.125 (+4) | 16 | 2 (-8) | 4.125 | 0.125 (+4) | 4 | 1 (-4) | 4.125 | - | - | - | - |
| <i>C. neoformans</i> var. <i>neoformans</i> | WM629 / VNIV | 0.015 | - | - | - | - | 0.015 (0) | 128 | 16 (-8) | 1 | 0.03 (+2) | 8 | 4 (-2) | 2.63 | 0.015 (0) | 2 | 1 (-2) | 1.63 | - | - | - | - |
| | JEC21α / VNIV | 0.007 | - | - | - | - | 0.0035 (-2) | 128 | 16 (-8) | 0.69 | 0.0035 (-2) | 4 | 2 (-2) | 0.84 | 0.007 (0) | 2 | 1 (-2) | 1.5 | - | - | - | - |
| <i>C. gattii</i> | R265 / VGIIa | 0.06 | 0.03 (-2) | 128 | 64 (-2) | 1.5 | 0.015 (-4) | 128 | 64 (-2) | 0.65 | 0.03 (-2) | 32 | 16 (-2) | 1.25 | 0.06 (0) | 4 | 2 (-2) | 1.25 | 0.06 (0) | 2 | 2 (0) | 2 |
| | R272 / VGIIb | 0.06 | 0.06 (0) | 64 | 64 (0) | 2 | 0.015 (-4) | 128 | 64 (-2) | 0.75 | 0.03 (-2) | 8 | 4 (-2) | 1 | 0.06 (0) | 2 | 1 (-2) | 1.25 | 0.06 (0) | 1 | 1 (0) | 2 |
| | 97/170 / VGII | 0.5 | 0.5 (0) | 64 | 64 (0) | 1.5 | 0.03 (-16) | 128 | 64 (-2) | 0.56 | 0.5 (0) | 4 | 1 (-4) | 1.57 | 0.25 (-2) | 1 | 1 (0) | 1.5 | 0.5 (0) | 2 | 2 (0) | 2 |
| <i>S. cerevisiae</i> | S288C | 0.125 | 0.125 (0) | 16 | 16 (0) | 2 | 0.06 (-2) | 16 | 8 (-2) | 1 | 0.06 (-2) | 64 | 64 (0) | 1.5 | 0.06 (-2) | 2 | 1 (-2) | 1 | 0.125 (0) | 0.5 | 0.5 (0) | 2 |
| CASPOFUNGIN | | CAS MIC | | | | | | | | | | | | | | | | | | | | |
| <i>C. neoformans</i> var. <i>grubii</i> | KN99α / VNI | 2 | 1 (-2) | 64 | 64 (0) | 1.5 | 2 (0) | 64 | 64 (0) | 2 | 1 (-2) | 16 | 4 (-4) | 0.64 | 1 (-2) | 8 | 0.5 (-16) | 0.59 | 2 (0) | 2 | 2 (0) | 2 |
| | R265 / VGIIa | 4 | 2 (-2) | 64 | 64 (0) | 1.37 | 1 (-4) | 128 | 64 (-2) | 0.68 | 2 (-2) | 32 | 2 (-16) | 0.53 | 2 (-2) | 4 | 0.5 (-8) | 0.625 | 4 (0) | 2 | 2 (0) | 2 |
| <i>C. gattii</i> | R272 / VGIIb | 2 | 1 (-2) | 128 | 64 (-2) | 1.27 | 0.5 (-4) | 128 | 64 (-2) | 0.75 | 1 (-2) | 32 | 32 (0) | 0.87 | 1 (-2) | 2 | 1 (-2) | 1 | 2 (0) | 1 | 1 (0) | 2 |
| | 97/170 / VGII | 4 | 4 (0) | 64 | 64 (0) | 2 | 2 (-2) | 128 | 64 (-2) | 0.87 | 2 (-2) | 8 | 2 (-4) | 0.75 | 2 (-2) | 2 | 0.5 (-4) | 0.65 | 4 (0) | 1 | 1 (0) | 2 |
| <i>S. cerevisiae</i> | S288C | 0.06 | 0.03 (-2) | 16 | 4 (-4) | 0.63 | 0.03 (-2) | 8 | 8 (0) | 1.75 | 0.06 (0) | 64 | 64 (0) | 1.5 | 0.06 (0) | 4 | 2 (-2) | 1.5 | 0.06 (0) | 1 | 0.5 (-2) | 1.125 |

- = Not done.

Bold denotes significant synergy (≤ 0.5) or antagonism (> 4).

Green = decreased requirement for A in presence of IC; yellow = increased requirement for A in presence of IC.

Chapter 4 Appendix

Appendix 4.1. *S. cerevisiae* S288C, *C. neoformans* H99 and *C. gattii* 97/170 RNA samples

| Experiment | Organism | Labelling | Sample name | Illumina Lane |
|---------------------|----------|-----------|-------------|---------------|
| AMB+LF Synergy | S288C | 1B | CAL | L1 |
| | S288C | 2F | AMB+LF | L1 |
| | S288C | 2I | AMB | L1 |
| | S288C | 3F | CA | L1 |
| | S288C | 3G | CAL | L1 |
| | S288C | 4E | AMB | L1 |
| | S288C | 4I | CAL | L1 |
| | S288C | 5C | AMB+LF | L2 |
| | S288C | 5G | CA | L2 |
| | S288C | 8A | CA | L2 |
| | S288C | 9D | AMB+LF | L2 |
| | S288C | 9E | AMB | L2 |
| | H99 | 1C | AMB | L1 |
| | H99 | 2G | AMB+LF | L1 |
| | H99 | 2K | CA | L1 |
| | H99 | 3D | CAL | L1 |
| | H99 | 4A | AMB | L1 |
| | H99 | 5A | AMB+LF | L1 |
| | H99 | 5F | AMB | L2 |
| | H99 | 5L | CA | L2 |
| H99 | 6F | CAL | L2 | |
| H99 | 7B | CAL | L2 | |
| H99 | 8G | CA | L2 | |
| H99 | 8H | AMB+LF | L2 | |
| LF only* | S288C | 10B | LF | - |
| | S288C | 10D | LF | - |
| | S288C | 10F | LF | - |
| | S288C | 10G | CLF | - |
| | S288C | 10H | CLF | - |
| | S288C | 10I | CLF | - |
| VRC+EDTA Antagonism | H99 | 1H | VRC | L1 |
| | H99 | 2J | VRC+EDTA | L1 |
| | H99 | 3E | C | L1 |
| | H99 | 4F | VRC+EDTA | L1 |
| | H99 | 5E | VRC+EDTA | L2 |
| | H99 | 5I | C | L2 |
| | H99 | 6G | C | L2 |
| | H99 | 7J | VRC | L2 |
| | H99 | 8B | VRC | L2 |
| | 97/170 | 1I | C | L1 |
| | 97/170 | 2B | VRC | L1 |
| | 97/170 | 3J | VRC+EDTA | L1 |
| | 97/170 | 4C | VRC | L1 |
| | 97/170 | 5J | VRC+EDTA | L2 |
| | 97/170 | 6E | VRC+EDTA | L2 |
| | 97/170 | 7D | C | L2 |
| | 97/170 | 8K | C | L2 |
| | 97/170 | 9F | VRC | L2 |

*LF only samples were sequenced using Next-Seq.

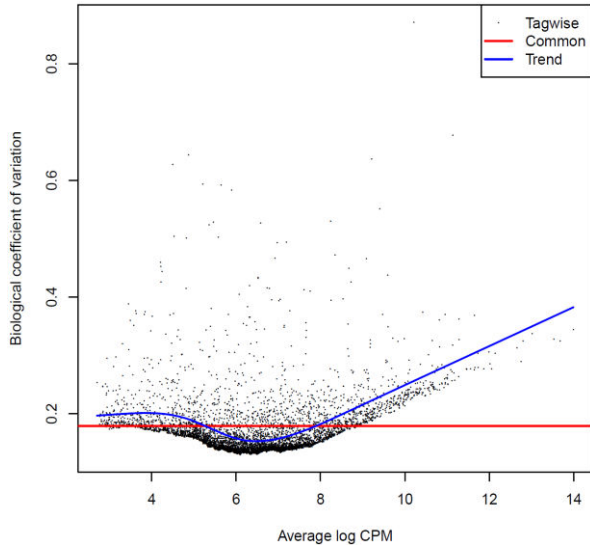
CA = corresponding control for AMB treatment. CAL = corresponding control for AMB+LF treatment. CLF = corresponding control for LF treatment. C = corresponding control for VRC and VRC+EDTA treatments,

Appendix 4.2. List of primers designed in this study that were used to construct and confirm knock-out mutants in *S. cerevisiae* S288C

| Primer type | 5' – 3' sequence |
|----------------------------------|--|
| KanB | CTGCAGCGAGGAGCCGTAAT |
| KanC | TGATTTTGATGACGAGCGTAAT |
| NatB* | ATTCGTCGTCGATTTCGTC |
| NatC* | TACATGAGCATGCCCTGC |
| <i>aft1</i> _A | AGCAGAAACAGAATTCGCATATTAC |
| <i>aft1</i> _B | CTTATCTTCAAAGTTGGGTAAGTGGG |
| <i>aft1</i> _D | CAAAATTAATGACAGAGGGAGAGAA |
| <i>atg1</i> _A | AAGTTAAGTACCAAGGCCATCTTTT |
| <i>atg1</i> _B | TAAAATGGGTAAGTTGTAGATCCCA |
| <i>atg1</i> _D | TATAGCCAAAGGCAAGTACTAAACG |
| <i>cch1</i> _A | AGAAAATGTAATTTGGCATGTCATT |
| <i>cch1</i> _B | GCTATAACTACTGAAGCTACGCCTG |
| <i>cch1</i> _D | AATCCCTTCTAATGGGTAAGTCTTG |
| <i>grx4</i> _A | CCAAAATTGAAGTTGTTTGGAAATAC |
| <i>grx4</i> _B | CATCTATTGATAAAAACCGGACATC |
| <i>grx4</i> _C | ATATGAAAGAAATGTGATGATGGCT |
| <i>met32</i> _A | CGCTTAGTACGCCACAGTTTATATT |
| <i>met32</i> _B | GCGTTTTCTTTTTAACCTTTATGT |
| <i>met32</i> _D | CCAAGAACTTGAGTATTTGACAGGT |
| <i>mtd1</i> _A | TATCTTTTTCTAGTCCAAGTCCTG |
| <i>mtd1</i> _B | CTATGCATTTCTCCACATACAGTCT |
| <i>mtd1</i> _D | GATATCATGGGTGATAAATGGGTA |
| <i>tpk2</i> _A | TACAATTCTGGCCTTCTTACCTAAA |
| <i>tpk2</i> _B | TTGCTACAGGATTAGGAAATCTTTG |
| <i>tpk2</i> _D | TAATTTTTGCACTGAGATCATGAGA |
| <i>yap5</i> _A | GTATTTTAGTTTACCTATTGGGCCG |
| <i>yap5</i> _B | ATCTGTTCCAGTTCTTTACAAACG |
| <i>yap5</i> _D | TATAGGCATAGTAAGCGGTACCTTG |
| <i>yct1</i> _A | CAATAGTGTTTGAAGTTCTTCCATT |
| <i>yct1</i> _B | GTGAATATTTTCCATAACGAAATGC |
| <i>yct1</i> _D | AGGCTAGAGGGTTACTAGTCTCTG |
| <i>yor387c</i> _A* | TTCGGATCTTTCCTAAACGG |
| <i>yor387c</i> _C* | ACTCTTGGGCAGACACCG |
| <i>yor387c</i> _D* | TGACAAGAAAACCATCTGCG |
| <i>vel1</i> _A | AAGGTAGTAATTTTCATGCATTCTCG |
| <i>vel1</i> _C | ATCTTACCACCAATATCAACACTT |
| <i>vel1</i> _D | TTACTTTTATCTTGTAGGCAAACCG |
| <i>zap1</i> _A | CTGCGATTTACTCTAGGGATCTTC |
| <i>zap1</i> _B | CTCAGATATGTCTTTCTTTGTCGGT |
| <i>zap1</i> _D | CTTCGGTTACCTAGTTGCACTCAT |
| <i>yor387c</i> _S1* [#] | TTCTGATAGATTGTACAATCTCAAGAAATCAAGAACAACAACCATACCATGcgtacgctgcaggctcgac |
| <i>yor387c</i> _S2* [#] | TAAAAAATACTTAAATATGTCTACAGATTATGCAGCTGGAAAAATCAatcgatgaattcgagctcg |

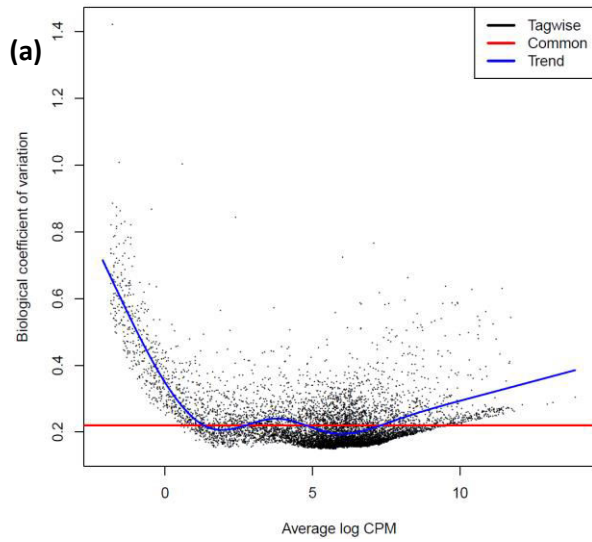
*Primers for other genes analysed in this study were obtained from the Yeast Deletion Project [341]. [#]Sequences from the plasmid cassette are in lower case.

Appendix 4.3. BCV of LF only transcripts.

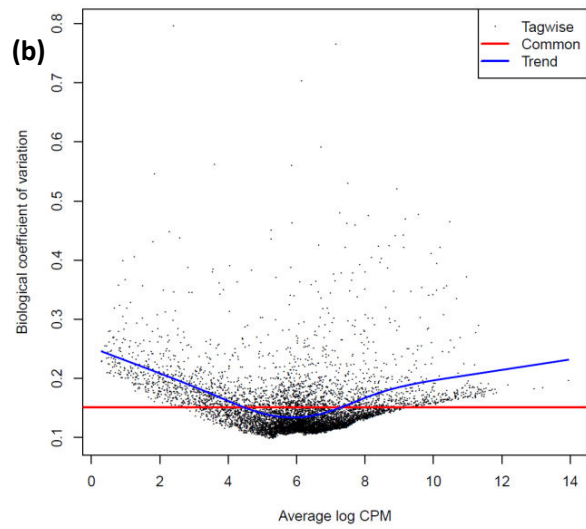


BCV = 0.1869.

Appendix 4.4. BCV of *C. neoformans* H99 transcripts in AMB+LF synergy.

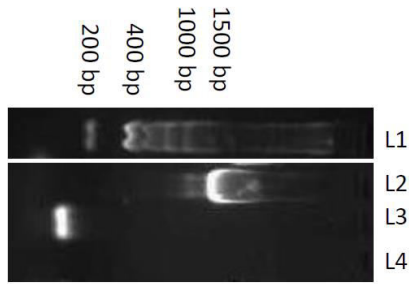


BCV = 0.2179 before sample 5A deletion



BCV = 0.1511 after 5A deletion

Appendix 4.5. Plasmid cassette construct for *YOR387C* deletion



L1: 1 Kb ladder (Bioline). L2: *yor387c_S1* and *yor387c_S2* primers stitched to pFA6a-natNT2 plasmid cassette using LongAmp® *Taq* 2 X master mix. Expected band size is 1460 bp. L3: Negative control (no DNA template). L4: Blue juice loading dye.

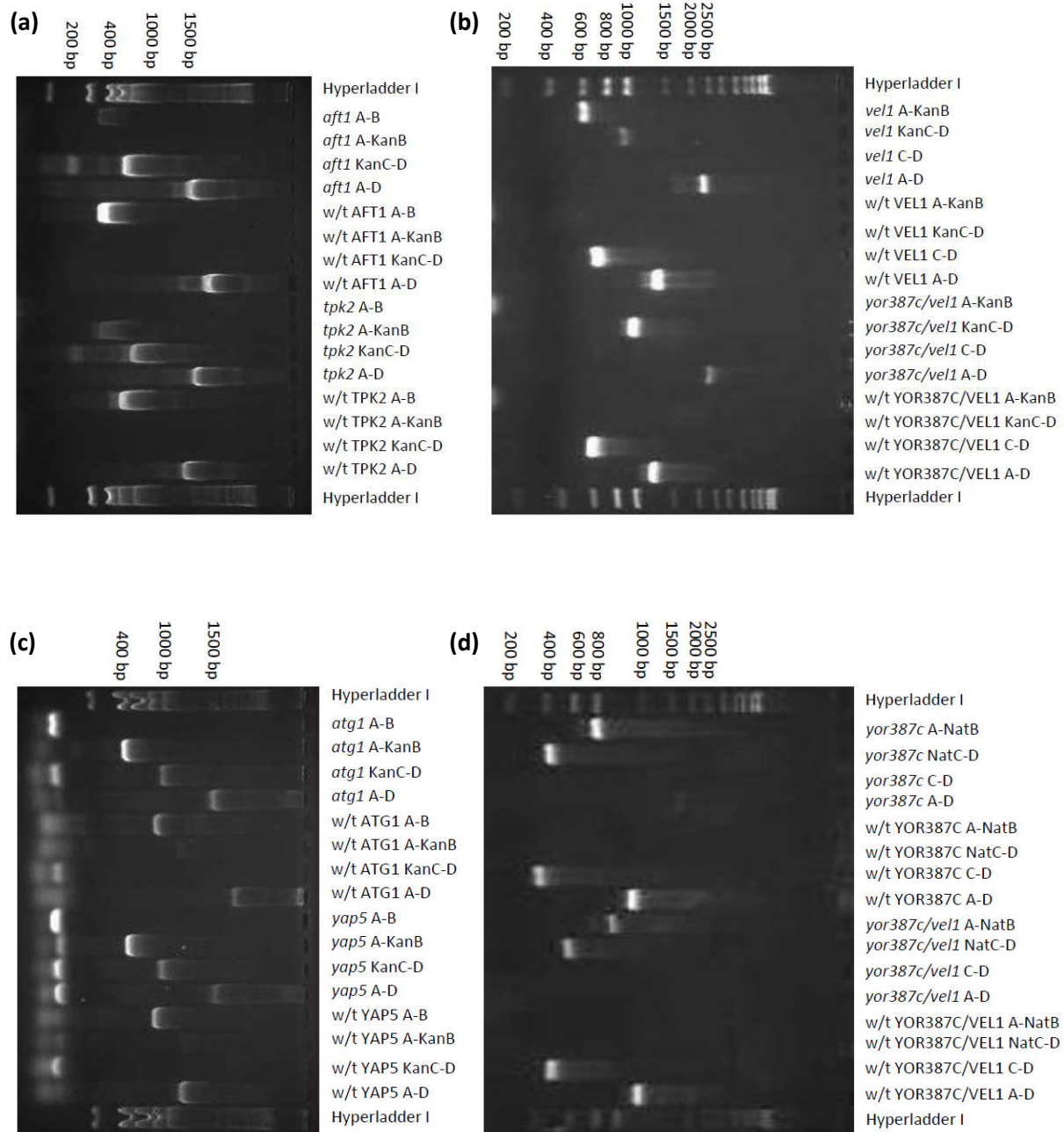
Appendix 4.6. Expected amplification band sizes (base pairs) of gene knock-out confirmation primer sets in *S. cerevisiae* BY4741

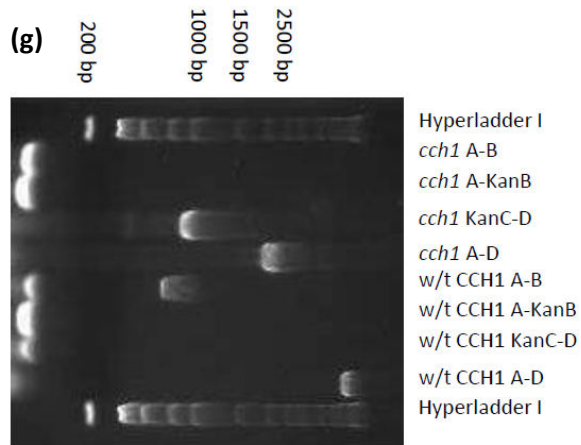
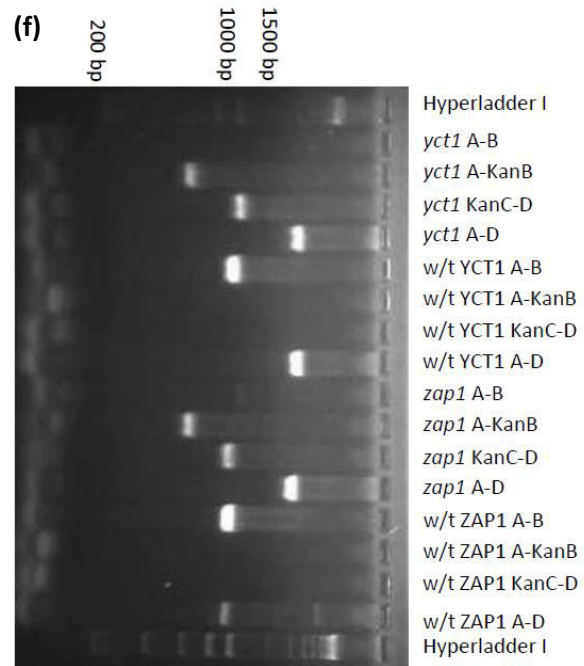
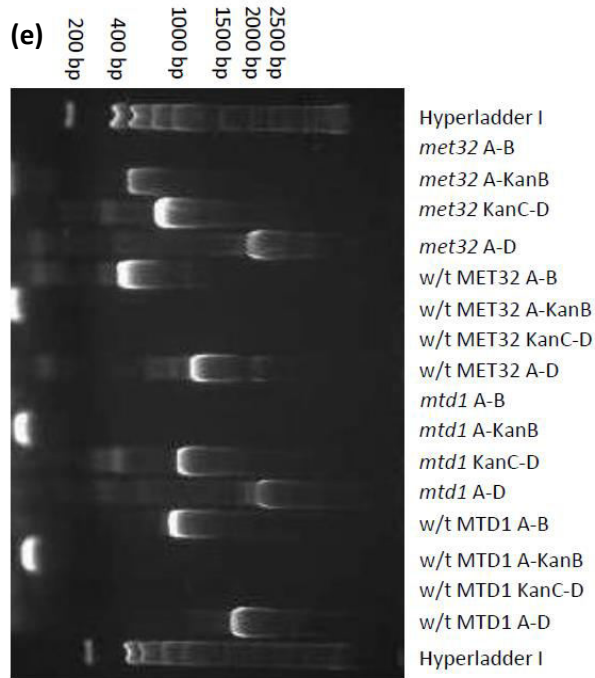
| Gene ID | Mutant | Primer combinations | | | | | |
|-----------------|-----------------|---------------------|--------|-----|--------|-----------------------|-----------------------|
| | | A-B | A-KanB | C-D | C-KanD | A-D K.O. ^a | A-D W.T. ^b |
| <i>YGL071W</i> | <i>aft1Δ</i> | 689 | 658 | ND | 985 | 2031 | 2790 |
| <i>YGL180W</i> | <i>atg1Δ</i> | 865 | 546 | ND | 946 | 2150 | 3260 |
| <i>YGR217W</i> | <i>cch1Δ</i> | 702 | 551 | ND | 936 | 2148 | 6681 |
| <i>YDR253C</i> | <i>met32Δ</i> | 557 | 638 | ND | 870 | 2166 | 1158 |
| <i>YKR080W</i> | <i>mtd1Δ</i> | 882 | 640 | ND | 1015 | 2313 | 1692 |
| <i>YPL203W</i> | <i>tpk2Δ</i> | 875 | 655 | ND | 1021 | 2344 | 1903 |
| <i>YIR018W</i> | <i>yap5Δ</i> | 834 | 551 | ND | 910 | 2119 | 1273 |
| <i>YLL55W</i> | <i>yct1Δ</i> | 936 | 576 | ND | 988 | 2222 | 2234 |
| <i>YOR387C*</i> | <i>yor387cΔ</i> | ND | 1010 | 499 | 632 | 1989 | 1260 |
| <i>YGL258W</i> | <i>vel1Δ</i> | ND | 616 | 624 | 928 | 2202 | 1239 |
| <i>YJL056C</i> | <i>zap1Δ</i> | 945 | 560 | ND | 886 | 2104 | 3163 |

^aknock-out. ^b wild type. *ORF replaced with CloNAT resistance marker.

ND = not done.

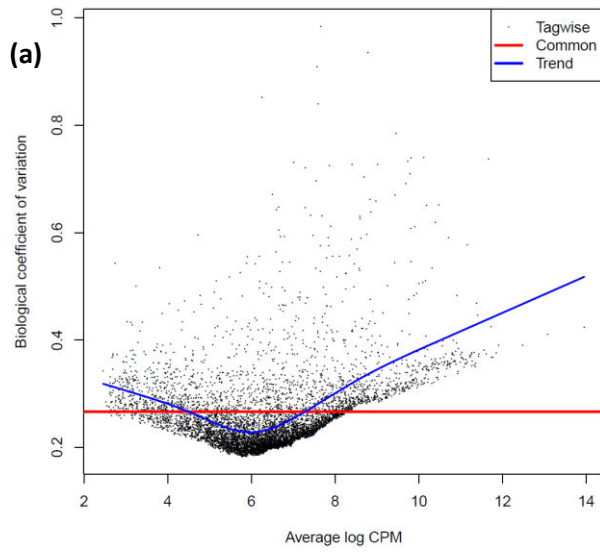
Appendix 4.7. PCR confirmations of gene knock-outs in *S. cerevisiae* BY4741



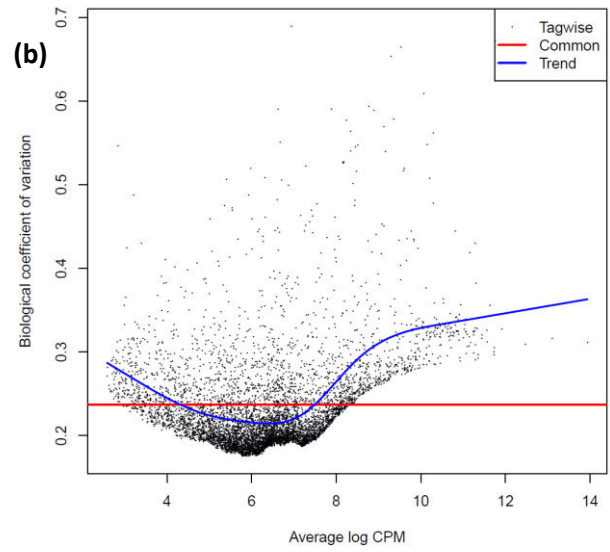


PCR confirmations of **(a)** *aft1Δ* and *tpk2Δ*, **(b)** *vel1Δ* and *vel1Δ* in the *yor387cΔ/vel1Δ* double mutant, **(c)** *atg1Δ* and *yap5Δ*, **(d)** *yor387cΔ* and *yor387cΔ* in the *yor387cΔ/vel1Δ* double mutant, **(e)** *met32Δ* and *mtd1Δ*, **(f)** *yct1Δ* and *zap1Δ* and **(g)** *cch1Δ*. Expected band sizes are present in Appendix 4.6.

Appendix 4.8. BCV of *C. neoformans* H99 transcripts in VRC+EDTA antagonism.



BCV = 0.2666 before sample 7J deletion



BCV = 0.2373 after 7J deletion.

REFERENCES

1. Garcia-Solache, M.A. and A. Casadevall, *Global warming will bring new fungal diseases for mammals*. MBio, 2010. **1**(1): p. e00061-10.
2. Brandt, M. and B. Park, *Think fungus - prevention and control of fungal infections*. Emerging Infectious Diseases, 2013. **19**(10): p. 1688-1689.
3. Brown, G.D., et al., *Hidden killers: human fungal infections*. Science Translational Medicine, 2012. **4**(165): p. 165rv13.
4. Del Poeta, M., et al., *Synergistic antifungal activities of bafilomycin A(1), fluconazole, and the pneumocandin MK-0991/caspofungin acetate (L-743,873) with calcineurin inhibitors FK506 and L-685,818 against Cryptococcus neoformans*. Antimicrobial Agents and Chemotherapy, 2000. **44**(3): p. 739-46.
5. Chen, Y.-L., et al., *Posaconazole exhibits in vitro and in vivo synergistic antifungal activity with caspofungin or FK506 against Candida albicans*. PLoS One, 2013. **8**(3): p. e57672.
6. Xu, Y., et al., *Proteomic analysis reveals a synergistic mechanism of fluconazole and berberine against fluconazole-resistant Candida albicans: endogenous ROS augmentation*. Journal of Proteome Research, 2009. **8**(11): p. 5296-5304.
7. Zhang, X.L., et al., *Proteomic analysis reveals that Adh1p is involved in a synergistic fluconazole and tetrandrine mechanism against Candida albicans*. Pharmazie, 2013. **68**(12): p. 951-4.
8. Johnson, L., *Iron and siderophores in fungal-host interactions*. Mycological Research, 2008. **112**: p. 170-183.
9. Zarembler, K.A., et al., *Antifungal activities of natural and synthetic iron chelators alone and in combination with azole and polyene antibiotics against Aspergillus fumigatus*. Antimicrobial Agents and Chemotherapy, 2009. **53**(6): p. 2654-6.
10. Kuipers, M.E., et al., *Synergistic fungistatic effects of lactoferrin in combination with antifungal drugs against clinical Candida isolates*. Antimicrobial Agents and Chemotherapy, 1999. **43**(11): p. 2635-41.
11. Simmer, M. and D. Secko, *A peach of a pathogen: Cryptococcus neoformans*. The Science Creative Quaterly 2003(2).
12. Hagen, F., et al., *Recognition of seven species in the Cryptococcus gattii/Cryptococcus neoformans species complex*. Fungal genetics and biology : FG & B, 2015. **78**: p. 16-48.
13. Lin, X. and J. Heitman, *The biology of the Cryptococcus neoformans species complex*. Annual Review of Microbiology, 2006. **60**: p. 69-105.
14. Chayakulkeeree, M. and J.R. Perfect, *Cryptococcosis*. Infectious Disease Clinics of North America, 2006. **20**(3): p. 507-44, v-vi.
15. Aminnejad, M., et al., *Identification of novel hybrids between Cryptococcus neoformans var. grubii VNI and Cryptococcus gattii VGII*. Mycopathologia, 2012. **173**(5-6): p. 337-46.
16. Bovers, M., et al., *Unique hybrids between the fungal pathogens Cryptococcus neoformans and Cryptococcus gattii*. FEMS Yeast Research, 2006. **6**(4): p. 599-607.
17. Bovers, M., et al., *AIDS patient death caused by novel Cryptococcus neoformans x C. gattii hybrid*. Emerging Infectious Diseases, 2008. **14**(7): p. 1105-8.
18. Sorrell, T.C., *Cryptococcus neoformans variety gattii*. Medical Mycology, 2001. **39**(2): p. 155-68.
19. Perfect, J.R., *The triple threat of cryptococcosis: it's the body site, the strain, and/or the host*. MBio, 2012. **3**(4).
20. Barchiesi, F., et al., *Comparative analysis of pathogenicity of Cryptococcus neoformans serotypes A, D and AD in murine cryptococcosis*. The Journal of Infection, 2005. **51**(1): p. 10-6.

21. Chong, H.S., et al., *In vitro* susceptibility of the yeast pathogen *Cryptococcus* to fluconazole and other azoles varies with molecular genotype. *Journal of Clinical Microbiology*, 2010. **48**(11): p. 4115-20.
22. Cogliati, M., *Global Molecular Epidemiology of Cryptococcus neoformans and Cryptococcus gattii: An Atlas of the Molecular Types*. Scientifica, 2013. **2013**: p. 675213.
23. da Costa, M.M., et al., *Cryptococcosis, a risk for immunocompromised and immunocompetent individuals* *The Open Epidemiology Journal* 2013. **6**: p. 9-17.
24. Mitchell, T.G. and J.R. Perfect, *Cryptococcosis in the era of AIDS--100 years after the discovery of Cryptococcus neoformans*. *Clinical Microbiology Reviews*, 1995. **8**(4): p. 515-48.
25. Antinori, S., *New Insights into HIV/AIDS-Associated Cryptococcosis*. *International Scholarly Research Network AIDS*, 2013. **2013**: p. 22.
26. Park, B.J., et al., *Estimation of the current global burden of cryptococcal meningitis among persons living with HIV/AIDS*. *Aids*, 2009. **23**(4): p. 525-30.
27. Park, J., et al., *Update on the global burden of cryptococcosis (oral abstract)*. *Mycoses*, 2014. **57**(Supplement s1): p. 5-32.
28. Chen, S.C., W. Meyer, and T.C. Sorrell, *Cryptococcus gattii* infections. *Clinical Microbiology Reviews*, 2014. **27**(4): p. 980-1024.
29. Min, K.H. and K.J. Kwon-Chung, *The biochemical basis for the distinction between the two Cryptococcus neoformans varieties with CGB medium*. *Zentralbl Bakteriol Mikrobiol Hyg A*, 1986. **261**(4): p. 471-80.
30. Espinel-Ingroff, A., et al., *Cryptococcus neoformans-Cryptococcus gattii species complex: an international study of wild-type susceptibility endpoint distributions and epidemiological cutoff values for fluconazole, itraconazole, posaconazole, and voriconazole*. *Antimicrobial Agents and Chemotherapy*, 2012. **56**(11): p. 5898-906.
31. Trilles, L., et al., *In vitro* antifungal susceptibility of *Cryptococcus gattii*. *Journal of Clinical Microbiology*, 2004. **42**(10): p. 4815-7.
32. Varma, A. and K.J. Kwon-Chung, *Heteroresistance of Cryptococcus gattii to fluconazole*. *Antimicrobial Agents and Chemotherapy*, 2010. **54**(6): p. 2030-2311.
33. Ellis, D.H. and T.J. Pfeiffer, *Natural habitat of Cryptococcus neoformans var. gattii*. *Journal of Clinical Microbiology*, 1990. **28**(7): p. 1642-1644.
34. Springer, D.J. and V. Chaturvedi, *Projecting global occurrence of Cryptococcus gattii*. *Emerging Infectious Diseases*, 2010. **16**(1): p. 14-20.
35. Stephen, C., et al., *British Columbia: Multispecies outbreak of cryptococcosis on southern Vancouver Island, British Columbia*. *The Canadian Veterinary Journal*, 2002. **43**(10): p. 792-794.
36. Datta, K., et al., *Spread of Cryptococcus gattii into Pacific Northwest region of the United States*. *Emerging Infectious Diseases*, 2009. **15**(8): p. 1185-91.
37. Byrnes, E.J., III, et al., *Emergence and pathogenicity of highly virulent Cryptococcus gattii genotypes in the northwest United States*. *PLoS Pathogens*, 2010. **6**(4): p. e1000850.
38. Woods, M.L., 2nd, et al., *HIV combination therapy: partial immune restitution unmasking latent cryptococcal infection*. *Aids*, 1998. **12**(12): p. 1491-4.
39. Kathiravan, M.K., et al., *The biology and chemistry of antifungal agents: a review*. *Bioorganic and Medicinal Chemistry*, 2012. **20**(19): p. 5678-5698.
40. Perfect, J.R., et al., *Clinical practice guidelines for the management of cryptococcal disease: 2010 update by the Infectious Diseases Society of America*. *Clinical Infectious Diseases : an Official Publication of the Infectious Diseases Society of America*, 2010. **50**(3): p. 291-322.
41. Sorrell, T.C. and S.C. Chen, *Recent advances in management of cryptococcal meningitis: commentary*. *F1000 Medicine Reports*, 2010. **2**: p. 82.

42. Day, J.N., et al., *Combination antifungal therapy for cryptococcal meningitis*. New England Journal of Medicine, 2013. **368**(14): p. 1291-1302.
43. Loyse, A., et al., *Cryptococcal meningitis: improving access to essential antifungal medicines in resource-poor countries*. The Lancet Infectious Diseases, 2013. **13**(7): p. 629-637.
44. Meyer, A.-C. and M. Jacobson, *Asymptomatic cryptococemia in resource-limited settings*. Current HIV/AIDS Reports, 2013. **10**(3): p. 254-263.
45. Vermes, A., H.J. Guchelaar, and J. Dankert, *Flucytosine: a review of its pharmacology, clinical indications, pharmacokinetics, toxicity and drug interactions*. The Journal of Antimicrobial Chemotherapy, 2000. **46**(2): p. 171-9.
46. Cheong, J.W. and J. McCormack, *Fluconazole resistance in cryptococcal disease: emerging or intrinsic?* Medical Mycology, 2013. **51**(3): p. 261-9.
47. Nguyen, P., et al., *Fluconazole resistance in Cryptococcus neoformans: an emerging threat to the immune-compromised*, in *IDWeek™ Advancing Science, Improving Care*. 2012: San Diego, CA.
48. Collier, R., *Drug patents: the evergreening problem*. Canadian Medical Association Journal, 2013. **185**(9): p. E385-E386.
49. Balkovec, J.M., et al., *Discovery and development of first in class antifungal caspofungin (CANCIDAS(R))-a case study*. Natural Product Reports, 2014. **31**(1): p. 15-34.
50. Butts, A. and D.J. Krysan, *Antifungal drug discovery: something old and something new*. PLoS Pathogens, 2012. **8**(9): p. e1002870.
51. Vengurlekar, S., R. Sharma, and P. Trivedi, *Efficacy of some natural compounds as antifungal agents*. Pharmacognosy Reviews, 2012. **6**(12): p. 91-99.
52. Caffrey, P., et al., *Amphotericin biosynthesis in Streptomyces nodosus: deductions from analysis of polyketide synthase and late genes*. Chemistry and Biology, 2001. **8**(7): p. 713-23.
53. Letscher-Bru, V. and R. Herbrecht, *Caspofungin: the first representative of a new antifungal class*. The Journal of Antimicrobial Chemotherapy, 2003. **51**(3): p. 513-21.
54. Butts, A., et al., *A repurposing approach identifies off-patent drugs with fungicidal cryptococcal activity, a common structural chemotype, and pharmacological properties relevant to the treatment of cryptococcosis*. Eukaryotic Cell, 2013. **12**(2): p. 278-87.
55. Campbell, B.C., K.L. Chan, and J.H. Kim, *Chemosensitization as a means to augment commercial antifungal agents*. Frontiers in Microbiology, 2012. **3**.
56. Mukherjee, P.K., et al., *Combination treatment of invasive fungal infections*. Clinical Microbiology Reviews, 2005. **18**(1): p. 163-94.
57. Reed, C., et al., *Deferasirox, an iron-chelating agent, as salvage therapy for rhinocerebral mucormycosis*. Antimicrobial Agents and Chemotherapy, 2006. **50**(11): p. 3968-9.
58. Soummer, A., et al., *Failure of deferasirox, an iron chelator agent, combined with antifungals in a case of severe zygomycosis*. Antimicrobial Agents and Chemotherapy, 2008. **52**(4): p. 1585-6.
59. Pahl, J., et al., *A randomized, blinded, multicenter trial of lipid-associated amphotericin B alone versus in combination with an antibody-based inhibitor of heat shock protein 90 in patients with invasive candidiasis*. Clinical Infectious Diseases : an Official Publication of the Infectious Diseases Society of America, 2006. **42**(10): p. 1404-13.
60. Ejim, L., et al., *Combinations of antibiotics and nonantibiotic drugs enhance antimicrobial efficacy*. Nature Chemical Biology, 2011. **7**(6): p. 348-50.
61. Fischbach, M.A., *Combination therapies for combating antimicrobial resistance*. Current Opinion in Microbiology, 2011. **14**(5): p. 519-523.
62. Johnson, M.D. and J.R. Perfect, *Use of antifungal combination therapy: agents, order, and timing*. Current Fungal Infection Reports, 2010. **4**(2): p. 87-95.
63. Meletiadis, J., et al., *Defining fractional inhibitory concentration index cutoffs for additive interactions based on self-drug additive combinations, Monte Carlo simulation analysis, and in*

- vitro-in vivo correlation data for antifungal drug combinations against Aspergillus fumigatus.* Antimicrobial Agents and Chemotherapy, 2010. **54**(2): p. 602-9.
64. Bushby, S.R., *Synergy of trimethoprim-sulfamethoxazole.* Canadian Medical Association Journal, 1975. **112**(13 Spec No): p. 63-66.
 65. Huovinen, P., *Resistance to trimethoprim-sulfamethoxazole.* Clinical Infectious Diseases : An Official Publication of the Infectious Diseases Society of America, 2001. **32**(11): p. 1608-14.
 66. Sorbera, M., et al., *Ceftolozane/tazobactam: a new option in the treatment of complicated gram-negative infections.* Pharmacy and Therapeutics, 2014. **39**(12): p. 825-832.
 67. Kontoyiannis, D.P., et al., *Calcineurin inhibitor agents interact synergistically with antifungal agents in vitro against Cryptococcus neoformans isolates: correlation with outcome in solid organ transplant recipients with cryptococcosis.* Antimicrobial Agents and Chemotherapy, 2008. **52**(2): p. 735-8.
 68. Rodero, L., et al., *In vitro susceptibility studies of Cryptococcus neoformans isolated from patients with no clinical response to amphotericin B therapy.* The Journal of Antimicrobial Chemotherapy 2000. **45**(2): p. 239-42.
 69. Zhai, B., et al., *The antidepressant sertraline provides a promising therapeutic option for neurotropic cryptococcal infections.* Antimicrobial Agents and Chemotherapy, 2012. **56**(7): p. 3758-66.
 70. Faria, N.C., et al., *Enhanced activity of antifungal drugs using natural phenolics against yeast strains of Candida and Cryptococcus.* Letters in Applied Microbiology, 2011. **52**(5): p. 506-13.
 71. Steinbach, W.J., et al., *In vitro interactions between antifungals and immunosuppressants against Aspergillus fumigatus.* Antimicrobial Agents and Chemotherapy, 2004. **48**(5): p. 1664-9.
 72. Kobayashi, T., et al., *Synergistic antifungal effect of lactoferrin with azole antifungals against Candida albicans and a proposal for a new treatment method for invasive candidiasis.* Japanese Journal of Infectious Diseases, 2011. **64**(4): p. 292-6.
 73. Ibrahim, A.S., et al., *The iron chelator deferasirox protects mice from mucormycosis through iron starvation.* The Journal of Clinical Investigation, 2007. **117**(9): p. 2649-57.
 74. Ibrahim, A.S., et al., *The iron chelator deferasirox enhances liposomal amphotericin B efficacy in treating murine invasive pulmonary aspergillosis.* Journal of Antimicrobial Chemotherapy, 2010. **65**(2): p. 289-92.
 75. Crichton, R., *Solution chemistry of iron in biological media,* in *Inorganic Biochemistry of Iron Metabolism.* 2002, John Wiley & Sons, Ltd. p. 1-15.
 76. Bayeva, M., et al., *When less is more: novel mechanisms of iron conservation.* Trends in Endocrinology & Metabolism, 2013. **24**(11): p. 569-577.
 77. Crichton, R., *The importance of iron for biological systems,* in *Inorganic Biochemistry of Iron Metabolism: From Molecular Mechanisms to Clinical Consequences.* 2002, John Wiley & Sons, Ltd. p. 17-48.
 78. Robins-Browne, R.M. and J.K. Prpic, *Effects of iron and desferrioxamine on infections with Yersinia enterocolitica.* Infection and Immunity, 1985. **47**(3): p. 774-779.
 79. Potrykus, J., et al., *Conflicting interests in the pathogen–host tug of war: fungal micronutrient scavenging versus mammalian nutritional immunity.* PLoS Pathogens, 2014. **10**(3): p. e1003910.
 80. Oliveira, F., S. Rocha, and R. Fernandes, *Iron metabolism: from health to disease.* Journal of Clinical Laboratory Analysis, 2014. **28**(3): p. 210-218.
 81. Outten, C.E. and A.N. Albetel, *Iron sensing and regulation in Saccharomyces cerevisiae: ironing out the mechanistic details.* Current Opinion in Microbiology, 2013. **16**(6): p. 662-8.
 82. Philpott, C.C. and O. Protchenko, *Response to iron deprivation in Saccharomyces cerevisiae.* Eukaryotic Cell, 2008. **7**(1): p. 20-7.

83. Kaplan, J., et al., *Iron-dependent metabolic remodeling in S. cerevisiae*. *Biochimica et Biophysica Acta*, 2006. **1763**: p. 646-651.
84. Puig, S., S.V. Vergara, and D.J. Thiele, *Cooperation of two mRNA-binding proteins drives metabolic adaptation to iron deficiency*. *Cell Metabolism*, 2008. **7**(6): p. 555-564.
85. Puig, S., E. Askeland, and D.J. Thiele, *Coordinated remodeling of cellular metabolism during iron deficiency through targeted mRNA degradation*. *Cell*, 2005. **120**(1): p. 99-110.
86. Rutherford, J.C., et al., *Activation of the iron regulon by the yeast Aft1/Aft2 transcription factors depends on mitochondrial but not cytosolic iron-sulfur protein biogenesis*. *The Journal of Biological Chemistry*, 2005. **280**(11): p. 10135-40.
87. Chen, O.S., et al., *Transcription of the yeast iron regulon does not respond directly to iron but rather to iron-sulfur cluster biosynthesis*. *The Journal of Biological Chemistry*, 2004. **279**(28): p. 29513-8.
88. Li, L., et al., *A role for iron-sulfur clusters in the regulation of transcription factor Yap5-dependent high iron transcriptional responses in yeast*. *The Journal of Biological Chemistry*, 2012. **287**(42): p. 35709-21.
89. Li, L., et al., *Yap5 is an iron-responsive transcriptional activator that regulates vacuolar iron storage in yeast*. *Molecular and Cellular Biology*, 2008. **28**(4): p. 1326-37.
90. Pimentel, C., et al., *The role of the Yap5 transcription factor in remodeling gene expression in response to Fe bioavailability*. *PLoS One*, 2012. **7**(5): p. e37434.
91. Pujol-Carrion, N., et al., *Glutaredoxins Grx3 and Grx4 regulate nuclear localisation of Aft1 and the oxidative stress response in Saccharomyces cerevisiae*. *Journal of Cell Science*, 2006. **119**(Pt 21): p. 4554-64.
92. Philpott, C.C., S. Leidgens, and A.G. Frey, *Metabolic remodeling in iron-deficient fungi*. *Biochimica et Biophysica Acta (BBA) - Molecular Cell Research*, 2012. **1823**(9): p. 1509-1520.
93. Cyert, M.S. and C.C. Philpott, *Regulation of cation balance in Saccharomyces cerevisiae*. *Genetics*, 2013. **193**(3): p. 677-713.
94. Jung, W.H., et al., *Iron source preference and regulation of iron uptake in Cryptococcus neoformans*. *PLoS Pathogens*, 2008. **4**(2): p. e45.
95. Lian, T., et al., *Iron-regulated transcription and capsule formation in the fungal pathogen Cryptococcus neoformans*. *Molecular Microbiology*, 2005. **55**(5): p. 1452-1472.
96. Jung, W.H. and J.W. Kronstad, *Iron and fungal pathogenesis: a case study with Cryptococcus neoformans*. *Cellular Microbiology*, 2008. **10**(2): p. 277-284.
97. Tangen, K.L., et al., *The iron- and cAMP-regulated gene SIT1 influences ferrioxamine B utilization, melanization and cell wall structure in Cryptococcus neoformans*. *Microbiology*, 2007. **153**(Pt 1): p. 29-41.
98. Saikia, S., et al., *Role of ferric reductases in iron acquisition and virulence in the fungal pathogen Cryptococcus neoformans*. *Infection and Immunity*, 2014. **82**(2): p. 839-50.
99. Jacobson, E.S., A.J. Troy, and K.J. Nyhus, *Mitochondrial functioning of constitutive iron uptake mutations in Cryptococcus neoformans*. *Mycopathologia*, 2005. **159**: p. 1-6.
100. Cadieux, B., et al., *The mannoprotein Cig1 supports iron acquisition from heme and virulence in the pathogenic fungus Cryptococcus neoformans*. *The Journal of Infectious Diseases*, 2013. **207**(8): p. 1339-47.
101. Hu, G., et al., *Cryptococcus neoformans requires the ESCRT protein Vps23 for iron acquisition from heme, for capsule formation, and for virulence*. *Infection and Immunity*, 2013. **81**(1): p. 292-302.
102. Pilas, B., et al., *The effect of melanin on iron associated decomposition of hydrogen peroxide*. *Free Radical Biology & Medicine*, 1988. **4**(5): p. 285-93.

103. Jung, W.H., et al., *HapX positively and negatively regulates the transcriptional response to iron deprivation in Cryptococcus neoformans*. PLoS Pathogens, 2010. **6**(11): p. e1001209.
104. Jung, W.H., et al., *Iron regulation of the major virulence factors in the AIDS-associated pathogen Cryptococcus neoformans*. PLoS Biology, 2006. **4**(12): p. e410.
105. Kronstad, J.W., G. Hu, and W.H. Jung, *An encapsulation of iron homeostasis and virulence in Cryptococcus neoformans*. Trends in Microbiology, 2013. **21**(9): p. 457-65.
106. Ding, C., et al., *Essential metals in Cryptococcus neoformans: acquisition and regulation*. Current Fungal Infection Reports, 2014. **8**(2): p. 153-162.
107. Jung, W.H. and J.W. Kronstad, *Iron influences the abundance of the iron regulatory protein Cir1 in the fungal pathogen Cryptococcus neoformans*. FEBS Letters, 2011. **585**(20): p. 3342-3347.
108. Lee, H., et al., *Regulatory diversity of TUP1 in Cryptococcus neoformans*. Eukaryotic Cell, 2009. **8**(12): p. 1901-8.
109. Chang, Y.C., et al., *Sre1p, a regulator of oxygen sensing and sterol homeostasis, is required for virulence in Cryptococcus neoformans*. Molecular Microbiology, 2007. **64**(3): p. 614-29.
110. Cramer, K.L., et al., *Transcription factor Nrg1 mediates capsule formation, stress response, and pathogenesis in Cryptococcus neoformans*. Eukaryotic Cell, 2006. **5**(7): p. 1147-56.
111. O'Meara, T.R., et al., *Interaction of Cryptococcus neoformans Rim101 and protein kinase A regulates capsule*. PLoS Pathogens, 2010. **6**(2): p. e1000776.
112. Chun, Cheryl D., Jessica C.S. Brown, and Hiten D. Madhani, *A major role for capsule-independent phagocytosis-inhibitory mechanisms in mammalian infection by Cryptococcus neoformans*. Cell Host & Microbe. **9**(3): p. 243-251.
113. Vartivarian, S.E., et al., *Regulation of cryptococcal capsular polysaccharide by iron*. The Journal of Infectious Diseases, 1993. **167**(1): p. 186-90.
114. Polacheck, I., V.J. Hearing, and K.J. Kwon-Chung, *Biochemical studies of phenoloxidase and utilization of catecholamines in Cryptococcus neoformans*. Journal of Bacteriology, 1982. **150**(3): p. 1212-1220.
115. Hu, G., et al., *Microevolution during serial mouse passage demonstrates FRE3 as a virulence adaptation gene in Cryptococcus neoformans*. MBio, 2014. **5**(2): p. e00941-14.
116. Jung, W.H., et al., *Role of ferroxidases in iron uptake and virulence of Cryptococcus neoformans*. Eukaryotic Cell, 2009. **8**(10): p. 1511-1520.
117. Jung, W.H. and J.W. Kronstad, *The iron-responsive, GATA-type transcription factor Cir1 influences mating in Cryptococcus neoformans*. Molecules and Cells, 2011. **31**(1): p. 73-7.
118. Zaragoza, O., et al., *The capsule of the fungal pathogen Cryptococcus neoformans*. Advances in Applied Microbiology, 2009. **68**: p. 133-216.
119. Casadevall, A., A.L. Rosas, and J.D. Nosanchuk, *Melanin and virulence in Cryptococcus neoformans*. Current Opinion in Microbiology, 2000. **3**(4): p. 354-358.
120. Kwon-Chung, K.J., I. Polacheck, and T.J. Popkin, *Melanin-lacking mutants of Cryptococcus neoformans and their virulence for mice*. Journal of Bacteriology, 1982. **150**(3): p. 1414-21.
121. Kwon-Chung, K.J. and J.C. Rhodes, *Encapsulation and melanin formation as indicators of virulence in Cryptococcus neoformans*. Infection and Immunity, 1986. **51**(1): p. 218-223.
122. Kirschner, M.W., *The meaning of systems biology*. Cell, 2005. **121**(4): p. 503-504.
123. Bork, P. and L. Serrano, *Towards cellular systems in 4D*. Cell, 2005. **121**(4): p. 507-509.
124. Liu, E.T., *Systems biology, integrative Biology, predictive Biology*. Cell, 2005. **121**(4): p. 505-506.
125. Chandramouli, K. and P.-Y. Qian, *Proteomics: challenges, techniques and possibilities to overcome biological sample complexity*. Human Genomics and Proteomics : HGP, 2009. **2009**: p. 239204.
126. Graves, P.D. and J.D. Tugwood, *Generation and analysis of transcriptomics data*. Methods in Molecular Biology, 2011. **691**: p. 167-85.

127. Wang, Z., M. Gerstein, and M. Snyder, *RNA-Seq: a revolutionary tool for transcriptomics*. Nature Reviews Genetics, 2009. **10**(1): p. 57-63.
128. Maier, T., M. Güell, and L. Serrano, *Correlation of mRNA and protein in complex biological samples*. FEBS Letters, 2009. **583**(24): p. 3966-3973.
129. Stephens, N.A., et al., *Using transcriptomics to identify and validate novel biomarkers of human skeletal muscle cancer cachexia*. Genome Medicine, 2010. **2**(1): p. 1.
130. Zarate-Blades, C.R., C.L. Silva, and G.A. Passos, *The impact of transcriptomics on the fight against tuberculosis: focus on biomarkers, BCG vaccination, and immunotherapy*. Clinical & Developmental Immunology, 2011. **2011**: p. 192630.
131. Costa, V., et al., *Uncovering the complexity of transcriptomes with RNA-Seq*. Journal of Biomedicine & Biotechnology, 2010. **2010**: p. 853916.
132. Haider, S. and R. Pal, *Integrated analysis of transcriptomic and proteomic data*. Current Genomics, 2013. **14**(2): p. 91-110.
133. Wolf, J.B., *Principles of transcriptome analysis and gene expression quantification: an RNA-seq tutorial*. Mol Ecol Resour, 2013. **13**(4): p. 559-72.
134. Mutz, K.O., et al., *Transcriptome analysis using next-generation sequencing*. Current Opinion in Biotechnology, 2013. **24**(1): p. 22-30.
135. Lee, R.E., et al., *Genome-wide expression profiling of the response to ciclopirox olamine in Candida albicans*. The Journal of Antimicrobial Chemotherapy, 2005. **55**(5): p. 655-62.
136. Silva, A.P., et al., *Transcriptional profiling of azole-resistant Candida parapsilosis strains*. Antimicrobial Agents and Chemotherapy, 2011. **55**(7): p. 3546-56.
137. Florio, A.R., et al., *Genome-wide expression profiling of the response to short-term exposure to fluconazole in Cryptococcus neoformans serotype A*. BMC Microbiology, 2011. **11**: p. 97.
138. Liu, J., et al., *Whole transcriptome analysis of Penicillium digitatum strains treated with prochloraz reveals their drug-resistant mechanisms*. BMC Genomics, 2015. **16**: p. 855.
139. Lopez-Moya, F., et al., *Neurospora crassa transcriptomics reveals oxidative stress and plasma membrane homeostasis biology genes as key targets in response to chitosan*. Molecular BioSystems, 2016. **12**(2): p. 391-403.
140. Gkarmiri, K., et al., *Transcriptomic changes in the plant pathogenic fungus Rhizoctonia solani AG-3 in response to the antagonistic bacteria Serratia proteamaculans and Serratia plymuthica*. BMC Genomics, 2015. **16**: p. 630.
141. Janbon, G., et al., *Analysis of the genome and transcriptome of Cryptococcus neoformans var. grubii reveals complex RNA expression and microevolution leading to virulence attenuation*. PLoS Genetics, 2014. **10**(4): p. e1004261.
142. Gillece, J.D., et al., *Whole genome sequence analysis of Cryptococcus gattii from the Pacific Northwest reveals unexpected diversity*. PLoS One, 2011. **6**(12): p. e28550.
143. Billmyre, R.B., et al., *Highly recombinant VGII Cryptococcus gattii population develops clonal outbreak clusters through both sexual macroevolution and asexual microevolution*. MBio, 2014. **5**(4): p. e01494-14.
144. Chong, H.S., *Proteomic study of intrinsic azole resistance in Cryptococcus gattii* in Science. 2011, University of Sydney: University of Sydney, Australia. p. 291.
145. Loftus, B.J., et al., *The genome of the basidiomycetous yeast and human pathogen Cryptococcus neoformans*. Science, 2005. **307**(5713): p. 1321-4.
146. Institute, C.a.L.S., *Reference method for broth dilution antifungal susceptibility testing of yeasts; approved standard - third edition*. 2008, CLSI: Wayne, Pennsylvania
147. Kontoyiannis, D.P. and R.E. Lewis, *Toward more effective antifungal therapy: the prospects of combination therapy*. British Journal of Haematology, 2004. **126**(2): p. 165-175.

148. Lewis, R.E. and D.P. Kontoyiannis, *Rationale for combination antifungal therapy*. Pharmacotherapy, 2001. **21**(8 Pt 2): p. 149s-164s.
149. Dockrell, D.H., *Salvage therapy for invasive aspergillosis*. The Journal of Antimicrobial Chemotherapy, 2008. **61 Suppl 1**: p. i41-4.
150. Johnson, M.D. and J.R. Perfect, *Combination antifungal therapy: what can and should we expect?* Bone Marrow Transplantation, 2007. **40**(4): p. 297-306.
151. Lupetti, A., et al., *Molecular targeted treatments for fungal infections: the role of drug combinations*. Trends in Molecular Medicine, 2003. **9**(6): p. 269-276.
152. Liu, S., et al., *Combination of fluconazole with non-antifungal agents: a promising approach to cope with resistant Candida albicans infections and insight into new antifungal agent discovery*. International Journal of Antimicrobial Agents, 2014. **43**(5): p. 395-402.
153. Spitzer, M., et al., *Cross-species discovery of syncretic drug combinations that potentiate the antifungal fluconazole*. Molecular Systems Biology, 2011. **7**: p. 499.
154. Spellberg, B., et al., *Safety and outcomes of open-label deferasirox iron chelation therapy for mucormycosis*. Antimicrobial Agents and Chemotherapy, 2009. **53**(7): p. 3122-5.
155. Ibrahim, A.S., et al., *Deferiprone iron chelation as a novel therapy for experimental mucormycosis*. The Journal of Antimicrobial Chemotherapy, 2006. **58**(5): p. 1070-3.
156. Ibrahim, A.S., et al., *Combination therapy of murine mucormycosis or aspergillosis with iron chelation, polyenes, and echinocandins*. Antimicrobial Agents and Chemotherapy, 2011. **55**(4): p. 1768-70.
157. Lee, J.J., et al., *Interaction index and different methods for determining drug interaction in combination therapy*. Journal of Biopharmaceutical Statistics, 2007. **17**(3): p. 461-480.
158. Vazquez, J.A., *Combination antifungal therapy against Candida species: the new frontier-are we there yet?* Medical Mycology, 2003. **41**(5): p. 355-68.
159. Goldoni, M. and C. Johansson, *A mathematical approach to study combined effects of toxicants in vitro: evaluation of the Bliss independence criterion and the Loewe additivity model*. Toxicology in Vitro, 2007. **21**(5): p. 759-769.
160. Hindler, J., *Antimicrobial susceptibility testing*, in *Clinical Microbiology Procedures Handbook*, H. Isenberg, Editor. 1995, ASM Press: Washington, DC. p. 5.18.11–15.18.20.
161. Te Dorsthorst, D.T.A., et al., *In vitro interaction of flucytosine combined with amphotericin B or fluconazole against thirty-five yeast isolates determined by both the fractional inhibitory concentration index and the response surface approach*. Antimicrobial Agents and Chemotherapy, 2002. **46**(9): p. 2982-2989.
162. Odds, F.C., *Synergy, antagonism, and what the chequerboard puts between them*. The Journal of Antimicrobial Chemotherapy, 2003. **52**(1): p. 1.
163. Buckheit, R. and R.D. Lunsford, *In vitro performance and analysis of combination anti-infective evaluations*, in *Antimicrobial Drug Resistance*, D. Mayers, Editor. 2009, Humana Press. p. 1135-1149.
164. Greco, W.R., G. Bravo, and J.C. Parsons, *The search for synergy: a critical review from a response surface perspective*. Pharmacological Reviews, 1995. **47**(2): p. 331-85.
165. Prichard, M.N. and J. C. Shipman, *A three-dimensional model to analyze drug-drug interactions*. Antiviral Research, 1990. **14**: p. 181-206.
166. Jumbe, N.L.n.S. and G. Drusano, *A model-based PK/PD antimicrobial chemotherapy drug development platform to simultaneously combat infectious diseases and drug resistance*, in *Clinical Trial Simulations*, H.H.C. Kimko and C.C. Peck, Editors. 2011, Springer New York. p. 251-279.
167. Prichard, M.N., K.R. Aseltine, and C.J. Shipman, *MacSynergyTM II*. 1992: University of Michigan.

168. Dutcher, J.D., *The discovery and development of amphotericin B*. Diseases of the Chest 1968. **54**: p. Suppl 1:296-8.
169. Gagos, M., et al., *Binding of antibiotic amphotericin B to lipid membranes: monomolecular layer technique and linear dichroism-FTIR studies*. Molecular Membrane Biology, 2005. **22**(5): p. 433-42.
170. Cowen, L.E. and W.J. Steinbach, *Stress, drugs, and evolution: the role of cellular signaling in fungal drug resistance*. Eukaryotic cell, 2008. **7**(5): p. 747-64.
171. Gray, K.C., et al., *Amphotericin primarily kills yeast by simply binding ergosterol*. PNAS, 2012. **109**(7): p. 2234-2239.
172. Ellis, D., *Amphotericin B: spectrum and resistance*. The Journal of Antimicrobial Chemotherapy, 2002. **49 Suppl 1**: p. 7-10.
173. Forastiero, A., et al., *Candida tropicalis antifungal cross-resistance is related to different azole target (Erg11p) modifications*. Antimicrobial Agents and Chemotherapy, 2013. **57**(10): p. 4769-81.
174. Joseph-Horne, T., et al., *Cross-resistance to polyene and azole drugs in Cryptococcus neoformans*. Antimicrobial Agents and Chemotherapy, 1995. **39**(7): p. 1526-9.
175. Kelly, S.L., et al., *Resistance to fluconazole and cross-resistance to amphotericin B in Candida albicans from AIDS patients caused by defective sterol delta5,6-desaturation*. FEBS Letters, 1997. **400**(1): p. 80-2.
176. Sutton, D.A., et al., *In vitro amphotericin B resistance in clinical isolates of Aspergillus terreus, with a head-to-head comparison to voriconazole*. Journal of Clinical Microbiology, 1999. **37**(7): p. 2343-5.
177. Ghannoum, M.A. and L.B. Rice, *Antifungal agents: mode of action, mechanisms of resistance, and correlation of these mechanisms with bacterial resistance*. Clinical Microbiology Reviews, 1999. **12**(4): p. 501-17.
178. Carrillo-Munoz, A.J., et al., *Antifungal agents: mode of action in yeast cells*. Revista Espanola de Quimioterapia: Publicacion Oficial de la Sociedad Espanola de Quimioterapia, 2006. **19**(2): p. 130-9.
179. Loyse, A., et al., *Flucytosine and cryptococcosis: time to urgently address the worldwide accessibility of a 50-year-old antifungal*. The Journal of Antimicrobial Chemotherapy, 2013. **68**(11): p. 2435-44.
180. Fera, M.T., E. La Camera, and A. De Sarro, *New triazoles and echinocandins: mode of action, in vitro activity and mechanisms of resistance*. Expert Review of Anti-Infective Therapy, 2009. **7**(8): p. 981-98.
181. Zonios, D.I. and J.E. Bennett, *Update on azole antifungals*. Seminars in Respiratory and Critical Care Medicine, 2008. **29**(2): p. 198-210.
182. Warrilow, A.G., et al., *Azole affinity of sterol 14alpha-demethylase (CYP51) enzymes from Candida albicans and Homo sapiens*. Antimicrobial Agents and Chemotherapy, 2013. **57**(3): p. 1352-60.
183. Espinel-Ingroff, A., *In vitro fungicidal activities of voriconazole, itraconazole, and amphotericin B against opportunistic moniliaceous and dematiaceous fungi*. Journal of Clinical Microbiology, 2001. **39**(3): p. 954-958.
184. Sionov, E., et al., *Heteroresistance to fluconazole in Cryptococcus neoformans is intrinsic and associated with virulence*. Antimicrobial Agents and Chemotherapy 2009. **53**(7): p. 2804-15.
185. Sionov, E., et al., *Cryptococcus neoformans overcomes stress of azole drugs by formation of disomy in specific multiple chromosomes*. PLoS Pathogens, 2010. **6**(4): p. e1000848.
186. Girmenia, C., *New generation azole antifungals in clinical investigation*. Expert Opinion on Investigational Drugs, 2009. **18**(9): p. 1279-95.

187. Santos, J.R., et al., *Dynamic interaction between fluconazole and amphotericin B against Cryptococcus gattii*. Antimicrobial Agents and Chemotherapy, 2012. **56**(5): p. 2553-8.
188. Barchiesi, F., et al., *Interactions between triazoles and amphotericin B against Cryptococcus neoformans*. Antimicrobial Agents and Chemotherapy, 2000. **44**(9): p. 2435-41.
189. Schwarz, P., et al., *In vitro interaction of flucytosine with conventional and new antifungals against Cryptococcus neoformans clinical isolates*. Antimicrobial Agents and Chemotherapy, 2003. **47**(10): p. 3361-3364.
190. Ding, J.C., et al., *Effect of severity of meningitis on fungicidal activity of flucytosine combined with fluconazole in a murine model of cryptococcal meningitis*. Antimicrobial Agents and Chemotherapy, 1997. **41**(7): p. 1589-1593.
191. Nussbaum, J.C., et al., *Combination flucytosine and high-dose fluconazole compared with fluconazole monotherapy for the treatment of cryptococcal meningitis: a randomized trial in Malawi*. Clinical Infectious Diseases: An Official Publication of the Infectious Diseases Society of America, 2010. **50**(3): p. 338-44.
192. Bruggemann, R.J., et al., *Clinical relevance of the pharmacokinetic interactions of azole antifungal drugs with other coadministered agents*. Clinical Infectious Diseases: An Official Publication of the Infectious Diseases Society of America, 2009. **48**(10): p. 1441-58.
193. Barchiesi, F., et al., *In vitro interactions of itraconazole with flucytosine against clinical isolates of Cryptococcus neoformans*. The Journal of Antimicrobial Chemotherapy 1999. **44**(1): p. 65-70.
194. Polak, A., *Combination therapy of experimental candidiasis, cryptococcosis, aspergillosis and wangiellosis in mice*. Chemotherapy, 1987. **33**(5): p. 381-395.
195. Iovannitti, C., et al., *Itraconazole and flucytosine+itraconazole combination in the treatment of experimental cryptococcosis in hamsters*. Mycoses, 1995. **38**(11-12): p. 449-52.
196. Van Cutsem, J., *Therapy of experimental meningeal and disseminated cryptococcosis*. Mycoses, 1993. **36**(11-12): p. 357-67.
197. Johnson, L.B. and C.A. Kauffman, *Voriconazole: a new triazole antifungal agent*. Clinical Infectious Diseases: an Official Publication of the Infectious Diseases Society of America, 2003. **36**(5): p. 630-7.
198. Gazzoni, A.F., et al., *Efficacy of intrathecal administration of liposomal amphotericin B combined with voriconazole in a murine model of cryptococcal meningitis*. International Journal of Antimicrobial Agents, 2012. **39**(3): p. 223-7.
199. Silva, E.G., et al., *Voriconazole, combined with amphotericin B, in the treatment for pulmonary cryptococcosis caused by C. neoformans (serotype A) in mice with severe combined immunodeficiency (SCID)*. Mycopathologia, 2012. **173**(5-6): p. 445-449.
200. Gamaletsou, M.N., et al., *Successful salvage therapy of refractory HIV-related cryptococcal meningitis with the combination of liposomal amphotericin B, voriconazole, and recombinant interferon- γ* . Diagnostic Microbiology and Infectious Disease, 2012. **74**(4): p. 409-411.
201. Maligie, M.A. and C.P. Selitrennikoff, *Cryptococcus neoformans resistance to echinocandins: (1,3) beta-glucan synthase activity is sensitive to echinocandins*. Antimicrobial Agents and Chemotherapy, 2005. **49**(7): p. 2851-6.
202. Lanigan, R.S. and T.A. Yamarik, *Final report on the safety assessment of EDTA, calcium disodium EDTA, diammonium EDTA, dipotassium EDTA, disodium EDTA, TEA-EDTA, tetrasodium EDTA, tripotassium EDTA, trisodium EDTA, HEDTA, and trisodium HEDTA*. International Journal of Toxicology, 2002. **21** Suppl 2: p. 95-142.
203. Abrunhosa, L. and A. Venancio, *In vitro antifungal effect of EDTA disodium salt in tested black Aspergilli*. Asian Journal of Biochemistry, 2008. **3**(3): p. 176-181.
204. Seely, D.M., P. Wu, and E.J. Mills, *EDTA chelation therapy for cardiovascular disease: a systematic review*. BMC Cardiovascular Disorders, 2005. **5**: p. 32.

205. Elihu, N., S. Anandasbapathy, and W.H. Frishman, *Chelation therapy in cardiovascular disease: ethylenediaminetetraacetic acid, deferoxamine, and dexrazoxane*. Journal of Clinical Pharmacology, 1998. **38**(2): p. 101-5.
206. Cranton, E.M. *Scientific rationale for EDTA chelation therapy in treatment of atherosclerosis and diseases of aging*. 2013 03.07.2014 03.07.2014]; Available from: <http://drcranton.com/chelation/freeradical.htm>.
207. Kubo, I., S.H. Lee, and T.J. Ha, *Effect of EDTA alone and in combination with polygodial on the growth of Saccharomyces cerevisiae*. Journal of Agricultural and Food Chemistry, 2005. **53**(5): p. 1818-22.
208. Hachem, R., et al., *EDTA as an adjunct antifungal agent for invasive pulmonary aspergillosis in a rodent model*. Antimicrobial Agents and Chemotherapy, 2006. **50**(5): p. 1823-7.
209. El-Sharif, A.A. and M.H. Hussain, *Chitosan-EDTA new combination is a promising candidate for treatment of bacterial and fungal infections*. Current Microbiology, 2011. **62**(3): p. 739-45.
210. Ates, M., B.G. Akdeniz, and B.H. Sen, *The effect of calcium chelating or binding agents on Candida albicans*. Oral Surgery, Oral Medicine, Oral Pathology, Oral Radiology, and Endodontics, 2005. **100**(5): p. 626-30.
211. Robinson, D.J. and J.H. Raschke, *Inactivation of Tobacco Rattle Virus by EDTA, and the role of divalent metal ions in the stability of the virus*. Journal of General Virology, 1977. **34**: p. 547-550.
212. Reidmiller, J.S., et al., *Antimicrobial properties of the chelating agent EDTA on Streptococcal bovine mastitis isolates*. Journal of Food Protection, 2006. **69**(6): p. 1460-2.
213. Hinton, A.J. and K.D. Ingram, *Comparison of the antibacterial activity of chelating agents using the agar diffusion method*. International Journal of Poultry Science, 2010. **9**(11): p. 1023-1026.
214. Lambert, R.J., G.W. Hanlon, and S.P. Denyer, *The synergistic effect of EDTA/antimicrobial combinations on Pseudomonas aeruginosa*. Journal of Applied Microbiology, 2004. **96**(2): p. 244-53.
215. Al-Bakri, A.G., G. Othman, and Y. Bustanji, *The assessment of the antibacterial and antifungal activities of aspirin, EDTA and aspirin-EDTA combination and their effectiveness as antibiofilm agents*. Journal of Applied Microbiology, 2009. **107**(1): p. 280-6.
216. Venkatesh, M., et al., *Novel synergistic antibiofilm combinations for salvage of infected catheters*. Journal of Medical Microbiology, 2009. **58**(Pt 7): p. 936-44.
217. Ramage, G., B.L. Wickes, and J.L. Lopez-Ribot, *Inhibition on Candida albicans biofilm formation using divalent cation chelators (EDTA)*. Mycopathologia, 2007. **164**(6): p. 301-6.
218. Ward, P.P. and O.M. Conneely, *Lactoferrin: role in iron homeostasis and host defense against microbial infection*. Biometals, 2004. **17**(3): p. 203-8.
219. Adlerova, L., A. Bartoskova, and M. Faldyna, *Lactoferrin: a review*. Veterinarni Medicina, 2008. **9**(53): p. 457-468.
220. García-Montoya, I.A., et al., *Lactoferrin a multiple bioactive protein: an overview*. Biochimica et Biophysica Acta (BBA) - General Subjects, 2012. **1820**(3): p. 226-236.
221. Jenssen, H. and R.E. Hancock, *Antimicrobial properties of lactoferrin*. Biochimie, 2009. **91**(1): p. 19-29.
222. Zarembek, K.A., et al., *Human polymorphonuclear leukocytes inhibit Aspergillus fumigatus conidial growth by lactoferrin-mediated iron depletion*. Journal of Immunology, 2007. **178**(10): p. 6367-73.
223. Wakabayashi, H., et al., *Inhibition of hyphal growth of azole-resistant strains of Candida albicans by triazole antifungal agents in the presence of lactoferrin-related compounds*. Antimicrobial Agents and Chemotherapy, 1998. **42**(7): p. 1587-91.
224. Kim, W.-S., M.M. Rahman, and K.-I. Shimazaki, *Antibacterial activity and binding ability of bovine lactoferrin against Pseudomonas spp*. Journal of Food Safety, 2008. **28**(1): p. 23-33.

225. Lahoz, E., et al., *Fungistatic activity of iron-free bovin lactoferrin against several fungal plant pathogens and antagonists*. Natural Product Research, 2008. **22**(11): p. 955-961.
226. Soukka, T., J. Tenovuo, and M. Lenander-Lumikari, *Fungicidal effect of human lactoferrin against Candida albicans*. FEMS Microbiol Lett, 1992. **69**(3): p. 223-8.
227. Sinha, M., et al., *Antimicrobial lactoferrin peptides: the hidden players in the protective function of a multifunctional protein*. International Journal of Peptides, 2013. **2013**: p. 12.
228. Viejo-Diaz, M., M.T. Andres, and J.F. Fierro, *Different anti-Candida activities of two human lactoferrin-derived peptides, Lfpep and kaliocin-1*. Antimicrobial Agents and Chemotherapy, 2005. **49**(7): p. 2583-8.
229. Mishra, B., et al., *A novel antimicrobial peptide derived from modified N-terminal domain of bovine lactoferrin: design, synthesis, activity against multidrug-resistant bacteria and Candida*. Biochimica et Biophysica Acta, 2013. **1828**(2): p. 677-86.
230. Grammatikova, N.E., et al., *In vitro study of antimicrobial activity of lactoferrins from various sources*. Antibiotiki i Khimioterapiia, 2010. **55**(7-8): p. 4-9.
231. Sengupta, J., et al., *Effects of lactoferricin B against keratitis-associated fungal biofilms*. Journal of Infection and Chemotherapy, 2012. **18**(5): p. 698-703.
232. Moreau-Marquis, S., B. Coutermarsh, and B.A. Stanton, *Combination of hypothiocyanite and lactoferrin (ALX-109) enhances the ability of tobramycin and aztreonam to eliminate Pseudomonas aeruginosa biofilms growing on cystic fibrosis airway epithelial cells*. Journal of Antimicrobial Chemotherapy, 2015. **70**(1): p. 160-6.
233. Petitclerc, D., et al., *Efficacy of a lactoferrin-penicillin combination to treat {beta}-lactam-resistant Staphylococcus aureus mastitis*. Journal of Dairy Science, 2007. **90**(6): p. 2778-87.
234. Naidu, A.S., et al., *Activated lactoferrin and fluconazole synergism against Candida albicans and Candida glabrata vaginal isolates*. The Journal of Reproductive Medicine, 2004. **49**(10): p. 800-7.
235. Venkatesh, M.P. and L. Rong, *Human recombinant lactoferrin acts synergistically with antimicrobials commonly used in neonatal practice against coagulase-negative staphylococci and Candida albicans causing neonatal sepsis*. Journal of Medical Microbiology, 2008. **57**(Pt 9): p. 1113-21.
236. ESFA Panel on Dietetic Products, N.a.A.N., *Scientific opinion on bovine lactoferrin*. European Food Safety Authority Journal, 2012. **10**(5): p. 2701-2727.
237. Manzoni, P., et al., *Lactoferrin and prevention of late-onset sepsis in the pre-term neonates*. Early Human Development, 2010. **86 Suppl 1**: p. 59-61.
238. Carrillo-Munoz, A.J., et al., *Ciclopiroxolamine: in vitro antifungal activity against clinical yeast isolates*. International Journal of Antimicrobial Agents, 2002. **20**(5): p. 375-9.
239. Zhou, H., et al., *The antitumor activity of the fungicide ciclopirox*. International Journal of Cancer, 2010. **127**(10): p. 2467-77.
240. Abrams, B.B., H. Hanel, and T. Hoehler, *Ciclopirox olamine: a hydroxypyridone antifungal agent*. Clinics in Dermatology, 1991. **9**(4): p. 471-7.
241. Carlson-Banning, K.M., et al., *Toward repurposing ciclopirox as an antibiotic against drug-resistant Acinetobacter baumannii, Escherichia coli, and Klebsiella pneumoniae*. PLoS One, 2013. **8**(7): p. e69646.
242. Niewerth, M., et al., *Ciclopirox olamine treatment affects the expression pattern of Candida albicans genes encoding virulence factors, iron metabolism proteins, and drug resistance factors*. Antimicrobial Agents and Chemotherapy, 2003. **47**(6): p. 1805-17.
243. Sigle, H.C., et al., *Oxygen accessibility and iron levels are critical factors for the antifungal action of ciclopirox against Candida albicans*. The Journal of Antimicrobial Chemotherapy, 2005. **55**(5): p. 663-73.

244. Eberhard, Y., et al., *Chelation of intracellular iron with the antifungal agent ciclopirox olamine induces cell death in leukemia and myeloma cells*. Blood, 2009. **114**(14): p. 3064-73.
245. Matsuki, M., et al., *Effects of antifungal drugs on proliferation signals in Candida albicans*. Biological and Pharmaceutical Bulletin, 2006. **29**(5): p. 919-22.
246. Gupta, A.K. and Y. Kohli, *In vitro susceptibility testing of ciclopirox, terbinafine, ketoconazole and itraconazole against dermatophytes and nondermatophytes, and in vitro evaluation of combination antifungal activity*. The British Journal of Dermatology, 2003. **149**(2): p. 296-305.
247. Neufeld, E.J., *Update on iron chelators in thalassemia*. Hematology / The Education Program of the American Society of Hematology. American Society of Hematology. Education Program, 2010. **2010**: p. 451-5.
248. Richardson, D.R., *The therapeutic potential of iron chelators*. Expert Opinion on Investigational Drugs, 1999. **8**(12): p. 2141-2158.
249. Kontoghiorghes, G.J., et al., *Transfusional iron overload and chelation therapy with deferoxamine and deferiprone (L1)*. Transfusion science, 2000. **23**(3): p. 211-23.
250. Porter, J.B., et al., *Recent insights into interactions of deferoxamine with cellular and plasma iron pools: Implications for clinical use*. Annals of the New York Academy of Sciences, 2005. **1054**: p. 155-68.
251. Dias-Melicio, L.A., et al., *Inhibitory effect of deferoxamine on Paracoccidioides brasiliensis survival in human monocytes: reversal by holotransferrin not by apotransferrin*. Revista do Instituto de Medicina Tropical de Sao Paulo, 2005. **47**(5): p. 263-6.
252. Sheppard, L.N. and G.J. Kontoghiorghes, *Competition between deferiprone, desferrioxamine and other chelators for iron and the effect of other metals*. Arzneimittel-Forschung, 1993. **43**(6): p. 659-63.
253. Flournoy, D.J., *In vitro antimicrobial properties of deferoxamine mesylate*. European Journal of Clinical Microbiology and Infectious Diseases: Official Publication of the European Society of Clinical Microbiology, 1991. **10**(7): p. 597-8.
254. Gordeuk, V.R., et al., *Iron chelation with desferrioxamine B in adults with asymptomatic Plasmodium falciparum parasitemia*. Blood, 1992. **79**(2): p. 308-12.
255. Kim, C.M. and S.H. Shin, *Effect of iron-chelator deferiprone on the in vitro growth of staphylococci*. Journal of Korean Medical Science, 2009. **24**(2): p. 289-95.
256. van Asbeck, B.S., et al., *Inhibition of bacterial multiplication by the iron chelator deferoxamine: potentiating effect of ascorbic acid*. European Journal of Clinical Microbiology, 1983. **2**(5): p. 426-31.
257. Clarkson, A.B., et al., *Action of deferoxamine against Pneumocystis carinii*. Antimicrobial Agents and Chemotherapy, 2001. **45**(12): p. 3560-3565.
258. Shander, A. and J.D. Sweeney, *Overview of current treatment regimens in iron chelation therapy*. US Hematology, 2009. **2**(1): p. 56-9.
259. Boelaert, J.R., et al., *Deferoxamine augments growth and pathogenicity of Rhizopus, while hydroxypyridinone chelators have no effect*. Kidney International, 1994. **45**(3): p. 667-71.
260. Symeonidis, A.S., *The role of iron and iron chelators in zygomycosis*. Clinical Microbiology and Infection: The Official Publication of the European Society of Clinical Microbiology and Infectious Diseases, 2009. **15 Suppl 5**: p. 26-32.
261. Cappellini, M.D. and L. Zanaboni, *Efficacy and safety of deferasirox*. US Hematology, 2009. **2**(1): p. 68-79.
262. Dubey, A.P., S. Sudha, and A. Parakh, *Deferasirox: the new oral iron chelator*. Indian Pediatrics, 2007. **44**(8): p. 603-7.
263. Heli, H., S. Mirtorabi, and K. Karimian, *Advances in iron chelation: an update*. Expert Opinion on Therapeutic Patents, 2011. **21**(6): p. 819-56.

264. Kontoghiorghes, G.J., K. Neocleous, and A. Kolnagou, *Benefits and risks of deferiprone in iron overload in thalassaemia and other conditions: comparison of epidemiological and therapeutic aspects with deferoxamine*. Drug Safety: An International Journal of Medical Toxicology and Drug Experience, 2003. **26**(8): p. 553-84.
265. Devanur, L.D., et al., *Chelator-facilitated removal of iron from transferrin: relevance to combined chelation therapy*. The Biochemical journal, 2008. **409**(2): p. 439-47.
266. Kontoghiorghes, G.J., *New concepts of iron and aluminium chelation therapy with oral L1 (deferiprone) and other chelators. A review*. The Analyst, 1995. **120**(3): p. 845-51.
267. Lesic, B., J. Foulon, and E. Carniel, *Comparison of the effects of deferiprone versus deferoxamine on growth and virulence of Yersinia enterocolitica*. Antimicrobial Agents and Chemotherapy, 2002. **46**(6): p. 1741-5.
268. Kontoghiorghes, G.J., et al., *The role of iron and chelators on infections in iron overload and non iron loaded conditions: prospects for the design of new antimicrobial therapies*. Hemoglobin, 2010. **34**(3): p. 227-39.
269. Holbein, B.E. and R. Mira de Orduna, *Effect of trace iron levels and iron withdrawal by chelation on the growth of Candida albicans and Candida vini*. FEMS Microbiology Letters, 2010. **307**(1): p. 19-24.
270. Chan, G.C., et al., *Effects of chelators (deferoxamine, deferiprone and deferasirox) on the growth of Klebsiella pneumoniae and Aeromonas hydrophila isolated from transfusion-dependent thalassemia patients*. Hemoglobin, 2009. **33**(5): p. 352-60.
271. Neupane, G.P. and D.M. Kim, *In vitro time-kill activities of ciprofloxacin alone and in combination with the iron chelator deferasirox against Vibrio vulnificus*. European Journal of Clinical Microbiology and Infectious Diseases, 2010. **29**(4): p. 407-410.
272. Lewis, R.E., et al., *Activity of deferasirox in Mucorales: influences of species and exogenous iron*. Antimicrobial Agents and Chemotherapy, 2011. **55**(1): p. 411-3.
273. Zanette, R.A., et al., *Complex interaction of deferasirox and Pythium insidiosum: iron-dependent attenuation of growth in vitro and immunotherapy-like enhancement of immune responses in vivo*. PLoS One, 2015. **10**(3): p. e0118932.
274. Kontoyiannis, D.P., *Deferasirox lacks in vitro activity against Fusarium and Scedosporium species and black molds*. Virulence, 2011. **2**(3): p. 257-258.
275. Spellberg, B., et al., *The Deferasirox-AmBisome Therapy for Mucormycosis (DEFEAT Mucor) study: a randomized, double-blinded, placebo-controlled trial*. The Journal of Antimicrobial Chemotherapy, 2012. **67**(3): p. 715-22.
276. Farnaud, S. and R.W. Evans, *Lactoferrin-a multifunctional protein with antimicrobial properties*. Molecular Immunology, 2003. **40**(7): p. 395-405.
277. Bellamy, W., et al., *Antifungal properties of lactoferricin B, a peptide derived from the N-terminal region of bovine lactoferrin*. Letters in Applied Microbiology, 1994. **18**(4): p. 230-233.
278. Kondori, N., et al., *Fungicidal activity of human lactoferrin-derived peptides based on the antimicrobial alpha region*. International Journal of Antimicrobial Agents, 2011. **37**(1): p. 51-7.
279. Silva, T., et al., *Structural diversity and mode of action on lipid membranes of three lactoferrin candidacidal peptides*. Biochimica et Biophysica Acta (BBA) - Biomembranes, 2013. **1828**(5): p. 1329-1339.
280. Manzoni, P., et al., *Clinical use of lactoferrin in preterm neonates: an update*. Minerva Pediatrica, 2010. **62**(3 Suppl 1): p. 101-4.
281. Enrique, M., et al., *Antimicrobial action of synthetic peptides towards wine spoilage yeasts*. International Journal of Food Microbiology, 2007. **118**(3): p. 318-25.

282. Flora, S.J.S. and V. Pachauri, *Chelation in metal intoxication*. International Journal of Environmental Research and Public Health, 2010. **7**(7): p. 2745-2788.
283. Robertson, E.J., J.M. Wolf, and A. Casadevall, *EDTA inhibits biofilm formation, extracellular vesicular secretion, and shedding of the capsular polysaccharide glucuronoxylomannan by Cryptococcus neoformans*. Applied and Environmental Microbiology, 2012. **78**(22): p. 7977-84.
284. Ruhil, S., et al., *In vitro evaluation of combination of polyenes with EDTA against Aspergillus spp. by different methods (FICI and CI Model)*. Journal of Applied Microbiology, 2014. **117**(3): p. 643-53.
285. Gupta, A.K. and T. Plott, *Ciclopirox: a broad-spectrum antifungal with antibacterial and anti-inflammatory properties*. International Journal of Dermatology, 2004. **43 Suppl 1**: p. 3-8.
286. Wanner, R.M., et al., *Epolones induce erythropoietin expression via hypoxia-inducible factor-1 α activation*. Blood, 2000. **96**(4): p. 1558-1565.
287. Sakurai, K., et al., *Studies on uptake of 6-cyclohexyl-1-hydroxy-4-methyl-2(1H)-pyridone ethanamine salt (Hoe 296) by Candida albicans*. Chemotherapy, 1978. **24**(3): p. 146-153.
288. Gupta, A.K. and A.R. Skinner, *Ciclopirox for the treatment of superficial fungal infections: a review*. International Journal of Dermatology, 2003. **42 Suppl 1**: p. 3-9.
289. Subissi, A., et al., *Ciclopirox: recent nonclinical and clinical data relevant to its use as a topical antimycotic agent*. Drugs, 2010. **70**(16): p. 2133-52.
290. Weir, S.J., et al., *The repositioning of the anti-fungal agent ciclopirox olamine as a novel therapeutic agent for the treatment of haematologic malignancy*. Journal of Clinical Pharmacy and Therapeutics, 2011. **36**(2): p. 128-34.
291. Oliveira, P.C., et al., *Ciclopirox olamine: an antifungal alternative against cryptococcosis*. Letters in Applied Microbiology, 2010. **51**(5): p. 485-9.
292. Kokjohn, K., et al., *Evaluation of in vitro activity of ciclopirox olamine, butenafine HCl and econazole nitrate against dermatophytes, yeasts and bacteria*. International Journal of Dermatology, 2003. **42 Suppl 1**: p. 11-7.
293. Kim, J., et al., *A defect in iron uptake enhances the susceptibility of Cryptococcus neoformans to azole antifungal drugs*. Fungal Genetics and Biology, 2012. **49**(11): p. 955-966.
294. Van Cutsem, J. and J.R. Boelaert, *Effects of deferoxamine, feroxamine and iron on experimental mucormycosis (zygomycosis)*. Kidney International, 1989. **36**(6): p. 1061-8.
295. Jacobson, E.S., A.P. Goodner, and K.J. Nyhus, *Ferrous iron uptake in Cryptococcus neoformans*. Infection and Immunity, 1998. **66**(9): p. 4169-75.
296. Yun, C.W., et al., *Desferrioxamine-mediated iron uptake in Saccharomyces cerevisiae. Evidence for two pathways of iron uptake*. Journal of Biological Chemistry, 2000. **275**(14): p. 10709-15.
297. Espinel-Ingroff, A., et al., *Cryptococcus neoformans-Cryptococcus gattii species complex: an international study of wild-type susceptibility endpoint distributions and epidemiological cutoff values for amphotericin B and flucytosine*. Antimicrobial Agents and Chemotherapy, 2012. **56**(6): p. 3107-13.
298. Pfaller, M.A., et al., *Clinical breakpoints for the echinocandins and Candida revisited: integration of molecular, clinical, and microbiological data to arrive at species-specific interpretive criteria*. Drug Resistance Updates: Reviews and Commentaries in Antimicrobial and Anticancer Chemotherapy, 2011. **14**(3): p. 164-76.
299. Meletiadis, J., et al., *Assessing in vitro combinations of antifungal drugs against yeasts and filamentous fungi: comparison of different drug interaction models*. Medical Mycology, 2005. **43**(2): p. 133-52.
300. Acosta-Zaldivar, M., et al., *Human lactoferrin triggers a mitochondrial- and caspase-dependent regulated cell death in Saccharomyces cerevisiae*. Apoptosis, 2016. **21**(2): p. 163-73.

301. Chudzik, B., et al., *A new look at the antibiotic amphotericin B effect on Candida albicans plasma membrane permeability and cell viability functions*. European Biophysics Journal: EBJ, 2015. **44**(1): p. 77-90.
302. Linares, C.E., et al., *Fluconazole and amphotericin-B resistance are associated with increased catalase and superoxide dismutase activity in Candida albicans and Candida dubliniensis*. Revista da Sociedade Brasileira de Medicina Tropical, 2013. **46**(6): p. 752-8.
303. Mesa-Arango, A.C., et al., *The production of reactive oxygen species is a universal action mechanism of amphotericin B against pathogenic yeasts and contributes to the fungicidal effect of this drug*. Antimicrobial Agents and Chemotherapy, 2014. **58**(11): p. 6627-38.
304. Sokol-Anderson, M.L., J. Brajtburg, and G. Medoff, *Amphotericin B-induced oxidative damage and killing of Candida albicans*. The Journal of Infectious Diseases, 1986. **154**(1): p. 76-83.
305. Fiori, A. and P. Van Dijck, *Potent synergistic effect of doxycycline with fluconazole against Candida albicans is mediated by interference with iron homeostasis*. Antimicrobial Agents and Chemotherapy, 2012. **56**(7): p. 3785-96.
306. Crestani, J., et al., *Proteomic profiling of the influence of iron availability on Cryptococcus gattii*. Journal of Proteome Research, 2012. **11**(1): p. 189-205.
307. Shakoury-Elizeh, M., et al., *Metabolic response to iron deficiency in Saccharomyces cerevisiae*. The Journal of Biological Chemistry., 2010. **285**(19): p. 14823-18833.
308. Laniado-Laborin, R. and M.N. Cabrales-Vargas, *Amphotericin B: side effects and toxicity*. Revista Iberoamericana de Micologia, 2009. **26**(4): p. 223-7.
309. Zhang, L., et al., *High-throughput synergy screening identifies microbial metabolites as combination agents for the treatment of fungal infections*. Proceedings of the National Academy of Sciences, 2007. **104**(11): p. 4606-4611.
310. Brown, J.C., et al., *Unraveling the biology of a fungal meningitis pathogen using chemical genetics*. Cell, 2014. **159**(5): p. 1168-87.
311. Jansen, G., et al., *Chemogenomic profiling predicts antifungal synergies*. Molecular Systems Biology, 2009. **5**.
312. Chen, X., et al., *ASDCD: Antifungal Synergistic Drug Combination Database*. PLoS ONE, 2014. **9**(1): p. e86499.
313. Borisy, A.A., et al., *Systematic discovery of multicomponent therapeutics*. Proceedings of the National Academy of Sciences, 2003. **100**(13): p. 7977-7982.
314. Zhai, B., et al., *Polymyxin B, in combination with fluconazole, exerts a potent fungicidal effect*. Journal of Antimicrobial Chemotherapy, 2010. **65**(5): p. 931-938.
315. Kaneko, Y., et al., *Combinatory effect of fluconazole and FDA-approved drugs against Candida albicans*. Journal of Infection and Chemotherapy : Official Journal of the Japan Society of Chemotherapy, 2013. **19**(6): p. 1141-5.
316. Yin, N., et al., *Synergistic and antagonistic drug combinations depend on network topology*. PLoS One, 2014. **9**(4): p. e93960.
317. Yilancioglu, K., et al., *Target-independent prediction of drug synergies using only drug lipophilicity*. Journal of Chemical Information and Modeling, 2014. **54**(8): p. 2286-93.
318. Hu, Y. and J. Bajorath, *Compound promiscuity: what can we learn from current data?* Drug Discovery Today, 2013. **18**(13-14): p. 644-650.
319. Gregori-Puigjané, E., et al., *Identifying mechanism-of-action targets for drugs and probes*. Proceedings of the National Academy of Sciences, 2012. **109**(28): p. 11178-11183.
320. Cokol, M., et al., *Systematic exploration of synergistic drug pairs*. Molecular Systems Biology, 2011. **7**(1).
321. Li, L.P., et al., *Synergistic antifungal activity of berberine derivative B-7b and fluconazole*. PLoS One, 2015. **10**(5): p. e0126393.

322. Ashburner, M., et al., *Gene Ontology: tool for the unification of biology*. *The Gene Ontology Consortium*. *Nature Genetics*, 2000. **25**(1): p. 25-29.
323. Beissbarth, T. and T.P. Speed, *Gostat: find statistically overrepresented gene ontologies within a group of genes*. *Bioinformatics*, 2004. **20**(9): p. 1464-5.
324. Kohonen, T., *Self-organized formation of topologically correct feature maps*. *Biological Cybernetics*, 1982. **43**(1): p. 59-69.
325. Hans, B. and W. Henry, *Analysis of Large-Scale OMIC Data Using Self Organizing Maps*, in *Encyclopedia of Information Science and Technology, Third Edition*, K.-P. Mehdi, Editor. 2015, IGI Global: Hershey, PA, USA. p. 1642-1653.
326. Tamayo, P., et al., *Interpreting patterns of gene expression with self-organizing maps: methods and application to hematopoietic differentiation*. *Proceedings of the National Academy of Sciences of the United States of America*, 1999. **96**(6): p. 2907-12.
327. Törönen, P., et al., *Analysis of gene expression data using self-organizing maps*. *FEBS Letters*, 1999. **451**(2): p. 142-146.
328. Kohl, M., S. Wiese, and B. Warscheid, *Cytoscape: software for visualization and analysis of biological networks*, in *Data Mining in Proteomics*, M. Hamacher, M. Eisenacher, and C. Stephan, Editors. 2011, Humana Press. p. 291-303.
329. Shannon, P., et al., *Cytoscape: a software environment for integrated models of biomolecular interaction networks*. *Genome Research*, 2003. **13**(11): p. 2498-504.
330. Altmann, K., M. Durr, and B. Westermann, *Saccharomyces cerevisiae as a model organism to study mitochondrial biology: general considerations and basic procedures*. *Methods in Molecular Biology*, 2007. **372**: p. 81-90.
331. Drubin, D., *The yeast Saccharomyces cerevisiae as a model organism for the cytoskeleton and cell biology*. *Cell Motility and the Cytoskeleton*, 1989. **14**(1): p. 42-9.
332. Cherry, J.M., et al., *Saccharomyces Genome Database: the genomics resource of budding yeast*. *Nucleic Acids Research*, 2012. **40**(Database issue): p. D700-5.
333. Nasheuer, H.-P., et al., *Initiation of eukaryotic DNA replication: Regulation and mechanisms*, in *Progress in Nucleic Acid Research and Molecular Biology*. 2002, Academic Press. p. 41-94.
334. Murakami, C. and M. Kaeberlein, *Quantifying yeast chronological life span by outgrowth of aged cells*. *Journal of visualized experiments : JoVE*, 2009(27): p. 1156.
335. Miller-Fleming, L., F. Giorgini, and T.F. Outeiro, *Yeast as a model for studying human neurodegenerative disorders*. *Biotechnology Journal*, 2008. **3**(3): p. 325-38.
336. Schacherer, J., et al., *Genome-wide analysis of nucleotide-level variation in commonly used Saccharomyces cerevisiae strains*. *PLoS One*, 2007. **2**(3): p. e322.
337. Mortimer, R.K. and J.R. Johnston, *Genealogy of principal strains of the yeast genetic stock center*. *Genetics*, 1986. **113**(1): p. 35-43.
338. Goffeau, A., et al., *Life with 6000 genes*. *Science*, 1996. **274**(5287): p. 546-567.
339. Engel, S.R., et al., *The reference genome sequence of Saccharomyces cerevisiae: then and now*. *G3: Genes|Genomes|Genetics*, 2014. **4**(3): p. 389-398.
340. Brachmann, C.B., et al., *Designer deletion strains derived from Saccharomyces cerevisiae S288C: a useful set of strains and plasmids for PCR-mediated gene disruption and other applications*. *Yeast*, 1998. **14**(2): p. 115-32.
341. Kelly, D.E., D.C. Lamb, and S.L. Kelly, *Genome-wide generation of yeast gene deletion strains*. *Comparative and Functional Genomics*, 2001. **2**(4): p. 236-242.
342. Botstein, D. and G.R. Fink, *Yeast: an experimental organism for 21st century biology*. *Genetics*, 2011. **189**(3): p. 695-704.
343. Fasolo, J., et al., *Diverse protein kinase interactions identified by protein microarrays reveal novel connections between cellular processes*. *Genes & Development*, 2011. **25**(7): p. 767-778.

344. Bastos de Oliveira, F.M. and M.B. Smolka, *Identification of DNA damage checkpoint-dependent protein interactions in Saccharomyces cerevisiae using quantitative mass spectrometry*. *Methods in Molecular Biology* 2014. **1156**: p. 251-263.
345. Balakrishnan, R., et al., *YeastMine - an integrated data warehouse for Saccharomyces cerevisiae data as a multipurpose tool-kit*. *Database*, 2012. **2012**: p. bar062.
346. Zhang, L., et al., *Response of gene expression in Saccharomyces cerevisiae to amphotericin B and nystatin measured by microarrays*. *The Journal of Antimicrobial Chemotherapy*, 2002. **49**(6): p. 905-15.
347. Gasch, A.P., et al., *Genomic expression programs in the response of yeast cells to environmental changes*. *Molecular Biology of the Cell*, 2000. **11**(12): p. 4241-4257.
348. Spellman, P.T., et al., *Comprehensive identification of cell cycle-regulated genes of the yeast Saccharomyces cerevisiae by microarray hybridization*. *Molecular Biology of the Cell* 1998. **9**(12): p. 3273-97.
349. Maziarz, E.K. and J.R. Perfect, *Cryptococcosis*. *Infectious Disease Clinics of North America*, 2016. **30**(1): p. 179-206.
350. Nielsen, K., et al., *Sexual cycle of Cryptococcus neoformans var. grubii and virulence of congenic α and α isolates*. *Infection and Immunity*, 2003. **71**(9): p. 4831-4841.
351. Perfect, J.R. and A. Casadevall, *The history of Cryptococcus and Cryptococcosis*, in *Cryptococcus: from human pathogen to model yeast*. 2011, ASM Press: Washington, DC. p. 17-26.
352. Liu, O.W., et al., *Systematic genetic analysis of virulence in the human fungal pathogen Cryptococcus neoformans*. *Cell*, 2008. **135**(1): p. 174-188.
353. Jung, K.-W., et al., *Systematic functional profiling of transcription factor networks in Cryptococcus neoformans*. *Nature Communications*, 2015. **6**(6757).
354. Ianiri, G. and A. Idnurm, *Essential gene discovery in the basidiomycete Cryptococcus neoformans for antifungal drug target prioritization*. *MBio*, 2015. **6**(2).
355. Kim, H., et al., *Network-assisted genetic dissection of pathogenicity and drug resistance in the opportunistic human pathogenic fungus Cryptococcus neoformans*. *Scientific reports*, 2015. **5**(8767): p. 8767.
356. Chong, H.S., et al., *Time-course proteome analysis reveals the dynamic response of Cryptococcus gattii cells to fluconazole*. *PLoS One*, 2012. **7**(8): p. e42835.
357. Maeng, S., et al., *Comparative transcriptome analysis reveals novel roles of the Ras and cyclic AMP signaling pathways in environmental stress response and antifungal drug sensitivity in Cryptococcus neoformans*. *Eukaryotic Cell*, 2010. **9**(3): p. 360-78.
358. Ferreira, M., et al., *Transcriptome analysis of Aspergillus fumigatus exposed to voriconazole*. *Current Genetics*, 2006. **50**(1): p. 32-44.
359. Liu, T.T., et al., *Genome-wide expression profiling of the response to azole, polyene, echinocandin, and pyrimidine antifungal agents in Candida albicans*. *Antimicrobial Agents and Chemotherapy*, 2005. **49**(6): p. 2226-36.
360. Simpson, J.T., et al., *ABYSS: a parallel assembler for short read sequence data*. *Genome Research*, 2009. **19**(6): p. 1117-23.
361. Compeau, P.E.C., P.A. Pevzner, and G. Tesler, *How to apply de Bruijn graphs to genome assembly*. *Nature Biotechnology*, 2011. **29**(11): p. 987-991.
362. Earl, D., et al., *Assemblathon 1: A competitive assessment of de novo short read assembly methods*. *Genome Research*, 2011. **21**(12): p. 2224-2241.
363. Stanke, M., et al., *Gene prediction in eukaryotes with a generalized hidden Markov model that uses hints from external sources*. *BMC Bioinformatics*, 2006. **7**: p. 62-62.
364. Nagalakshmi, U., K. Waern, and M. Snyder, *RNA-Seq: a method for comprehensive transcriptome analysis*. *Current Protocols in Molecular Biology*, 2001. **Chapter 4**: p. Unit 4.11. 1-13.

365. Ewing, B. and P. Green, *Base-calling of automated sequencer traces using phred. II. Error probabilities*. Genome Research, 1998. **8**(3): p. 186-94.
366. Cox, M.P., D.A. Peterson, and P.J. Biggs, *SolexaQA: At-a-glance quality assessment of Illumina second-generation sequencing data*. BMC Bioinformatics, 2010. **11**: p. 485.
367. Trapnell, C., L. Pachter, and S.L. Salzberg, *TopHat: discovering splice junctions with RNA-Seq*. Bioinformatics, 2009. **25**(9): p. 1105-1111.
368. Anders, S., P.T. Pyl, and W. Huber, *HTSeq-a Python framework to work with high-throughput sequencing data*. Bioinformatics, 2014. **31**(2): p. 166-9.
369. Chen, Y., A.L. Lun, and G. Smyth, *Differential expression analysis of complex RNA-Seq experiments using edgeR*, in *Statistical Analysis of Next Generation Sequencing Data*, S. Datta and D. Nettleton, Editors. 2014, Springer International Publishing. p. 51-74.
370. Benjamini, Y. and Y. Hochberg, *Controlling the false discovery rate: a practical and powerful approach to multiple testing*. Journal of the Royal Statistical Society: Series B (Statistical Methodology), 1995. **57**(1): p. 289-300.
371. Kohonen, T., *Self-Organizing Maps*. Third ed. Springer Series in Information Sciences ed. T. Kohonen, M.R. Schroeder, and T.S. Huang. 2001, Springer-Verlag New York, Inc.: Springer Berlin Heidelberg. 528.
372. Wehren, R. and L.M.C. Buydens, *Self- and super-organizing maps in R: the kohonen package*. Journal of Statistical Software, 2007. **21**(5): p. 1-19.
373. Team, R.D.C., *R: A language and environment for statistical computing*. . 2005, R Foundation for Statistical Computing: Vienna, Austria.
374. Camacho, C., et al., *BLAST+: architecture and applications*. BMC Bioinformatics, 2009. **10**: p. 421.
375. Falcon, S. and R. Gentleman, *Using GOstats to test gene lists for GO term association*. Bioinformatics, 2007. **23**(2): p. 257-8.
376. Pollard, K.S., S. Dudoit, and M.J. van der Laan, *Multiple testing procedures: the multtest package and applications to genomics*, in *Bioinformatics and Computational Biology Solutions Using R and Bioconductor*, R. Gentleman, et al., Editors. 2005, Springer New York. p. 249-271.
377. Uniprot, *UniProt: a hub for protein information*. Nucleic Acids Research, 2015. **43**(Database issue): p. D204-12.
378. Binns, D., et al., *QuickGO: a web-based tool for Gene Ontology searching*. Bioinformatics, 2009. **25**(22): p. 3045-6.
379. Fischer, S., et al., *Using OrthoMCL to assign proteins to OrthoMCL-DB groups or to cluster proteomes into new ortholog groups*. Current Protocols in Bioinformatics 2011. **Chapter 6**: p. Unit 6.12.1-19.
380. Conesa, A., et al., *Blast2GO: a universal tool for annotation, visualization and analysis in functional genomics research*. Bioinformatics, 2005. **21**(18): p. 3674-6.
381. Smoot, M.E., et al., *Cytoscape 2.8: new features for data integration and network visualization*. Bioinformatics, 2011. **27**(3): p. 431-2.
382. Teixeira, M.C., et al., *The YEASTRACT database: an upgraded information system for the analysis of gene and genomic transcription regulation in Saccharomyces cerevisiae*. Nucleic Acids Research, 2014. **42**(Database issue): p. D161-6.
383. Pang, C.N., et al., *A multidimensional matrix for systems biology research and its application to interaction networks*. Journal of Proteome Research, 2012. **11**(11): p. 5204-20.
384. Kanehisa, M., et al., *KEGG for integration and interpretation of large-scale molecular data sets*. Nucleic Acids Research, 2012. **40**(Database issue): p. D109-14.
385. Janke, C., et al., *A versatile toolbox for PCR-based tagging of yeast genes: new fluorescent proteins, more markers and promoter substitution cassettes*. Yeast, 2004. **21**(11): p. 947-62.

386. Gietz, R.D. and R. Woods, *Yeast transformation by the LiAc/SS carrier DNA/PEG method*, in *Yeast Protocol*, W. Xiao, Editor. 2006, Humana Press. p. 107-120.
387. McCarthy, D.J., Y. Chen, and G.K. Smyth, *Differential expression analysis of multifactor RNA-Seq experiments with respect to biological variation*. *Nucleic Acids Research*, 2012. **40**(10): p. 4288-97.
388. Wiemken, A., *Trehalose in yeast, stress protectant rather than reserve carbohydrate*. *Antonie van Leeuwenhoek*, 1990. **58**(3): p. 209-217.
389. Filomeni, G., D. De Zio, and F. Cecconi, *Oxidative stress and autophagy: the clash between damage and metabolic needs*. *Cell Death & Differentiation*, 2015. **22**(3): p. 377-388.
390. Philpott, C.C., *Iron uptake in fungi: a system for every source*. *Biochimica et Biophysica Acta (BBA) - Molecular Cell Research*, 2006. **1763**(7): p. 636-645.
391. MacDiarmid, C.W., L.A. Gaither, and D. Eide, *Zinc transporters that regulate vacuolar zinc storage in *Saccharomyces cerevisiae**. *The EMBO Journal*, 2000. **19**(12): p. 2845-55.
392. Glerum, D.M., A. Shtanko, and A. Tzagoloff, *SCO1 and SCO2 act as high copy suppressors of a mitochondrial copper recruitment defect in *Saccharomyces cerevisiae**. *The Journal of Biological Chemistry*, 1996. **271**(34): p. 20531-5.
393. Gross, C., et al., *Identification of the copper regulon in *Saccharomyces cerevisiae* by DNA microarrays*. *The Journal of Biological Chemistry*, 2000. **275**(41): p. 32310-6.
394. Vest, K.E., et al., *Copper import into the mitochondrial matrix in *Saccharomyces cerevisiae* is mediated by Pic2, a mitochondrial carrier family protein*. *The Journal of Biological Chemistry*, 2013. **288**(33): p. 23884-92.
395. Yamaguchi-Iwai, Y., A. Dancis, and R.D. Klausner, *Aft1: a mediator of iron regulated transcriptional control in *Saccharomyces cerevisiae**. *The EMBO Journal*, 1995. **14**(6): p. 1231-9.
396. Eide, D.J., *Zinc transporters and the cellular trafficking of zinc*. *Biochimica et Biophysica Acta (BBA) - Molecular Cell Research*, 2006. **1763**(7): p. 711-722.
397. Zhao, H. and D.J. Eide, *Zap1p, a metalloregulatory protein involved in zinc-responsive transcriptional regulation in *Saccharomyces cerevisiae**. *Molecular and Cellular Biology*, 1997. **17**(9): p. 5044-52.
398. Belenky, P., D. Camacho, and J.J. Collins, *Fungicidal drugs induce a common oxidative-damage cellular death pathway*. *Cell Reports*, 2013. **3**(2): p. 350-8.
399. Leadsham, J.E. and C.W. Gourelay, *cAMP/PKA signaling balances respiratory activity with mitochondria dependent apoptosis via transcriptional regulation*. *BMC Cell Biology*, 2010. **11**: p. 92.
400. Lemasters, J.J., *Selective mitochondrial autophagy, or mitophagy, as a targeted defense against oxidative stress, mitochondrial dysfunction, and aging*. *Rejuvenation Research*, 2005. **8**(1): p. 3-5.
401. Benaroudj, N., D.H. Lee, and A.L. Goldberg, *Trehalose accumulation during cellular stress protects cells and cellular proteins from damage by oxygen radicals*. *The Journal of Biological Chemistry*, 2001. **276**(26): p. 24261-7.
402. Go, Y.-M., J.D. Chandler, and D.P. Jones, *The cysteine proteome*. *Free Radical Biology and Medicine*, 2015. **84**: p. 227-245.
403. Wu, C.Y., et al., *Repression of sulfate assimilation is an adaptive response of yeast to the oxidative stress of zinc deficiency*. *The Journal of Biological Chemistry*, 2009. **284**(40): p. 27544-56.
404. Ullrich, T.C., M. Blaesse, and R. Huber, *Crystal structure of ATP sulfurylase from *Saccharomyces cerevisiae*, a key enzyme in sulfate activation*. *The EMBO Journal*, 2001. **20**(3): p. 316-329.
405. Schwenn, J., F. Krone, and K. Husmann, *Yeast PAPS reductase: properties and requirements of the purified enzyme*. *Archives of Microbiology*, 1988. **150**(4): p. 313-319.

406. Forlani, N., E. Martegani, and L. Alberghina, *Posttranscriptional regulation of the expression of MET2 gene of Saccharomyces cerevisiae*. Biochimica et Biophysica Acta (BBA) - Gene Structure and Expression, 1991. **1089**(1): p. 47-53.
407. Blaiseau, P.L., et al., *Met31p and Met32p, two related zinc finger proteins, are involved in transcriptional regulation of yeast sulfur amino acid metabolism*. Molecular and Cellular Biology, 1997. **17**(7): p. 3640-8.
408. Iraqui, I., et al., *Characterisation of Saccharomyces cerevisiae ARO8 and ARO9 genes encoding aromatic aminotransferases I and II reveals a new aminotransferase subfamily*. Molecular Genetics and Genomics, 1998. **257**(2): p. 238-48.
409. Park, H. and A.T. Bakalinsky, *SSU1 mediates sulphite efflux in Saccharomyces cerevisiae*. Yeast, 2000. **16**(10): p. 881-8.
410. Fontecave, M., *Iron-sulfur clusters: ever-expanding roles*. Nature Chemical Biology, 2006. **2**(4): p. 171-4.
411. Kaur, J. and A.K. Bachhawat, *Yct1p, a novel, high-affinity, cysteine-specific transporter from the yeast Saccharomyces cerevisiae*. Genetics, 2007. **176**(2): p. 877-90.
412. Carrillo, E., et al., *Characterizing the roles of Met31 and Met32 in coordinating Met4-activated transcription in the absence of Met30*. Molecular Biology of the Cell, 2012. **23**(10): p. 1928-42.
413. Suzuki, K., et al., *Selective transport of α -mannosidase by autophagic pathways: identification of a novel receptor, Atg34p*. The Journal of Biological Chemistry, 2010. **285**(39): p. 30019-30025.
414. Dulubova, I., et al., *Convergence and divergence in the mechanism of SNARE binding by Sec1/Munc18-like proteins*. Proceedings of the National Academy of Sciences of the United States of America, 2003. **100**(1): p. 32-7.
415. Mijaljica, D. and R.J. Devenish, *Nucleophagy at a glance*. Journal of Cell Science, 2013. **126**(Pt 19): p. 4325-30.
416. Stolz, A. and D.H. Wolf, *Endoplasmic reticulum associated protein degradation: a chaperone assisted journey to hell*. Biochimica et Biophysica Acta (BBA) - Molecular Cell Research, 2010. **1803**(6): p. 694-705.
417. Gentzsch, M. and W. Tanner, *The PMT gene family: protein O-glycosylation in Saccharomyces cerevisiae is vital*. The EMBO journal, 1996. **15**(21): p. 5752-9.
418. Kumanovics, A., et al., *Identification of FRA1 and FRA2 as genes involved in regulating the yeast iron regulon in response to decreased mitochondrial iron-sulfur cluster synthesis*. The Journal of Biological Chemistry, 2008. **283**(16): p. 10276-86.
419. Eide, D.J., *Homeostatic and adaptive responses to zinc deficiency in Saccharomyces cerevisiae*. The Journal of Biological Chemistry, 2009. **284**(28): p. 18565-9.
420. Wu, C.Y., et al., *Differential control of Zap1-regulated genes in response to zinc deficiency in Saccharomyces cerevisiae*. BMC Genomics, 2008. **9**: p. 370.
421. Wu, Y.H., A.G. Frey, and D.J. Eide, *Transcriptional regulation of the Zrg17 zinc transporter of the yeast secretory pathway*. Biochemical Journal, 2011. **435**(1): p. 259-66.
422. Cyert, M.S., *Calcineurin signaling in Saccharomyces cerevisiae: how yeast go crazy in response to stress*. Biochemical and Biophysical Research Communications, 2003. **311**(4): p. 1143-1150.
423. Hay, J.C., *Calcium: a fundamental regulator of intracellular membrane fusion?* EMBO Reports, 2007. **8**(3): p. 236-240.
424. Malhotra, J.D. and R.J. Kaufman, *Endoplasmic reticulum stress and oxidative stress: a vicious cycle or a double-edged sword?* Antioxidants and redox signaling, 2007. **9**(12): p. 2277-93.
425. Measday, V., et al., *Systematic yeast synthetic lethal and synthetic dosage lethal screens identify genes required for chromosome segregation*. Proceedings of the National Academy of Sciences of the United States of America 2005. **102**(39): p. 13956-61.

426. Cebollero, E. and F. Reggiori, *Regulation of autophagy in yeast Saccharomyces cerevisiae*. Biochimica et Biophysica Acta (BBA) - Molecular Cell Research, 2009. **1793**(9): p. 1413-21.
427. Cheong, H., et al., *The Atg1 kinase complex is involved in the regulation of protein recruitment to initiate sequestering vesicle formation for nonspecific autophagy in Saccharomyces cerevisiae*. Molecular Biology of the Cell, 2008. **19**(2): p. 668-81.
428. Groppi, S., et al., *Glucose-induced calcium influx in budding yeast involves a novel calcium transport system and can activate calcineurin*. Cell Calcium, 2011. **49**(6): p. 376-86.
429. Kanzaki, M., et al., *Molecular identification of a eukaryotic, stretch-activated nonselective cation channel*. Science, 1999. **285**(5429): p. 882-6.
430. Bonilla, M., K.K. Nastase, and K.W. Cunningham, *Essential role of calcineurin in response to endoplasmic reticulum stress*. The EMBO Journal, 2002. **21**(10): p. 2343-2353.
431. Locke, E.G., et al., *A homolog of voltage-gated Ca(2+) channels stimulated by depletion of secretory Ca(2+) in yeast*. Molecular and Cellular Biology, 2000. **20**(18): p. 6686-94.
432. Viladevall, L., et al., *Characterization of the calcium-mediated response to alkaline stress in Saccharomyces cerevisiae*. The Journal of Biological Chemistry, 2004. **279**(42): p. 43614-24.
433. Ghislat, G. and E. Knecht, *Ca(2+)-sensor proteins in the autophagic and endocytic traffic*. Current Protein & Peptide Science, 2013. **14**(2): p. 97-110.
434. de Castro, P.A., et al., *The involvement of the Mid1/Cch1/Yvc1 calcium channels in Aspergillus fumigatus virulence*. PLoS One, 2014. **9**(8): p. e103957.
435. Toda, T., et al., *Three different genes in S. cerevisiae encode the catalytic subunits of the cAMP-dependent protein kinase*. Cell, 1987. **50**(2): p. 277-87.
436. Robertson, L.S., et al., *The yeast A kinases differentially regulate iron uptake and respiratory function*. Proceedings of the National Academy of Sciences of the United States of America, 2000. **97**(11): p. 5984-8.
437. Mattiazzi Usaj, M., et al., *Yeast Saccharomyces cerevisiae adiponectin receptor homolog Izh2 is involved in the regulation of zinc, phospholipid and pH homeostasis*. Metallomics, 2015. **7**(9): p. 1338-51.
438. De Nicola, R., et al., *Physiological and transcriptional responses of Saccharomyces cerevisiae to zinc limitation in chemostat cultures*. Applied and Environmental Microbiology, 2007. **73**(23): p. 7680-92.
439. Kung, L.A., et al., *Global analysis of the glycoproteome in Saccharomyces cerevisiae reveals new roles for protein glycosylation in eukaryotes*. Molecular Systems Biology, 2009. **5**: p. 308-308.
440. Terashima, H., et al., *Sequence-based approach for identification of cell wall proteins in Saccharomyces cerevisiae*. Current Genetics, 2002. **40**(5): p. 311-316.
441. Zhao, X.Q. and F.W. Bai, *Zinc and yeast stress tolerance: micronutrient plays a big role*. Journal of Biotechnology, 2012. **158**(4): p. 176-83.
442. Askwith, C., et al., *The FET3 gene of S. cerevisiae encodes a multicopper oxidase required for ferrous iron uptake*. Cell, 1994. **76**(2): p. 403-10.
443. Almeida, R.S., D. Wilson, and B. Hube, *Candida albicans iron acquisition within the host*. FEMS Yeast Research, 2009. **9**(7): p. 1000-1012.
444. Caza, M. and J.W. Kronstad, *Shared and distinct mechanisms of iron acquisition by bacterial and fungal pathogens of humans*. Frontiers in Cellular and Infection Microbiology, 2013. **3**: p. 80.
445. Ene, I.V., et al., *Carbon source-induced reprogramming of the cell wall proteome and secretome modulates the adherence and drug resistance of the fungal pathogen Candida albicans*. Proteomics, 2012. **12**(21): p. 3164-3179.
446. Narasimhan, M.L., et al., *Osmotin is a homolog of mammalian adiponectin and controls apoptosis in yeast through a homolog of mammalian adiponectin receptor*. Molecular Cell, 2005. **17**(2): p. 171-180.

447. Villa, N.Y., et al., *Phylogenetic and preliminary phenotypic analysis of yeast PAQR receptors: potential antifungal targets*. Journal of Molecular Evolution, 2011. **73**(3-4): p. 134-52.
448. Kupchak, B.R., et al., *Dissecting the regulation of yeast genes by the osmotin receptor*. Biochemical and Biophysical Research Communications 2008. **374**(2): p. 210-3.
449. Aouida, M., et al., *A Saccharomyces cerevisiae assay system to investigate ligand/AdipoR1 interactions that lead to cellular signaling*. PLoS One, 2013. **8**(6): p. e65454.
450. Villa, N.Y., et al., *Sphingolipids function as downstream effectors of a fungal PAQR*. Molecular Pharmacology, 2009. **75**(4): p. 866-75.
451. Lyons, T.J., et al., *Metalloregulation of yeast membrane steroid receptor homologs*. Proceedings of the National Academy of Sciences of the United States of America, 2004. **101**(15): p. 5506-5511.
452. Dickson, R.C., C. Sumanasekera, and R.L. Lester, *Functions and metabolism of sphingolipids in Saccharomyces cerevisiae*. Progress in Lipid Research, 2006. **45**(6): p. 447-465.
453. Siafakas, A.R., et al., *Lipid rafts in Cryptococcus neoformans concentrate the virulence determinants phospholipase B1 and Cu/Zn superoxide dismutase*. Eukaryotic Cell, 2006. **5**(3): p. 488-98.
454. Mannhaupt, G., et al., *Yeast homoserine kinase. Characteristics of the corresponding gene, THR1, and the purified enzyme, and evolutionary relationships with other enzymes of threonine metabolism*. European Journal of Biochemistry, 1990. **191**(1): p. 115-22.
455. Kingsbury, J.M. and J.H. McCusker, *Homoserine toxicity in Saccharomyces cerevisiae and Candida albicans homoserine kinase (thr1Δ) mutants*. Eukaryotic Cell, 2010. **9**(5): p. 717-28.
456. Kingsbury, J.M. and J.H. McCusker, *Threonine biosynthetic genes are essential in Cryptococcus neoformans*. Microbiology, 2008. **154**(Pt 9): p. 2767-75.
457. Kingsbury, J.M. and J.H. McCusker, *Fungal homoserine kinase (thr1Δ) mutants are attenuated in virulence and die rapidly upon threonine starvation and serum incubation*. Eukaryotic Cell, 2010. **9**(5): p. 729-37.
458. Jastrzębowska, K. and I. Gabriel, *Inhibitors of amino acids biosynthesis as antifungal agents*. Amino Acids, 2015. **47**(2): p. 227-249.
459. Law, V., et al., *DrugBank 4.0: shedding new light on drug metabolism*. Nucleic Acids Research 2014. **42**(Database issue): p. D1091-7.
460. Finn, R.D., et al., *Pfam: the protein families database*. Nucleic Acids Research, 2014. **42**(Database issue): p. D222-30.
461. West, M.G., C.K. Barlowe, and D.R. Appling, *Cloning and characterization of the Saccharomyces cerevisiae gene encoding NAD-dependent 5,10-methylenetetrahydrofolate dehydrogenase*. The Journal of Biological Chemistry, 1993. **268**(1): p. 153-60.
462. Blankenship, J.R., et al., *Teaching old drugs new tricks: reincarnating immunosuppressants as antifungal drugs*. Curr Opin Investig Drugs, 2003. **4**(2): p. 192-9.
463. Agarwal, A.K., et al., *Genome-wide expression profiling of the response to polyene, pyrimidine, azole, and echinocandin antifungal agents in Saccharomyces cerevisiae*. The Journal of biological chemistry, 2003. **278**(37): p. 34998-5015.
464. Andres, M.T. and J.F. Fierro, *Antimicrobial mechanism of action of transferrins: selective inhibition of H⁺-ATPase*. Antimicrobial Agents and Chemotherapy, 2010. **54**(10): p. 4335-42.
465. Andrés, M.T., M. Viejo-Díaz, and J.F. Fierro, *Human lactoferrin induces apoptosis-like cell death in Candida albicans: critical role of K⁺-channel-mediated K⁺ efflux*. Antimicrobial Agents and Chemotherapy, 2008. **52**(11): p. 4081-4088.
466. Viejo-Díaz, M., M.T. Andres, and J.F. Fierro, *Modulation of in vitro fungicidal activity of human lactoferrin against Candida albicans by extracellular cation concentration and target cell metabolic activity*. Antimicrobial Agents and Chemotherapy, 2004. **48**(4): p. 1242-8.

467. Viejo-Diaz, M., M.T. Andres, and J.F. Fierro, *Effects of human lactoferrin on the cytoplasmic membrane of Candida albicans cells related with its candidacidal activity*. FEMS Immunology and Medical Microbiology, 2004. **42**(2): p. 181-5.
468. Gonzalez-Parraga, P., et al., *Amphotericin B induces trehalose synthesis and simultaneously activates an antioxidant enzymatic response in Candida albicans*. Biochim Biophys Acta, 2011. **1810**(8): p. 777-83.
469. Sangalli-Leite, F., et al., *Amphotericin B mediates killing in Cryptococcus neoformans through the induction of a strong oxidative burst*. Microbes and Infection, 2011. **13**(5): p. 457-67.
470. Kovacic, P. and A. Cooksy, *Novel, unifying mechanism for amphotericin B and other polyene drugs: electron affinity, radicals, electron transfer, autoxidation, toxicity, and antifungal action*. Medicinal Chemical Communications, 2012. **3**(3): p. 274-280.
471. Ferreira, G.F., et al., *The role of oxidative and nitrosative bursts caused by azoles and amphotericin B against the fungal pathogen Cryptococcus gattii*. The Journal of Antimicrobial Chemotherapy, 2013. **68**(8): p. 1801-11.
472. Stephen, D.W. and D.J. Jamieson, *Glutathione is an important antioxidant molecule in the yeast Saccharomyces cerevisiae*. FEMS Microbiology Letters, 1996. **141**(2-3): p. 207-12.
473. Fujita, Y., et al., *Homocysteine accumulation causes a defect in purine biosynthesis: further characterization of Schizosaccharomyces pombe methionine auxotrophs*. Microbiology, 2006. **152**(Pt 2): p. 397-404.
474. Perna, A.F., et al., *Possible mechanisms of homocysteine toxicity*. Kidney International, 2003. **63**(S84): p. S137-S140.
475. Landau, G., et al., *Chapter fourteen - detection of oxidative damage in response to protein misfolding in the endoplasmic reticulum*, in *Methods in Enzymology*, C. Enrique and P. Lester, Editors. 2013, Academic Press. p. 231-250.
476. Chakravarthi, S., C.E. Jessop, and N.J. Bulleid, *The role of glutathione in disulphide bond formation and endoplasmic-reticulum-generated oxidative stress*. EMBO Reports, 2006. **7**(3): p. 271-275.
477. Sevier, C.S., et al., *Modulation of cellular disulfide-bond formation and the ER redox environment by feedback regulation of Ero1*. Cell, 2007. **129**(2): p. 333-44.
478. Eide, D.J., *The oxidative stress of zinc deficiency*. Metallomics, 2011. **3**(11): p. 1124-9.
479. Kaloriti, D., et al., *Mechanisms underlying the exquisite sensitivity of Candida albicans to combinatorial cationic and oxidative stress that enhances the potent fungicidal activity of phagocytes*. MBio, 2014. **5**(4): p. e01334-14.
480. Kaloriti, D., et al., *Combinatorial stresses kill pathogenic Candida species*. Medical Mycology, 2012. **50**(7): p. 699-709.
481. Bahn, Y.S. and K.W. Jung, *Stress signaling pathways for the pathogenicity of cryptococcus*. Eukaryot Cell, 2013. **12**(12): p. 1564-77.
482. Kaiser, P., et al., *Regulation of transcription by ubiquitination without proteolysis: Cdc34/SCF^{Met30}-mediated inactivation of the transcription factor Met4*. Cell, 2000. **102**(3): p. 303-314.
483. Tokunaga, M., A. Kawamura, and K. Kohno, *Purification and characterization of BiP/Kar2 protein from Saccharomyces cerevisiae*. The Journal of Biological Chemistry, 1992. **267**(25): p. 17553-9.
484. Hsu, C.-L., et al., *Endoplasmic reticulum stress regulation of the Kar2p/BiP chaperone alleviates proteotoxicity via dual degradation pathways*. Molecular Biology of the Cell, 2012. **23**(4): p. 630-641.
485. Normington, K., et al., *S. cerevisiae encodes an essential protein homologous in sequence and function to mammalian BiP*. Cell, 1989. **57**(7): p. 1223-36.

486. Kimata, Y., et al., *Genetic evidence for a role of BiP/Kar2 that regulates Ire1 in response to accumulation of unfolded proteins*. *Molecular Biology of the Cell* 2003. **14**(6): p. 2559-69.
487. Sidrauski, C. and P. Walter, *The transmembrane kinase Ire1p is a site-specific endonuclease that initiates mRNA splicing in the unfolded protein response*. *Cell*, 1997. **90**(6): p. 1031-1039.
488. Ellis, C.D., et al., *Zinc and the Msc2 zinc transporter protein are required for endoplasmic reticulum function*. *The Journal of Cell Biology*, 2004. **166**(3): p. 325-335.
489. Wu, C.Y., et al., *Regulation of the yeast TSA1 peroxiredoxin by ZAP1 is an adaptive response to the oxidative stress of zinc deficiency*. *The Journal of Biological Chemistry*, 2007. **282**(4): p. 2184-95.
490. Kato, M. and W. Wickner, *Ergosterol is required for the Sec18/ATP-dependent priming step of homotypic vacuole fusion*. *The EMBO journal*, 2001. **20**(15): p. 4035-40.
491. Zhang, Y.Q., et al., *Requirement for ergosterol in V-ATPase function underlies antifungal activity of azole drugs*. *PLoS Pathogens*, 2010. **6**(6): p. e1000939.
492. Kagan, S., et al., *Toxicity mechanisms of amphotericin B and its neutralization by conjugation with arabinogalactan*. *Antimicrobial Agents and Chemotherapy*, 2012. **56**(11): p. 5603-11.
493. Waterman, S.R., et al., *Role of CTR4 in the Virulence of Cryptococcus neoformans*. *MBio*, 2012. **3**(5).
494. Fu, D., T.J. Beeler, and T.M. Dunn, *Sequence, mapping and disruption of CCC2, a gene that cross-complements the Ca(2+)-sensitive phenotype of csg1 mutants and encodes a P-type ATPase belonging to the Cu(2+)-ATPase subfamily*. *Yeast*, 1995. **11**(3): p. 283-92.
495. Ko, Y.-J., et al., *Remodeling of Global Transcription Patterns of Cryptococcus neoformans Genes Mediated by the Stress-Activated HOG Signaling Pathways*. *Eukaryotic Cell*, 2009. **8**(8): p. 1197-1217.
496. Bermingham-McDonogh, O., E.B. Gralla, and J.S. Valentine, *The copper, zinc-superoxide dismutase gene of Saccharomyces cerevisiae: cloning, sequencing, and biological activity*. *Proceedings of the National Academy of Sciences*, 1988. **85**(13): p. 4789-4793.
497. Hortschansky, P., et al., *Interaction of HapX with the CCAAT-binding complex—a novel mechanism of gene regulation by iron*. *The EMBO Journal*, 2007. **26**(13): p. 3157-3168.
498. Pujol-Carrion, N., et al., *The MAP kinase Slt2 is involved in vacuolar function and actin remodeling in Saccharomyces cerevisiae mutants affected by endogenous oxidative stress*. *Appl Environ Microbiol*, 2013. **79**(20): p. 6459-71.
499. Fujita, M. and T. Kinoshita, *GPI-anchor remodeling: Potential functions of GPI-anchors in intracellular trafficking and membrane dynamics*. *Biochimica et Biophysica Acta (BBA) - Molecular and Cell Biology of Lipids*, 2012. **1821**(8): p. 1050-1058.
500. Hong, W. and S. Lev, *Tethering the assembly of SNARE complexes*. *Trends in Cell Biology*, 2014. **24**(1): p. 35-43.
501. Karunakaran, S., et al., *SNAREs, HOPS and regulatory lipids control the dynamics of vacuolar actin during homotypic fusion in S. cerevisiae*. *J Cell Sci*, 2012. **125**(Pt 7): p. 1683-92.
502. Geddes, J., *Proteomic profiling of the pathogenic fungus Cryptococcus neoformans upon regulation of the cyclic-AMP/protein kinase A signaling pathway*, in *Microbiology and Immunology*. 2015, The University of British Columbia: Vancouver. p. 349.
503. Olesen, J.T. and L. Guarente, *The HAP2 subunit of yeast CCAAT transcriptional activator contains adjacent domains for subunit association and DNA recognition: model for the HAP2/3/4 complex*. *Genes Dev*, 1990. **4**(10): p. 1714-29.
504. Choi, J.N., et al., *Influence of Iron Regulation on the Metabolome of Cryptococcus neoformans*. *PLoS ONE*, 2012. **7**(7): p. e41654.
505. Upadhyya, R., et al., *Global Transcriptome Profile of Cryptococcus neoformans during Exposure to Hydrogen Peroxide Induced Oxidative Stress*. *PLoS ONE*, 2013. **8**(1): p. e55110.

506. Kadowaki, H. and H. Nishitoh, *Signaling Pathways from the Endoplasmic Reticulum and Their Roles in Disease*. Genes, 2013. **4**(3): p. 306-333.
507. Alberts, B., et al., *Transport from the ER through through the Golgi Aparatus in Molecular Biology of the Cell 2002*, Garland Science New York
508. Cooper, G.M., *The endoplasmic reticulum*, in *The Cell: A Molecular Approach*, S. (MA), Editor. 2000, Sinauer Associates
509. Gerlach, Q.J., et al., *A tight-knit group: protein glycosylation, endoplasmic reticulum stress and the unfolded protein response*, in *Endoplasmic Reticulum Stress in Health and Disease*, P. Agostinis and S. Afshin, Editors. 2012, Springer Netherlands: Dordrecht. p. 23-39.
510. Hohmann, S., *Osmotic stress signaling and osmoadaptation in yeasts*. Microbiology and Molecular Biology Reviews, 2002. **66**(2): p. 300-372.
511. Ljungdahl, P.O. and B. Daignan-Fornier, *Regulation of amino acid, nucleotide, and phosphate metabolism in Saccharomyces cerevisiae*. Genetics, 2012. **190**(3): p. 885-929.
512. Kwok, E. and D. Kosman, *Iron in yeast: Mechanisms involved in homeostasis*, in *Molecular Biology of Metal Homeostasis and Detoxification*, M. Tamas and E. Martinoia, Editors. 2006, Springer Berlin Heidelberg. p. 59-99.
513. Gunter, T.E., et al., *Mitochondrial calcium transport: mechanisms and functions*. Cell Calcium, 2000. **28**(5): p. 285-296.
514. Iannuzzi, C., et al., *The role of zinc in the stability of the marginally stable IscU scaffold protein*. Protein Science, 2014. **23**(9): p. 1208-1219.
515. Chillappagari, S., et al., *Copper stress affects iron homeostasis by destabilizing iron-sulfur cluster formation in Bacillus subtilis*. J Bacteriol, 2010. **192**(10): p. 2512-24.
516. Stehling, O. and R. Lill, *The role of mitochondria in cellular iron-sulfur protein biogenesis: mechanisms, connected processes, and diseases*. Cold Spring Harb Perspect Biol, 2013. **5**(8): p. a011312.
517. Reeder, N.L., et al., *Zinc Pyrithione Inhibits Yeast Growth through Copper Influx and Inactivation of Iron-Sulfur Proteins*. Antimicrobial Agents and Chemotherapy, 2011. **55**(12): p. 5753-5760.
518. Yasokawa, D., et al., *DNA microarray analysis suggests that zinc pyrithione causes iron starvation to the yeast Saccharomyces cerevisiae*. J Biosci Bioeng, 2010. **109**(5): p. 479-86.
519. Schneider, R.d.O., et al., *Zap1 Regulates Zinc Homeostasis and Modulates Virulence in <italic>Cryptococcus gattii</italic>*. PLoS ONE, 2012. **7**(8): p. e43773.
520. Borjihan, H., et al., *The vacuole-targeting fungicidal activity of amphotericin B against the pathogenic fungus Candida albicans and its enhancement by allicin*. J Antibiot, 2009. **62**(12): p. 691-697.
521. McAbee, D.D., *Isolated rat hepatocytes acquire iron from lactoferrin by endocytosis*. Biochemical Journal, 1995. **311**(Pt 2): p. 603-609.
522. Zhao, H., et al., *Regulation of zinc homeostasis in yeast by binding of the Zap1 transcriptional activator to zinc-responsive promoter elements*. Journal of Biological Chemistry, 1998. **273**(44): p. 28713-28720.
523. Cannon, R.D., et al., *Efflux-mediated antifungal drug resistance*. Clinical Microbiology Reviews, 2009. **22**(2): p. 291-321, Table of Contents.
524. Prasad, R. and M.K. Rawal, *Efflux pump proteins in antifungal resistance*. Frontiers in Pharmacology, 2014. **5**(202): p. 10.3389/fphar.2014.00202.
525. Yang, M.L., et al., *Fluconazole susceptibility in Cryptococcus gattii Is dependent on the ABC transporter Pdr11*. Antimicrobial Agents and Chemotherapy 2015. **60**(3): p. 1202-7.
526. Keeratavasee, S., et al., *Heteroresistance to fluconazole among isolates of Cryptococcus neoformans in Northern Thailand*. African Journal of Microbiology Research, 2013. **7**(32): p. 4096-4102.

527. Price, C.T.D., I.R. Lee, and J.E. Gustafson, *The effects of salicylate on bacteria*. The International Journal of Biochemistry & Cell Biology, 2000. **32**(10): p. 1029-1043.
528. Wood, K.B. and P. Cluzel, *Trade-offs between drug toxicity and benefit in the multi-antibiotic resistance system underlie optimal growth of E. coli*. BMC Systems Biology, 2012. **6**(48): p. 10.1186/1752-0509-6-48.
529. Ferrari, S., et al., *Loss of mitochondrial functions associated with azole resistance in Candida glabrata results in enhanced virulence in mice*. Antimicrob Agents Chemother, 2011. **55**(5): p. 1852-60.
530. Cheng, S., et al., *A Candida albicans Petite Mutant Strain with Uncoupled Oxidative Phosphorylation Overexpresses MDR1 and Has Diminished Susceptibility to Fluconazole and Voriconazole*. Antimicrobial Agents and Chemotherapy, 2007. **51**(5): p. 1855-1858.
531. Sanglard, D., F. Ischer, and J. Bille, *Role of ATP-binding-cassette transporter genes in high-frequency acquisition of resistance to azole antifungals in Candida glabrata*. Antimicrob Agents Chemother, 2001. **45**(4): p. 1174-83.
532. Panepinto, J.C., et al., *Overexpression of TUF1 restores respiratory growth and fluconazole sensitivity to a Cryptococcus neoformans vad1Δ mutant*. Microbiology, 2010. **156**(Pt 8): p. 2558-2565.
533. Veatch, J.R., et al., *Mitochondrial dysfunction leads to nuclear genome instability via an iron-sulfur cluster defect*. Cell, 2009. **137**(7): p. 1247-1258.
534. Thomas, E., et al., *Mitochondria influence CDR1 efflux pump activity, Hog1-mediated oxidative stress pathway, iron homeostasis, and ergosterol levels in Candida albicans*. Antimicrob Agents Chemother, 2013. **57**(11): p. 5580-99.
535. Sun, N., et al., *Azole susceptibility and transcriptome profiling in Candida albicans mitochondrial electron transport chain complex I mutants*. Antimicrobial Agents and Chemotherapy, 2013. **57**(1): p. 532-42.
536. Elferink, J.G., *The effect of ethylenediaminetetraacetic acid on yeast cell membranes*. Protoplasma, 1974. **80**(1): p. 261-8.
537. Bahn, Y.-S., et al., *A unique fungal two-component system regulates stress responses, drug sensitivity, sexual development, and virulence of Cryptococcus neoformans*. Molecular Biology of the Cell, 2006. **17**(7): p. 3122-3135.
538. Bradshaw, P.C. and D.R. Pfeiffer, *Release of Ca²⁺ and Mg²⁺ from yeast mitochondria is stimulated by increased ionic strength*. BMC Biochemistry, 2006. **7**(1): p. 1-12.
539. D'Souza, C.A., et al., *Genome variation in Cryptococcus gattii, an emerging pathogen of immunocompetent hosts*. MBio, 2011. **2**(1): p. e00342-10.
540. Casadevall, A. and J.R. Perfect, *Cryptococcosis*. 1998, Washington, D.C.: ASM Press.
541. Pfaller, M.A., *Antifungal Drug Resistance: Mechanisms, Epidemiology, and Consequences for Treatment*. The American Journal of Medicine. **125**(1): p. S3-S13.
542. Chen, Y., et al., *The Cryptococcus neoformans transcriptome at the site of human meningitis*. MBio, 2014. **5**(1): p. e01087-13.
543. Brand, Martin D. and David G. Nicholls, *Assessing mitochondrial dysfunction in cells*. Biochemical Journal, 2011. **435**(Pt 2): p. 297-312.
544. Cai, J., J. Yang, and D. Jones, *Mitochondrial control of apoptosis: the role of cytochrome c*. Biochimica et Biophysica Acta (BBA) - Bioenergetics, 1998. **1366**(1-2): p. 139-149.
545. George, N.I., et al., *An iterative leave-one-out approach to outlier detection in RNA-Seq data*. PLoS ONE, 2015. **10**(6): p. e0125224.
546. Palma-Guerrero, J., et al., *Comparative transcriptomic analyses of Zymoseptoria tritici strains show complex lifestyle transitions and intraspecific variability in transcription profiles*. Molecular Plant Pathology, 2016. **17**(6): p. 845-859.

547. Matsumura, H., et al., *Transcriptome analysis reveals an unexpected role of a collagen tyrosine kinase receptor gene, Ddr2, as a regulator of ovarian function*. *Physiological Genomics*, 2009. **39**(2): p. 120-129.
548. Moya, A., et al., *Whole transcriptome analysis of the coral *Acropora millepora* reveals complex responses to CO₂-driven acidification during the initiation of calcification*. *Molecular Ecology*, 2012. **21**(10): p. 2440-2454.
549. Lamoth, F., et al., *Antifungal activity of compounds targeting the Hsp90-calcineurin pathway against various mould species*. *Journal of Antimicrobial Chemotherapy*, 2015. **70**(5): p. 1408-1411.
550. Zhang, J., et al., *Antifungal activity of geldanamycin alone or in combination with fluconazole against *Candida* species*. *Mycopathologia*, 2013. **175**(3-4): p. 273-9.
551. Pagani, M.A., et al., *Disruption of iron homeostasis in *Saccharomyces cerevisiae* by high zinc levels: a genome-wide study*. *Molecular Microbiology*, 2007. **65**(2): p. 521-537.
552. Qin, Y., et al., *Measuring steady-state and dynamic endoplasmic reticulum and Golgi Zn(2+) with genetically encoded sensors*. *Proceedings of the National Academy of Sciences of the United States of America*, 2011. **108**(18): p. 7351-7356.
553. Schrettl, M., et al., *Siderophore biosynthesis but not reductive iron assimilation is essential for *Aspergillus fumigatus* virulence*. *The Journal of Experimental Medicine*, 2004. **200**(9): p. 1213-9.
554. Zhang, Y., S. Muend, and R. Rao, *DYSREGULATION OF ION HOMEOSTASIS BY ANTIFUNGAL AGENTS*. *Frontiers in Microbiology*, 2012. **3**.
555. Vicentefranqueira, R., et al., *Targeting zinc homeostasis to combat *Aspergillus fumigatus* infections*. *Frontiers in Microbiology*, 2015. **6**: p. 160.
556. Gupta, S.S., et al., *Antifungal activity of amiodarone is mediated by disruption of calcium homeostasis*. *J Biol Chem*, 2003. **278**(31): p. 28831-9.
557. Han, K., E. Do, and W.H. Jung, *A human fungal pathogen *Cryptococcus neoformans* expresses three distinct iron permease homologs*. *J Microbiol Biotechnol*, 2012. **22**(12): p. 1644-1652.
558. Do, E., et al., *The ZIP family zinc transporters support the virulence of *Cryptococcus neoformans**. *Medical Mycology*, 2016. **54**(6): p. 605-615.
559. Moastafa, T.M., et al., *Study on the therapeutic benefit on lactoferrin in patients with colorectal cancer receiving chemotherapy*. *International Scholarly Research Notices*, 2014. **2014**: p. 10.
560. Kaito, M., et al., *Effect of lactoferrin in patients with chronic hepatitis C: combination therapy with interferon and ribavirin*. *Journal of Gastroenterology and Hepatology*, 2007. **22**(11): p. 1894-7.
561. Guntupalli, K., et al., *A phase 2 randomized, double-blind, placebo-controlled study of the safety and efficacy of talactoferrin in patients with severe sepsis*. *Critical Care Medicine*, 2013. **41**(3): p. 706-16.
562. Manzoni, P., et al., *Bovine lactoferrin prevents invasive fungal infections in very low birth weight infants: a randomized controlled trial*. *Pediatrics*, 2012. **129**(1): p. 116-23.
563. Todd, R.B., et al., *Prevalence of transcription factors in ascomycete and basidiomycete fungi*. *BMC Genomics*, 2014. **15**(1): p. 1-12.
564. Nikolaou, E., et al., *Phylogenetic diversity of stress signalling pathways in fungi*. *BMC Evolutionary Biology*, 2009. **9**(1): p. 1-18.
565. Goddard, M.R. and D. Greig, **Saccharomyces cerevisiae*: a nomadic yeast with no niche?* *FEMS Yeast Research*, 2015. **15**(3): p. fov009.
566. Ménez, C., et al., *Interaction between miltefosine and amphotericin B: consequences for their activities towards intestinal epithelial cells and *Leishmania donovani* promastigotes in vitro*. *Antimicrobial Agents and Chemotherapy*, 2006. **50**(11): p. 3793-3800.

567. Bollenbach, T., *Antimicrobial interactions: mechanisms and implications for drug discovery and resistance evolution*. Current Opinion in Microbiology, 2015. **27**: p. 1-9.
568. Hill, J.A., T.R. O'Meara, and L.E. Cowen, *Fitness Trade-Offs Associated with the Evolution of Resistance to Antifungal Drug Combinations*. Cell Rep, 2015.
569. Sanguinetti, M., et al., *Role of AFR1, an ABC transporter-encoding gene, in the in vivo response to fluconazole and virulence of Cryptococcus neoformans*. Infection and Immunity, 2006. **74**(2): p. 1352-9.
570. Ahmad, A., A. Khan, and N. Manzoor, *Reversal of efflux mediated antifungal resistance underlies synergistic activity of two monoterpenes with fluconazole*. European Journal of Pharmaceutical Sciences, 2013. **48**(1-2): p. 80-86.